New Developments in the Crystal Chemistry of Selected Borophosphates and Phosphates

DISSERTATION

zur Erlangung des akademischen Grades

Doctor rerum naturalium
(Dr. rer. nat.)

vorgelegt

der Fakultät Mathematik und Naturwissenschaften
der Technischen Universität Dresden

von

M. Sc. Prashanth W. Menezes

geboren am 02.05.1979 in Puttur, Indien

Eingereicht am 09.07.2009

Die Dissertation wurde in der Zeit von Oktober 2004 bis
Juni 2009 im Max-Planck-Institut für Chemische Physik fester Stoffe angefertigt.

Hope is the companion of power and the mother of success.
For who so hopes strongly has within him the gift of miracles.

- Samuel Smiles

Tag der Verteidigung: 19.10.2009
Gutachter:
Prof. Dr. Rüdiger Kniep
Prof. Dr. Michael Ruck

Acknowledgement

This is perhaps the easiest and hardest chapter that I have to write. It will be simple to name all the people that helped to get this done, but it will be tough to thank them enough. I will nonetheless try…

In the first place, I would like to express my gratitude to my mentor and guide, Prof. R. Kniep, the director of Max Planck Institute for Chemical Physics of Solids for his supervision, advice, and guidance right from the nascent stage of this research till its completion. Above all he provided me unflinching encouragement and support in various ways. His passion towards science, his scientific intuition and foresight made him a constant oasis of ideas which enriched my growth as a student, a researcher and a scientist. His strong belief in the concept of "learning by doing" exceptionally inspired me during my failures and persuaded me to strive for success. I am truly indebted to him.

I gratefully acknowledge my supervisor, Dr. S. Hoffmann for his advice and crucial contribution, which made him a backbone of this research and so to this thesis. His involvement, with his originality has triggered and nourished my intellectual maturity that I will benefit from, for a long time to come. Throughout my thesis–writing period, he provided encouragement, good teaching, good company, and lots of good ideas. I thank him for his detailed review and constructive criticism during the preparation of this thesis. I would have been lost without him.

I sincerely thank Dr. Yu. Prots for single–crystal measurements and for his untiring help during my difficult moments especially with the single crystal structure refinements. I am obligated to him for reading my manuscripts.

I have also benefited from the advice and guidance of Dr. G. Kreiner which was fruitful in shaping up my ideas and research.

Collective and individual acknowledgments are also owed to my colleagues at MPI – CPfS whose presence perpetually refreshed and helped me in various ways. In particular, I would like to mention Dr. H. Borrmann, Dr. R. Cardoso and Mr. S.

Hückmann for X–ray data collections and related discussions, Dr. G. Auffermann and Ms. A. Völzke for chemical analyses, Ms. Susann Scharsach for TG / DTA measurements, Dr. U. Burkhardt, Dr. R. Ramlau, and Mrs. P. Scheppan for SEM and EDX analyses, Dr. W. Schnelle and Mr. R. Koban for magnetic measurements and Ms. J. Buder for infrared measurements.

This thesis research was made a lot easier by my lab mates, Dr. Y.-X. Huang, Dr. B. Ewald, Dr. W. Liu, Dr. M. Yang, Mr. Z. Lin, Ms. S. Chen, Mr. F. Gruchow and Mr. A. Topcu who created a pleasant working atmosphere. Without their constant support, my life at the institute would have been a lot less satisfying. I thank them all. Special thanks go to Dr. Y.-X. Huang and Dr. B. Ewald for all the interesting discussions and the critical reviews.

I am grateful to the secretaries for assisting me in many different ways. Mrs. K. Demian, Mrs. C. Strohbach, Mrs. K. Klein and Ms. S. Zücker deserve special mention for their indispensable help dealing with travel, administration and bureaucratic matters during my stay in Dresden.

I convey special acknowledgements to Dr. M. Schmidt, Dr. E. Dashjav and Dr. J. Hunger who amidst their busy schedules agreed to be internal referees for my papers.

The last five years have been very rich and enjoyable owing to the presence of my colleagues and friends inside and outside the institute. It is pleasure to mention few of my friends and colleagues Dr. S. Nair, Dr. M. Kumar, Mr. J. Hirale, Dr. D. Kasinathan, Dr. A. Rajarajan, Mrs. A. Thomas, Dr. S. Rössler, Dr. H. Tlatlic, Dr. J. Makongo, Ms. K. Wagner, Dr. C. Göbel, Mr. Y. Ötzan, Dr. S. Singh, Dr. R. Nath, Mrs. J. Bendyna and Mr. S. Boulfelfel for the lunch meeting, tea breaks and weekend parties, also Dr. A. Wosylus for being such a good officemate and who always ready to lend a hand. I acknowledge the support of my friends Dr. S. Sapra, Dr. A. Sapra, Mr. K. Kumar, Dr. A. Bajpai, Dr. N. Kumar, Dr. M. Vyas, Dr. B. Gowd, Dr. B. Nandan, Mr. A. Nanjundan, Dr. N. Manik, Dr. K. Koepernik and Ms. S. Kuramoto for their great friendship outside office. They have been there through all my ups and downs.

I was extraordinarily fortunate in having D. D. Sarma as my professor in Indian Institute of Science, India. I could never have embarked and started all of this without his prior teachings thus opened up unknown areas to me. Thank you.

Words fail me to express my appreciation to my girlfriend Ms. R. Pais whose dedication, love and persistent confidence in me, has taken the load off my shoulder. Furthermore, I would like to thank Mr. R. Pais and Mrs. M. Pais for their constant support.

None of these experiences would have occurred if not for the perpetual support of my parents, my father, Fredrick Menezes, my mother, Cecelia Menezes and my brothers Pradeep and Pramod, who deserve special mention for their inseparable support and prayers. The knowledge that they will always be there to pick up the pieces is what allows me to repeatedly risk getting shattered. To them I dedicate this thesis.

Finally, I would like to thank everyone who was significant in the successful completion of my thesis as well as expressing my sincere apologies for failing to mention in person each and everyone.

Thank you God for continuously showering your blessings upon me...

CONTENTS

1 Introduction and Objective

This chapter covers the general introduction and the structural chemistry of borophosphates which was proposed in 1998 and then modified in 2007 in order to understand the basic principles of borophosphates. Subsequently, it will discuss their syntheses, structural developments and applications and will give an overview on *3d* transition metal borophosphates. Finally, the main objectives of this thesis will be dealt with.

1.1 General Introduction

Borates have long been a focus of research for their variety of structure types, high laser–damage tolerance and high optical quality [1-5]. Increasing interest has been observed in the synthesis and development of metal phosphates with open framework structure due to their rich structural chemistry and potential applications in catalysis, adsorbents and ion–exchangers [6-10]. It was assumed that a combination of borate and phosphate characteristics may show exciting structural architecture and properties both of borates and phosphates namely, optical, catalytic, as molecular sieves, as an ion exchanger and corrosion protector. Keeping these aspects in mind, the systematic investigation on borophosphates was started in 1994 [11].

Borophosphates are intermediate compounds of systems M_xO_y–B_2O_3–P_2O_5–(H_2O) (*M* = main group or transition metal) which contain complex anionic structures built of interconnected trigonal–planar BO_3 and / or BO_4 and PO_4 groups and their partially protonated species (*Figure 1.1*) [12].

Although the intensive research on borophosphates has been carried throughout these years, numerous applications are already established. Several borophosphates have been applied in optical industries (non–linear optical materials) [13-19]. The catalytic properties of borophosphates are well established and widely used in the petroleum industry [20, 21]. Some borophosphates doped with rare earth metals exhibit luminescence and fluorescence effects [22-25]. Applications of borophosphates as corrosion protecting materials were also successful [26]. Borophosphates can be used as coating on metal surfaces, consequently acting as corrosion protectors [27]. In addition, several borophosphate compounds have been used as antioxidants and fire proofing agents [28].

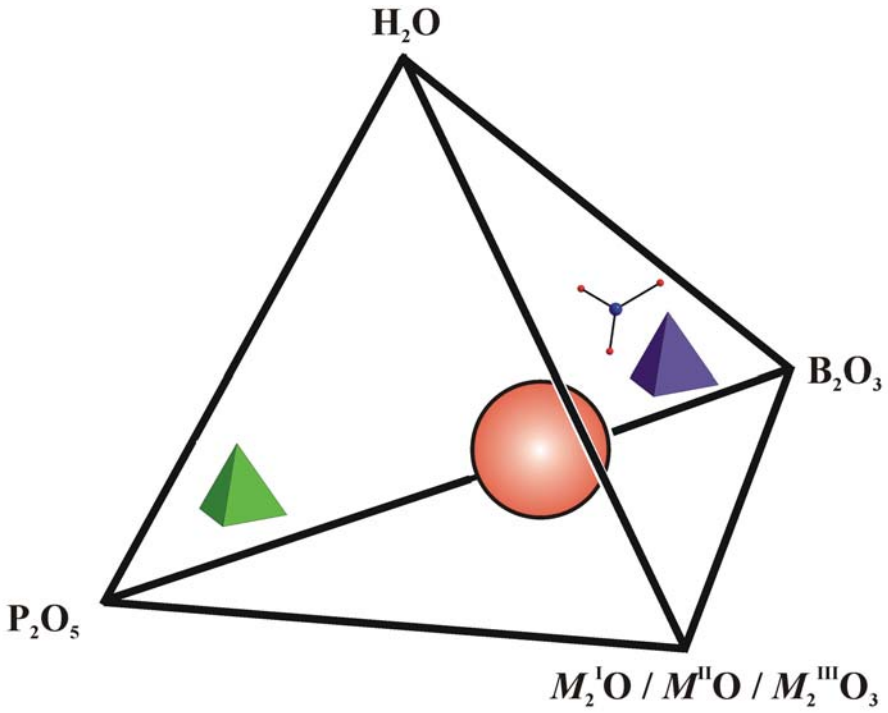

Figure 1.1: *Borophosphates (schematically by the red ball) are intermediate compounds of systems M_xO_y–B_2O_3–P_2O_5–(H_2O) (M = main group or transition metal). The complex anionic structures of borophosphates are built of interconnected trigonal–planar BO_3 (ball and stick) and / or BO_4 (blue tetrahedron) and PO_4 (green tetrahedron) groups and their partially protonated species. Not included: Templated Borophosphates.*

1.2 Structural Chemistry of Borophosphates

A first approach to the development of a structural chemistry of borophosphates is based on the linking principles of the primary building units (BO_3, BO_4 and PO_4) following the general line of silicate crystal chemistry [12]. The classification of borophosphates is exclusively focused on the anionic partial structures, although it is clear that the cations (charge, size, and coordination behavior) have a significant influence even on the dimensionality of the anionic structural units.

Phosphorus in borophosphates is always four–fold coordinated. However, boron can be surrounded by three or four oxygen atoms. The construction of complex borophosphate anions comprise of trigonal–planar BO_3 and / or tetrahedral BO_4 and PO_4 groups (protonated and non–protonated) exclusively linked *via* common corners to form isolated species, oligomers, rings, chains, layers and even frameworks. Initially, structural classifications of borophosphates were divided into **“anhydrous”**

and **"hydrated"** on the basis of the molar B : P ratio. The following principles in the structural chemistry of borophosphates were proposed in 1998 [12].

- Compounds with the molar ratio B : P = 6 : 1 to 2 : 1 (boron rich) contain boron in three–fold **and** tetrahedral coordination (later described as mixed–coordinated borophosphates).
- The complex borophosphate anions of **anhydrous** borophosphates consist of isolated species, oligomers and chains, whereas anions of **hydrated** borophosphates form in addition rings, layers and frameworks.
- Non–bridging corners of borate species (BO_3 and BO_4) in hydrated phases correspond to OH –groups.
- Analogies to the structural chemistry of borates are also given by the frequent formation of three–membered rings.
- P—O—P linking is not observed.

Combining and extending the classification principles of the borophosphate structural chemistry given in 1998 [12], a new approach was proposed in 2007 in terms of dimensionality (spatiality) of complex borophosphate anionic partial structures and the molar B : P ratio [29]. The five new structural classification criteria are given as follows.

- **Tetrahedral borophosphates:** The large majority of borophosphates comprises anionic arrangements that are exclusively containing boron (BO_4) and phosphorus tetrahedra (PO_4). In the simplest case exactly one borate and one phosphate tetrahedron are condensed *via* a common oxygen vertex to form a dimer. Tetrahedral borophosphates are realized only with the composition B : P = 1 : 1 to 1 : 4.
- **Mixed–coordinated borophosphates:** Borophosphates with mixed–coordinated anions comprise of a trigonal–planar borate group (BO_3), and / or boron tetrahedra (BO_4) and phosphorus tetrahedra (PO_4). The mixed–coordinated borophosphates show a large variety in composition with B : P ratios ranging from 6 : 1 to 1 : 3.
- **Metalloborophosphates:** Up to date, metalloborophosphates exclusively comprise three–dimensional anionic partial structures built of BO_4 and PO_4

tetrahedra which are unique to a ratio of metallate, borate and phosphate polyhedra with the composition *M* : B : P = 1 : 1 : 2 and 2 : 1 : 3.

- **Anion–substituted compounds and border cases:** Borophosphates in which the oxoligands of the complex anions are substituted are belonging to this group. Only a small number of borophosphates with anion–substitution (fluorine–substituted) are known up to now.
- **Borate–phosphates**: The group of borate–phosphates comprises isolated borate (BO_3, BO_4) and phosphate species (PO_4). Additionally, further oxide or hydroxide ions may be present in the compounds.

The observed dimensionalities of the complex borophosphate anions with respect to the existence of B : P ratios is shown in *Figure 1.2*. The layers and the frameworks (D = 2–3) are only observed in a small range of composition between B : P = 1 : 1 and 1 : 2. Furthermore, tetrahedral borophosphates have been observed only between B : P = 1 : 1 and 1 : 4 which exclusively contain isolated species, oligomers and rings. All borate rich (B : P = 6 : 1 to 1 : 1) compounds known to date comprise mixed–coordinated anions as indicated by dark grey regions (*Figure 1.2*).

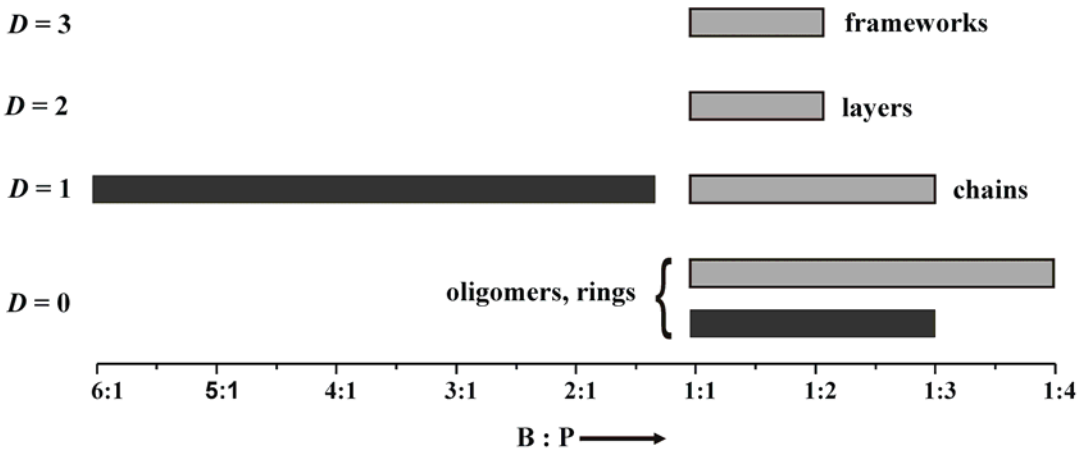

Figure 1.2: *Dimensionality of complex borophosphate anionic partial structures; mixed coordinated (dark grey) and tetrahedral (light grey) borophosphates. Layers and frameworks (D = 2 – 3) are observed with compositions between B : P = 1 : 1 and 1 : 2. The oligomers, rings and chains are known within the composition range from B : P = 6 : 1 to 1 : 4.*

Borophosphates are prepared by employing several techniques such as high temperature solid state [11], hydrothermal [12, 30], microwave–assisted [31, 32], solvothermal [30], precursor [31, 33], flux [34] and chemical transport reactions [31, 35]. However, hydrothermal methods and high temperature solid state reactions are commonly adopted. The mild hydrothermal route [36] (T ≈ 200 ºC, Teflon autoclave) has produced a substantial number of new borophosphates with a wide variety of structural patterns. The number of borophosphates prepared from high temperature solid state reactions is less in comparison with those obtained by hydrothermal methods due to the fact that single phase materials are hard to obtain and the formation of glasses is often encountered [37-39]. Hydrothermal synthesis usually refers to heterogeneous reactions in aqueous media above 100 °C and 1 bar. Possible advantages of the hydrothermal method over other techniques include the ability to create crystalline phases which are not stable at the melting point. Also, materials which have a high vapour pressure near their melting points can be grown by the hydrothermal method [36, 37]. The method is also particularly suitable for the growth of large good quality crystals while maintaining good control over their composition. Even, compounds with elements in oxidation states that are difficult to attain by other routes can be obtained in closed systems by hydrothermal synthesis. For borophosphates, the temperature and the degree of filling are the main factors influencing the pressure conditions.

1.3 Transition Metal Borophosphates

Transition (*3d*) metal borophosphates are of interest with respect to their catalytic, thermal and magnetic properties [40]. Synthesis and characterization of a broad new spectrum of borophosphates with magnetically active cations is, thus, studied systematically in various Ph.D. theses (C. Hauf [14], I. Boy [41], H. Engelhardt [42], G. Schäfer [43], Y.–X. Huang [44] and B. Ewald [45]) and diverse structural features have been observed. Also out of the two known borophosphate minerals [46, 47] one of them contains transition metal ion ($Mn_3(OH)_2[B(OH)_4][PO_4]$, Seamanite).

Focusing on the objective of this Ph.D. work, an overview on *3d* transition metal (Sc – Zn) containing borophosphates (templated borophosphates are not under consideration) has been prepared. The list below (*Table 1.1* to *Table 1.5*) describes the

existing transition metal borophosphates and their complex anionic borophosphate units.

Table 1.1: *Tetrahedral borophosphates containing 3d transition metals (highlighted in bold) with B : P ratios 1 : 1 to 1 : 4 (tetrahedra: BO_4 = blue, PO_4 = green; spheres: H = pink). The sequence is given by N, where N is the number of interconnected groups.*

Compound	Complex borophosphate anion
Oligomers	
$M^{I}\mathbf{M^{III}}[BP_2O_7(OH)_3]$ (M^{I} = Na, K; $\mathbf{M^{III}}$ **= V, Fe**) [48, 49] $Na_{14}[Na > \{(\mathbf{V}O)_2BP_2O_{10}\}_5]\cdot nH_2O$ [50][b] $M^{I}{}_{17}[A > \{(\mathbf{V}O)_2BP_2O_{10}\}_6]\cdot nH_2O$[b] ($M^{I}$ = NH_4, K, Cs) [50] $Cs\mathbf{V_3}(H_2O)_2[B_2P_4O_{16}(OH)_4]$ [51] $Li\mathbf{Cu_2}[BP_2O_8(OH)_2]$ [52]	**N = 3** 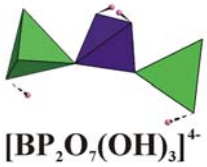 $[BP_2O_7(OH)_3]^{4-}$ Unbranched tetrahedral triple built from $(HO)_2BO_2$ sharing common apices with two PO_4 tetrahedra
$(NH_4)_5\mathbf{V_3}[BP_3O_{19}]\cdot H_2O$ [53] $(NH_4)_4\mathbf{Mn_9}[BP_3O_{11}(OH)_2]_2[HPO_4]_2[PO_4]_2$[a] [54]	**N = 4**  $[BP_3O_9(OH)]^{4-}$ Open–branched tetramer built from a central $(HO)BO_3$ tetrahedron sharing common O–corners with one $(HO)PO_3$, one $(HO)_2PO_2$ and one PO_4 tetrahedron

N = 6

Mg_{1-x}**Ni**$_x$ $(H_2O)_2[BPO_4(OH)_2]$ (x = 0.5) [55]

Unbranched six–membered ring of alternating $(HO)_2BO_2$ and PO_4 tetrahedra

N = 6

K**V**$[BP_2O_8(OH)]$ [56]

K**Fe**$^{III}[BP_2O_8(OH)]$ [48]

Na**Co**$[BP_2O_8(OH)]$ [57]

Open–branched four–membered ring of $(HO)BO_3$ and PO_4 tetrahedra sharing common corners with two additionally branching PO_4 tetrahedra

N = 6

Na_4**Cu**$_3[B_2P_4O_{15}(OH)_2]\cdot[HPO_4]_2$[a] [58]

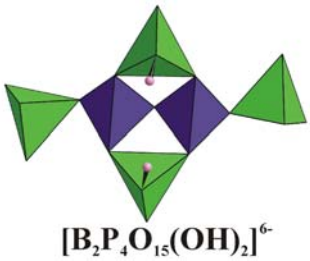

Double loop–branched hexamer built from BO_4, PO_4 and $(HO)PO_3$ tetrahedra

N = 12

$K_6\mathbf{Cu_2}[B_4P_8O_{28}(OH)_6]$ [59]

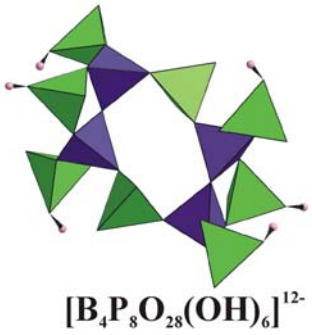

$[B_4P_8O_{28}(OH)_6]^{12-}$

Open–branched central six–membered ring built from BO_4 and PO_4 tetrahedra with additional loop–branchings by $(HO)PO_3$ groups

Chains

$\mathbf{Fe^{II}}[B_2P_2O_7(OH)_5]$ [60]

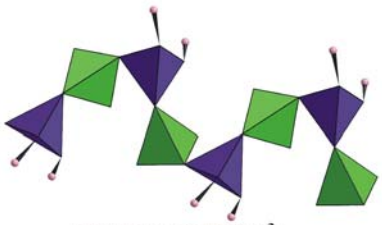

$^1_\infty[B_2P_2O_7(OH)_5]^{3-}$

Unbranched single chain built from alternating $(HO)_2BO_2$ and $(HO)PO_3$ tetrahedra

$\boldsymbol{M^{II}}[BPO_4(OH)_2]$
($\boldsymbol{M^{II}}$ **= Mn, Fe, Co, Ni**) [61, 62]

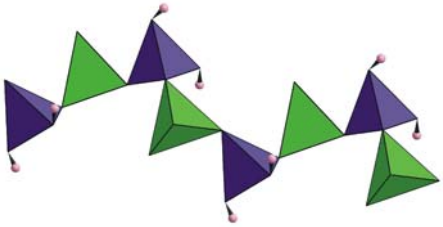

$^1_\infty[BPO_4(OH)_2]^{2-}$

Unbranched single chain built from alternating $(HO)_2BO_2$ and PO_4 tetrahedra

$M^{I}\boldsymbol{M}^{III}[BP_2O_8(OH)]$
(M^{I} = NH_4, Rb, Cs; $\boldsymbol{M}^{III}$ = **V, Fe,** $\mathbf{Fe_{0.53}V_{0.47}}$) [63-66]

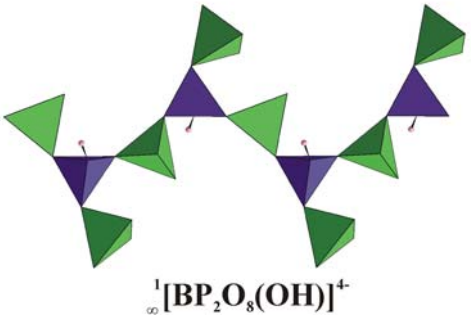

Open–branched single chain built from alternating $(HO)BO_3$ and PO_4 tetrahedra

$\boldsymbol{M}^{III}(H_2O)_2[BP_2O_8]\cdot H_2O$
($\boldsymbol{M}^{III}$ = **Sc, Fe**) [67, 68]

$\boldsymbol{M}^{III}(H_2O)_2[BP_2O_8]$
($\boldsymbol{M}^{III}$ = **Sc, Fe**) [67, 68]

$M^{I}\boldsymbol{M}^{II}(H_2O)_2[BP_2O_8]\cdot H_2O$
(M^{I} = Li–K, NH_4; $\boldsymbol{M}^{II}$ = **Mn–Zn**) [69]

Na**Mn**$(H_2O)_2[BP_2O_8]\cdot H_2O$ [70]

(H_3O)**Zn**$(H_2O)_2[BP_2O_8]\cdot H_2O$ [71]

K**Fe**$(H_2O)_2[BP_2O_8]\cdot 0.5H_2O$ [72]

$(H_3O)_{0.5}\boldsymbol{M}^{II}_{1.25}(H_2O)[BP_2O_8]\cdot H_2O$
($\boldsymbol{M}^{II}$ = **Mn, Co**) [73]

$(NH_4)_{0.4}\mathbf{Fe}^{II}_{0.55}\mathbf{Fe}^{III}_{0.5}(H_2O)_2[BP_2O_8]\cdot 0.6H_2O$ [74]

$(NH_4)_{0.5}\mathbf{Fe}^{II}_{0.5}\mathbf{Fe}^{III}_{0.5}(H_2O)_2[BP_2O_8]\cdot 0.5H_2O$ [75]

$\{(NH_4)_x\mathbf{Co}_{(3-x)/2}\}(H_2O)_2[BP_2O_8]\cdot zH_2O$
(x = 0.5) [76]

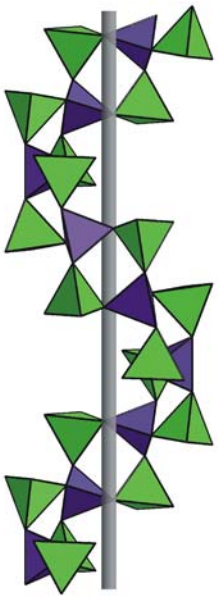

Spiral ribbon built from four–membered tetrahedral rings in which the BO_4 and PO_4 groups are alternate

Layers

Cu$(H_2O)_2[B_2P_2O_8(OH)_2]\cdot H_2O$ [77]

Mg_{1-x}**Co**$_x(H_2O)_2[B_2P_2O_8(OH)_2]\cdot H_2O$ (x = 0.25) [78]

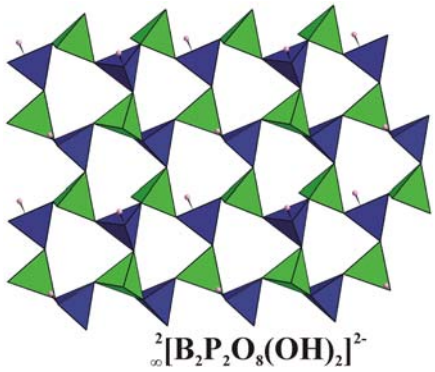

Unbranched single layer with alternating $(HO)BO_3$ and PO_4 tetrahedra

Rb_2**Co$_3$**$(H_2O)_2[B_4P_6O_{24}(OH)_2]$ [79]

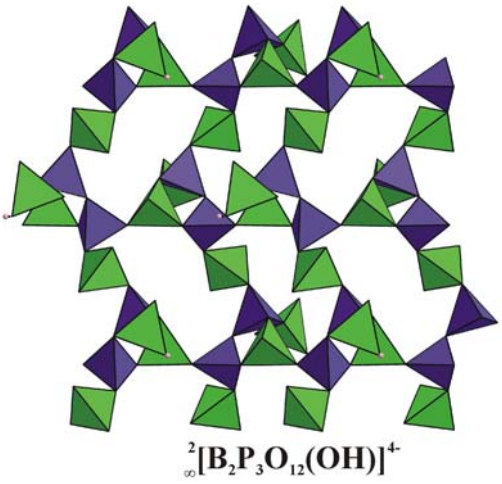

Layer of BO_4, PO_4 and $(HO)PO_3$ tetrahedra connected *via* common vertices

[a] Compound contains isolated PO_4 tetrahedra besides the borophosphate anions.

[b] The borophosphate trimers are interconnected by V_2O_8 units forming cluster anions. In such a crystal structure, some of the cations (alkali–metal or ammonium) are located inside the anions indicated by > in the formulas

Table 1.2: *Mixed–coordinated borophosphates containing transition 3d metals (highlighted in bold) with B : P ratios 6 : 3 to 1 : 3 (tetrahedra: BO_4 = blue, PO_4 = green; spheres: B = blue, O = red). The sequence is given by N, where N is the number of interconnected groups.*

Compound	Complex borophosphate anion
	Oligomer
	N = 2
Co$_5$[BPO$_6$][PO$_4$]$_2$[a][34]	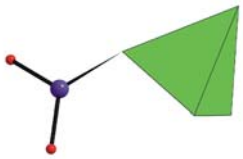 $[BPO_6]^{4-}$
	A trigonal–planar BO_3 unit is connected to a PO_4 tetrahedron
	N = 4
M*^{III}**[BP$_3$O$_{12}$] (M*^{III} = V, Cr, Fe**) [15, 80, 81]	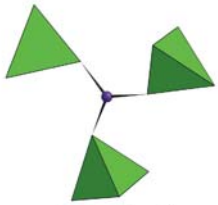 $[BP_3O_{12}]^{6-}$
	A trigonal–planar BO_3 unit is connected to three PO_4 tetrahedra
	Chains
Na$_2$***M*^{II}**[B$_3$P$_2$O$_{11}$(OH)]·0.67H$_2$O (***M*^{II} = Mn–Zn**) [82, 83] Na$_5$(H$_3$O)***M*$^{II}_3$**[B$_3$P$_2$O$_{11}$(OH)]$_3$·2H$_2$O (***M*^{II} = Mn–Zn**) [84]	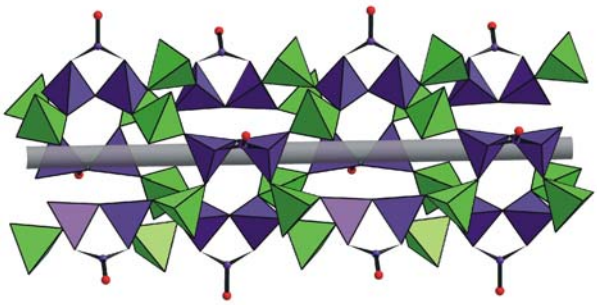 $[B_3P_2O_{11}(OH)]^{4-}$
	One–dimensional borophosphate tubes built from 12–membered rings by sharing common O–corners with BO_4 tetrahedra and PO_4 tetrahedra. Loop–branching BO_3 units are at the borders.

[a] Compound contains isolated PO_4 / $(HO)PO_3$ tetrahedra besides the borophosphate anions.

Table 1.3: *Metalloborophosphates containing transition 3d metals (highlighted in bold) with M : B : P ratio 1 : 1 : 2 (tetrahedra: BO_4 = blue, PO_4 = green, ZnO_4 = light grey)*

Compound	Complex borophosphate anion
$M^I[\mathbf{Zn}BP_2O_8]$ (M^I = NH_4, K, Rb, Cs) [85, 86] $NH_4[\mathbf{Zn_{1-x}Co_x})BP_2O_8]$ [87] $Na[\mathbf{Zn}BP_2O_8]\cdot H_2O$ [88]	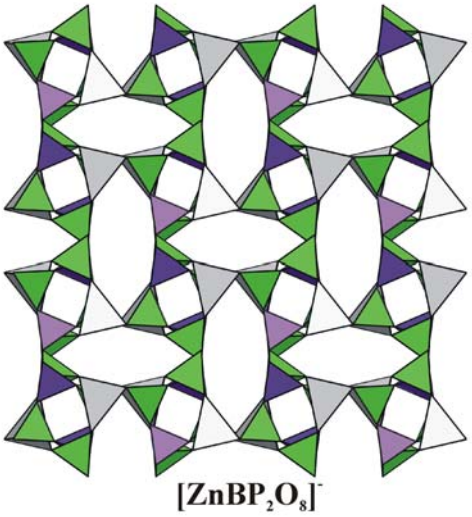 **$[ZnBP_2O_8]^-$** Frameworks built from BO_4, PO_4 and ZnO_4 tetrahedra

Table 1.4: *Border cases containing transition 3d metals (highlighted in bold) with B : P ratio 1: 1 (tetrahedra: BO_4 = blue, PO_4 = green, ZnO_4 = light grey)*

Compound	Complex borophosphate anion
$\mathbf{Zn}[BPO_4(OH)_2]$ [89]	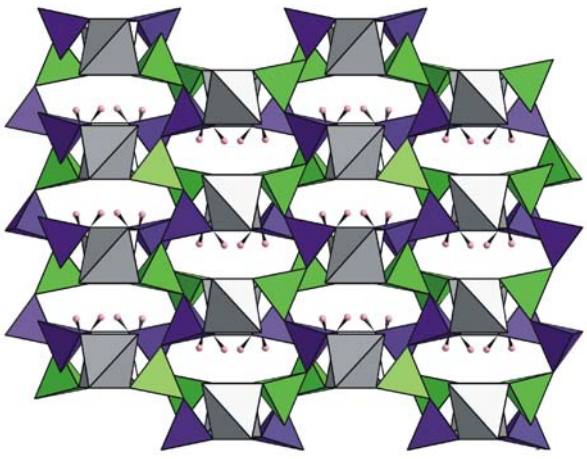 **$Zn[BPO_4(OH)_2]$** Open–branched single chains of alternating $(HO_2)BO_2$ and PO_4 tetrahedra interconnected by $ZnO_2(OH)_2$ tetrahedra forming a neutral framework

Table 1.5: *Borate–phosphates containing transition 3d metals (highlighted in bold) (tetrahedra: BO_4 = blue, PO_4 = green; spheres: O = red)*

Compound	Anion
$\boldsymbol{M^{II}_3}[BO_3][PO_4]$ ($\boldsymbol{M^{II}}$ = **Co, Zn**[a])	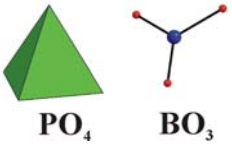 Isolated PO_4 tetrahedra and BO_3 groups
$\mathbf{Mn_3}(OH)_2[B(OH)_4][PO_4]$ [90-92]	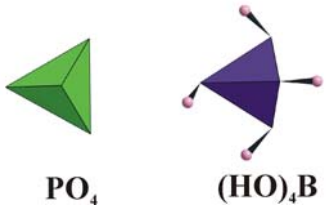 Isolated PO_4 tetrahedra and $(HO)_4B$ groups

[a] High and low temperature forms with different space groups have been reported.

1.4 Aim of the Work

The main objective of the present work was to synthesize, characterize and to study the properties of new selected *3d* transition metal borophosphates. The selected four elements are scandium (Sc), iron (Fe), cobalt (Co) and nickel (Ni) due to their interesting contributions to borophosphate structural chemistry. The mild hydrothermal method was employed for the syntheses.

Objective 1: Numerous borophosphates containing transition metals (V – Zn) with alkali–metals (Li – Cs) have been reported in the past ten years (*Table 1.1* to *Table 1.5*). Scandium is the most recent trivalent metal to attract interest as a framework forming element. Only a few compounds are known representing scandium based open framework structures, e.g. scandium phosphates, organically templated phosphates, phosphonates, and fluorophosphates, respectively [93-96]. In 2006 [67], the first scandium borophosphate was synthesized exhibiting remarkable thermal properties. However, there is still no report on incorporation of alkali–metals and

alkaline–earth metals into scandium based borophosphate compounds. In this regard, we started to investigate the role of alkali–metals (Li – Cs) and alkaline–earth metals (Mg – Ba) on crystal structure formation and the thermal properties of scandium containing borophosphates (*Figure 1.3*).

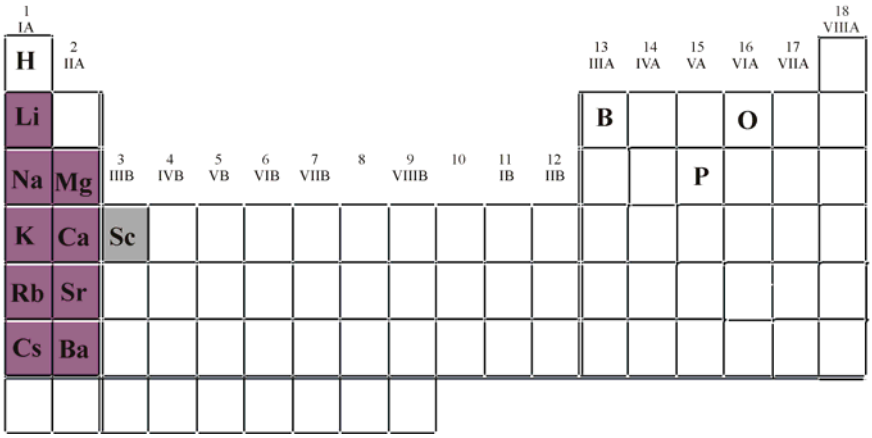

Figure 1.3: *Selected elements for objective 1: alkali– and alkaline–earth – scandium – borophosphates.*

Objective 2: It is well known from the borophosphate structural chemistry that the charge of the complex anionic partial structures of borophosphates can either be compensated by one type of cation (M^{I}, M^{II} or M^{III}) or by a combination of them ($M^{I}M^{II}$ or $M^{I}M^{III}$) retaining the anionic partial structure [12, 29]. Depending on the shape and the size of the M^{I} ion it is possible to control the shape and size of cavities or channels in the framework structures. There are only very few examples where the charge of the complex borophosphate anion is compensated with two divalent metals ($M1^{II}M2^{II}$). Therefore, in order to prove the existence of such compounds and to investigate the effect of two divalent ($M1^{II}M2^{II}$) cations on the crystal structure, the thermal and magnetic properties, we considered to investigate borophosphates with alkaline–earth metals (Mg – Ba) and selected the transition metals (Fe, Co, Ni) (*Figure 1.4*).

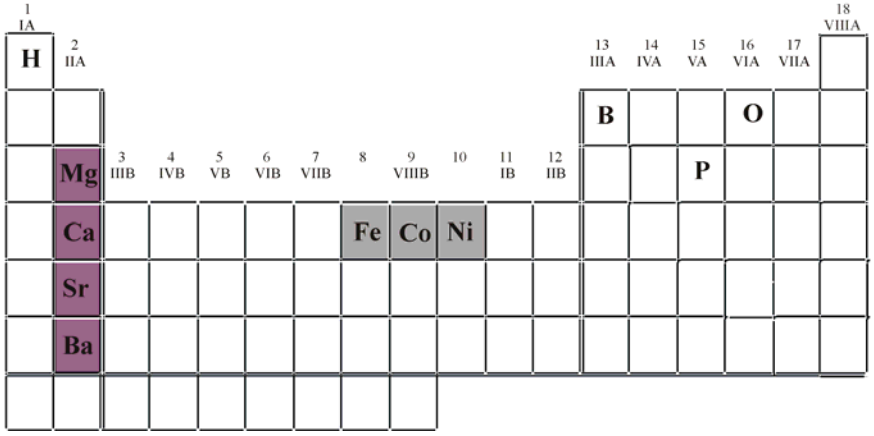

Figure 1.4: *Selected elements for objective 2: alkaline–earth – 3d transition metal – borophosphates.*

Objective 3: Recently, the focus was directed to borophosphates which exclusively contain transition metals as the cationic component. This led to the discovery of compounds with infinite chiral chains of condensed transition metal octahedra showing antiferromagnetic behavior [61]. In search of new (2D) examples among the borophosphates we proposed to carry out our research on borophosphates containing the transition metals Fe, Co or Ni (single transition element) and combinations of Fe, Co and Ni. (*Figure 1.5*)

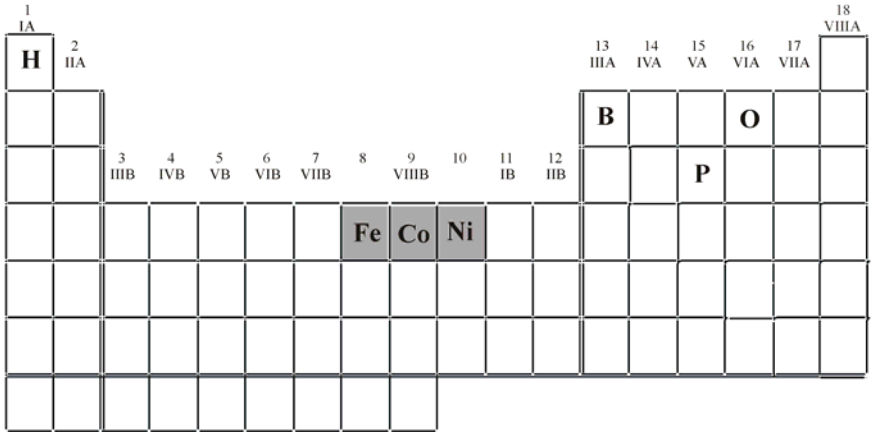

Figure 1.5: *Selected elements for objective 3: 3d transition metal – borophosphates.*

2 Experimental

This chapter starts with a report on the techniques employed for the preparation, the chemicals and their quality used for the experiments. Later on, brief descriptions on the materials characterizations are given, such as powder X–ray diffraction, single crystal X–ray diffraction, scanning electron microscopy, inductively coupled plasma–atomic emission spectroscopy, energy dispersive X–ray analyses, thermal analyses, infrared spectroscopy and temperature dependent magnetic susceptibilities.

2.1 Methods of Preparation

The hydrothermal synthesis is one of conventional procedures for the preparation of borophosphates and phosphates [36, 97, 98]. The method involves heating the reactants in a closed vessel together with water. The pressure within the vessel increases with increasing temperature. Above its normal boiling temperature (100 °C) the system is referred as 'super–heated aqueous system'.

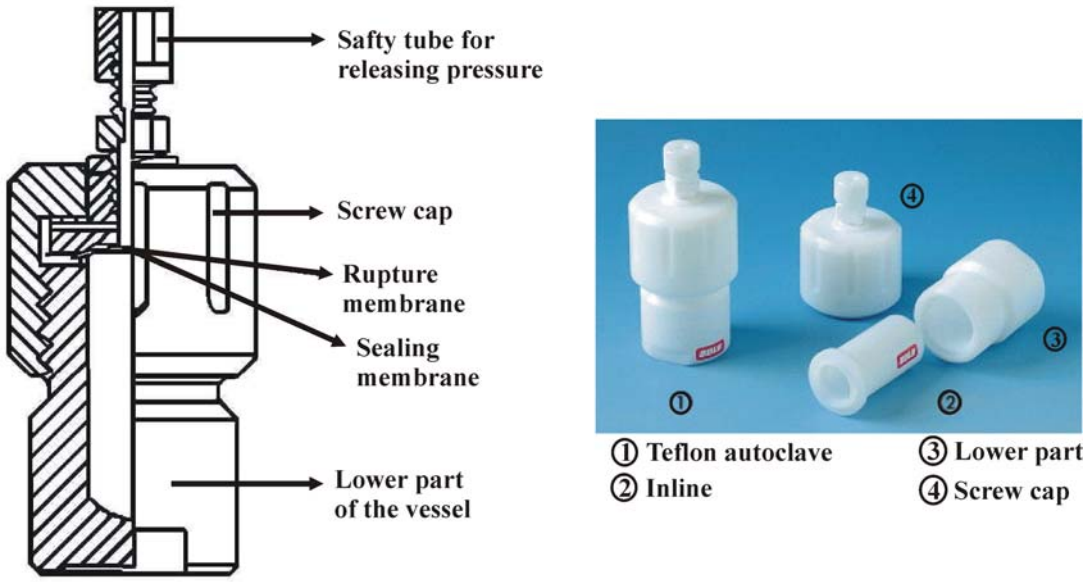

Figure 2.1: *Reaction vessel employed for hydrothermal syntheses below 170 °C (Teflon autoclave, ROTH BOLA. Source of picture: user manual, BOHLENDER GmbH)*

The reaction vessels used in this work are (1) Teflon autoclaves (*ROTH*, *BOLA,* reaction volume 10 ml or 20 ml) for reaction temperatures lower than 170 °C as shown in *Figure 2.1* and (2) Teflon–lined stainless steel autoclaves (*BERGHOF*,

reaction volume 25 ml) as shown in *Figure 2.2* and usually used at higher temperatures (170 °C to 240 °C).

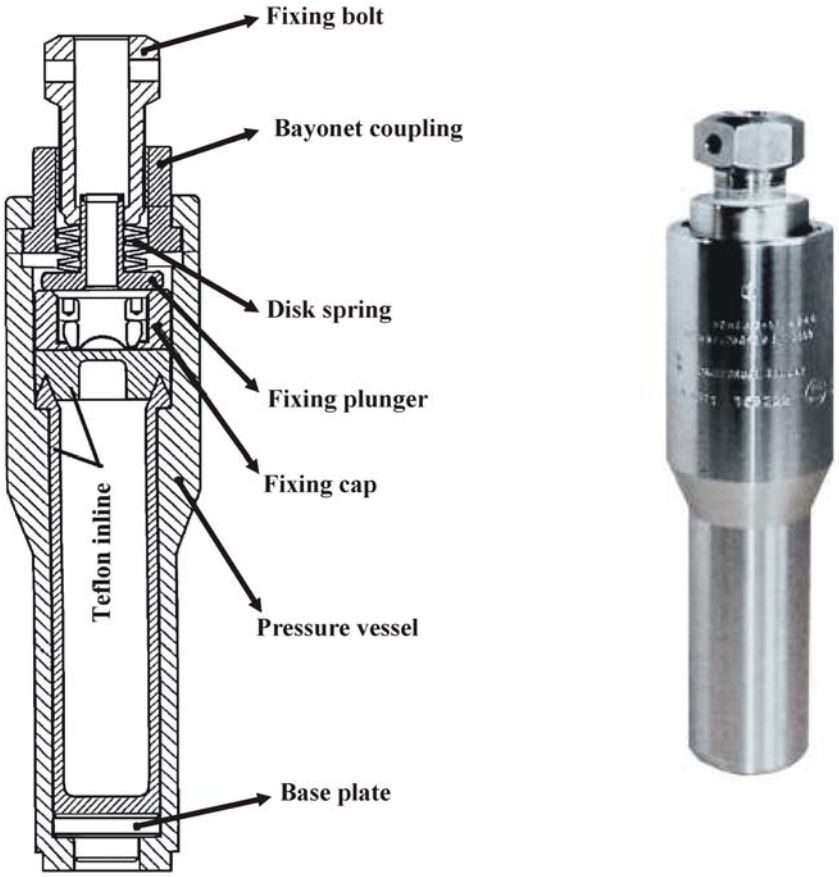

Figure 2.2: *Reaction vessel employed for hydrothermal syntheses up to 240 °C (Stainless steel autoclave, BERGHOF. Source of picture: user manual, BERGHOF GmbH)*

The general method of preparation of borophosphates and phosphates is described as follows: A mixture of the reagents is homogenized in 10 ml water and stirred slowly while heating from room temperature to higher temperatures (≈ 80 °C) for four hours. The pH is adjusted to acidic conditions (pH = 1 – 3) by addition of 37 % HCl. The reaction mixture is then filled into Teflon autoclaves with different filling degrees (20 – 70 %) and heated under autogenous pressure in an oven (140 – 240 °C) for 1 – 60 days. The solid reaction products are separated by filtration, washed with deionized water and then with hot water, filtered and washed again with acetone and finally dried at 60 °C in air. The problems associated with the preparation of borophosphates and phosphates with specified compositions consist in choosing the optimum conditions for their synthesis. Structure and composition of the resulting

borophosphates and phosphates depend on the parameters of the synthesis (the temperature, the degree of filling of an autoclave, the concentration of the starting material, the pH of the medium, the duration of synthesis). One of the criteria for the existence of complex borophosphates is the presence of a strongly acidic medium. From practical experience, in most of cases acid conditions lead to borophosphates and more basic conditions to phosphates.

2.2 Chemicals and Quality

An overview of the chemicals and their purity used for the hydrothermal syntheses of borophosphates and phosphates is given in *Appendix 1*. As transition metal–, alkali– and alkaline earth–metal sources the respective oxides, hydroxides, halides, carbonates, oxalates and acetates were used. The phosphate and borate sources were 85 % H_3PO_4, P_2O_5, B_2O_3, and H_3BO_3 besides other alkali–metal and ammonium phosphates / borates.

2.3 Materials Characterization

2.3.1 Powder X–ray Diffraction

Powder X–ray diffraction investigations were extensively used as the primary tool for the characterization of the final reaction products. The powder patterns of the products are compared with the powder patterns from database or with simulated powder patterns from single crystal structure data (ICSD [P1] and PDF [P2]). The phase purity of the reaction products was initially checked using the powder X–ray diffraction pattern collected on a *HUBER* Image Foil Guinier Camera G670 (Cu $K_{\alpha 1}$–radiation, Germanium (111) monochromator and Co $K_{\alpha 1}$–radiation, Quartz (101)) and on a *STOE* Stadi MP diffractometer equipped with a primary–beam germanium monochromator. X–ray powder investigations were carried out either by using glass capillaries or flat foils on aluminum rings. For flat foils, the samples were finely ground and spread over the foil with a solution of hexane and vaseline and for the capillary measurements, the fine powder was filled into the glass capillary with a 0.3 mm inner diameter. Continuous scan data were collected in the 2θ range of 5 – 110° with a step width of 0.005° for foils and 2θ range of 3 – 100° with a step width of 0.02° for glass capillaries. The final data handling was made by using the program *WinXPOW* [P3] software package (*STOE*, version 1.2). The lattice parameters of

some of the compounds were determined using lanthanum hexaboride (LaB_6) as an internal standard. The *WinCSD* (version 2000) program package [P4] was used for the least–squares refinements.

2.3.2 Single Crystal X–ray Diffraction

Suitable single crystals were selected under a polarizing microscope and glued on a thin glass fiber with a two–component adhesive (UHV). The Laue method was initially used to check the quality of the specimens. Intensity data collection was performed on a *RIGAKU AFC7* four–circle diffractometer equipped with a Mercury–CCD detector and a fine focused sealed tube X–ray source (Mo K_α–radiation, λ = 0.71073 Å, graphite monochromator). The collected data were subjected to Lorentz, polarization and absorption correction. Initial models of the crystal structures were obtained by direct methods. The crystal structures were refined using least–squares refinements with the program *SHELXL–97* included in the program package *WinGX* [P5-P8]. The quality of the structure model was evaluated by R–values, which indicate the agreement between observed (F_o) and calculated (F_c) F values. R1 is given by:

$$R1 = \Sigma \, ||F_o| - |F_c|| \, / \, \Sigma \, |F_o|$$

The wR2 based on F^2 is defined as

$$wR2 = \{ \Sigma \, [w \, (F_o^2 - F_c^2)^2] \, / \, \Sigma \, [w \, (F_o^2)^2] \}^{1/2}$$

where

$$w = 1 \, / \, \sigma^2 \, (F_o^2) + (aP)^2 + bP$$

σ is the statistical error of a measured intensity F^2, the parameters a and b are chosen to minimize the differences in variances for reflection in different ranges of intensity and diffraction angles

and

$$P = 2F_c^2 + \max \, (F_o^2, 0) \, / \, 3$$

Goodness of fit (GooF) is another important factor for evaluating the quality of a crystal structure refinement; it is always based on F^2 and is given by:

$$GooF = S = \{\Sigma [w (F_o^2 - F_c^2)_2] / (n - p)\}^{1/2}$$

where *n* resembles the number of reflections and *p* represents the total number of parameters refined. A correct structure model usually requires S ≈ 1. The crystal structures were visualized and analyzed using the program *DIAMOND* version 3.1f [P9].

2.3.3 Chemical Analysis

In the present work, the Inductively Coupled Plasma–Optical Emission Spectrometry (ICP–OES) was applied to analyze metals like scandium, iron, cobalt, nickel, zinc, alkaline earth–metals, alkali–metals and non metals like phosphorus and boron in the reaction products. The analyses were performed with a *VARIAN VISTA RL SPECTROMETER* (excited by Ar plasma with radial observation). The samples were dissolved in an acid solution (chloronitrous acid). The solution was then aspirated into a plasma chamber. The emission was detected by an optical spectrometer. The results of three measurements were averaged.

The simultaneous determination of hydrogen and nitrogen contents were analyzed in a *LECO CHNS–932* system, which applies the hot extraction method [99]. About 2 mg of a sample in a tin capsule was exposed to high temperature combustion (approximately 1000 ºC) in an enriched oxygen environment in which H is converted to H_2O and N to N_2. H_2O is measured using an infrared detector whereas N_2 is determined *via* thermal conductivity detection. The samples analyzed for oxygen are burnt in a high–carbon environment inside the pyrolysis furnace *VFT–900* at a temperature of approximately 1300 ºC in a stream of helium to form CO. The CO is swept from the furnace and converted to CO_2 which is then measured by an infrared detector. In general, the measured total O–value was too low because the oxygen of the H_2O molecules (crystal water) was only incompletely detected.

2.3.4 Scanning Electron Microscopy (SEM) and Energy Dispersive X–ray Analysis (EDX)

Scanning electron microscopy (SEM) was applied for examining texture, morophology and surface details of the crystals under investigation. Energy dispersive X–ray (EDX) analyses were used to half–quantitatively determine the elements

present on the sample surface (typically 0.05 mm) by detecting the energy and intensity of emitted X–rays. The samples were placed on a substrate (sample holder) and sputtered with gold for SEM and with carbon for EDX in order to increase the surface conductivity. The energy dispersive X–ray measurements were carried out on a *PHILIPS XL 30* (SEM integrated with EDX). Data handling and analytical processing were done by use of the software package *EDAX*. The drawback of this technique is given by the fact that it can not detect elements below an atomic number of ten; therefore boron (in borophosphates) can not be determined by EDX (ICP–OES was used instead).

2.3.5 Thermal Analysis

Thermal analyses (TG / DTA) were carried out to determine changes in weight and the temperature difference of a sample and a reference to give informations on reactions, decompositions, phase transitions and recrystallization events. For some borophosphates, the de– and re–hydration behavior was also examined. Simultaneous constant rate thermogravimetry (TG) and difference thermal analyses (DTA) were performed on a *NETZSCH STA 449* in a glovebox filled with argon. The powdered sample (30 – 50 mg) was placed in an open 85 μL PtRh crucible (Netzsch) and typically heated by 5 K / min to 1000 ºC in a continuous argon flow (200 mL / h, Messer–Griesheim 99.999 % purified with *ALPHAGAZ O2*–Free–System). Cooling was done with the same rate. The data were analyzed by applying the program *Proteus* (version 4.8.3, *NETZSCH*). Selected compounds were also investigated by a thermobalance coupled to a mass spectrometer (*SKIMMER STA409 CD NETZSCH*) in order to identify the evolved gases.

2.3.6 Infrared Spectroscopy

IR spectroscopy was performed to confirm the presence of —OH groups and H_2O in the crystal structures of the investigated borophosphates and phosphates. A mixture of 1.5 mg sample and 150 mg of KBr (Merck, Uvasol for IR spectroscopy) was ground and pressed with a pressure of 10×10^4 N / cm^2 to a transparent tablet. The IR spectrum was recorded on a *BRUKER* spectrometer (IFS 66 v / S; Globar (MIR), KBr, DTGS detector; program Opus / IR 3.0.3) in the wavenumber range 4000 – 400 cm^{-1}. The observed IR absorption bands (especially —OH bands) were compared with literature data from known borophosphates and phosphates.

2.3.7 Magnetic Susceptibility

The magnetic susceptibility of the phase pure compounds containing transition metals (*3d*) was measured with a *SQUID* magnetometer (Quantum Design, MPMS XL 7). A quartz tube was used as a sample holder for the powdered compounds. The blank signal of the tube was subtracted before data evaluation. The magnetic susceptibilities were measured in the temperature range 1.8 K – 400 K by applying an external magnetic field of 1 Tesla.

3 Results and Discussion

3.1 Alkali–Metal Scandium Borophosphates

This chapter is composed of two main parts. The first part starts by giving details on synthesis and crystal structure determinations of two isotypic alkali–metal (K and Rb) scandium borophosphates. Next, the anionic partial structure and thermochemical properties are briefly described. The second part of this chapter deals with synthesis and structural characterization of the first cesium scandium borophosphate, which contains a new borophosphate oligomer with boron in three– and four fold coordination. This oligomer was observed in the structural chemistry of borophosphates for the first time. Subsequently, this chapter discusses the three types of anionic partial structures observed for borophosphates containing alkali–metals (M^{I}) and trivalent metals (M^{III}) with $M^{I} : M^{III} = 1 : 1$.

3.1.1 $M^{I}Sc[BP_2O_8(OH)]$ (M^{I} = K, Rb)

3.1.1.1 Synthesis

$KSc[BP_2O_8(OH)]$: Single crystals of $KSc[BP_2O_8(OH)]$ (*Figure 3.1a*) were obtained under mild hydrothermal conditions from a mixture of 0.2500 g Sc_2O_3, 0.2769 g $K_2B_4O_7{\cdot}4H_2O$ and 1.1051 g K_2HPO_4 in the molar ratio K : Sc : B : P = 4 : 1 : 1 : 1.75. 10 ml of deionized water were added and the system was stirred at 100 ºC. In the mean time, 2 ml HCl (37 %) were added to adjust the pH value to 1. The mixture was filled into a 10 ml Teflon–lined autoclave (filling degree 30 %) and heated at 170 ºC under autogenous pressure for two weeks.

$RbSc[BP_2O_8(OH)]$: Single crystals of $RbSc[BP_2O_8(OH)]$ (*Figure 3.1b*) used for structure determinations were isolated from a sample synthesized hydrothermally by using a mixture of 0.2500 g Sc_2O_3, 1.009 g RbOH, 0.6043 g H_3BO_3 and 2.8126 g phosphoric acid (85 %) in the molar ratio Rb : Sc : B : P = 3 : 1 : 4 : 10. 10 ml of deionized water were added followed by 1 ml HCl (37 %) to adjust the pH value to 1. The mixture was placed in a 10 ml Teflon–lined autoclave (filling degree 30 %), treated under autogenous pressure at 170 ºC for 10 days, cooled down to 60 ºC and kept there for 12 hours before cooling down to ambient temperature.

The reaction products of both the compounds were filtered, washed with deionized water / acetone and dried at 60 ºC in air.

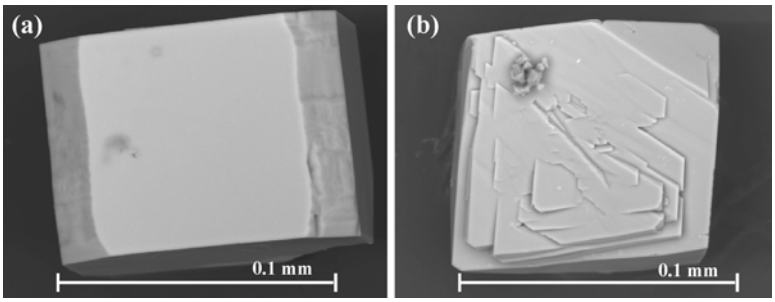

Figure 3.1: *SEM images of crystals of (a) $KSc[BP_2O_8(OH)]$ and (b) $RbSc[BP_2O_8(OH)]$*

The phase purity of the reaction products was initially checked using powder X–ray diffraction. A good fit of the observed and the calculated powder patterns (*Figure 3.2* and *Figure 3.3*) indicates that the sample is phase pure. The results of chemical analyses are given in *Table 3.1* and give a molar ratio K : Sc : B : P = 1.02 : 1.02 : 1 : 2 and Rb : Sc : B : P = 1 : 1.05 : 1.05 : 2.06 which is in accordance with the chemical formula obtained from the single–crystal structure refinements (K : Rb : Sc : B : P = 1 : 1 : 1 : 1 : 2). Except for boron and hydrogen the presence of the elements were additionally confirmed from EDX measurements. Infrared spectra were consistent with the presence of —OH groups (see *Appendix 5.4.1*).

Table 3.1: *Results of the chemical analyses of $KSc[BP_2O_8(OH)]$ and $RbSc[BP_2O_8(OH)$*

Element	Observed (e.s.d.) weight %	Calculated weight %
K	12.66(5)	12.95
Sc	14.79(9)	14.90
B	3.40(2)	3.58
P	19.56(8)	20.52
O	39.3(1)	47.71
H	0.43(1)	0.33
Rb	22.85(3)	24.55
Sc	12.64(9)	12.91
B	3.00(5)	3.10
P	17.09(2)	17.79
O	35.6(4)	41.36
H	0.39(4)	0.29

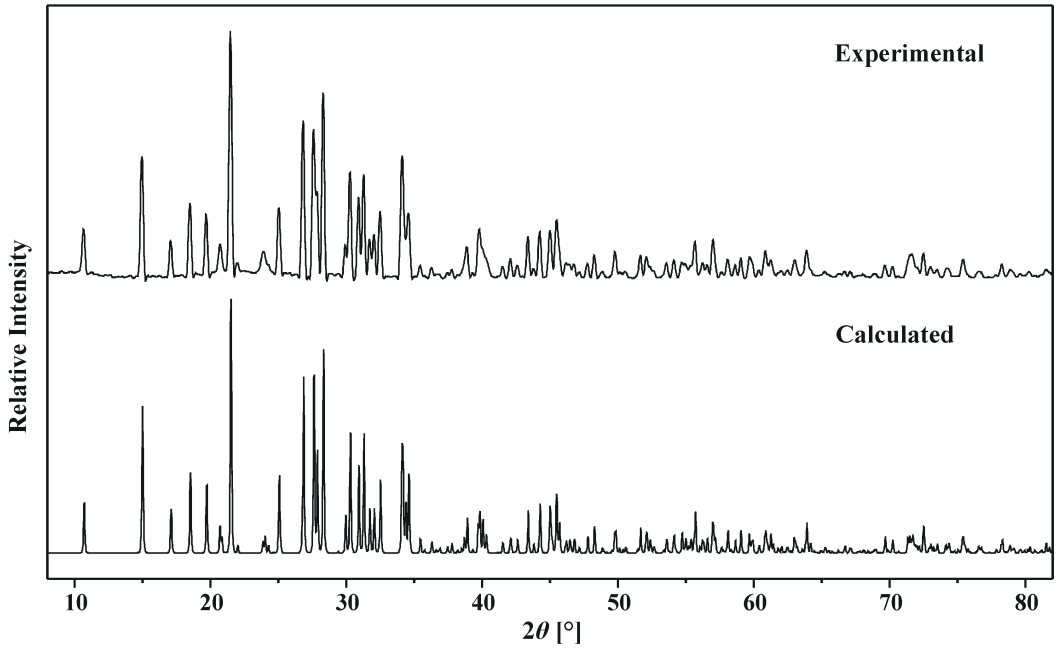

Figure 3.2: *Observed (background subtracted) and calculated powder X–ray diffraction patterns of $KSc[BP_2O_8(OH)]$ (Cu $K_{\alpha 1}$–radiation)*

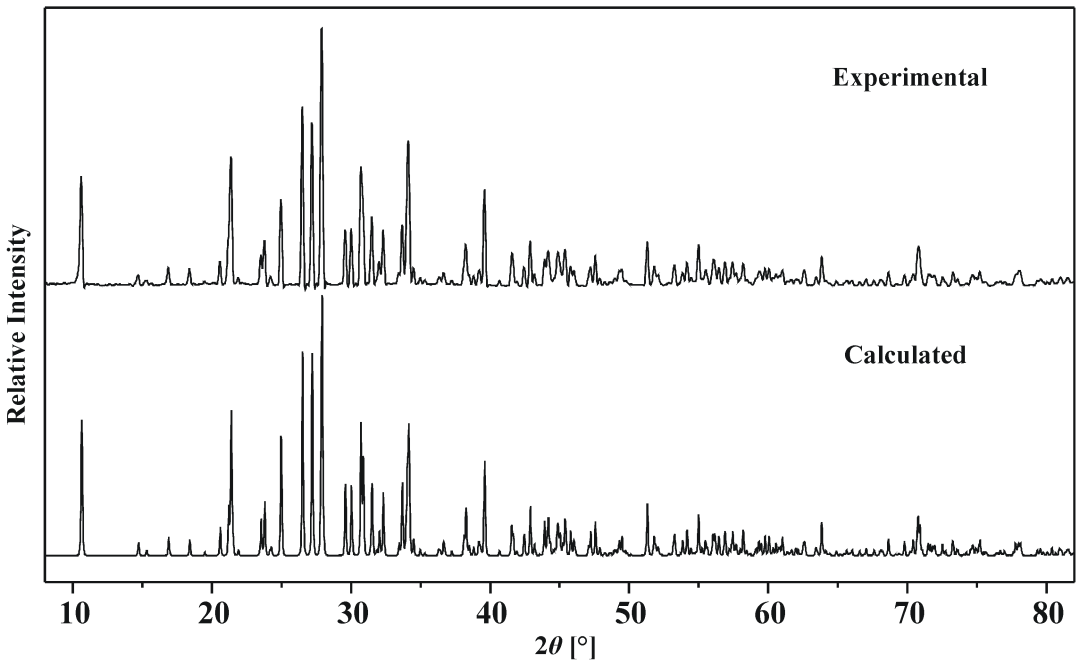

Figure 3.3: *Observed (background subtracted) and calculated powder X–ray diffraction patterns of $RbSc[BP_2O_8(OH)]$ (Cu $K_{\alpha 1}$–radiation)*

3.1.1.2 Crystal Structure Determination

Suitable colorless transparent single crystals of $KSc[BP_2O_8(OH)]$ and $RbSc[BP_2O_8(OH)]$ were selected and the X–ray data were collected. The crystal structures of $KSc[BP_2O_8(OH)]$ (triclinic, space group $P\bar{1}$ (No. 2), a = 5.2696(2) Å, b = 8.2739(8) Å, c = 8.3890(5) Å, α = 88.22(1)º, β = 79.701(6)º, γ = 86.67(1)º, Z = 2) and $RbSc[BP_2O_8(OH)]$ (triclinic, space group $P\bar{1}$ (No. 2), a = 5.3296(2) Å, b = 8.3919(8) Å, c = 8.4319(5) Å, α = 87.27(1)º, β = 80.124(6)º, γ = 86.60(1)º, Z = 2) were solved by direct methods. After anisotropic refinement of the heavier atoms, all hydrogen atoms were located from the Fourier difference maps and refined without applying any restraints. The refinement of atomic coordinates and anisotropic thermal parameters led to reliability factors R1 = 0.032 and wR2 = 0.072 ($I > 2\sigma(I)$) for $KSc[BP_2O_8(OH)]$ and R1 = 0.023 and wR2 = 0.065 ($I > 2\sigma(I)$) for $RbSc[BP_2O_8(OH)]$ considering 1918 and 2013 independent reflections, respectively.

The crystallographic data and refinement parameters for $KSc[BP_2O_8(OH)$ and $RbSc[BP_2O_8(OH)]$ are summarized in *Appendix 2* and *Appendix 3*. The final fractional atomic coordinates and equivalent / isotropic and anisotropic displacement factors for $KSc[BP_2O_8(OH)$ and $RbSc[BP_2O_8(OH)]$ are listed in *Appendix 4*, *Appendix 5*, *Appendix 6*, and *Appendix 7*, respectively.

3.1.1.3 Crystal Structure Description

The anionic partial structure of $M^{I}Sc[BP_2O_8(OH)]$ (M^{I} = K, Rb) comprises of open–branched four–membered rings (a loop–branched hexamer) $[B_2P_4O_{16}(OH)_2]^{8-}$, which is formed by alternating hydrogenborate ($(HO)BO_3$) and phosphate (PO_4) tetrahedra sharing common corners with two additionally branching phosphate tetrahedra as shown in *Figure 3.4a*.

The scandium coordination octahedra are connected to five different oligomers by sharing common oxygen corners (five corners are connected to PO_4 tetrahedra of five different oligomers and one to the $(HO)BO_3$ group) as shown in *Figure 3.4b*. The condensation of the borophosphate anions, $[B_2P_4O_{16}(OH)_2]^{8-}$, *via* $ScO_5(OH)$ coordination octahedra by sharing common corners results in an overall three–dimensional framework which contains channels extending along [100] as shown in *Figure 3.5*. The cross sections of the channels are defined by eight–membered rings consisting of two scandium coordination octahedra, four phosphate tetrahedra and two

hydrogenborate groups. The M^I ions (M^I= K, Rb) ions reside within the channels. The structure also contains six– and three–membered rings consisting of combinations of scandium coordination octahedra, phosphate tetrahedra and hydrogenborate groups.

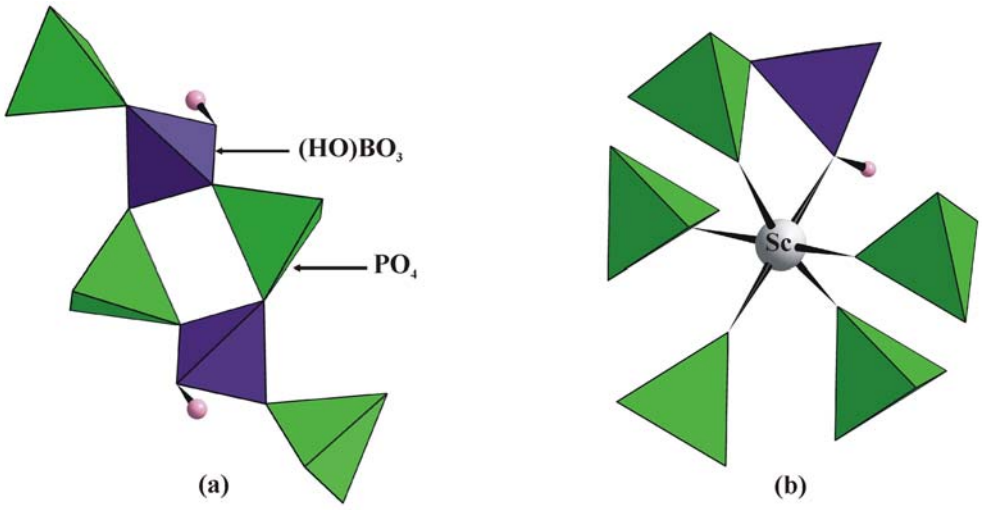

Figure 3.4: *(a) The anionic partial structure of $M^ISc[BP_2O_8(OH)]$ (M^I= K, Rb) comprises of open–branched four–membered rings $[B_2P_4O_{16}(OH)_2]^{8-}$, which are formed by alternating hydrogenborate and phosphate tetrahedra sharing common corners and two additionally branching phosphate tetrahedra, (b) Coordination octahedron of Sc^{3+} (five PO_4 tetrahedra and one $(HO)BO_3$ group) formed by the oxygen atoms of five different surrounding oligomers.*

For $KSc[BP_2O_8(OH)]$, the B—O distances and the O—B—O angles for the hydrogenborate tetrahedron range from 1.457(3) Å to 1.482(3) Å and 105.20(18)° to 112.64(19)°, respectively. For $RbSc[BP_2O_8(OH)]$, the B—O distances and the O—B—O angles cover the range from 1.458(3) Å to 1.479(3) Å and 105.39(19)° to 112.0(2)°, respectively. Similarly, the P—O distances and the O—P—O angles for $KSc[BP_2O_8(OH)]$ were found to be in the range of 1.5112(16) Å to 1.5661(17) Å and 105.36(9)° to 112.73(10)° whereas for $RbSc[BP_2O_8(OH)]$, the P—O distances and the O—P—O angels range between 1.5097(18) Å and 1.5641(19) Å, and 105.12(10)° and 113.41(11)°, respectively.

The Sc—O distances for $KSc[BP_2O_8(OH)]$ and $RbSc[BP_2O_8(OH)]$ range from 2.0556(16) Å to 2.1361(17) Å and 2.0583(18) Å to 2.1333(18) Å, respectively. A notably longer distance *d*(Sc—OH) = 2.1503(17) Å and 2.1565(19) Å is also observed for $KSc[BP_2O_8(OH)]$ and $RbSc[BP_2O_8(OH)]$. In $KSc[BP_2O_8(OH)]$, the shortest Sc···Sc distance is 5.3095(1) Å (in four–membered rings) whereas in

$RbSc[BP_2O_8(OH)]$, the shortest Sc···Sc distance is 5.2932(1) Å. Both, potassium and rubidium (residing within the eight–membered rings) are surrounded by ten oxygen atoms with the K—O and the Rb—O distances ranging from 2.8291(16) Å to 3.1181(18) Å and 2.8937(18) Å to 3.3061(19) Å, respectively. Selected bond lengths and bond angles for the compounds $M^{I}Sc[BP_2O_8(OH)]$ (M^{I}= K, Rb) are given in *Appendix 8* and *Appendix 9*, respectively.

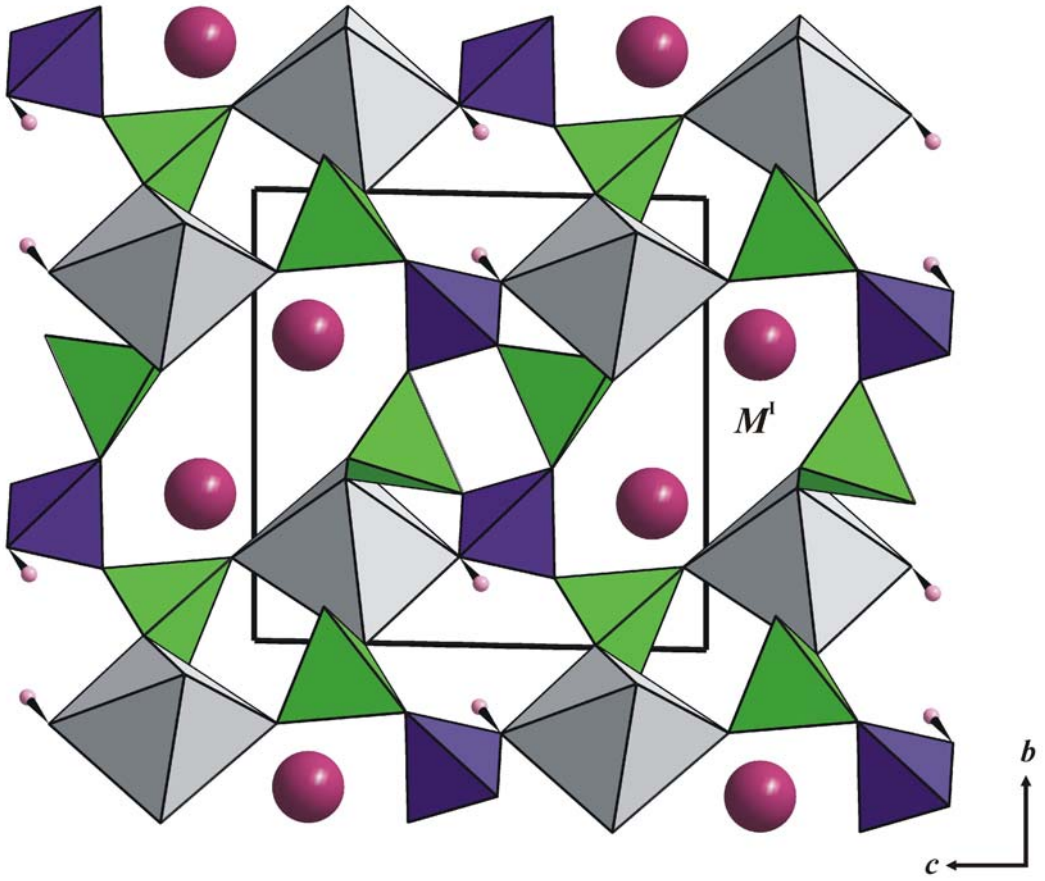

Figure 3.5: *The crystal structure of $M^{I}Sc[BP_2O_8(OH)]$ (M^{I}= K, Rb) (view along [100]): The borophosphate anions (blue $(HO)BO_3$ groups and green PO_4 tetrahedra) are interconnected by ScO_6 octahedra (light grey) to form a three–dimensional network. The (violet) M^{I} ions (M^{I}= K, Rb) are located within the channels formed by the 8–membered rings. The unit cell is outlined.*

3.1.1.4 Thermal Analysis

The thermal behavior of $M^{I}Sc[BP_2O_8(OH)]$ (M^{I}= K, Rb) was analyzed by simultaneous constant rate thermogravimetry (TG) and difference thermal analysis (DTA). The samples were heated from 30 °C at 5 K / min to 1000 °C in a continuous

argon flow in Al_2O_3 crucibles and then cooled with the same rate. No melting is observed during thermal treatment of $M^{I}Sc[BP_2O_8(OH)]$ (M^{I}= K, Rb) until 1000 °C (*Figure 3.6* and *Figure 3.7*).

The TG curve of $KSc[BP_2O_8(OH)]$ shows an overall mass loss of 4.24 wt % which is higher than that of a hypothetical mass loss of half water (2.95 wt %, calculated) molecule per formula unit. The mass loss is slow till 640 °C and then a sudden drop is observed at 700 °C. The DTA shows an endothermic peak with a maximum at 695 °C as shown in *Figure 3.6*.

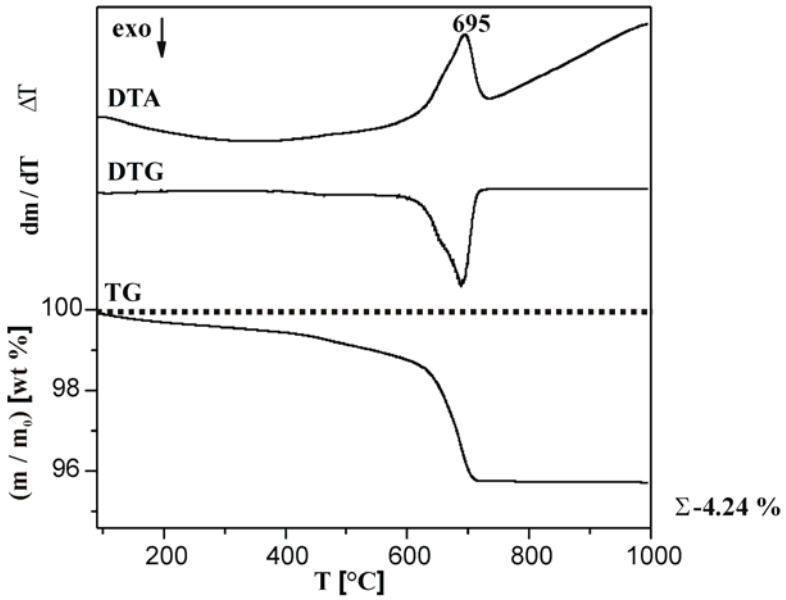

Figure 3.6: *Simultaneous thermogravimetry (TG) and difference thermal analysis (DTA) of $KSc[BP_2O_8(OH)]$ as well as the first derivative (DTG) of the TG trace. The total mass loss is given on the bottom right (calculated for ½ mol H_2O = 2.95 weight %).*

The TG curve of $RbSc[BP_2O_8(OH)]$ shows an overall mass loss of 3.07 wt % which is slightly higher compared to that of a hypothetical mass loss of half water (2.53 wt %, calculated) molecule per formula unit (*Figure 3.7*). A pronounced mass loss is observed at 710 °C. An exothermic peak in DTA was observed at 709 °C.

After DTA / TG investigations, the reaction products were subjected to powder X–ray diffraction and were compared with the reported powder patterns of compounds containing the elements Rb, Sc, P, B, and O in the respective oxides, hydroxides, phosphates, borates and borophosphates. However, the structural patterns observed could not be indexed with any of known compounds. Details of the thermal analyses

of both compounds are summarized in *Table 3.2* and the X–ray diffraction patterns after thermal treatment are shown in *Figure 3.8*.

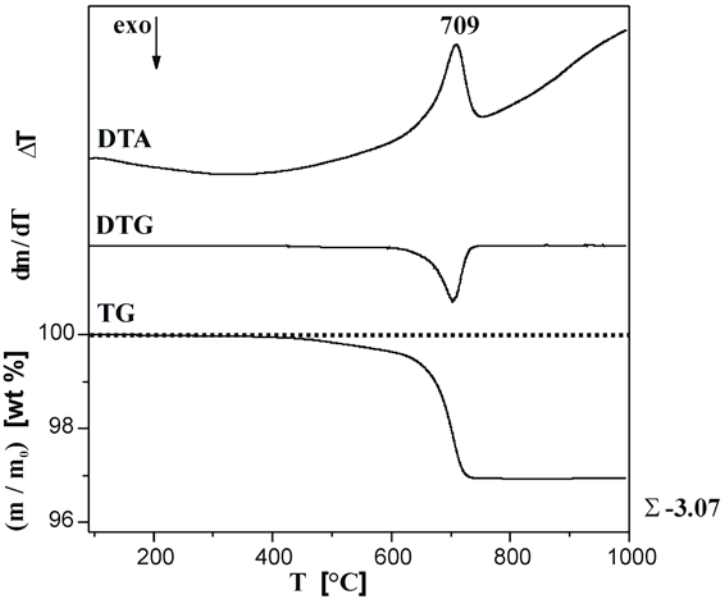

Figure 3.7: *Simultaneous thermogravimetry (TG) and difference thermal analysis (DTA) of $RbSc[BP_2O_8(OH)]$ as well as the first derivative (DTG) of the TG trace. The total mass loss is given on the bottom right (calculated for ½ mol H_2O = 2.53 weight %).*

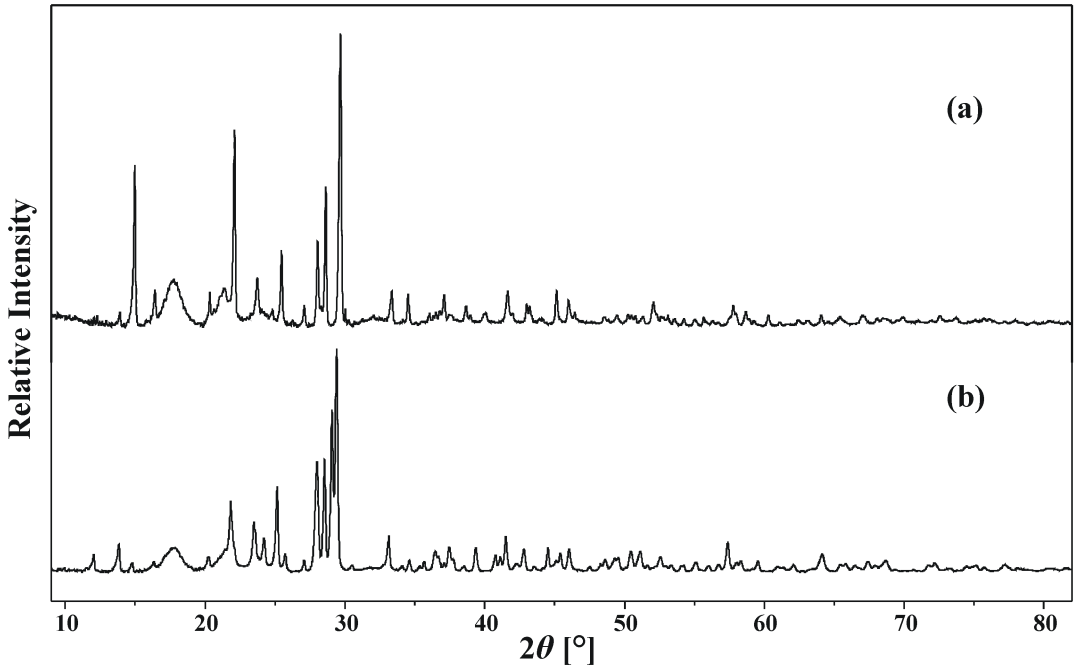

Figure 3.8: *Powder X–ray diffraction patterns of the (crystalline) reaction products after TG / DTA investigations up to 1000 °C of (a) $KSc[BP_2O_8(OH)]$ and (b) $RbSc[BP_2O_8(OH)]$ (Cu $K_{\alpha 1}$–radiation)*

Table 3.2: *Details of the thermal analyses of $KSc[BP_2O_8(OH)]$ and $RbSc[BP_2O_8(OH)]$*

Compound	Mol. Wt.[a]	Expt. mass loss[b]	Calc. mass loss[c]	Decomposition product
KSc	301.81	4.24	2.95 (½× H_2O)	Unidentified
RbSc	348.18	3.07	2.53 (½ × H_2O)	Unidentified

[a] molecular weight (g / mol), [b] experimental mass loss (wt %), [c] calculated mass loss (wt %)

3.1.2 $CsSc[B_2P_3O_{11}(OH)_3]$

3.1.2.1 Synthesis

Colorless single crystals of $CsSc[B_2P_3O_{11}(OH)_3]$ (*Figure 3.9*) used for crystal structure determinations were isolated from a sample synthesized hydrothermally from a mixture of 0.2500 g Sc_2O_3, 0.8152 g CsOH, 0.4483 g H_3BO_3 and 1.7764 g H_3PO_4 in the molar ratio Cs : Sc : B : P = 3 : 1 : 4 : 10. The pH value was adjusted to 1 by addition of 1 ml HCl (37 %). The mixture was then transferred into a 10 ml Teflon–lined autoclave (filling degree 30 %), treated under autogenous pressure at 170 ºC for 10 days, cooled down to 60 ºC and kept there for 12 hours before cooling down to ambient temperature. The reaction product was separated by filtration, washed with hot water / acetone, and dried in air at 60 ºC. The product consisted of transparent platy crystals with dimensions ranging from 0.1 to 0.4 mm.

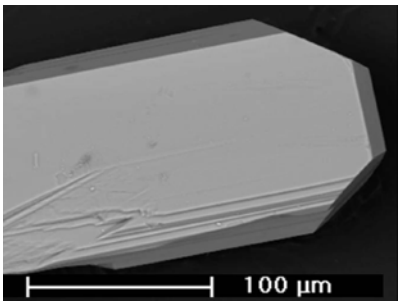

Figure 3.9: *SEM image of single crystal of $CsSc[B_2P_3O_{11}(OH)_3]$*

The results of the chemical analyses are given in *Table 3.3*. The elements cesium, scandium, boron and phosphorus were analyzed using ICP–OES, while the hot extraction method was applied for hydrogen. The molar ratio of the elements Cs : Sc : P : B = 1 : 1.03 : 2.99 : 1.98 is in accordance with the chemical formula obtained from the single–crystal structure refinements. Except for boron and hydrogen the presence of the elements were also confirmed by EDX measurements (Cs : Sc : P ≈ 1: 1: 2).

The phase purity of the reaction products was checked by powder XRD data as shown in *Figure 3.10*. The good fit between the observed and the calculated powder patterns confirms the purity of the product. The infrared spectrum was consistent with the presence of —OH groups (see *Appendix 5.4.2*).

Table 3.3: *Results of the chemical analysis of* $CsSc[B_2P_3O_{11}(OH)_3]$

Element	Observed (e.s.d.) weight %	Calculated weight %
Cs	24.68(14)	25.59
Sc	8.61(4)	8.66
B	3.99(2)	4.16
P	17.20(11)	17.89
O	33.65(31)	43.12
H	0.65(1)	0.58

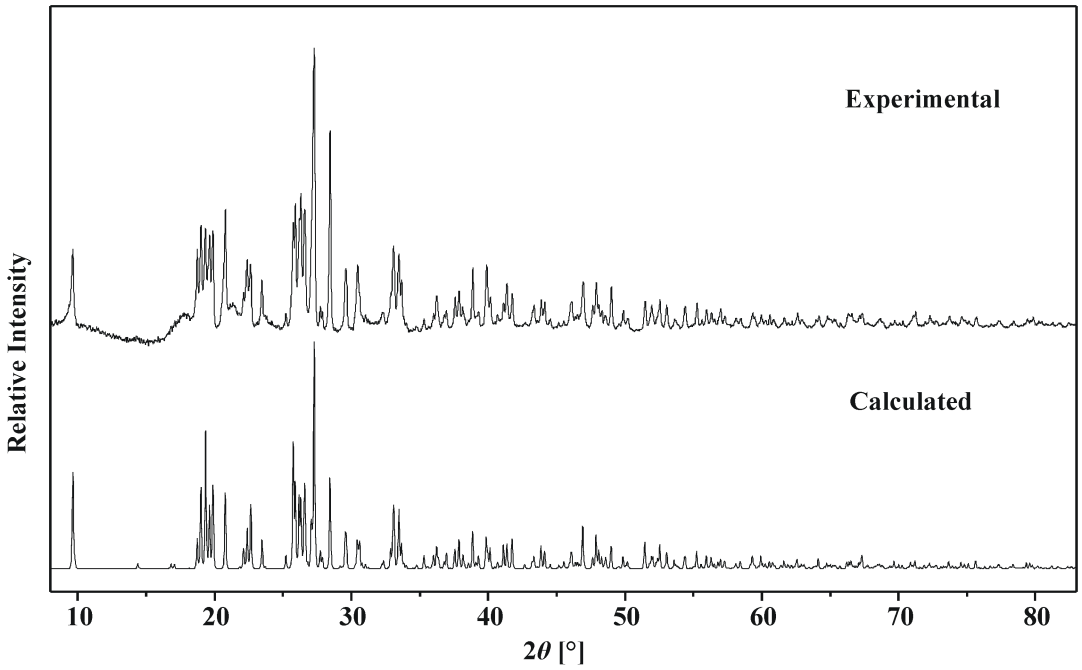

Figure 3.10: *Observed and calculated powder X–ray diffraction patterns of* $CsSc[B_2P_3O_{11}(OH)_3]$ *(Cu* $K_{\alpha 1}$*–radiation)*

3.1.2.2 Crystal Structure Determination

A suitable colorless single crystal of $CsSc[B_2P_3O_{11}(OH)_3]$ was selected. The crystal structure (orthorhombic, space group *Pnna* (No. 52), a = 13.0529(15) Å, b = 18.3403(17) Å, c = 10.3838(12) Å, Z = 8) was solved by direct methods. The positions of the hydrogen atoms could be located in the difference Fourier maps

(close to O3, O10 and O14), and their coordinates were refined as free variables. For the final anisotropic refinement step the isotropic displacement parameters of the hydrogen atoms were restrained to 1.2 U_{iso}(O). The refinement of the atomic coordinates and anisotropic thermal parameters led to reliability factors R1 = 0.044 and wR2 = 0.11 ($I > 2\sigma(I)$) considering 1676 independent reflections.

Crystallographic data and refinement parameters are summarized in *Appendix 10.* The final fractional atomic coordinates and equivalent / isotropic and anisotropic displacement factors are enlisted in *Appendix 11* and *Appendix 12.*

3.1.2.3 Crystal Structure Description

The crystal structure of $CsSc[B_2P_3O_{11}(OH)_3]$ contains a novel complex anion, $[B_2P_3O_{11}(OH)_3]^{4-}$, which is built of a central borate tetrahedron (B1) open–branched by two $(HO)PO_3$ tetrahedra (P1 and P2) and loop–branched by one PO_4 (P3) tetrahedron and a trigonal–planar $(HO)BO_2$ group (B2) by sharing common apices as shown in *Figure 3.11*.

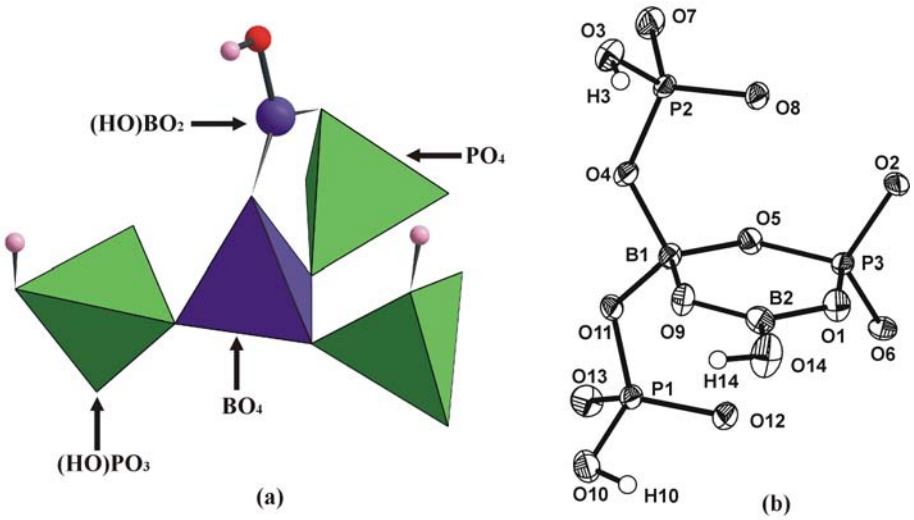

Figure 3.11: *Borophosphate complex $[B_2P_3O_{11}(OH)_3]^{4-}$ in the crystal structure of $CsSc[B_2P_3O_{11}(OH)_3]$ containing a central BO_4 tetrahedron (B1) open–branched by two $(HO)PO_3$ tetrahedra (P1 and P2) and loop–branched by one PO_4 tetrahedron (P3) and a trigonal–planar $(HO)BO_2$ (B2) group by sharing common apexes (a) polyhedral representation (b) ORTEP presentation (displacement ellipsoids are drawn at the 50% probability level).*

The oligomeric units are interlinked *via* common O corners of ScO_6 octahedra. By this, each scandium octahedron (ScO_6) is surrounded by six phosphate tetrahedra belonging to four different borophosphate oligomers (*Figure 3.12a*). As shown in *Figure 3.12b*, two borophosphate anions are connected to four ScO_6 octahedra, resulting in the formation of a cavity. A detailed analysis of this cavity (*Figure 3.13*) reveals similarities to a common secondary building unit (SBU) encountered in zeolites [100], and which can be described as a hexagonal prism (6–6 in the zeolite nomenclature). The borophosphate oligomers together with the ScO_6 octahedra are condensed to form layers running parallel (001), as shown in *Figure 3.14*. The Cs cations are located in between the layers.

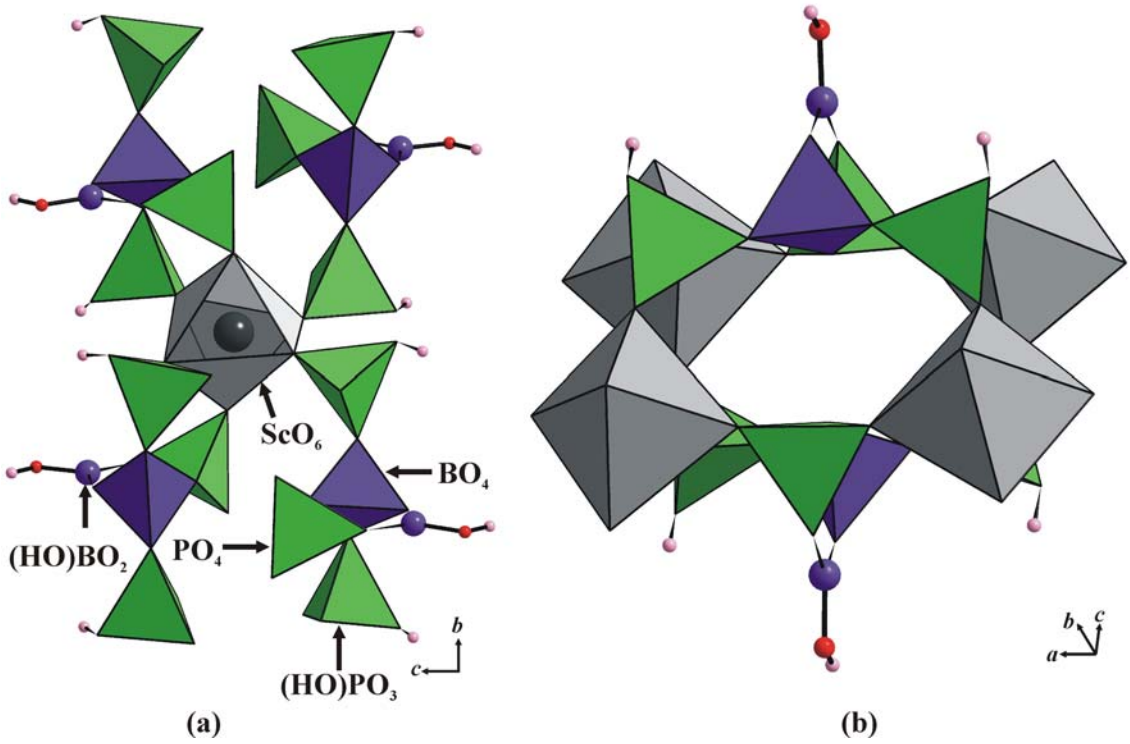

Figure 3.12: *(a) Linkage of six $(HO)PO_3$ tetrahedra of four oligomers to one ScO_6 octahedron by sharing common O – corners (scandium is shown as black sphere). (b) Cavity formed by four ScO_6 octahedra and two borophosphate anions $[B_2P_3O_{11}(OH)_3]^{4-}$ in the crystal structure of $CsSc[B_2P_3O_{11}(OH)_3]$.*

All of the atoms of the oligomeric unit represent independent crystallographic sites. The bondings within the oligomeric unit are listed in *Table 3.4*. The lengths of the bridging B—O bonds (B—O_{br}) for the borate tetrahedron (B1) range from 1.457(1) to 1.470(6) Å. In the case of the trigonal-planar boron unit, the bridging B—O bonds

(B— O_{br}) are notably shorter, with 1.361(8) and 1.397(1) Å. The shortest B—O bond is observed for the terminal B—OH bond, with 1.342(1) Å.

Table 3.4: *P—O and B—O bonds in $CsSc[B_2P_3O_{11}(OH)_3]$, standard deviations in units of last decimal in brackets ($O_{(t)}$ denotes terminal, $O_{(br)}$ bridging and $O_{(OH)}$ hydroxyl oxygen atoms)*

Atom–contact		d/Å	Atom–contact		d/Å
P1	—$O13_{(t)}$	1.490(4)	P3	—$O2_{(t)}$	1.497(4)
	—$O12_{(t)}$	1.498(4)		—$O6_{(t)}$	1.503(4)
	—$O11_{(br)}$	1.555(3)		—$O5_{(br)}$	1.540(4)
	—$O10_{(OH)}$	1.577(5)		—$O1_{(br)}$	1.576(6)
P2	—$O7_{(t)}$	1.482(6)	B1	—$O5_{(br)}$	1.457(1)
	—$O8_{(t)}$	1.522(4)		—$O11_{(br)}$	1.462(6)
	—$O4_{(br)}$	1.548(4)		—$O9_{(br)}$	1.466(1)
	—$O3_{(OH)}$	1.562(5)		—$O4_{(br)}$	1.470(6)
			B2	—$O14_{(OH)}$	1.342(1)
				—$O9_{(br)}$	1.361(8)
				—$O1_{(br)}$	1.397(1)

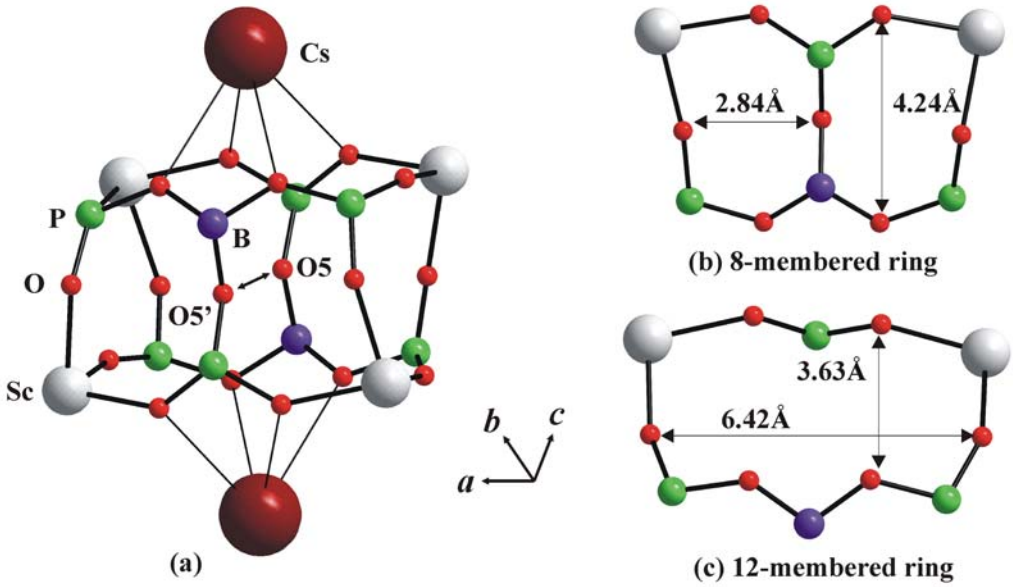

Figure 3.13: *(a) Details of the cage formed by six eight–membered rings (according to zeolite structure representation) and two twelve–membered rings with d(O5···O5') = 3.25 Å in the crystal structure of $CsSc[B_2P_3O_{11}(OH)_3]$, (b) eight–membered rings viewed from the side of (a) and (c) twelve–membered ring viewed from the top of (a).*

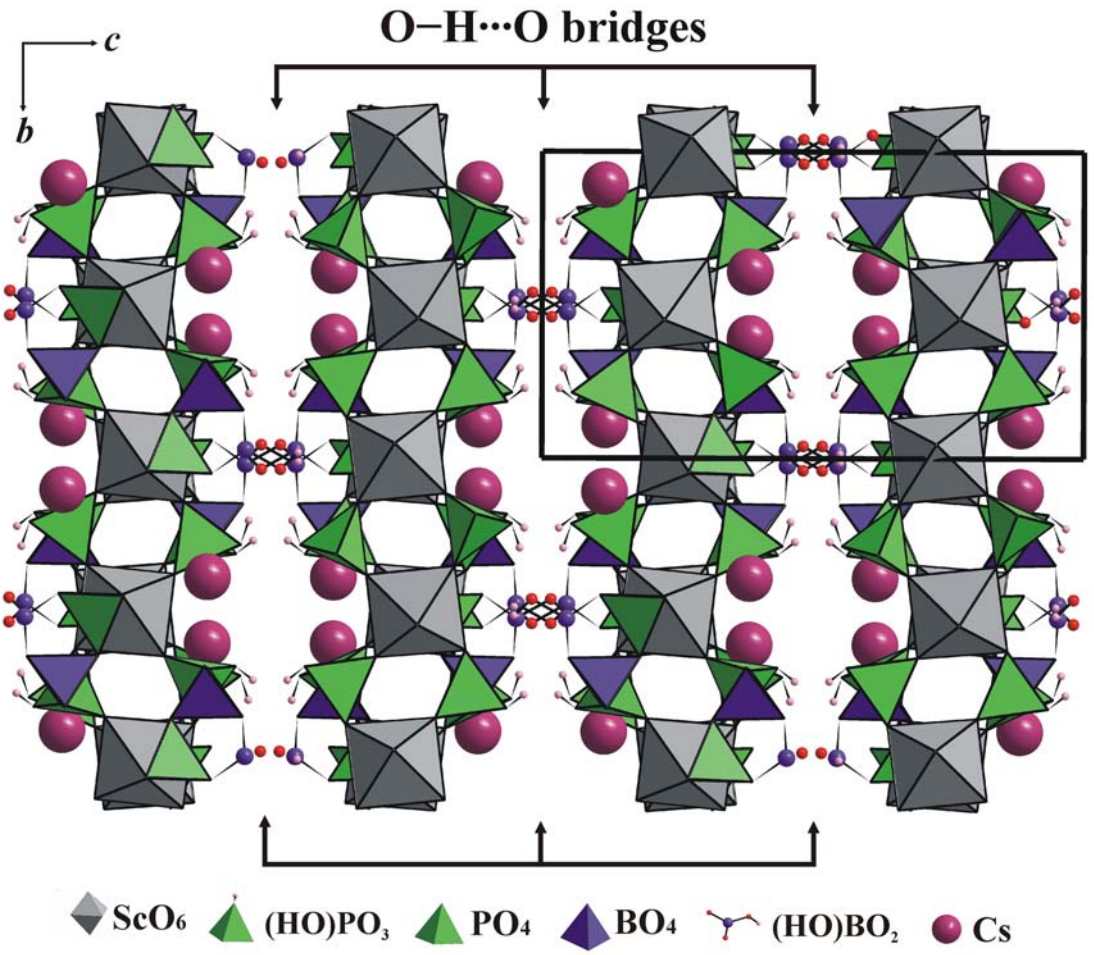

Figure 3.14: *Crystal structure of $CsSc[B_2P_3O_{11}(OH)_3]$ (view along [100]): layers consisting of interconnected borophosphate anions and ScO_6 octahedra are linked via hydrogen bonds. The Cs^+ ions (large violet spheres) are located in between the layers close to their borders. The unit cell is outlined.*

The shortest P—O distances are found for the terminal P—O bonds (P—O_t) in the phosphate tetrahedron (P3) and in the hydrogen phosphate groups (P1 and P2), varying from 1.4821(6) to 1.522(4) Å. The bridging P—O bonds (P—O_{br}) are in the range from 1.540(4) to 1.576(6) Å, and the two P—OH (P1 and P2) bond lengths are 1.562(5) and 1.577(5) Å, respectively. This is in accordance with the trend observed for pure phosphates [101]. The lengths of the Sc—O bonds range from 2.058(5) to 2.166(5) Å. The shortest interatomic distance within the cavity is 3.25 Å (O5···O5'). The Cs ions are situated above and below the six–membered rings with four contacts to neighbouring O atoms (d(Cs—O) = 3.181(5) – 3.334(4) Å) of the rings. Hydrogen bonds O—H···O are formed between the layers (*Figure 3.14*).

The protons H3, H10 and H14 (*Figure 3.15*) are attached to O3, O10 and O14 (with distances *d*(O3—H3) = 0.755(1) Å, *d*(O10—H10) = 0.865(1) Å and *d*(O14—H14) = 0.821(1) Å, and are involved in hydrogen bridges (O3—H3···O9 with *d*(O3···O9) = 2.754(1) Å, O10—H10···O14 with *d*(O10···O14) = 2.657(1) Å) and O14—H14···O8 with *d*(O14···O8) = 2.836(1) Å). Selected bond distances and bong angles are listed in *Appendix 13*.

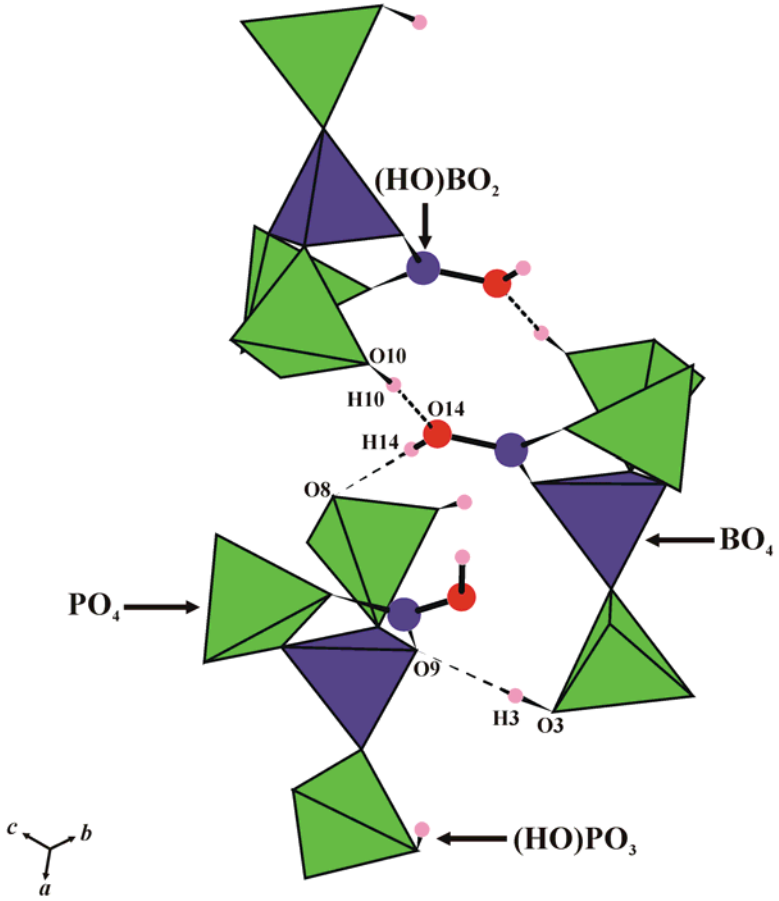

Figure 3.15: *Hydrogen bonding in the crystal structure of $CsSc[B_2P_3O_{11}(OH)_3]$. The protons H3, H10 and H14 (pink spheres) are attached to O3, O10 and O14 (red spheres) with distances d(O3—H3) = 0.755(1) Å, d(O10—H10) = 0.865(1) Å and d(O14—H14) = 0.821(1) Å, and are involved in hydrogen bridges (O3—H3···O9 with d(O3···O9) = 2.754(1) Å, O10—H10···O14 with d(O10···O14) = 2.657(1) Å) and O14—H14···O8 with d(O14···O8) = 2.836(1) Å).*

3.1.2.4 Thermal Analysis

The TG curve of $CsSc[B_2P_3O_{11}(OH)_3]$ (*Figure 3.16*, left) reveals a stepwise mass loss during heating, which is completed at about 700 °C with an overall mass loss of 6.3 wt %. Assuming that only water is released under the chosen experimental conditions, a value of 5.2 wt % (1½ mol of H_2O per formula unit) is expected. During heating, a broad structured endothermic effect is observed with maxima (786, 856, and 996 °C) coinciding with the individual steps of the mass loss. At 840 °C, an exothermic effect occurs without a change in the sample weight. For examination of the rehydration behavior (*Figure 3.16*, right), a new sample was heated under the same conditions up to 310 °C. The obtained product was then exposed to atmospheric moisture for several days and reheated to 1000 °C in a continuous argon flow. A sample that was heated to approximately the end of the second TG step at about 310 °C did not show any rehydration behavior.

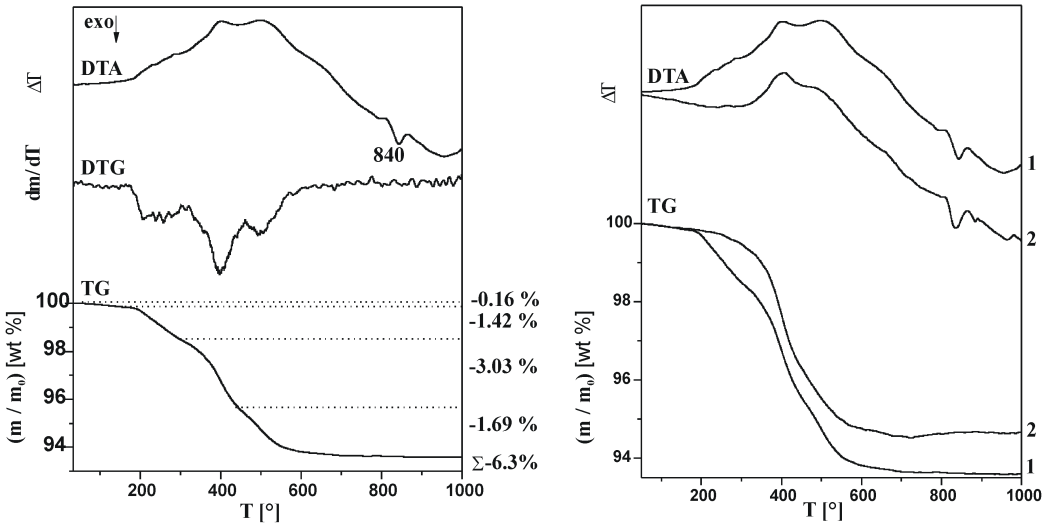

Figure 3.16: *Simultaneous thermogravimetry (TG) and difference thermal analysis (DTA) of $CsSc[B_2P_3O_{11}(OH)_3]$ as well as the first derivative (DTG) of the TG trace. The measured mass loss (weight %) of the four steps are given on the right (1 mol H_2O = 5.2 weight %) (Figure left). Comparison of simultaneous thermogravimetry (TG) and difference thermal analysis (DTA) traces of $CsSc[B_2P_3O_{11}(OH)_3]$ (1) and thermally pretreated $CsSc[B_2P_3O_{11}(OH)_3]$ (2). This sample was obtained by thermal treatment at 310 ºC followed by exposure to atmospheric moisture for several days (Figure right).*

The powder XRD pattern of the decomposition product (*Figure 3.17*) shows sharp reflections which could not be assigned to any known crystalline phase or phase mixture. The X–ray powder diffraction pattern could not be indexed after thermal treatment at 1000 °C.

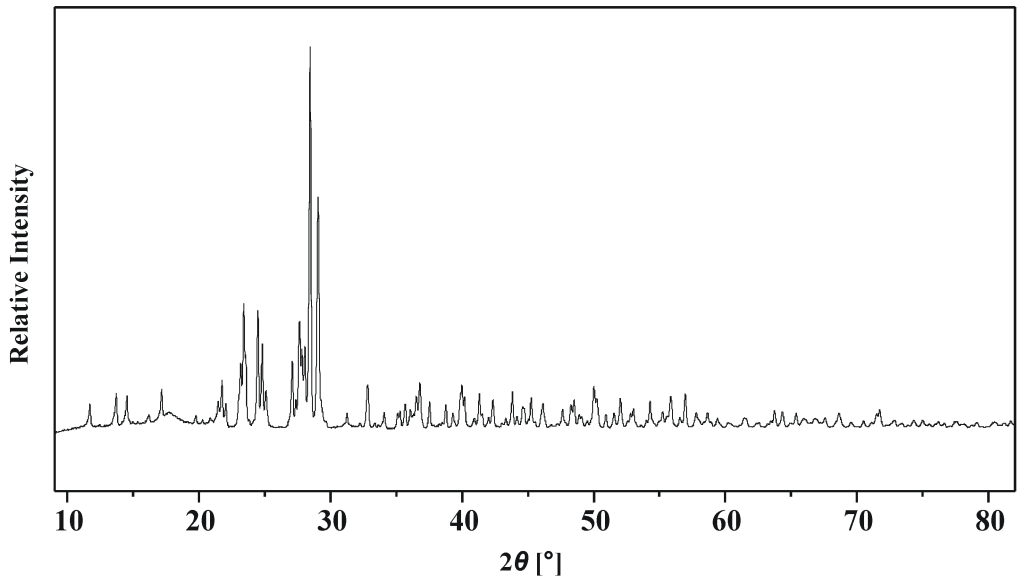

Figure 3.17: *Powder X–ray diffraction pattern of the decomposition product of* $CsSc[B_2P_3O_{11}(OH)_3]$ *heated up to 1000 °C (Cu* $K_{\alpha 1}$*–radiation)*

3.1.3 Discussion

In the course of our systematic investigations on the existence of alkali–metal scandium borophosphates, three different compounds were synthesized and structurally characterized by single–crystal XRD data: $KSc[BP_2O_8(OH)]$, $RbSc[BP_2O_8(OH)]$, and $CsSc[B_2P_3O_{11}(OH)_3]$. The borophosphates $KSc[BP_2O_8(OH)]$ and $RbSc[BP_2O_8(OH)]$ were found to be isotypic to $KFe^{III}[BP_2O_8(OH)]$ (triclinic, $P\bar{1}$) [48], which belongs to the group of borophosphates with B : P = 1 : 2. On the other hand, $CsSc[B_2P_3O_{11}(OH)_3]$ exhibits a new crystal structure with B : P = 2 : 3, although the molar ratio of the educts and the reaction conditions used for the preparation of all three compounds were kept invariant. Attempts to synthesize lithium– and sodium–scandium borophosphates ended up with respective phosphates ($Li_2Sc[(PO_4)(HPO_4)$, $NaSc(HPO_4)_2$) only.

With the successful synthesis of the scandium compounds, the group of borophosphates containing M^I as well as M^{III} (M^I = Na, K, Rb, Cs; M^{III} = Al, Ga, V,

Fe, Sc, In) is now represented by a total number of 22 (M^{I} : M^{III} = 1 : 1) members which are ordered in *Figure 3.18* according to their cationic radii.

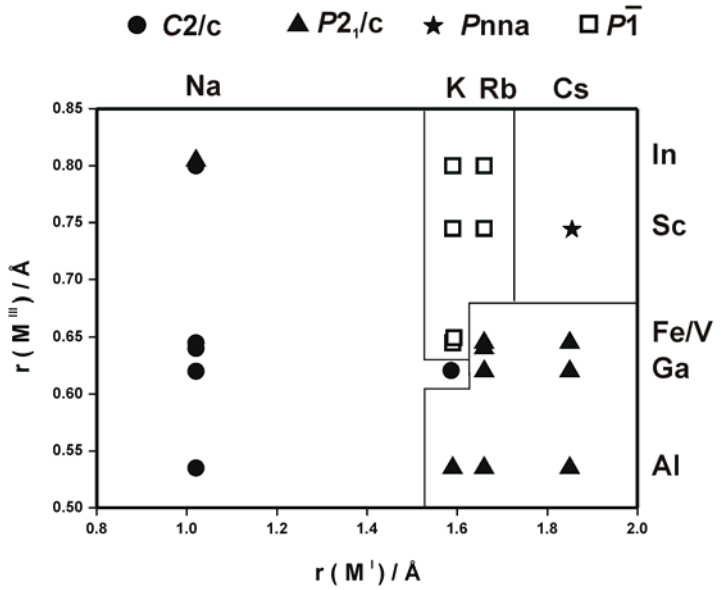

Figure 3.18: *Structure map for the known $M^{I}M^{III}$ borophosphates (M^{I} : M^{III} = 1 : 1) with general formulas $M^{I}M^{III}[BP_2O_7(OH)_3]$ (SPG: C2/c), $M^{I}M^{III}[BP_2O_8(OH)]$ (SPG: $P\bar{1}$), $M^{I}M^{III}[BP_2O_8(OH)]$ (SPG: $P2_1/c$) and $CsSc[B_2P_3O_{11}(OH)_3]$(SPG: Pnna).*

Three structure types were already observed for the known $M^{I}M^{III}$ borophosphates, namely, $M^{I}M^{III}[BP_2O_8(OH)]$ ($P2_1/c$; *Figure 3.19c*) [56, 64, 65, 102-106], $M^{I}M^{II}[BP_2O_7(OH)_3]$ ($C2/c$; *Figure 3.19a*) [48, 49, 105-108], and $M^{I}M^{III}[BP_2O_8(OH)]$ ($P\bar{1}$; *Figure 3.19b*) [48, 109, 110], which all consist of the same FBB in form of the borophosphate trimer $[BP_2O_{10}]$ (*Figure 3.19a*). In the crystal structure of $M^{I}M^{III}[BP_2O_7(OH)_3]$, the anionic partial structure (*Figure 3.19a*) consists of an unbranched tetrahedral triple $[BP_2O_7(OH)_3]^{4-}$, built of a dihydrogen borate tetrahedron sharing common corners with two hydrogenphosphate tetrahedra. This unit is present in all members containing sodium (*Figure 3.18*). Condensation of such units accompanied by the loss of one molecule of H_2O per unit can lead to the formation of either open–branched four–membered rings $[B_2P_4O_{16}(OH)_2]^{8-}$ (*Figure 3.19b*) or open–branched single chains $^1_\infty[BP_2O_8(OH)]^{4-}$ (*Figure 3.19c*). Examples with a higher degree of condensation are unknown for the combination $M^{I}M^{III}$ so far but can be realized by using the combinations $M^{I}M^{II}$ [69] $M^{II}_{0.5}$ M^{II}, or M^{III} [67, 68, 111] and result in a helical anion $^1_\infty[BP_2O_8]^{3-}$. For all of the $M^{I}M^{III}$ borophosphates

under consideration, the coordination number of boron and phosphorus is 4 (*Figure 3.19*). For the $CsSc[B_2P_3O_{11}(OH)_3]$ compound (also with B : P < 1), a completely different anionic partial structure is observed containing boron in the coordination numbers 3 and 4, respectively. Up to now, the occurrence of mixed coordination for boron was only reported for compounds with B : P > 1 containing complex chain anions [112-114] and the trigonal borate unit exclusively bonded to borate species.

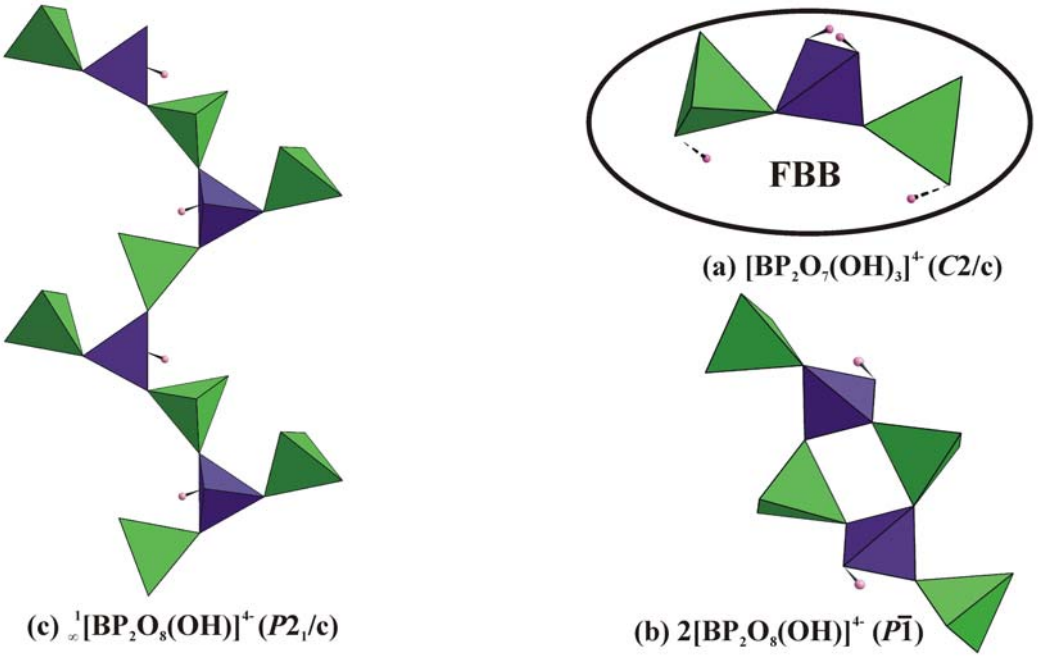

Figure 3.19: *Anionic partial borophosphate structures in compounds ($M^I : M^{III}$ = 1 : 1) with element combinations M^I (Na, K, Rb, and Cs) and M^{III} (Al, Ga, In, V, and Fe): (a) $M^IM^{III}[BP_2O_7(OH)_3]$ (SPG: C2/c); (b) $M^IM^{III}[BP_2O_8(OH)]$ (SPG: P$\bar{1}$); (c) $M^IM^{III}[BP_2O_8(OH)]$ (SPG: P2$_1$/c). All three anionic partial structures are built up from the common FBB $[BP_2O_7(OH)_3]^{3-}$.*

Considering borophosphates containing triangular borate units with B : P < 1, only four members are reported so far: $Co_5[BPO_6][PO_4]_2$ [34], $Cr_2[BP_3O_{12}]$ [15], $V_2[BP_3O_{12}]$ [81] prepared *via* a solid–state route and the templated compound $([C_6H_{12}N_2]VO(PO_3(OH)_4(B_3O_3OH)\cdot 4H_2O)$ ($C_6H_{12}N_2$) = DABCO) (*Figure 3.20*) [50]. In $Co[BPO_6][PO_4]_2$ (SPG: *P*2$_1$/*c*) [34], the anionic partial structure (*Figure 3.20a*) consists of a trigonal–planar borate unit that is connected to one phosphate tetrahedron, whereas in $Cr_2[BP_3O_{12}]$ (SPG: *P*3) [15] and $V_2[BP_3O_{12}]$ (SPG: *P*6$_3$/*m*) [81], the anionic partial structure (*Figure 3.20b*) consists of a trigonal–planar borate unit that is connected to three phosphate tetrahedra.

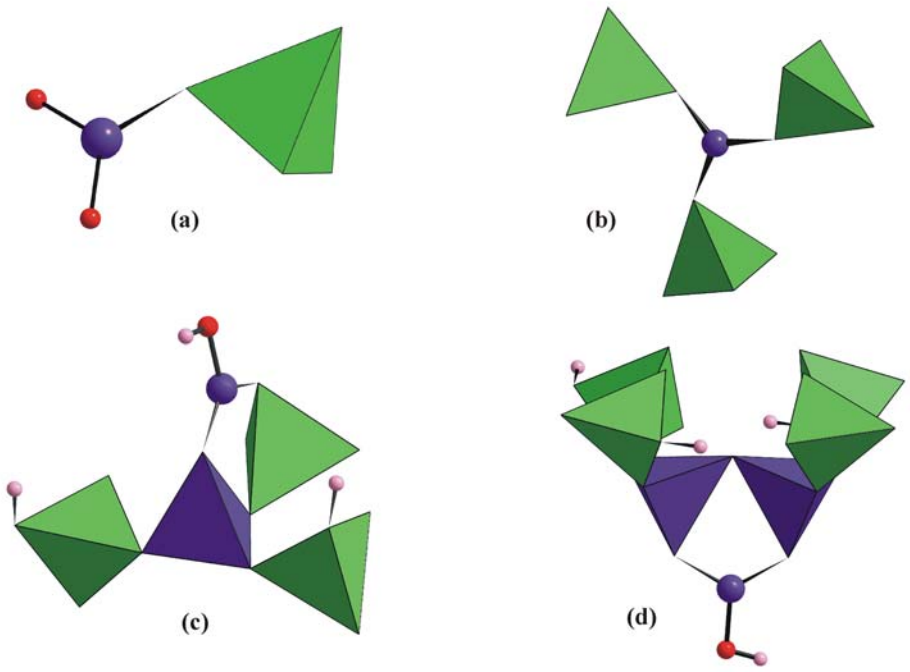

Figure 3.20: *Borophosphate complexes (B : P < 1) containing boron with coordination numbers 3 and 4: (a) $Co_5[BPO_6][PO_4]_2$ [34] (one PO_4 tetrahedron and one BO_3 group); (b) $Cr_2[BP_3O_{12}]$ [15] and $V_2[BP_3O_{12}]$ [81] (three PO_4 tetrahedra and one BO_3 group); (c) $CsSc[B_2P_3O_{11}(OH)_3]$ (two $(HO)PO_3$ groups, one PO_4 tetrahedra, one BO_4 tetrahedron and one $(HO)BO_2$ group); (d) $[C_6H_{12}N_2]_2VO(PO_3(OH)_4(B_3O_3OH)\cdot 4H_2O$ [50] (four $(HO)PO_3$ tetrahedra, two BO_4 tetrahedra and one $(HO)BO_2$ group).*

The only known example for an oligomeric templated borophosphate containing boron in coordination 3 and 4, respectively, is given by $[C_6H_{12}N_2]_2VO(PO_3(OH)_4(B_3O_3OH)\cdot 4H_2O$ ($P2_1/c$) [50] containing an oligomer built of a trimeric hydrogenborate group $(HO)B_3O_3$ and four hydrogenphosphate groups $((HO)PO_3)_4$ (*Figure 3.20d*). The trigonal–planar borate unit in this oligomer is connected to two borate tetrahedra, which are further connected to four hydrogenphosphate groups. In the crystal structure of $CsSc[B_2P_3O_{11}(OH)_3]$, the trigonal–planar borate unit is attached to one borate and one phosphate tetrahedron (*Figure 3.20c*). This arrangement of polyhedra was already predicted for borates but never observed [1, 2]. Considering the structural relationship between indium (III) and scandium (III) (*Figure 3.18*), several attempts has already been made to prepare a corresponding cesium indium borophosphate containing the novel oligomer, but despite all efforts, they were unsuccessful till now.

3.2 Alkali–Metal Scandium Hydrogenphosphates

This chapter extends the results discussed in the previous chapter. The main content of this chapter involves the synthesis, crystal structure and properties of five new alkali–metal scandium hydrogenphosphates which were prepared during the extensive study of their respective borophosphates. It also describes the principles and structural similarities between these five frameworks which contain the same building units and linkages.

3.2.1 $Li_2Sc[(PO_4)(HPO_4)]$ and $M^{I}Sc(HPO_4)_2$ (M^{I} = K, Rb, Cs, NH_4)

3.2.1.1 Synthesis

Single crystals for crystal structure determinations of $Li_2Sc[(PO_4)(HPO_4)]$, $KSc(HPO_4)_2$ and the isotypic $M^{I}Sc(HPO_4)_2$ (M^{I} = Rb, Cs, NH_4) were obtained under mild hydrothermal conditions.

$Li_2Sc[(PO_4)(HPO_4)]$: Single crystals of $Li_2Sc[(PO_4)(HPO_4)]$ (*Figure 3.21a*) were synthesized from 0.5000 g Sc_2O_3 and 2.2600 g LiH_2PO_4 in the molar ratio Li : Sc : P = 6 : 1 : 6. The pH was adjusted to 1 by addition of 1.5 ml HCl (37 %). The reaction mixture was transferred into a 10 ml Teflon autoclave (filling degree 30 %) and was heated under autogenous pressure at 170 ºC for two weeks.

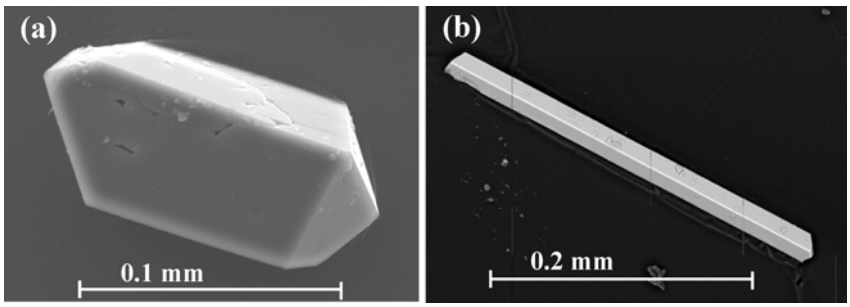

Figure 3.21: *SEM images of single crystals of (a) $Li_2Sc[(PO_4)(HPO_4)]$ (b) $KSc(HPO_4)_2$*

$KSc(HPO_4)_2$: Single crystals $KSc(HPO_4)_2$ (*Figure 3.21b*) were synthesized from acidic suspensions of 0.5000 g Sc_2O_3, 1.2629 g K_2HPO_4 and 2.5079 g H_3PO_4 in the molar ratio K : Sc : P = 2 : 1 : 6. The reaction mixture was homogenized in 10 ml water, the pH was adjusted to 1 by addition of 1 ml HCl (37 %) and the system was heated at 80 ºC for two hours. The reaction mixture was then filled into a 20 ml

Teflon autoclave (filling degree 45 %) and heated under autogenous pressure at 170 ºC for 8 days.

$RbSc(HPO_4)_2$: Single crystals of $RbSc(HPO_4)_2$ (*Figure 3.22a*) were prepared from a mixture of 0.5000 g Sc_2O_3, 0.3715 g RbOH, and 2.5079 g H_3PO_4. The mixture was heated at 80 ºC in deionized water (10 ml) with continuous stirring until the components were completely dissolved (molar ratio Sc : Rb : P = 1 : 1 : 6). The clear solution (pH = 1) was transferred into a Teflon autoclave (internal volume 20 ml) with filling degree 40 % and heated at 170 ºC for 7 days.

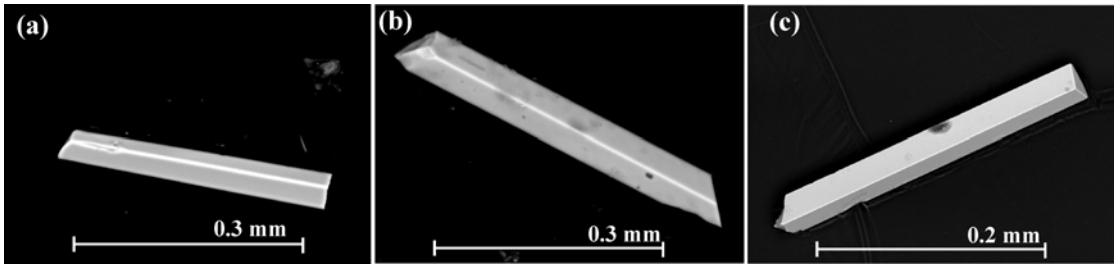

Figure 3.22: *SEM images of single crystals of isotypic series (a) $RbSC(HPO_4)_2$ (b) $CsSc(HPO_4)_2$ and (c) $NH_4Sc(HPO_4)_2$*

$CsSc(HPO_4)_2$: Single crystals of $CsSc(HPO_4)_2$ (*Figure 3.22b*) were yielded according to the molar ratio of 1 : 1 : 6 (Sc : Cs : P). A mixture of 0.5000 g Sc_2O_3, 0.5435 g CsOH and 2.5079 g H_3PO_4 was homogenized in 10 ml of water. The suspension was concentrated by heating at 80 ºC for two hours. The acidic mixture was then transferred into a 10 ml Teflon autoclave (filling degree 40 %) and heated under autogenous pressure at 170 ºC for 7 days.

$NH_4Sc(HPO_4)_2$: Single crystals of $NH_4Sc(HPO_4)_2$ (*Figure 3.22c*) were synthesized from 0.5002 g Sc_2O_3, 0.2241 g H_3BO_3 and 3.8302 g $(NH_4)_2HPO_4$ in the molar ratio NH_4 : Sc : P = 1 : 1 : 8. The pH value was adjusted to 1 by the addition of 3 ml HCl (37 %). The mixture was then filled into a 10 ml autoclave (filling degree 30 %) and heated under autogenous pressure at 170 ºC for 24 days.

In all cases, the reaction products contained crystals, which were separated by filtration, washed with hot water, filtered and washed again with acetone before they were dried at 60 ºC in air. The obtained transparent and colorless elongated prismatic crystals were up to 0.3 mm in length as shown in *Figure 3.21* and *Figure 3.22*. The phase purity of the reaction products was initially checked using X–ray powder

diffraction (*Figure 3.23* to *Figure 3.27*). The data fit well to the calculated powder patterns obtained from single crystal measurements.

The results of the chemical analyses are given in *Table 3.5*. The elements lithium, potassium, rubidium, cesium, scandium, boron and phosphorus were analyzed using ICP–OES, while the hot extraction method was applied for nitrogen and hydrogen. The molar ratios of the products were determined as Li : Sc : P = 1 : 1.5 : 2, K : Sc : P = 1 : 1.04 : 2.14, Rb : Sc : P = 1 : 1.12 : 2.18, Cs : Sc : P = 1 : 1.08 : 2.11 and N : Sc : P = 1 : 1 : 2.02. The values are in accordance with the chemical formulae obtained from the single–crystal structure refinements. Except for boron, hydrogen and nitrogen the presence of the elements were also confirmed by EDX measurements. The observed broad infra red absorption band at 3430 – 3564 cm^{-1} clearly indicates the presence of O—H groups (*Appendix 5.4.3*)

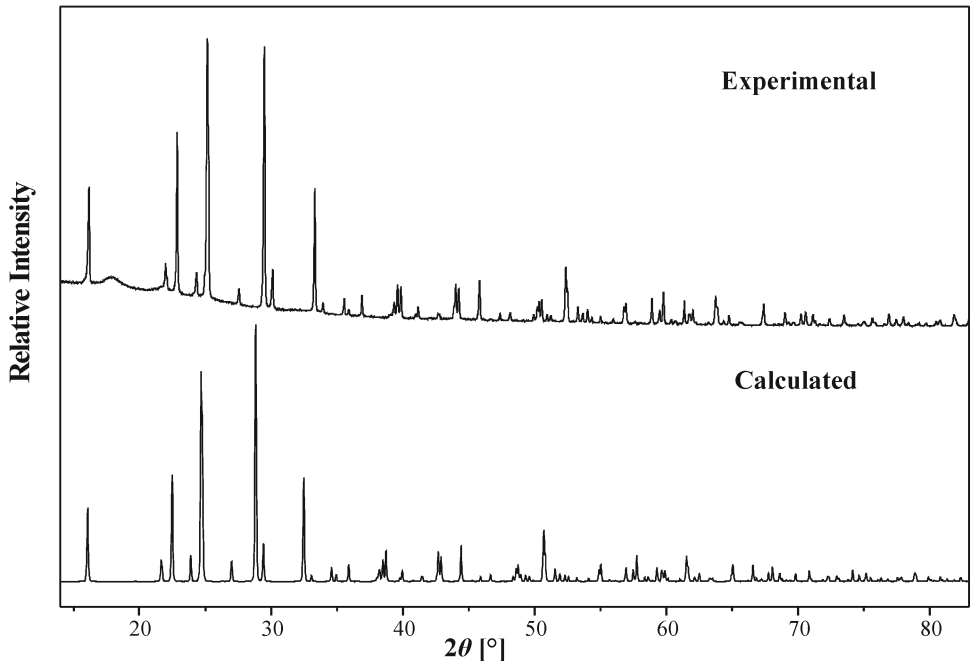

Figure 3.23: *Observed and calculated powder X–ray diffraction patterns of* $Li_2Sc[(PO_4)(HPO_4)]$ *(Cu* $K_{\alpha 1}$*–radiation)*

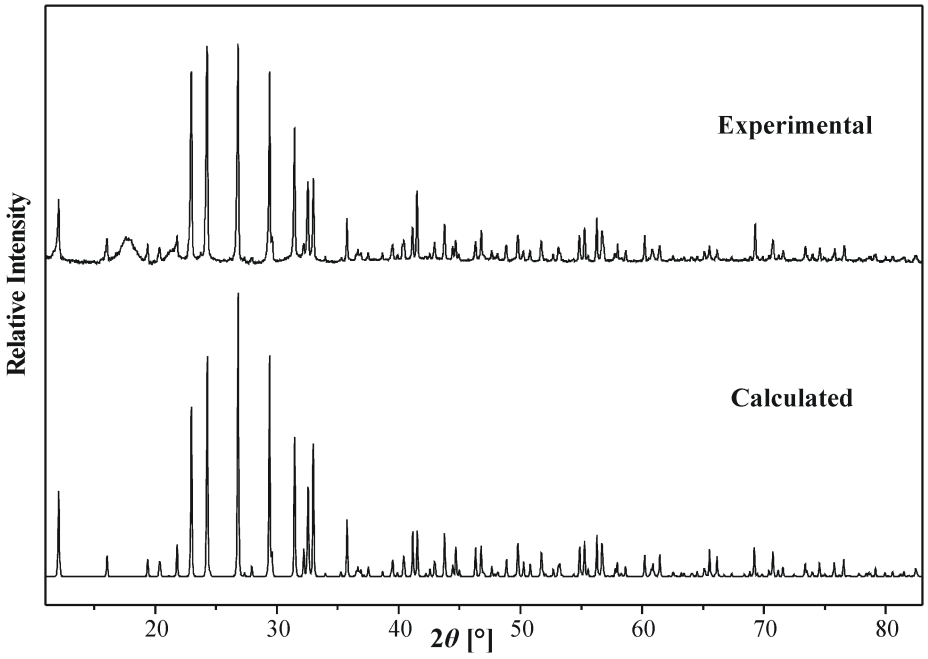

Figure 3.24: *Observed (background subtracted) and calculated powder X–ray diffraction patterns of* $KSc(HPO_4)_2$ *(Cu* $K_{\alpha 1}$*–radiation)*

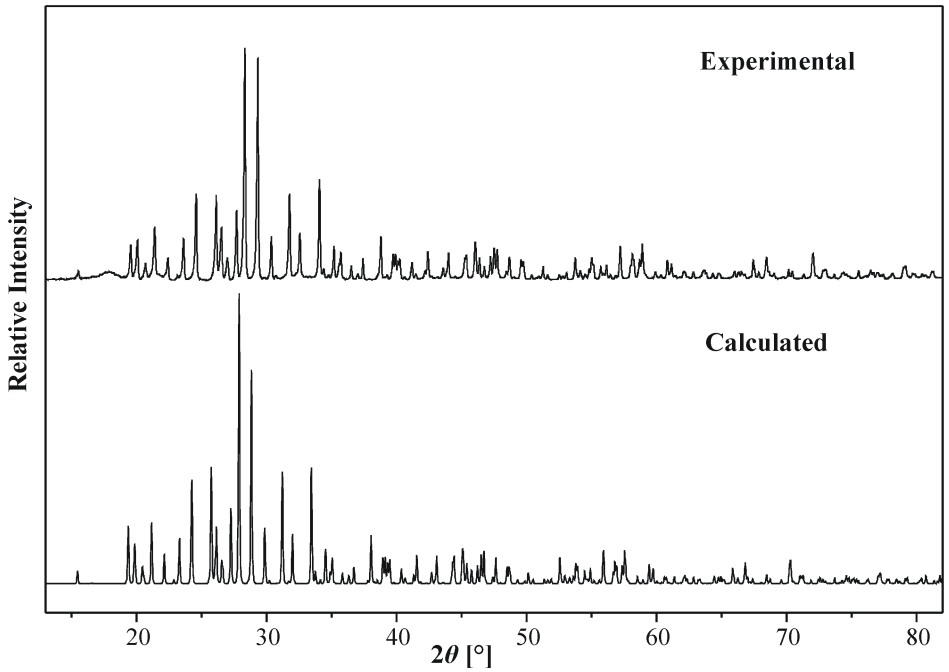

Figure 3.25: *Observed (background subtracted) and calculated powder X–ray diffraction patterns of* $RbSc(HPO_4)_2$ *(Cu* $K_{\alpha 1}$*–radiation)*

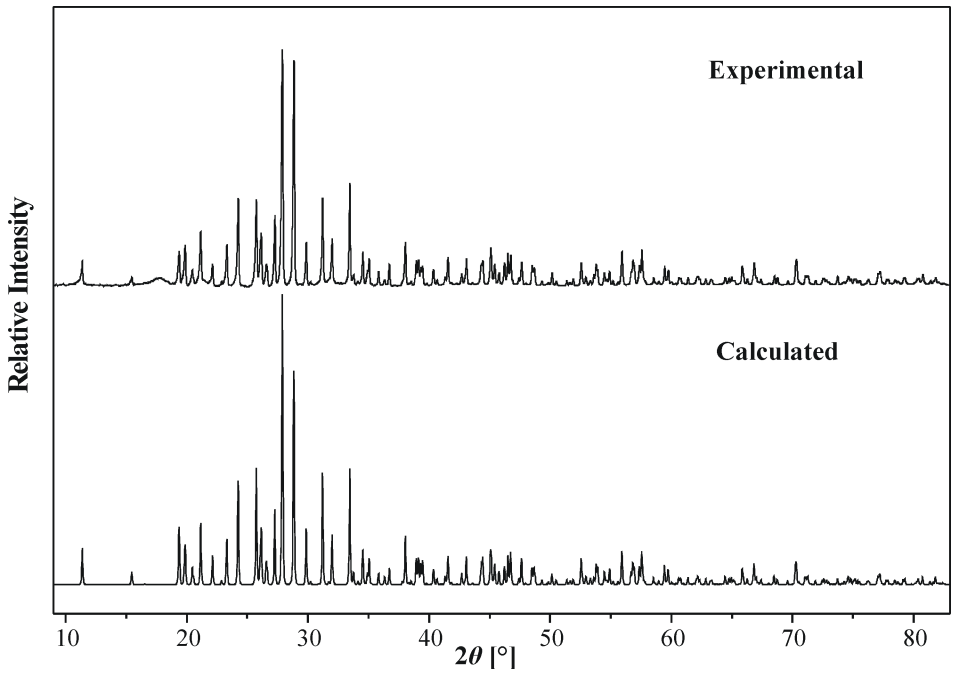

Figure 3.26: *Observed (background subtracted) and calculated powder X–ray diffraction patterns of $CsSc(HPO_4)_2$ (Cu $K_{\alpha 1}$–radiation)*

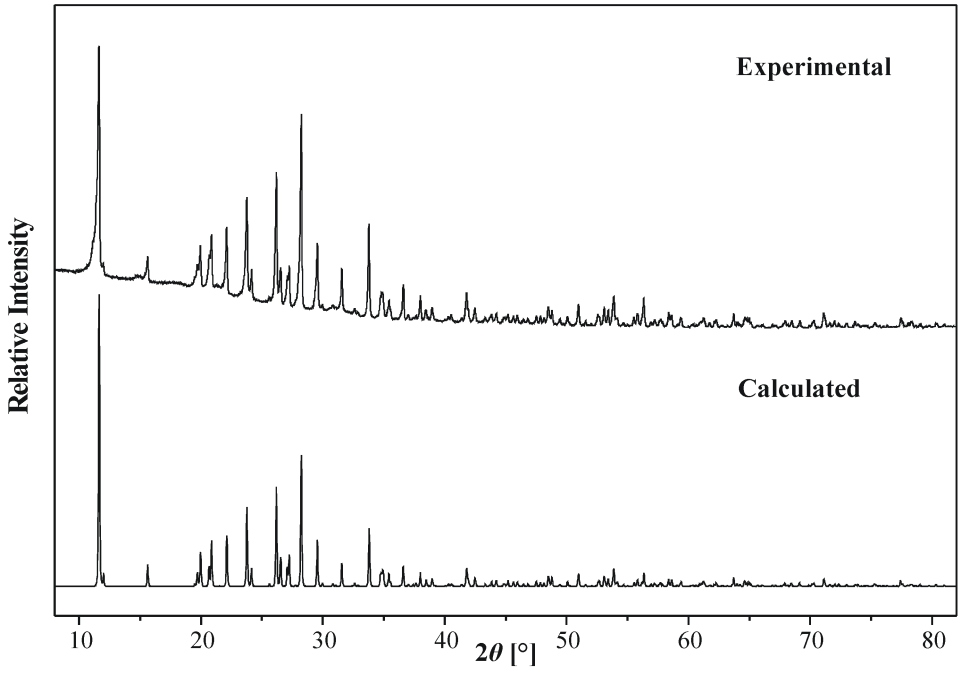

Figure 3.27: *Observed and calculated powder X–ray diffraction patterns of $NH_4Sc(HPO_4)_2$ (Cu $K_{\alpha 1}$–radiation)*

Table 3.5: *Results of the chemical analyses of $Li_2Sc[(PO_4)(HPO_4)]$ and $M^ISc(HPO_4)_2$ (M^I = K, Rb, Cs, NH_4)*

Element	Observed (e.s.d.) weight %	Calculated weight %
Li	3.02(06)	5.56
Sc	19.65(12)	18.00
P	24.80(13)	24.80
O	48.74(44)	51.24
H	0.39(05)	0.40
K	13.32(19)	14.17
Sc	16.06(04)	16.29
P	22.58(12)	22.44
O	33.54(15)	46.37
H	0.88(05)	0.73
Rb	24.46(20)	26.51
Sc	14.49(09)	13.94
P	19.32(12)	19.22
O	34.8(6)	39.7
H	0.85(02)	0.63
Cs	34.2(85)	35.94
Sc	12.54(05)	12.16
P	16.85(08)	16.75
O	30.51(12)	34.61
H	0.73(01)	0.55
N	5.43(06)	5.49
Sc	17.90(11)	17.63
P	24.34(07)	24.30
O	46.33(9)	50.20
H	2.42(02)	2.37

3.2.1.2 Crystal Structure Determinations

$Li_2Sc[(PO_4)(HPO_4)]$: A suitable prismatic crystal was selected and the data were collected on a single crystal diffractometer. The crystal structure was solved (monoclinic, space group $P12_1/n1$ (no. 14), a = 4.8582(12) Å, b = 8.1887(12) Å, c = 7.6683(18) Å, β = 104.111(7)°, Z = 2) as indicated by the isotypic relationship to $Li_2Fe^{III}[(PO_4)(HPO_4)]$ and $Li_2In[(PO_4)(HPO_4)]$ [115, 116]. The crystal structure was solved by direct methods and subsequently completed and refined by Fourier difference map analyses. The positions of Li, Sc, P, and O were located; the remaining hydrogen atom could not be deduced by this method. A total of 61 variables was refined to R_1 = 0.038 and wR_2 = 0.083 ($I > 2\sigma(I)$) considering 841 independent reflections.

$KSc(HPO_4)_2$: A needle–shaped crystal was selected for X–ray diffraction. Based on the systematic absences, the space group was determined (orthorhombic, space group *Pnma* (No. 62), a = 14.5095(2) Å, b = 5.4260(4) Å, c = 8.4882(5) Å, Z = 4). Direct methods and subsequent Fourier difference analyses were used to locate K, Sc, P and O atoms. One proton position out of two was determined from the Fourier difference maps. The refinement of the atomic coordinates and anisotropic thermal parameters led to reliability factors R1 = 0.045 and wR2 = 0.105 ($I > 2\sigma(I)$) considering 1332 independent reflections.

$M^{I}Sc(HPO_4)_2$ (M^{I} = Rb, Cs, NH_4): Foremost, the crystal structures of these three isotypic compounds $RbSc(HPO_4)_2$ (monoclinic, space group $P2_1/c$ (No. 14), a = 5.3214(6) Å, b = 8.9221(7) Å, c = 14.7579(12) Å, β = 94.967(5)°, Z = 4), $CsSc(HPO_4)_2$ (monoclinic, space group $P2_1/c$ (No. 14), a = 5.3639(4) Å, b = 9.1604(6) Å, c = 14.7052(10) Å, β = 93.727(4)°, Z = 4) and $NH_4Sc(HPO_4)_2$ (monoclinic, space group $P2_1/c$ (No. 14), a = 5.3211(5) Å, b = 8.8660(7) Å, c = 14.7909(12) Å, β = 95.266(4)°, Z = 4) were determined from single crystal X–ray data. In $CsSc(HPO_4)_2$, the positions of Cs, Sc, P, O were located by direct methods. The positions of the hydrogen atoms could be located in the difference Fourier maps (close to O4, and O8). The O—H distance was fixed to 0.80 Å during the refinement and the coordinates were refined as free variables. The refinement of the atomic coordinates and anisotropic thermal parameters led to reliability factors R1 = 0.035 and wR2 = 0.068 ($I > 2\sigma(I)$) considering 1926 independent reflections.

The crystals of both $RbSc(HPO_4)_2$ and $NH_4Sc(HPO_4)_2$ showed a reticular merohedry. The positions of Rb, Sc, P, O for $RbSc(HPO_4)_2$ and Sc, P, O, N for $NH_4Sc(HPO_4)_2$ were taken from structural data of the isotypic compound $CsSc(HPO_4)_2$. Subsequent introduction of the twin matrix −1 0 0 0 −1 0 0.5 0 1 and simultaneous refinement of the twin ratio together with the atomic coordinates and anisotropic thermal parameters led to reasonable structural models and residuals. The position of the protons could not be determined by Fourier difference map analyses for $M^{I}Sc(HPO_4)_2$ (M^{I} = Rb, NH_4).

Crystallographic data and refinement parameters of $Li_2Sc[(PO_4)(HPO_4)]$ and $M^{I}Sc(HPO_4)_2$ (M^{I} = K, Rb, Cs, NH_4) are summarized in *Appendix 14* to *Appendix 18*. The final fractional atomic coordinates and equivalent / isotropic and anisotropic displacement factors are enlisted in *Appendix 19* to *Appendix 28*.

3.2.1.3 Crystal Structure Description

$Li_2Sc[(PO_4)(HPO_4)]$: The crystal structure of $Li_2Sc[(PO_4)(HPO_4)]$ is an isotype of the Li—Fe and Li—In analogues [115, 116]. The crystal structure of the $Li_2Sc[(PO_4)(HPO_4)]$ is characterized by ScO_6 octahedra which are solely connected to six adjacent PO_4 tetrahedra *via* common O–corners (*Figure 3.28a*). Each PO_4 tetrahedron shares its unprotonated O–corners with three ScO_6 octahedra to form a three–dimensional network structure containing channels running along [100] as shown in *Figure 3.29*. The cross section of the channels is defined by eight–membered rings consisting of four ScO_6 octahedra and four phosphate tetrahedra. The Li cations reside within the channels.

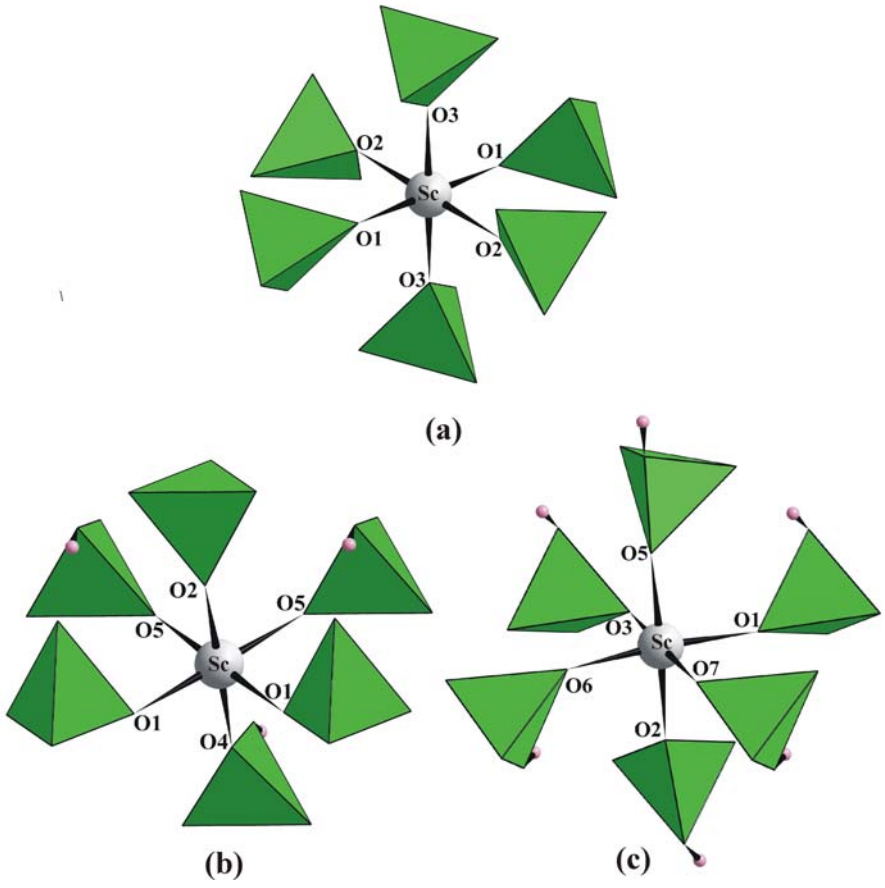

Figure 3.28: *Octahedral coordination of Sc^{3+} by oxygen atoms of six different phosphate / hydrogenphosphate groups in (a) $Li_2Sc[(PO_4)(HPO_4)]$, (b) $KSc(HPO_4)_2$ and (c) $M^ISc(HPO_4)_2$ (M^I = Rb, Cs, NH_4) Protons are shown by small pink spheres (protons which could not be deduced from the Fourier difference maps are omitted).*

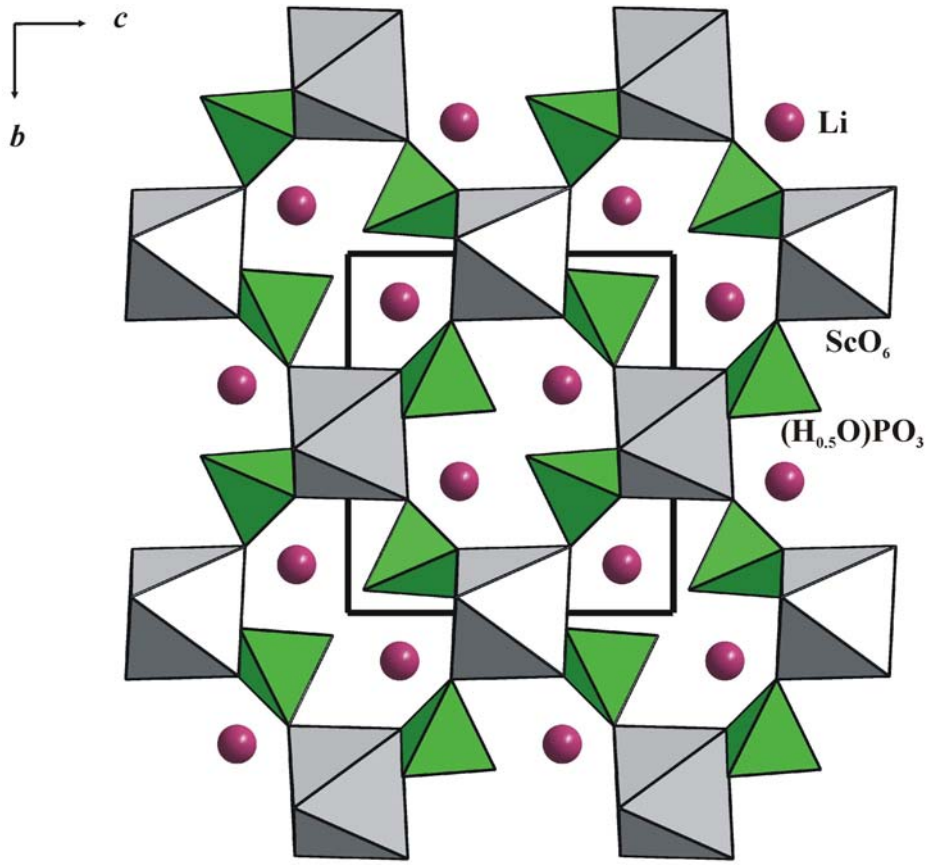

Figure 3.29: *Crystal structure of $Li_2Sc[(PO_4)(HPO_4)]$ (view along [100]): PO_4 tetrahedra (green) sharing their unprotonated O–corners with three ScO_6 octahedra (gray) to form a three–dimensional network. Li cations (violet) reside within the eight–membered channels. The unit cell is outlined.*

In the closest coordination sphere lithium atoms (CN = 5) are tetrahedrally coordinated by oxygen atoms from four different phosphate anions with Li—O distances ranging from 1.976(1) Å to 2.099(2) Å. An additional Li—O contact occurs at 2.418(2) Å to presumable protonated oxygen (O4). The Sc—O contacts within the ScO_6 octahedron are in the range from 2.073(2) Å to 2.131(2) Å. The P—O bond lengths within the PO_4 tetrahedra range from 1.529(2) Å to 1.550(2) Å. The bond lengths and angles of the phosphate tetrahedra and scandium octahedra are in the same range as observed in other related phosphates and borophosphates [101]. In analogy to the isotypic phases $Li_2Fe[(PO_4)(HPO_4)]$ and $Li_2In[(PO_4)(HPO_4)]$ the position of the proton (which could not be deduced from the Fourier difference maps) is assumed to take a position between two O4 atoms forming a symmetric O···H···O

bond (d(O4···O4) = 2.476(2) Å). Selected bond lengths and bond angles of $Li_2Sc[(PO_4)(HPO_4)]$ are given in *Appendix 29*.

$KSc(HPO_4)_2$: $KSc(HPO_4)_2$ represents a new structure type in the family of monohydrogen phosphates with general composition $M^I M^{III}(HPO_4)_2$. A selected part of the crystal structure of $KSc(HPO_4)_2$ is shown in *Figure 3.30*. ScO_6 octahedra share their oxygen corners with adjacent $(HO)PO_3$ tetrahedra. The $(HO)PO_3$ tetrahedra share three of their corners with neighbouring ScO_6 octahedra and the fourth ("free") oxygen binds to the proton (*Figure 3.28b*).

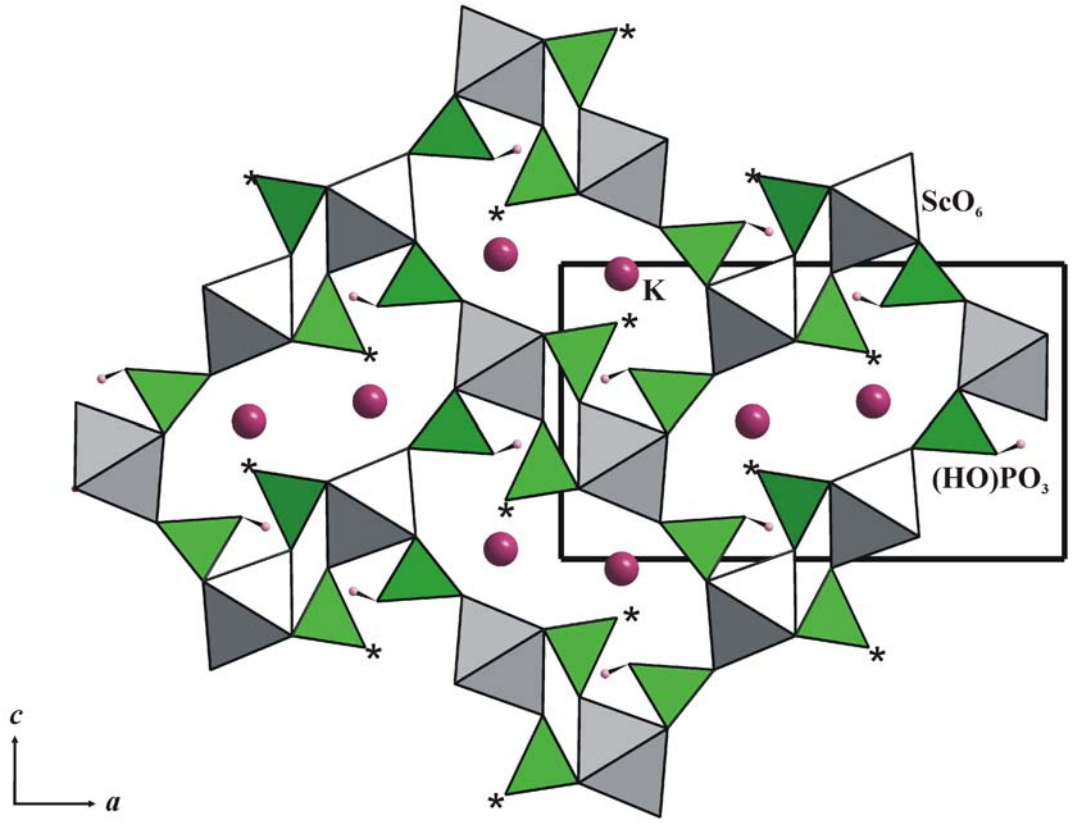

Figure 3.30: *Crystal structure of $KSc(HPO_4)_2$ viewed along [010]. ScO_6 octahedra (gray) are linked to $(HO)PO_3$ tetrahedra (green) to form a three–dimensional network with the K^+ ions (violet) inside the channels. Protons H6 (at O6) are shown as small (pink) spheres. The presumed proton at O3 (marked as *) could not be located. The protonated vertices of the PO_4 tetrahedra are directed inside the channels. The unit cell is outlined.*

The interconnection of the hydrogenphosphate groups with ScO_6 octahedra *via* common corners results in an overall three–dimensional framework forming channels

running along [010]. The cross sections of the channels are given by twelve–membered rings consisting of six scandium coordination octahedra and six hydrogenphosphate groups as well as four–membered rings consisting of two scandium coordination octahedra and two hydrogenphosphate tetrahedra. Potassium ions are located within those channels of the twelve–membered rings.

The Sc—O distances inside the octahedra range from 2.056(2) Å to 2.113(2) Å. The P—O bond lengths within the network range from 1.510(2) Å to 1.518(2) Å. The terminal bond lengths P—OH are increased to 1.583(3) Å (P1—O3) and 1.593(3) Å (P2—O6), respectively. O—P—O angles range from 105.54(16)° to 112.23(17)°. Proton H6 is attached to O6 (d(O6—H1) = 0.74(4) Å) and is involved in a hydrogen bridge (O6—H1···O2; d(O6···O2) = 2.887(3) Å). The second proton (attached to O3) could not be located from the Fourier difference maps. Since the P—OH bonds are generally longer compared to P—O bonds [101], the given position was assumed. Potassium was found to be ten–fold coordinated with K—O distances between 2.874(2) Å and 3.2184(15) Å. Selected interatomic distances and bond angles of $KSc(HPO_4)_2$ are listed in *Appendix 30*.

$M^{I}Sc(HPO_4)_2$ (M^{I} = Rb, Cs, NH_4): The crystal structure of the $M^{I}Sc(HPO_4)_2$ (M^{I} = Rb, Cs, NH_4) series is an isotype of β–$RbV^{III}(HPO_4)_2$ and $NH_4V^{III}(HPO_4)_2$ [117]. In the crystal structure of $M^{I}Sc(HPO_4)_2$ (M^{I} = Rb, Cs, NH_4), the ScO_6 octahedra share their six corners with adjacent $(HO)PO_3$ tetrahedra *(Figure 3.28c)*.

Condensation of the hydrogenphosphate groups with ScO_6 coordination octahedra *via* common corners results in an overall three–dimensional framework containing channels running along [100] as shown in *Figure 3.31*. The cross section of the channel is defined by twelve–membered rings consisting of six scandium coordination octahedra and six hydrogenphosphate groups. The M^{I} (M^{I} = Rb, Cs, NH_4) ions reside within the channels formed by the twelve–membered rings.

Selected interatomic distances and bond angles of $M^{I}Sc(HPO_4)_2$ (M^{I} = Rb, Cs, NH_4) are listed in *Appendix 31, Appendix 32* and *Appendix 33*. The Sc—O distances for $M^{I}Sc(HPO_4)_2$ (M^{I} = Rb, Cs, NH_4) are in the interval from 2.053(3) Å to 2.144(3) Å. The coordination of the P atom is slightly distorted with three shorter distances (1.503(3) – 1.529(3) Å) and one longer contact (1.597(3) – 1.600(3) Å). The latter oxygen atom binds to the proton. The angles of scandium octahedra and hydrogenphosphate groups are similar to other related phosphates and scandium

borophosphates [101]. The coordination number of rubidium was found to be eleven and the length of the Rb—O bonds ranges from 2.993(3) Å to 3.559 (3) Å. Cesium is twelve–fold coordinated by oxygen and the Cs—O contacts vary from 3.105(3) Å to 3.585(3) Å.

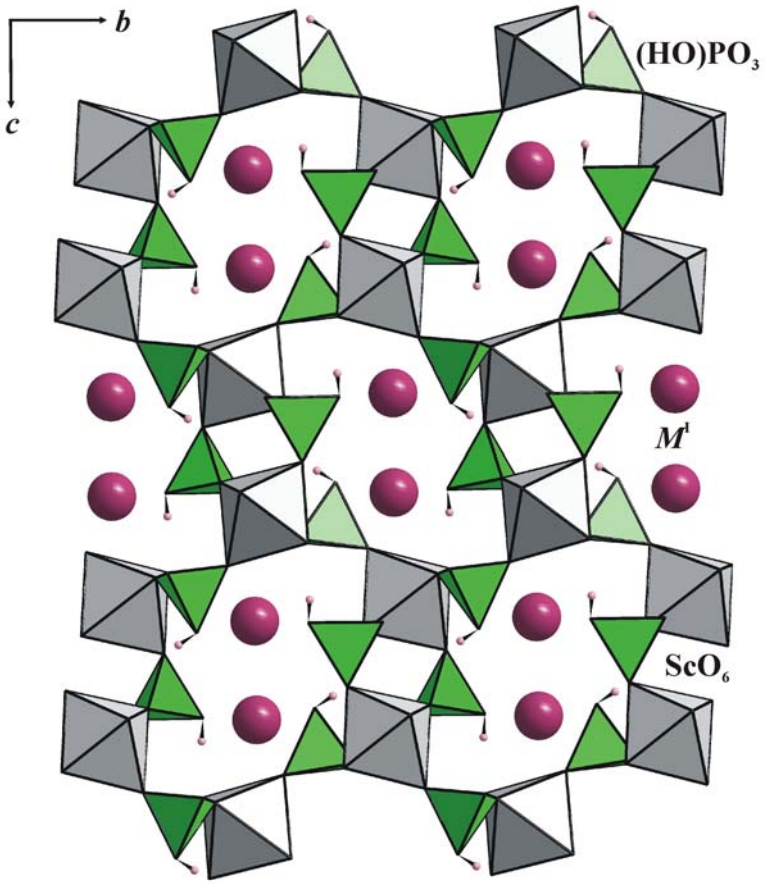

Figure 3.31: *Crystal structure of $M^{I}Sc(HPO_4)_2$ (M^{I} = Rb, Cs, NH_4) (view along [100]): The hydrogenphosphate groups (green) are connected to ScO_6 octahedra (gray) by sharing common corners to form a three–dimensional network. The channels of the frameworks are occupied by M^{I} (M^{I} = Rb, Cs, NH_4) ions (violet spheres). The unit cell is outlined.*

3.2.1.4 Thermal Analysis

The thermochemical properties were investigated by simultaneous constant rate thermogravimetry (TG) and difference thermal analyses (DTA) with heating and cooling rates of 5 K / min up to 1000 ºC in a continuous argon gas flow.

The TG curves for $Li_2Sc[(PO_4)(HPO_4)]$ and $M^{I}Sc(HPO_4)_2$ (M^{I} = K, Rb, Cs) showed a broad unresolved mass loss step (*Figure 3.32*) between 350 ºC and 600 ºC accompanied by an endothermic effect (*Figure 3.33*) in the DTA trace (maximum of

the peak: Li 539 ºC, K 369 ºC, Rb 365 ºC, Cs 384 ºC). The total mass losses observed are high in comparison with the calculated values suggesting that adsorbed water is also released up to the maximum temperature (exp. / theo.: Li 4.1 / 3.6 wt %, K 7.5 / 6.5 wt %, Rb 6.7 / 5.6 wt %, Cs 5.9 / 4.9 wt %). In addition to the broad mass loss (*Figure 3.34*) $NH_4Sc(HPO_4)_2$ exhibits a second one with the highest mass loss rate at 796 ºC also connected with an endothermic peak in the DTA curve (*Figure 3.35*). The experimentally determined mass loss of 18.0 wt % is in accordance with the release of 1 mole ammonia and 1½ mole of water per formula unit $NH_4Sc(HPO_4)_2$ (calc.: 17.3 wt %). Low temperature DTA investigations were performed for all compounds and did not show any transition until –180 ºC.

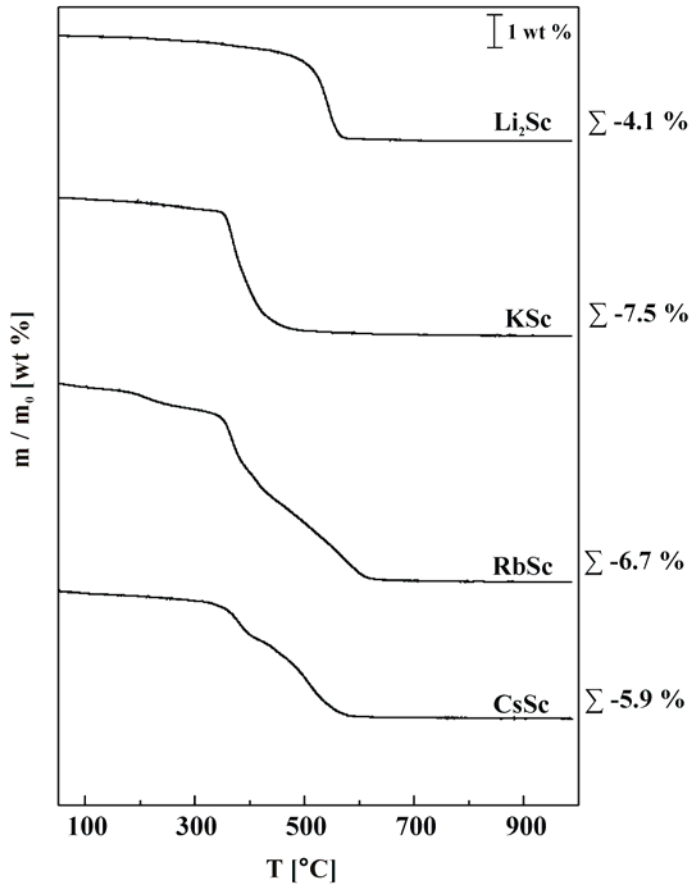

Figure 3.32: *Thermogravimetric curves recorded for $Li_2Sc[(PO_4)(HPO_4)]$, and $M^ISc(HPO_4)_2$ (M^I = K, Rb, Cs) with a heating rate of 5 K / min up to 1000 ºC. The recorded mass loss (weight %) is given at the right.*

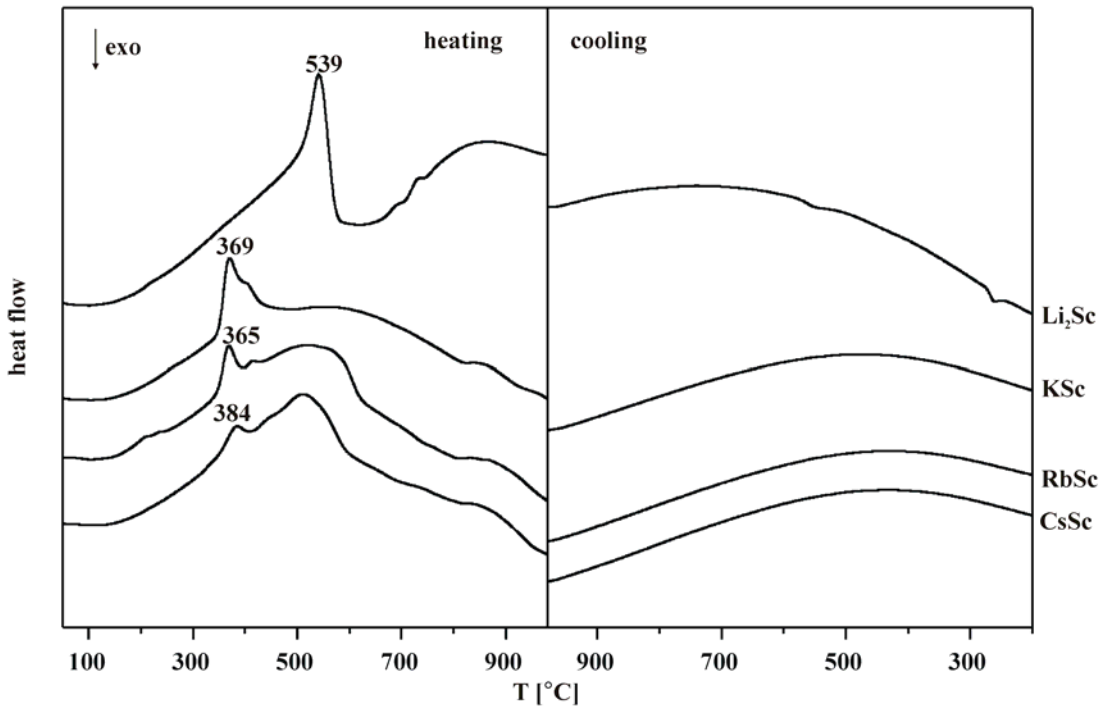

Figure 3.33: *DTA traces for the thermal decomposition of $Li_2Sc[(PO_4)(HPO_4)]$, and $M^ISc(HPO_4)_2$ (M^I = K, Rb, Cs) recorded for heating (left) and cooling (right) (rate ± 5 K / min).*

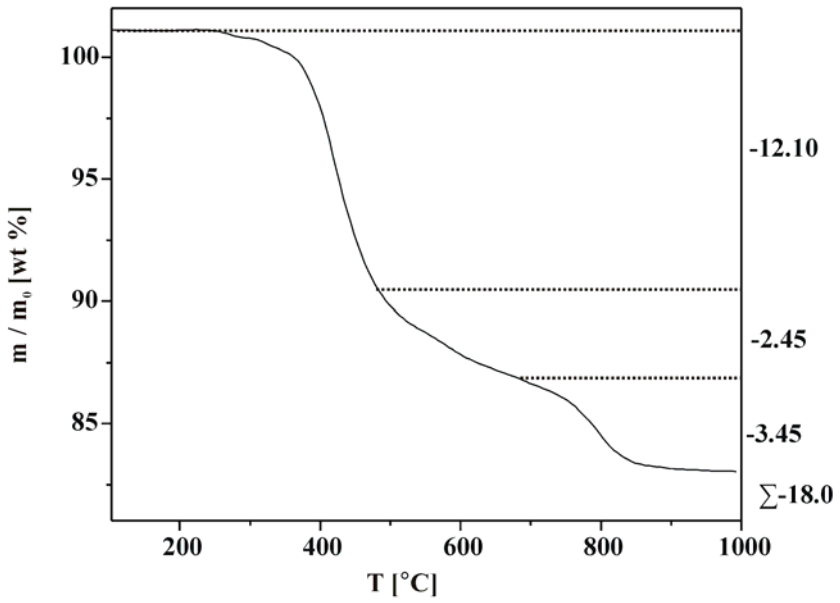

Figure 3.34: *Thermogravimetric curve recorded for $NH_4Sc(HPO_4)_2$ with a heating rate (not corrected by blank run) of 5 K / min. The measured mass loss (weight %) is given at the right.*

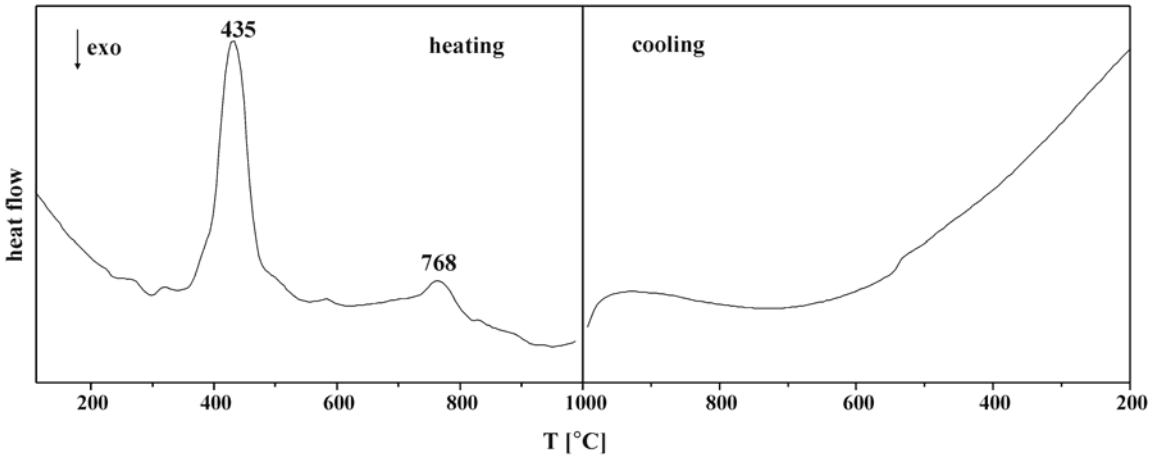

Figure 3.35: *DTA traces for the thermal decomposition of $NH_4Sc(HPO_4)_2$ recorded for heating (left) and cooling (right) (rate ± 5 K / min).*

The products after thermal decomposition were ascertained for $Li_2Sc[(PO_4)(HPO_4)]$ (mixture of $LiScP_2O_7$ and $Li_3Sc_2(PO_4)_3$) (*Figure 3.36*) and $KSc(HPO_4)_2$ (*Figure 3.37*; $KScP_2O_7$ together with an unidentified pattern). Completely new X–ray diffraction patterns (*Figure 3.38* and *Figure 3.39*) were obtained for the isotypic phases $M^ISc(HPO_4)_2$ (M^I = Rb, Cs, NH_4) (could not be indexed) indicating the formation of new phases by thermal decomposition. The results of the thermal investigations are summarized in *Table 3.6*.

Table 3.6: *Details of thermal analyses of $Li_2Sc[(PO_4)(HPO_4)]$ and $M^ISc(HPO_4)_2$ (M^I = K, Rb, Cs, NH_4)*

Compound	Mol. Wt.[a]	Expt. mass loss [b]	Calculated [c]	Decomposition product
Li_2Sc	249.79	4.1	3.60 (½ × H_2O)	$Li_3Sc_2(PO_4)_3$ [118] + LiScP2O7 [119]
KSc	276.02	7.5	6.52 (1 × H_2O)	$KScP_2O_7$ [120] + Unidentified
RbSc	322.38	6.7	5.58 (1 × H_2O)	Unidentified
CsSc	369.83	5.9	4.87 (1 × H_2O)	Unidentified
NH_4Sc	254.96	18.0	17.30 (1½ × H_2O) + (1 × NH_3)	Unidentified

[a] molecular weight (g / mol), [b] experimental mass loss (wt %), [c] calculated mass loss (wt %)

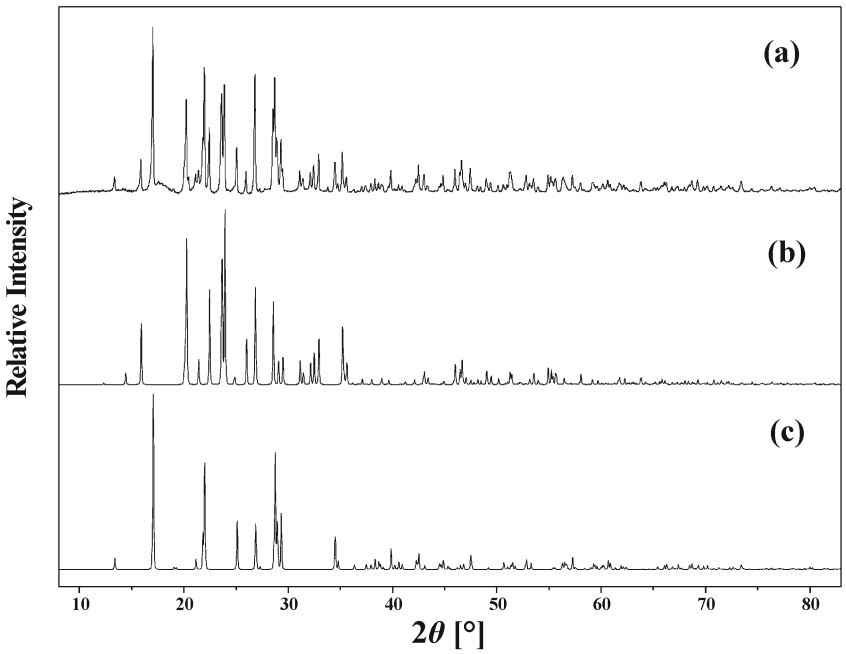

Figure 3.36: *Powder X–ray diffraction patterns (background subtracted) of (a) the decomposition product of $Li_2Sc[(PO_4)(HPO_4)]$ heated up to 1000 °C, compared with the calculated powder diffraction pattern of (b) $Li_3Sc_2(PO_4)_3$ [118] and (c) $LiScP_2O_7$ [119] (Cu $K_{\alpha 1}$–radiation)*

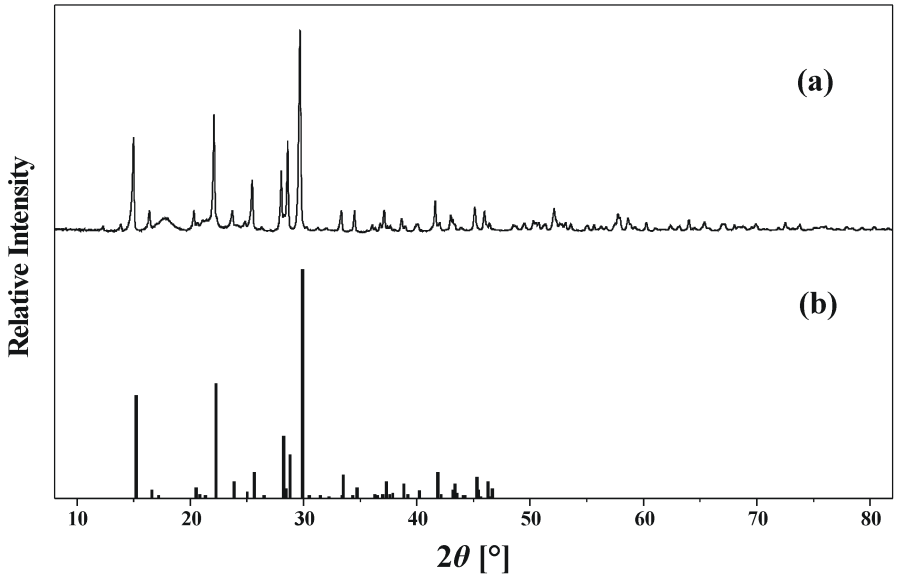

Figure 3.37: *Powder X–ray diffraction pattern (background subtracted) of (a) the decomposition product of $KSc(HPO_4)_2$ heated up to 1000 °C, compared with the tabulated peak positions of (b) $KScP_2O_7$ [120] (Cu $K_{\alpha 1}$–radiation)*

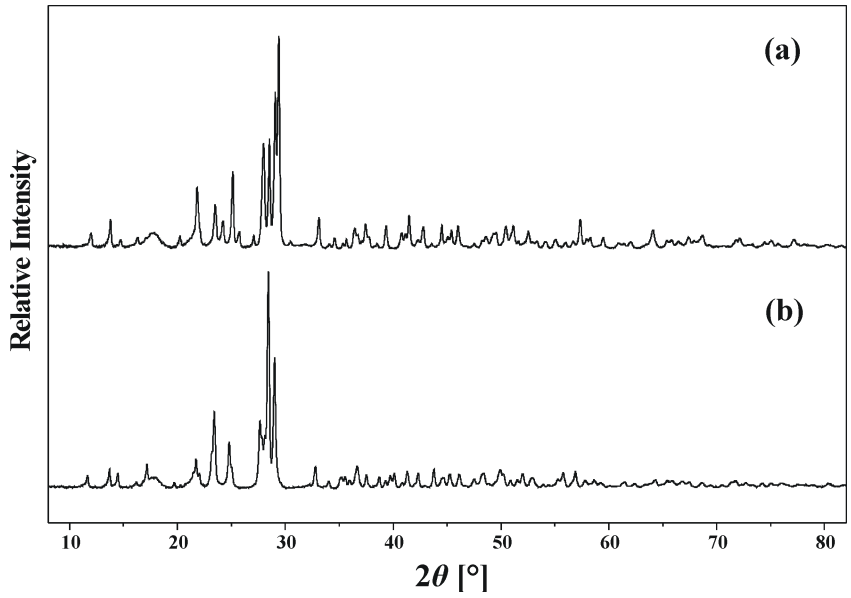

Figure 3.38: *Powder X–ray diffraction patterns of the crystalline products after TG / DTA investigations up to 1000 °C of (a) $RbSc(HPO_4)_2$ and (b) $CsSc(HPO_4)_2$ (Cu $K_{\alpha 1}$–radiation)*

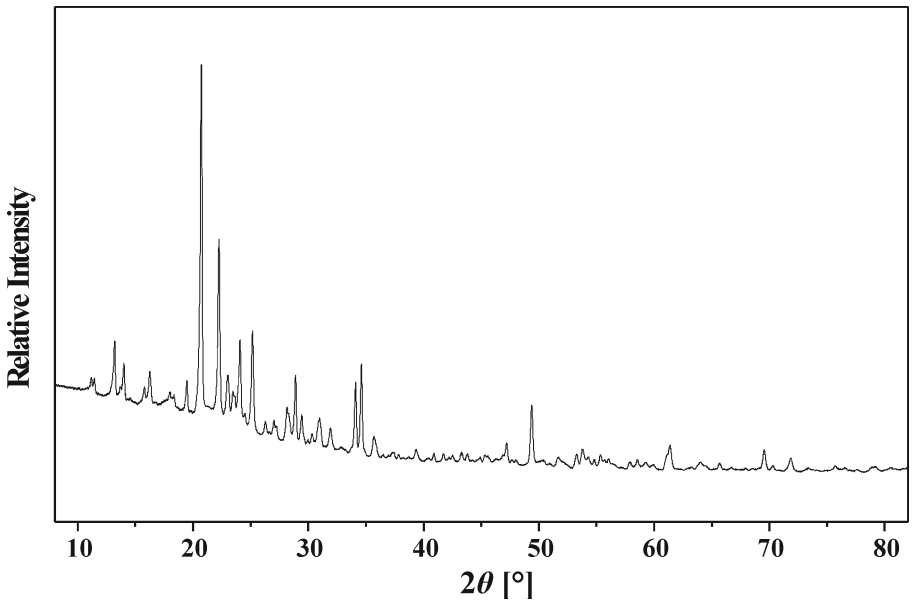

Figure 3.39: *Powder X–ray diffraction patterns of the crystalline products after TG / DTA investigations up to 1000 °C of $NH_4Sc(HPO_4)_2$ (Cu $K_{\alpha 1}$–radiation)*

3.2.2 Discussion

The crystal structures of $Li_2Sc[(PO_4)(HPO_4)]$, $KSc(HPO_4)_2$ and $M^ISc(HPO_4)_2$ (M^I = Rb, Cs, NH_4) contain frameworks built of vertex–sharing ScO_6 tetrahedra and PO_4 tetrahedra. The cavities and channels of the frameworks are occupied by the mono–valent cations (*Figure 3.40*). Variations in the sizes of M^I (M^I = Li, K, Rb, Cs, NH_4) in combination with Sc cations give rise to three different structure types. Thus, different types of frameworks are formed, the coordination polyhedra are distorted and the sizes of the channels and cavities are changed.

Significant structural similarities between the three frameworks are given by the fact that they contain the same building units and linkages within the framework. Expanding the Hawthorne M–T rules (M = six coordinated central metal atom, T = four coordinated phosphorus atom) [121] to $Li_2Sc[(PO_4)(HPO_4)]$, $KSc(HPO_4)_2$ and $M^ISc(HPO_4)_2$ (M^I = Rb, Cs, NH_4),

(a) only isolated ScO_6 and $(HO)PO_3$ groups are formed and a strict alteration between these two building units is observed,

(b) only three corners of the PO_4 tetrahedra are linked to neighbouring ScO_6 octahedra and the "free" O atom is always linked to a proton,

(c) ScO_6 octahedra are always connected to six PO_4 tetrahedra *via* sharing common corners,

(d) all these structures show the formation of channels.

However, the particular arrangements of ScO_6 octahedra and $(HO)PO_3$ tetrahedra are different in the crystal structures of $Li_2Sc[(PO_4)(HPO_4)]$, $KSc(HPO_4)_2$ and $M^ISc(HPO_4)_2$ (M^I = Rb, Cs, NH_4), which seems to depend on the size of the M^I ion [122]. For the smallest ion lithium (ionic radius 0.59 Å), only 8–membered channels (along *a*) are formed whereas the larger mono–valent ions K (ionic radius 1.69 Å), Rb (ionic radius 1.69 Å) and Cs (ionic radius 1.88 Å) require more space and consequently 12–membered channels constitute the framework [122]. The ammonium compound adopts the same structure as the rubidium phase which is in agreement with the observation from other ionic compounds that the space requirements for both ions are similar [122]. A brief summary on framework structures built up of ScO_6 octahedra and $(HO)PO_3$ tetrahedra as well as their characteristics are listed in *Table 3.7*. It seems to be essential that in all crystal structures, the protons bonded to the PO_4 tetrahedra are directed inside the channels. This arrangement of protons has an effect

on the channels (because of hydrogen bridges) and their presence compensates the negative charge of the frameworks [123].

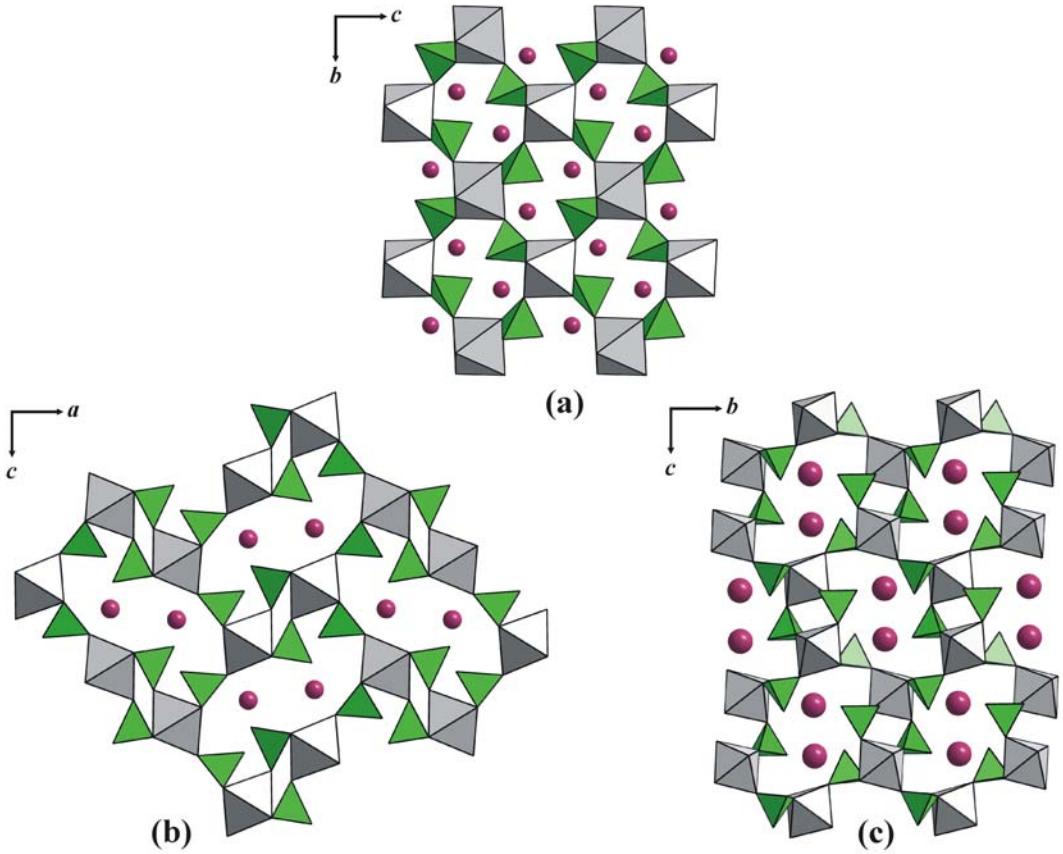

Figure 3.40: *Crystal structures of (a) $Li_2Sc[(PO_4)(HPO_4)]$; (b) $KSc(HPO_4)_2$ and (c) $M^{I}Sc(HPO_4)_2$ (M^{I} = Rb, Cs, NH_4) built from ScO_6 tetrahedra (light grey) and PO_4 tetrahedra (green) sharing common corners. The cavities and channels within the frameworks are occupied by M^{I} ions (violet spheres, M^{I}= Li, K, Rb, Cs, NH_4). Proton positions at the PO_4 tetrahedra are omitted for clarity.*

Monohydrogen phosphates of general composition $M^{I}M^{III}(HPO_4)_2$ are known for the group 13 elements Al, Ga, In and for the transition metals Sc, V, and Fe in combination with alkali–metals or ammonium ions (shown in *Table 3.8*). All of them are built of alternating $M^{III}O_6$ and $(HO)PO_3$ tetrahedra resulting in flexible frameworks manifesting 7 different structure types reported so far. Sequenced according to their crystal systems there are:

1) $NH_4Fe^{III}(HPO_4)_2$ [124], α–$RbFe(HPO_4)_2$ [125], α–$CsIn(HPO_4)_2$ [126], and α–$M^{I}V^{III}(HPO_4)_2$ (M^{I} = Rb, NH_4) [117, 127] crystallizing in $P\bar{1}$,

Table 3.7: *Summary on framework structures built up of ScO_6 octahedra and PO_4 tetrahedra and their characteristic structural elements (bold: this work).*

Cations	Ionic radii r^+ [Å] [122]	Coordination number	Volume per formula unit / Å^3	Description of the framework	Formula
Li^+	0.59	5	148.1	M—T [b], 8–membered channels (along *a*) with O···H—O bridges	**$Li_2Sc[(PO_4)(HPO_4)]$**
Na^+	1.02	6	163.4	M—T [b], 8–membered channels (along *a*)	$NaSc(HPO_4)_2$ [128]
K^+	1.55	9	259.8	M—T [b], cages (Langbeinite–type)	$K_2Sc_2[HPO_4][PO_4]_2$ [45]
K^+	1.59	10	167.1	M—T [b], 12–membered channels (along *b*)	**$KSc(HPO_4)_2$**
Rb^+	1.69	11	174.5	M—T [b], 12–membered channels (along *a*)	**$RbSc(HPO_4)_2$**
NH_4^+	1.51 [129]		173.7		**$NH_4Sc(HPO_4)_2$**
Cs^+	1.85	12	180.3		**$CsSc(HPO_4)_2$**
H_3O^+			172.1 [a]		$[H_3O^+]Sc(HPO_4)_2$ [93]

[a] measured at 173 K, [b] M = six coordinated central metal atom, T = four coordinated phosphorus atom, lattice parameters are given in *Table 3.8*

Table 3.8: *Structurally characterized monohydrogen phosphates (bold: this work) of general composition $M^{I}M^{III}(HPO_4)_2$.*

Compound	Space group	*a* (Å)	*b* (Å)	*c* (Å)	*α* (°)	*β* (°)	*γ* (°)
$NH_4Fe(HPO_4)_2$	$I\bar{1}$	9.834(4)	7.185(3)	14.159(4)	93.46(3)	85.58(3)	89.47(3) [124]
	$(P\bar{1})^a$	7.185	8.857	9.478	64.77	70.2	69.3(7)
α–$RbFe(HPO_4)_2$	$P\bar{1}$	7.202(4)	8.832(8)	9.450(8)	65.14(8)	70.04(6)	69.59(6) [125]
α–$CsIn(HPO_4)_2$	$P\bar{1}$	7.414(3)	9.011(3)	9.784(3)	65.52(3)	70.20(3)	69.55(3) [126]
α–$NH_4V(HPO_4)_2$	$P\bar{1}$	7.173(2)	8.841(2)	9.458(2)	65.08(2)	70.68(2)	69.59(2) [117]
α–$RbV(HPO_4)_2$	$P\bar{1}$	8.831(1)	9.450(2)	7.188(2)	109.55(2)	110.26(1)	65.34(1) [127]
	$(P\bar{1})^a$	7.188	8.831	9.450	65.34	70.45	69.7(4)
β–$RbV(HPO_4)_2$	$P2_1/c$	5.21(1)	8.789(8)	14.330(5)	90	94.39(4)	90 [117]
β–$NH_4V(HPO_4)_2$	$P2_1/c$	5.201(1)	8.738(2)	14.398(3)	90	94.83(1)	90 [117]
β–$RbIn(HPO_4)_2$	$P2_1/c$						
β–$CsIn(HPO_4)_2$	$P2_1/c$	5.3286(6)	9.1653(7)	14.7839(14)	90	93.839(9)	90 [130]
$RbSc(HPO_4)_2$	***P*2$_1$/c**	**5.3214(6)**	**8.9221(7)**	**14.7579(1)**	**90**	**94.967(5)**	**90**
$CsSc(HPO_4)_2$	***P*2$_1$/c**	**5.3639(4)**	**9.1604(6)**	**14.7052(1)**	**90**	**93.727(4)**	**90**
$NH_4Sc(HPO_4)_2$	***P*2$_1$/c**	**5.3211(4)**	**8.660(7)**	**14.7909(1)**	**90**	**96.265(4)**	**90**
$NH_4In(HPO_4)_2$	$P2_1/c$	9.665(1)	8.276(1)	9.5964(1)	90	116.15(1)	90 [131]
α–$RbIn(HPO_4)_2$	$P2_1/c$	9.705(2)	8.367(2)	9.528(2)	90	116.60(3)	90 [131]
$KIn(HPO_4)_2$	$P2_1/c$	9.623(1)	8.257(1)	9.4571(1)	90	115.72(1)	90 [131]
$NaSc(HPO_4)_2$	*C*1c1	10.444(9)	16.371(2)	9.055(7)	90	122.42(3)	90 [128]
$LiIn(HPO_4)_2$	*Pmnn*	5.490(6)	7.946(6)	6.929(6)	90	90	90 [132]
$KSc(HPO_4)_2$	***P*nma**	**5.4260(4)**	**8.4882(5)**	**14.5095(1)**	**90**	**90**	**90**
β–$RbFe(HPO_4)_2$	$R\bar{3}c$	8.160(1)	8.160(1)	52.75(1)	90	90	120 [126]
$RbGa(HPO_4)_2$	$R\bar{3}c$	8.118(1)	8.118(1)	51.943(4)	90	90	120 [126]
$RbAl(HPO_4)_2$	$R\bar{3}c$	8.058(1)	8.05811)	51.081(1)	90	90	120 [126]

[a] *The cell parameters ($I\bar{1}$) transformed into the reduced cell ($P\bar{1}$) for the comparibility reasons.*

2) β–$M^{I}V^{III}(HPO_4)_2$ (M^{I} = Rb, NH_4) [117], β–$M^{I}In(HPO_4)_2$ (M^{I} = Rb, Cs) [130] and the new compounds $M^{I}Sc(HPO_4)_2$ (M^{I} = Rb, Cs, NH_4) crystallizing in $P2_1/c$,

3) $M^{I}In(HPO_4)_2$ (M^{I} = K, Rb, NH_4) [131] also crystallizes in $P2_1/c$ with difference in lattice dimensions.

Three non–isotypic examples for the orthorhombic system are:

4) $NaSc(HPO_4)_2$ crystallizing in $C1c1$ [128],

5) $LiIn(HPO_4)_2$ in *Pmnn* [132] and

6) $KSc(HPO_4)_2$ in *Pnma*,

and finally three examples crystallizing in $R\bar{3}c$ with comparable huge unit cells,

7) $RbM^{III}(HPO_4)_2$ (M^{III} = Fe, Al, Ga) [126].

There are also examples with two different modifications of a compound, for instance α–$RbV^{III}(HPO_4)_2$ and β–$RbV^{III}(HPO_4)_2$ [117] which even more is caused by the flexibility of such kind of frameworks. Therefore, we already assume the existence of further modifications of $M^{I}Sc(HPO_4)_2$ (M^{I} = K, Rb, Cs, NH_4) and carried out first low temperature DTA investigations. However, no phase transition down to –180 ºC was observed.

3.3 Alkaline Earth–Transition Metal Borophosphates

In this chapter the results obtained from the systematic investigation of borophosphates containing alkaline earth– and transition metals (AE–T^{II} and AE–T^{III}) are discussed. Foremost, the different experimental conditions, the crystal structure determinations and the crystal structure descriptions for the first alkaline earth– and transition metal borophosphates are given. For the first time, a divalent alkaline–earth – trivalent transition metal (AE–T^{III}) borophosphate and a two–dimensional layered borophosphate were synthesized. In addition, a large group of helical borophosphates (AE–T^{II}) were synthesized and studied. Finally, the anionic partial structures obtained from alkaline earth– and transition metal borophosphates.

3.3.1 Ca*M2*^{II}[$BP_2O_7(OH)_3$] (*M2*^{II} = Fe, Ni)

3.3.1.1 Synthesis

CaFe[$BP_2O_7(OH)_3$]: Transparent (colorless) platy single crystals (*Figure 3.41*) were obtained under mild hydrothermal conditions from a mixture of 0.7453 g $Ca(OH)_2$, 1.0002 g $FeCl_2 \cdot 4H_2O$, 0.7003 g B_2O_3 and 3.4793 g H_3PO_4 in the molar ratio Ca : Fe : B : P = 1 : 2 : 2 : 6. The mixture was heated with 10 ml of deionized water for three hours and filled into a 20 ml Teflon–lined autoclave. The degree of filling was about 30 %. The autoclave was placed in the oven with subsequent heating at 170 ºC for 8 days.

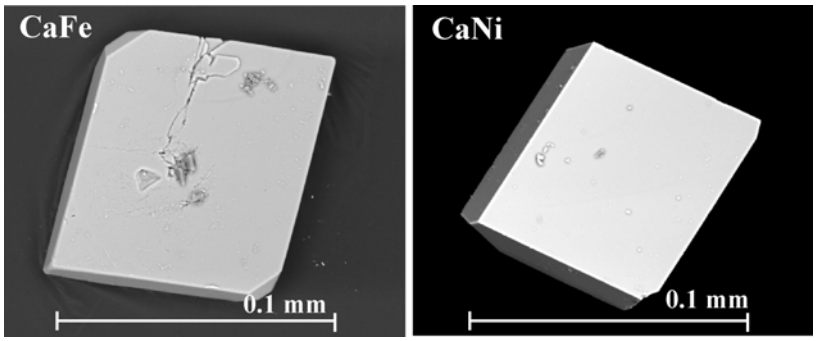

Figure 3.41: *SEM images of single crystals of CaFe[$BP_2O_7(OH)_3$] and CaNi[$BP_2O_7(OH)_3$]*

CaNi[$BP_2O_7(OH)_3$]: The light green platy crystals were obtained hydrothermally (*Figure 3.41*) from a mixture of 0.2480 g $Ca(OH)_2$, 0.2500 g NiO, 0.4606 g B_2O_3 and 2.3153 g H_3PO_4 in the molar ratio Ca : Ni : B : P = 1 : 1 : 4 : 6 together with 10 ml of

water. The mixture was filled into a 10 ml Teflon–lined autoclave (degree of filling was about 35 %, pH = 1). The autoclave was heated under autogenous pressure at 170 ºC for two weeks.

The reaction products were separated by filtration, washed with hot water / acetone and dried at 60 ºC in air. The platy crystals obtained from both $CaFe[BP_2O_7(OH)_3]$ and $CaNi[BP_2O_7(OH)_3]$ had dimensions ranging from 0.05 mm to 0.1 mm. The crystals obtained were in the form of by–products (minority phase). BPO_4 together with an unknown phase were the main products. The chemical compositions (Ca : Ni : Fe : P ≈ 1 : 1 : 1 : 2) are consistent with EDX analytical data.

3.3.1.2 Crystal Structure Determination

The crystal structures of $CaFe[BP_2O_7(OH)_3]$ (monoclinic, space group *C*1 2/*c*1 (No. 15), a = 10.2332(15) Å, b = 8.2391(8) Å, c = 9.1587(12) Å, β = 117.069(6)º, Z = 4) and $CaNi[BP_2O_7(OH)_3]$ (monoclinic, space group *C*1 2/*c*1 (No. 15), a = 10.2515(9) Å, b = 8.3364(5) Å, c = 9.1752(13) Å, β = 116.34(4)º, Z = 4) were solved by direct methods. After including anisotropic parameters of the heavier atoms in the refinement, the protons were located from Fourier difference maps and refined without applying any restrains. The position of the protons attached to the PO_4 group could not be located from the Fourier difference maps. The refinement of the atomic coordinates and anisotropic thermal parameters led to reliability factors R1 = 0.025 and wR2 = 0.062 for $CaFe[BP_2O_7(OH)_3]$ ($I > 2\sigma(I)$) and R1 = 0.028 and wR2 = 0.075 for $CaNi[BP_2O_7(OH)_3]$ ($I > 2\sigma(I)$) considering 1166 and 1111 independent reflections, respectively.

The crystallographic data and refinement parameters are summarized in *Appendix 34* and *Appendix 35*. The final fractional atomic coordinates and equivalent / isotropic and anisotropic displacement factors are enlisted in *Appendix 36* to *Appendix 39*.

3.3.1.3 Crystal Structure Description

The crystal structure of $Ca\mathit{M2}^{II}[BP_2O_7(OH)_3]$ ($\mathit{M2}^{II}$ = Fe, Ni) is an isotype of the $\mathit{M1}^{I}\mathit{M2}^{III}$ analogues ($\mathit{M1}^{I}$ = Na, K; $\mathit{M2}^{III}$ = Fe, Al, Ga, V) [48, 49, 107, 108, 133, 134]. The oligomeric borophosphate unit consists of an unbranched tetrahedral triple, $[BP_2O_7(OH)_3]^{4-}$, built up by a central dihyrogenborate tetrahedron, $[(HO)_2BO_2]$, sharing two common corners with two hydrogenphosphate tetrahedra, $[(H)_{1/2}OPO_3]$, as shown in *Figure 3.42a*. The $\mathit{M2}^{II}O_4(OH)_2$ coordination octahedra share common

O–corners with four hydrogenphosphate and common $O_{(OH)}$–corners of two hydrogenborate groups from the oligomeric units $[BP_2O_7(OH)_3]^{4-}$ (*Figure 3.42b*). The condensation of oligomers with the $M2^{II}$ coordination octahedra results in a three–dimensional framework characterized by elliptical channels running along [001] as shown in *Figure 3.43*. The cross section of the channels is defined by eight–membered rings formed by four $M2^{II}$ coordination octahedra, two hydrogenphosphate and two dihyrogenborate tetrahedra. Calcium ions (8–fold coordinated) are distributed within the channels.

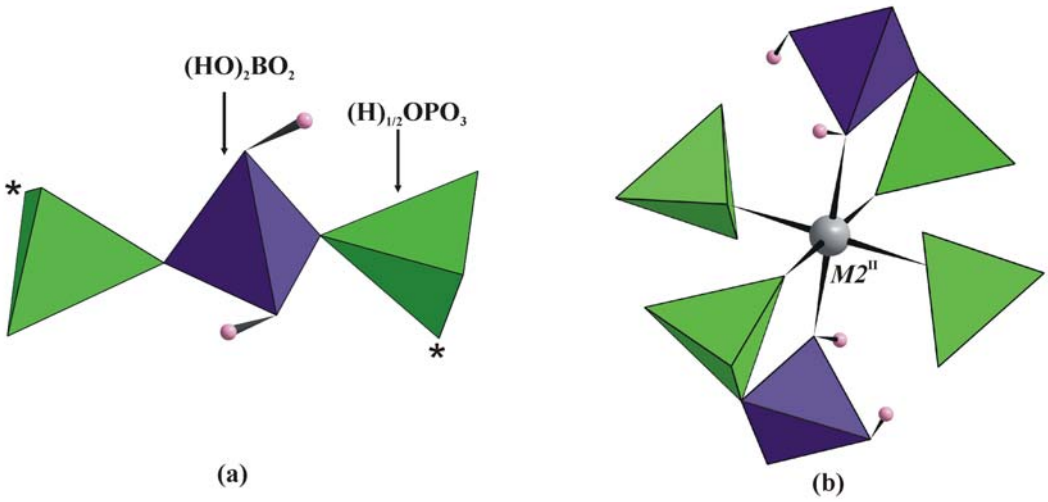

Figure 3.42: *(a) Anionic partial structure of* $CaM2^{II}[BP_2O_7(OH)_3]$ *(*$M2^{II}$ *= Fe, Ni) consisting of a central dihyrogenborate tetrahedron,* $[(HO)_2BO_2]$*, sharing two common corners with two hydrogenphosphate tetrahedra* $[(H)_{1/2}OPO_3]$*. Protons are represented by small pink spheres. Protons* $(H)_{1/2}$ *marked (*) could not be located from Fourier difference maps but assumed at that position in analogy to the isotypic compounds. (b) Octahedral coordination of* $M2^{II}$ *(*$M2^{II}$ *= Fe, Ni) by oxygen atoms of four different oligomers (four* $(H)_{1/2}OPO_3$ *tetrahedra and two* $(HO)_2BO_2$ *groups).*

In the crystal structure of $CaFe[BP_2O_7(OH)_3]$, B—O distances and O—B—O angles for the hydrogenborate tetrahedron range from 1.4606(18) Å to 1.486(2) Å and 101.35(18)° to 112.10(19)°, respectively. The P—O distances and the O—P—O angles were found to be in the range of 1.5014(7) Å to 1.5725(13) Å and 104.65(7)° to 113.75(7)°, respectively. The Fe—O distances and O—Fe—O angles take values from 2.0556(16) Å to 2.1503(17) Å and 88.52(3)° to 180.00(5)°, respectively. Calcium was found to be eight–fold coordinated by oxygen and the Ca—O contacts vary from 2.3814(13) Å to 2.5821(13) Å. The proton H5 is attached to O5 with

d(O5—H5) = 0.82(3) Å and *d*(O5···O1) = 2.748(1) Å. The second proton bound to O5 and the proton $(H)_{1/2}$ bound to O2 could not be determined but are assumed on that position in analogy to the isotypic phases. Selected bond lengths and bond angles of Ca*M2*^{II}[$BP_2O_7(OH)_3$] (*M2*^{II} = Fe, Ni) are listed in *Appendix 40* and in *Appendix 41*.

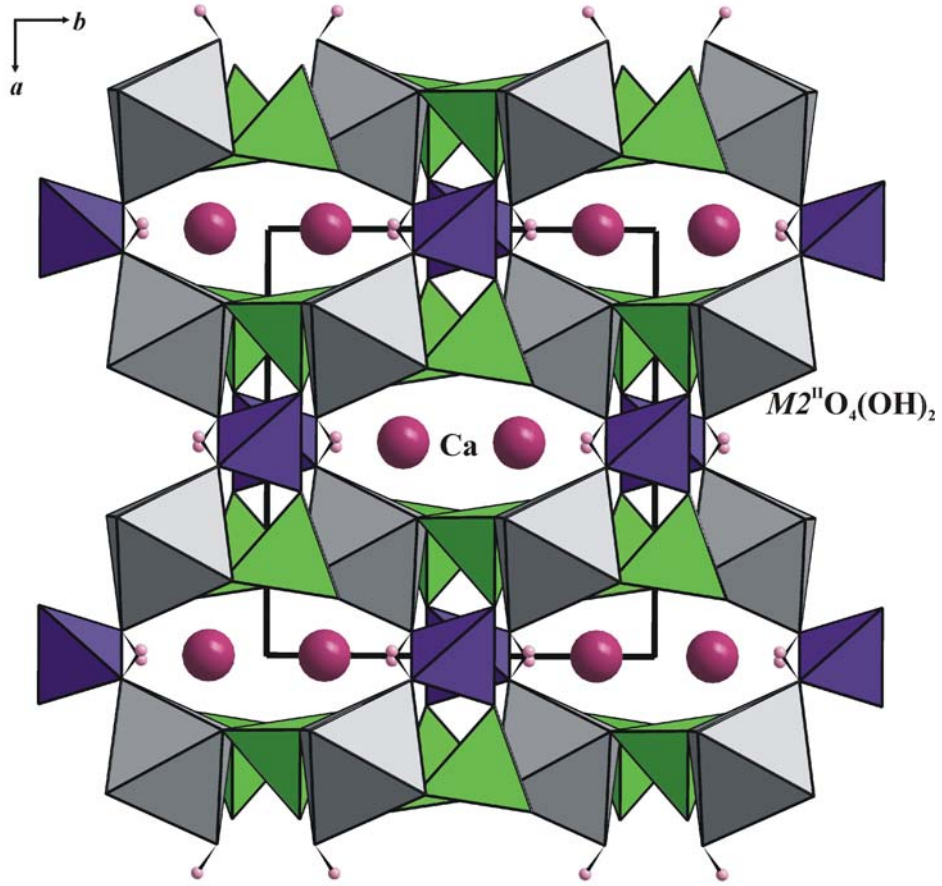

Figure 3.43: *Crystal structure of $CaM2^{II}[BP_2O_7(OH)_3]$ ($M2^{II}$ = Fe, Ni) (view along [001]): Borophosphate anions (blue $(HO)_2BO_2$ groups and green $(H)_{1/2}OPO_3$ tetrahedra) are interconnected via $M2^{II}O_4(OH)_2$ coordination octahedra (dark grey) to form a three–dimensional network. The calcium ions (violet spheres) are located within the channels formed by 8–membered rings. The unit cell is outlined.*

In case of $CaNi[BP_2O_7(OH)_3]$, the B—O distances and the O—B—O angles cover the range from 1.4447(19) Å to 1.498(2) Å and 100.93(17)° to 114.7(2)°, respectively. The P—O bond distances and the O—P—O bond angles have values from 1.5096(13) Å to 1.5655(13) Å and 103.38(8)° to 112.91(7)°, respectively. The Ni—O distances and O—Ni—O angles range between 2.0284(13) Å to 2.0931(14) Å and 88.58(7)° to 180.00(8)°, respectively. The calcium ion is eight–fold coordinated by oxygen and the

Ca—O distances vary from 2.3960(8) Å to 2.5961(13) Å. The protons H2 and H5 are attached to O2 and O5 with distances *d*(O2—H2 = 1.2713(15) Å, O5—H5 = 0.77(4) Å) and are involved in hydrogen bridges (*d*(O5···O2) = 2.966(3) Å and *d*(O2···O2) = 2.542(1) Å). The second proton $(H)_{1/2}$ bound to O1 (symmetric arrangement) could not be determined but was assumed in a position corresponding to the isotypic compounds.

3.3.2 Ba*M2*^{II}[$BP_2O_8(OH)$] (*M2*^{II} = Fe, Co)

3.3.2.1 Synthesis

BaFe[$BP_2O_8(OH)$]: Colorless platy crystals (*Figure 3.44*) were synthesized hydrothermally from a mixture of 0.87679 g $Ba(OH)_2{\cdot}8H_2O$, 1.0001 g $FeC_2O_4{\cdot}2H_2O$, 0.7740 g B_2O_3 and 3.8451 g H_3PO_4 in the molar ratio Ba : Fe : B : P = 0.5 : 1 : 2 : 6. The pH value was adjusted to 1 by the addition of 1 ml HCl (37 %). The mixture was heated at 80 ºC with 10 ml H_2O for 3 hours and filled into a 20 ml Teflon–lined autoclave. The degree of filling was about 30 %. The autoclave was heated at 170 ºC for 8 days.

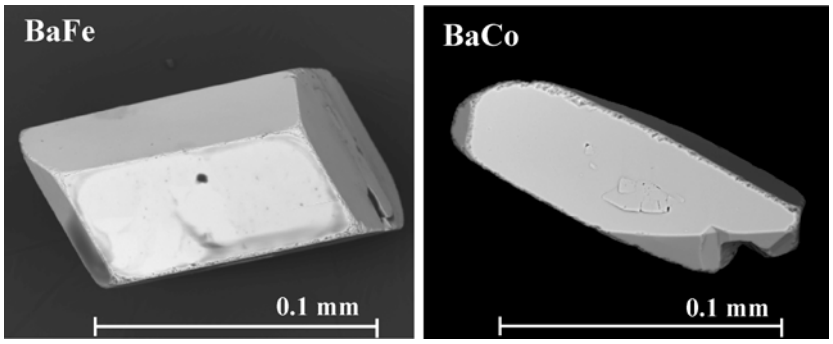

Figure 3.44: *SEM images of single crystals of BaFe[$BP_2O_8(OH)$] and BaCo[$BP_2O_8(OH)$]*

BaCo[$BP_2O_8(OH)$]: Pink platelets (*Figure 3.44*) were obtained from a mixture of 0.6332 g $Ba(OH)_2{\cdot}8H_2O$, 1.0001 g $Co(C_2H_3O_2)_2{\cdot}4H_2O$, 0.5590 g B_2O_3 and 2.7771 g H_3PO_4 in the molar ratio Ba : Co : B : P = 0.5 : 1 : 2 : 6. 10 ml of deionized water were added and the solution was stirred at 80 ºC. Meanwhile, 1 ml HCl (37 %) was added to adjust the pH value to 1. The mixture was filled into a 20 ml Teflon–lined autoclave (filling degree 40 %) and heated at 170 ºC under autogenous pressure for two weeks.

The reaction products in both cases were separated by filtration and washed with hot water / acetone and dried at 60 ºC in air. The reaction products contained crystals ranging from 0.05 mm to 0.1 mm in length. The crystals were obtained as by–products besides $Ca_{0.5}M2^{II}(H_2O)_2[BP_2O_8]\cdot H_2O$ ($M2^{II}$ = Fe, Co) as the main component. The chemical compositions (Ba : Fe : P = Ba : Co : P ≈ 1 : 1 : 2) are consistent with EDX analytical data.

3.3.2.2 Crystal Structure Determination

Selected single crystals of $BaFe[BP_2O_8(OH)$ (triclinic, space group $P\bar{1}$ (No. 2), a = 5.3393(4) Å, b = 8.0179(9) Å, c = 8.3443(10) Å, α = 89.047(15)º, β = 79.211(12)º, γ = 87.446(14)º, Z = 2) and $BaCo[BP_2O_8(OH)]$ (triclinic, space group $P\bar{1}$ (No. 2), a = 5.3147(3) Å, b = 7.9926(8) Å, c = 8.2936(8) Å, α = 88.634(14)º, β = 79.461(10)º, γ = 87.139(13)º, Z = 2) were used for crystal structure determinations and the structures were solved by direct methods. Subsequent Fourier difference analyses were used to locate Ca, Fe, Ni, P, B and O atoms. The position of the protons could not be located from the Fourier difference maps but their positions were assumed in analogy to the isotypic compounds. The refinement of the atomic coordinates and anisotropic thermal parameters led to reliability factors R1 = 0.034 ($I > 2\sigma(I)$) and wR2 = 0.083 for $BaFe[BP_2O_8(OH)]$ and R1 = 0.028 and wR2 = 0.067 for $BaCo[BP_2O_8(OH)]$ ($I > 2\sigma(I)$) considering 2252 and 2173 independent reflections, respectively.

Crystallographic data and refinement parameters are summarized in *Appendix 42* and *Appendix 43*. The final fractional atomic coordinates and equivalent / isotropic and anisotropic displacement factors are enlisted in *Appendix 44* to *Appendix 47*.

3.3.2.3 Crystal Structure Description

The crystal structure of $BaM2^{II}[BP_2O_8(OH)]$ ($M2^{II}$ = Fe, Co) is an isotype of the $M1^{I}M2^{III}$ analogues ($M1^{I}$ = K, Rb, NH_4; $M2^{III}$ = Fe, In) [48, 109, 110, 135]. The anionic partial structure comprises of open–branched four–membered rings $[B_2P_4O_{16}(OH)_2]^{8-}$, which are formed by alternating hydrogenborate and phosphate tetrahedra sharing common corners with two additional phosphate branches as shown in *Figure 3.45a*.

Each $M2^{II}$ coordination octahedra is connected to five different oligomers, $[B_2P_4O_{16}(OH)_2]^{8-}$, by sharing common oxygen corners (five corners are connected to PO_4 tetrahedra and one to the $(HO)BO_3$ group) as shown in *Figure 3.45b*. The

interconnection of the borophosphate anions with the $M2^{II}O_5(OH)$ (M^{II} = Fe, Co) coordination octahedra *via* common corners results in an overall three–dimensional framework containing channels running along [100] (*Figure 3.46*). The cross section of the channels is defined by eight–membered rings consisting of two $M2^{II}$ coordination octahedra, four phosphate tetrahedra and two hydrogenborate groups. Barium ions (10–fold coordinated) reside within the channels. Selected bond lengths and bond angles for $BaM2^{II}[BP_2O_8(OH)]$ ($M2^{II}$ = Fe, Co) are listed in *Appendix 48* and in *Appendix 49*.

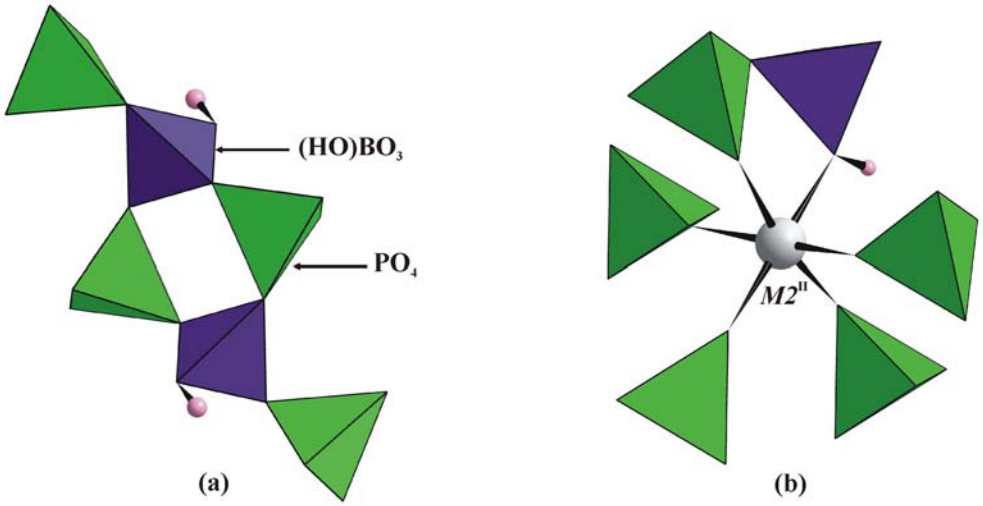

Figure 3.45: *(a) Anionic partial structure comprises of open–branched four–membered rings $[B_2P_4O_{16}(OH)_2]^{8-}$, which are formed by alternating $(HO)BO_3$ and PO_4 tetrahedra sharing common corners with two additional PO_4 branches (b) Octahedral coordination of $M2^{II}$ ($M2^{II}$ = Fe, Co) by oxygen atoms of five different oligomers (five PO_4 tetrahedra and one $(OH)BO_3$ group).*

B—O distances and O—B—O angles for the hydrogenborate tetrahedron in the crystal structure of $BaFe[BP_2O_8(OH)]$ range from 1.445(5) Å to 1.489(5) Å and 104.0(3)° to 113.2(3)°, respectively. P—O distances and O—P—O angles were found to be in the range of 1.512(3) Å to 1.590(3) Å and 103.93(15)° to 114.59(16)°, respectively. Fe—O distances and O—Fe—O angles inside the octahedra range from 2.077(3) Å to 2.255(3) Å and 81.14(10)° to 172.13(12)°, respectively. Barium was found to be ten–fold coordinated by oxygen and the Ba—O contacts vary from 2.741(3) Å to 3.020(3) Å.

In case of $BaCo[BP_2O_8(OH)]$, the B—O distances and the O—B—O angles for the hydrogenborate tetrahedron range from 1.446(5) Å to 1.492(5) Å and 104.43(3)° to 113.1(3)°, respectively. The P—O distances and the O—P—O angles have values between 1.506(3) Å to 1.590(3) Å and 103.57(15)° to 114.82(15)°, respectively. The Co—O distances and the O—Co—O angles range from 2.046(3) Å to 2.224(3) Å and 81.25(10)° to 172.62(12)°, respectively. Barium is ten–fold coordinated by oxygen and the Ba—O distance was found to be 2.742(3) Å to 2.998(3) Å. The position of the protons could not be determined and were assumed from isotypic compounds in order to maintain the charge balance [48].

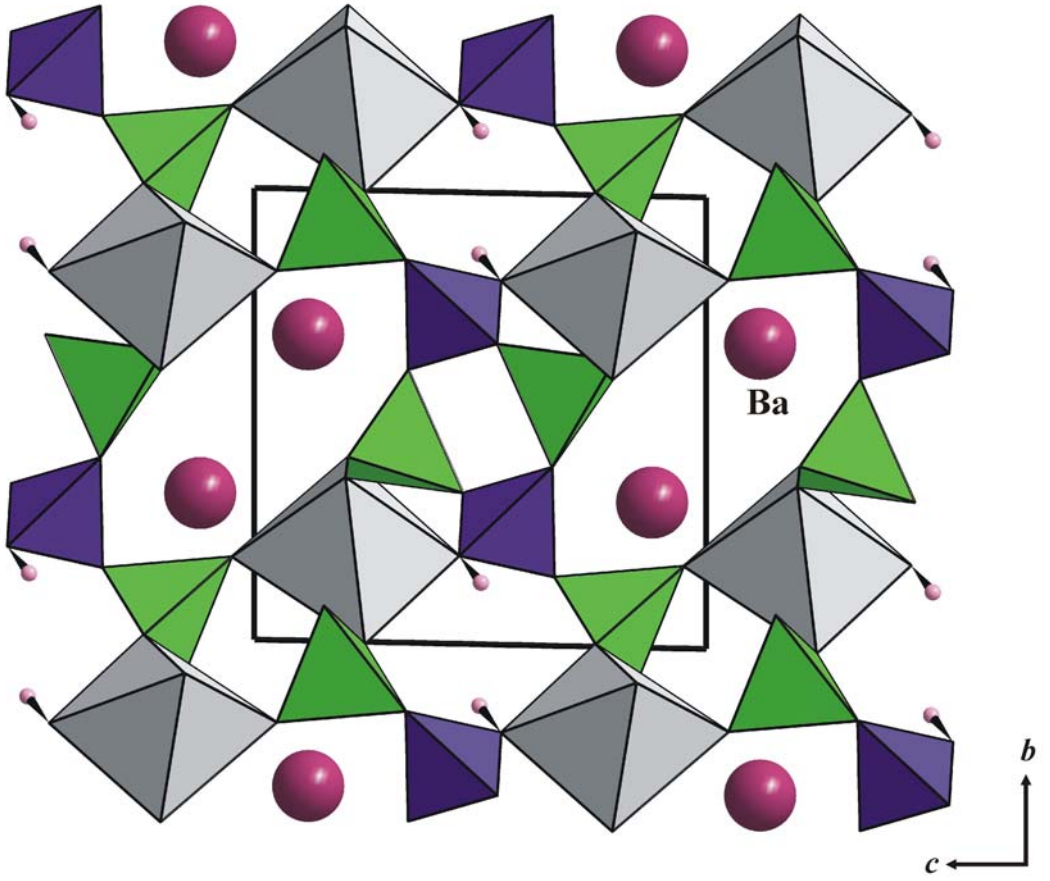

Figure 3.46: *Crystal structure of $BaM2^{II}[BP_2O_8(OH)]$ ($M2^{II}$ = Fe, Co) (view along [100]): The borophosphate anions (blue (HO)BO_3 groups, green PO_4 tetrahedra) are interconnected by $M2^{II}O_5(OH)$ octahedra (light grey) to form a three–dimensional network. Barium (violet spheres) is located within the channels. The unit cell is outlined.*

3.3.3 $SrFe^{III}[BP_2O_8(OH)_2]$

3.3.3.1 Synthesis

Colorless, transparent single crystals (*Figure 3.47*) of $SrFe^{III}[BP_2O_8(OH)_2]$ were prepared hydrothermally from a mixture of 0.7386 g $Sr(OH)_2{\cdot}8H_2O$, 0.5000 g $FeC_2O_4{\cdot}2H_2O$, 0.3870 g B_2O_3 and 1.9225 g H_3PO_4 in the molar ratio Sr : Fe : B : P = 1 : 1 : 2 : 6. The mixture was heated under stirring together with 10 ml of deionized water at 100 ºC for three hours. The pH value was adjusted to 1 by addition of 0.5 ml HCl (37 %). The reaction mixture was then filled into a Teflon–lined autoclave (filling degree 70 %) and heated under autogenous pressure at 80 ºC for 8 days. The reaction product was separated by filtration, washed with hot water, filtered and washed again with acetone and finally dried at 60 ºC in air.

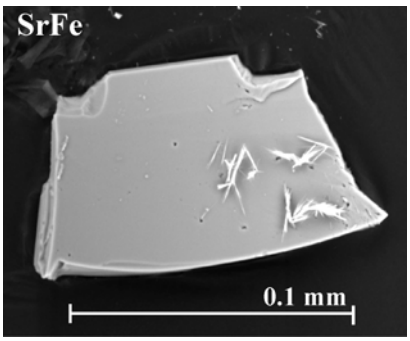

Figure 3.47: *SEM image of a single crystal of $SrFe^{III}[BP_2O_8(OH)_2]$*

The product consisted of transparent crystals of $SrFe^{III}[BP_2O_8(OH)_2]$ with dimensions ranging from 0.05 to 0.1mm. The chemical composition is consistent with EDX analytical data (Sr : Fe : P ≈ 1 :1 : 2).

3.3.3.2 Crystal Structure Determination

X–ray data were collected from suitable single crystals. The space group was determined to be triclinic $P\bar{1}$ (No. 2) (a = 6.6704(12) Å, b = 6.6927(13) Å, c = 9.3891(19) Å, α = 109.829(5)º, β = 102.068(6)º, γ = 103.151(3)º, Z = 2). Direct methods and subsequent Fourier difference analyses were used to locate Sr, Fe, P, B and O positions. Protons (H9 and H10) were determined from Fourier difference maps. The refinement of the atomic coordinates and anisotropic thermal parameters led to reliability factors R1 = 0.041 and wR2 = 0.101 considering 2244 independent

reflections ($I > 2\sigma(I)$). Attempts were also made to refine the crystal structure in space group $C2/c$ but without success (further details are given in the discussion). Crystallographic data and refinement parameters are summarized in *Appendix 50*. The final fractional atomic coordinates and equivalent / isotropic and anisotropic displacement factors are listed in *Appendix 51* and *Appendix 52*.

3.3.3.3 Crystal Structure Description

The oligomeric borophosphate unit of $SrFe^{III}[BP_2O_8(OH)_2]$ consists of an unbranched tetrahedral triple, $[BP_2O_8(OH)_2]^{5-}$, built up by a central dihyrogenborate tetrahedron, $(HO)_2BO_2$, sharing two common corners with two phosphate tetrahedra as shown in *Figure 3.48a*.

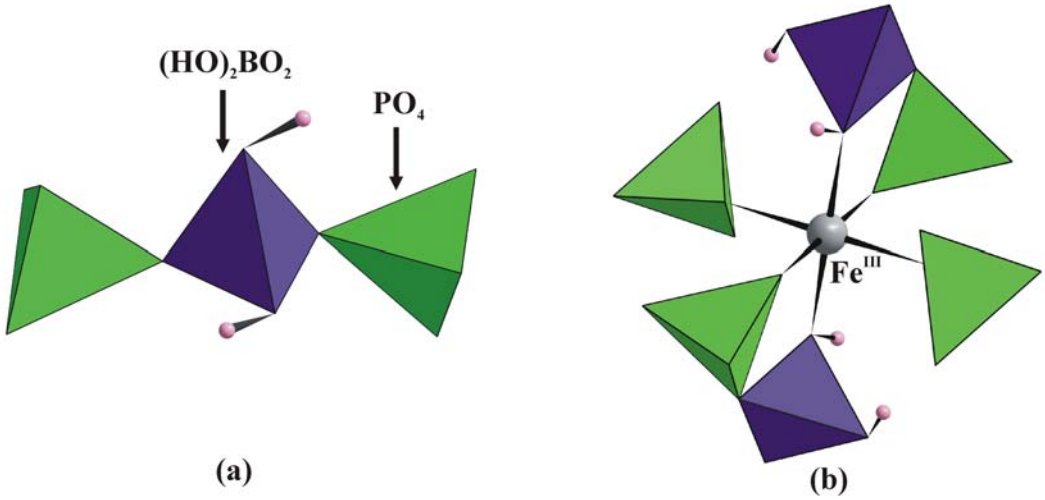

Figure 3.48: *(a) Anionic partial structure of $SrFe^{III}[BP_2O_8(OH)_2]$ consisting of an unbranched tetrahedral triple, $[BP_2O_8(OH)_2]^{5-}$, built up by a central $(HO)_2BO_2$, sharing two common corners with two PO_4 tetrahedra, (b) Octahedral coordination of Fe^{3+} by oxygen atoms of four different oligomers (four PO_4 tetrahedra and two $(HO)_2BO_2$ groups).*

The borophosphate oligomers are interconnected by Fe^{3+} ions, forming distorted isolated $FeO_4(OH)_2$ coordination octahedra *via* neighbouring O–corners of phosphate and $O_{(OH)}$–corners of hydrogenborate groups (*Figure 3.48b*). This interconnection results in a three–dimensional framework characterized by elliptical channels running along [011] (*Figure 3.49*). The cross section of the channels is defined by eight–membered rings formed by four iron coordination octahedra, two phosphate and two hydrogenborate tetrahedra. Strontium ions (10–fold coordinated) are distributed within the channels.

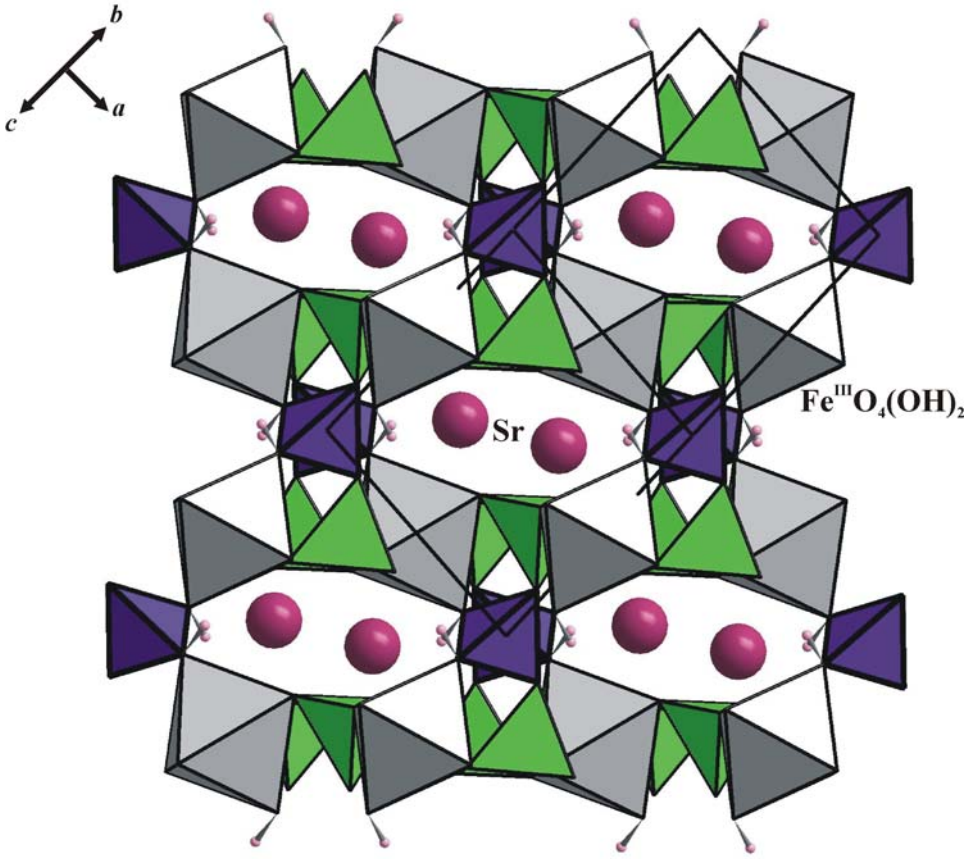

Figure 3.49: *Crystal structure of SrFe[$BP_2O_8(OH)_2$] viewed along [011]: The borophosphate anions (blue $(HO)_2BO_2$ groups, green PO_4 tetrahedra) are interconnected by $Fe^{III}O_4(OH)_2$ coordination octahedra (dark grey) to form a three–dimensional network. The Sr ions (violet spheres) are located within the channels formed by 8–membered rings. The unit cell is outlined.*

The Fe—O distances inside the octahedra and the O—Fe—O angles range from 1.989(2) Å to 2.163(3) Å and 87.39(11)° to 180.0(2)°, respectively. P—O bond lengths within the phosphate tetrahedra range from 1.506(3) Å to 1.575(3) Å. The O—P—O angles vary from 105.30(15)° to 113.05(17)°. In the dihyrogenborate tetrahedra the B—O distances range from 1.430(4) Å to 1.506(5) Å (with B—OH being the shortest). O—B—O angles take values between 102.3(3)° to 113.7(3)°. Bond distances (P—O, B—O) and the bond angles (O—P—O, O—B—O) in the oligomeric borophosphate groups are similar to those in related borophosphates [12, 29]. The protons H9 and H10 are attached to O9 and O10, respectively (d(O9—H9) = 0.89(6) Å, d(O10—H10) = 1.00(5) Å), and are involved in hydrogen bridges (O9—H9···O1 with d(O9···O1) = 3.106(3) Å and O10—H10···O5 with d(O10···O5) = 2.764(1) Å). Strontium is ten–fold coordinated by oxygen. The Sr—O contacts vary

from 2.519(3) Å to 3.084 (3) Å. Selected interatomic distances and bond angles are listed in *Appendix 53.*

3.3.3.4 Magnetic Susceptibility

Within the range of 40 – 400 K the temperature dependent magnetic susceptibility of $SrFe[BP_2O_8(OH)_2]$ can be described by a Curie–Weiss law with 6.1 μ_B (θ = –42.6 K). The effective magnetic moment derived from this measurement is comparable with the expected value of 5.9 – 6 μ_B for weak field octahedral coordination and five unpaired electrons for Fe^{III} [136].

3.3.4 $CaCo(H_2O)[BP_2O_8(OH)]\cdot H_2O$

3.3.4.1 Synthesis

Pink platelets (*Figure 3.50*) of $CaCo(H_2O)[BP_2O_8(OH)]\cdot H_2O$ were synthesized under mild hydrothermal conditions. A mixture of 0.2974 g $Ca(OH)_2$, 1.0005 g $Co(C_2H_3O_2)_2\cdot 4H_2O$, 0.5590 g B_2O_3 and 2.7771 g H_3PO_4, molar ratio Ca : Co : B : P = 1 : 1: 2 : 6, was heated to 80 ºC by stirring together with 10 ml of deionized water. Meanwhile, 1 ml HCl (37 %) was added to adjust the pH value to 1. The reaction mixture was then filled into a Teflon–lined autoclave (filling degree 40 %) and heated under autogenous pressure at 170 ºC for 7 days. The reaction product was filtered, washed with hot water / acetone and finally dried in air at 60 ºC.

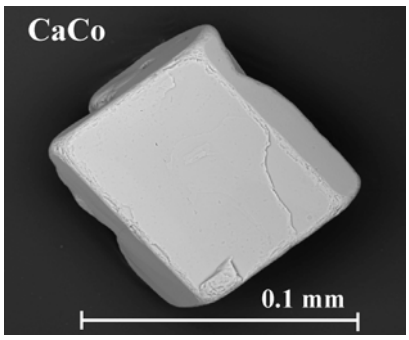

Figure 3.50: *SEM image of a single crystal of $CaCo(H_2O)[BP_2O_8(OH)]\cdot H_2O$*

The pink platelets of $CaCo(H_2O)[BP_2O_8(OH)]\cdot H_2O$ were obtained as a by–product (BPO_4 was the main product). Single crystals with dimensions ranging from 0.05 mm to 0.1 mm were isolated from the mixture. The chemical composition is consistent with EDX analytical data (Ca : Co : P ≈ 1 : 1 : 2).

3.3.4.2 Crystal Structure Determination

The crystal structure was solved in the triclinic space group $P\bar{1}$ (No. 2) (a = 6.5793(3) Å, b = 7.8320(1) Å, c = 8.8172(1) Å, α = 68.785(7)º, β = 82.719(6)º, γ = 73.985(9)º, Z = 2). Subsequent difference Fourier analyses led to the atomic coordinates of the heavy atoms. The H atoms were also located from Fourier difference maps and the O—H distances for the water molecule were constrained to vary around 0.80(5) Å during the final refinement. The refinement of the atomic coordinates and anisotropic displacement parameters led to reliability factors R1 = 0.043 and wR2 = 0.107 considering 2261 independent reflections ($I > 2\sigma(I)$).
The crystallographic data and refinement parameters are summarized in *Appendix 54*. The final fractional atomic coordinates and equivalent / isotropic and anisotropic displacement factors are listed in *Appendix 55* and *Appendix 56*.

3.3.4.3 Crystal Structure Description

The anionic partial structure of $CaCo(H_2O)[BP_2O_8(OH)]\cdot H_2O$ comprises open–branched four–membered rings, $[B_2P_4O_{16}(OH)_2]^{8-}$, which are formed by alternating hydrogenborate and phosphate tetrahedra sharing common corners with two additional phosphate branches as shown in *Figure 3.45a*. The dimer $Co_2O_8(H_2O)_2$ is formed by two $CoO_3O_{2/2}(H_2O)$ octahedra as shown in *Figure 3.51*.

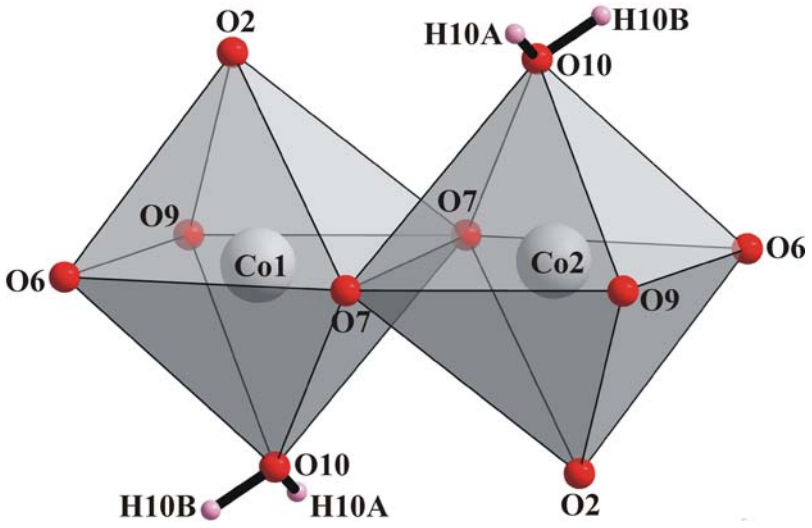

Figure 3.51: *Dimer of edge–sharing cobalt coordination octahedra in the crystal structure of $CaCo(H_2O)[BP_2O_8(OH)]\cdot H_2O$*

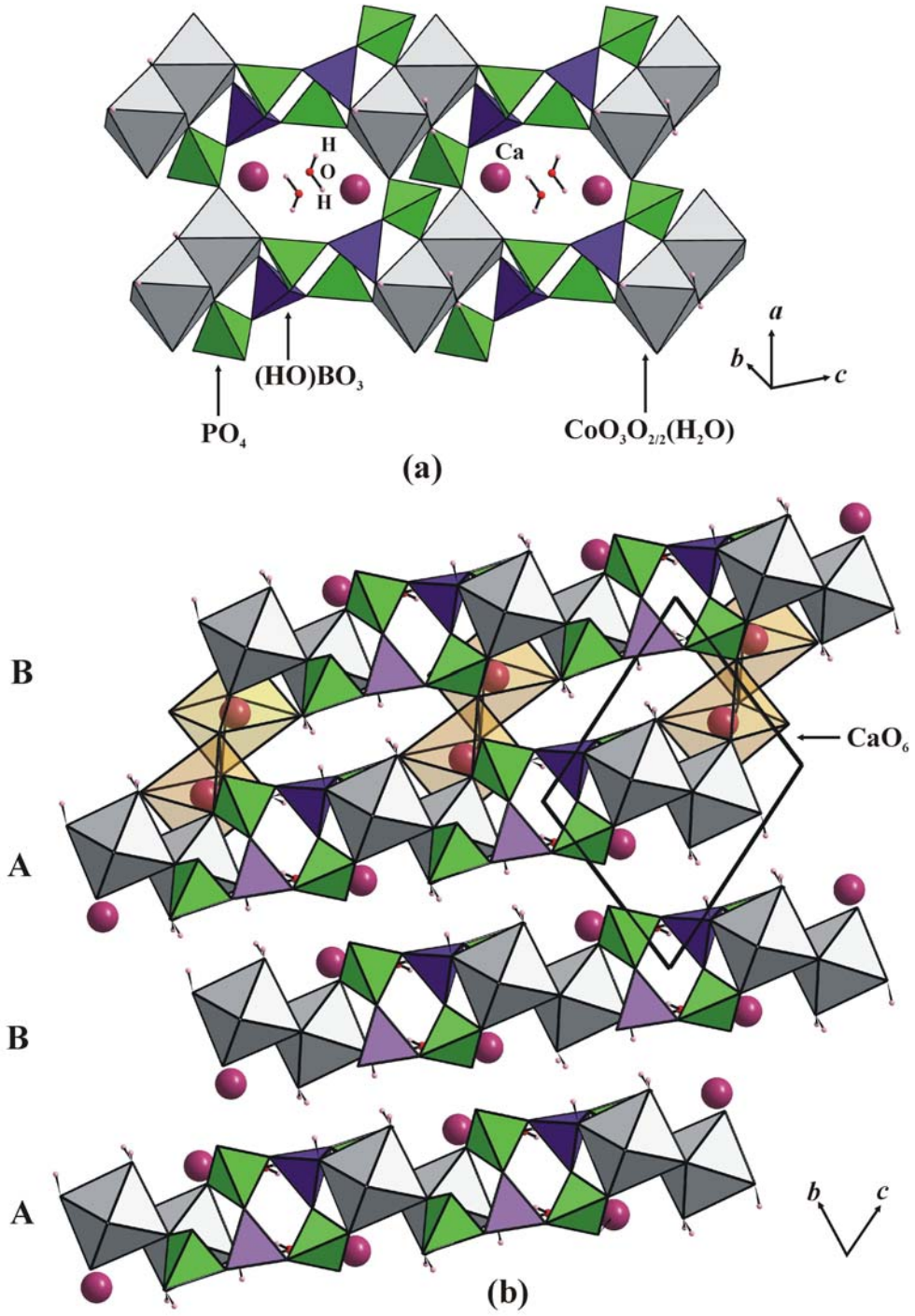

***Figure 3.52**: (a) Interconnection of borophosphate oligomers $[B_2P_4O_{16}(OH)_2]^{8-}$ with $Co_2O_8(H_2O)_2$ octahedral dimers to form layers containing eight–membered rings. Calcium ions and crystal water are located close to the eight–membered rings. (b) Crystal structure of $CaCo(H_2O)[BP_2O_8(OH)]\cdot H_2O$ viewed along [100], representing the stacking of the layers presented in (a) with the sequence ABAB... . CaO_6 coordination octahedra connecting the layers are presented in yellow colour. The unit cell is outlined.*

The interconnection of borophosphate oligomers with dimers of coordination octahedra, $CoO_3O_{2/2}(H_2O)$, results in layers containing eight–membered rings as shown in *Figure 3.52a*. Calcium ions and crystal water reside close to the eight–membered rings. The overall crystal structure of $CaCo(H_2O)[BP_2O_8(OH)]\cdot H_2O$ is characterized by stacking of the layers along [011] (*Figure 3.52b*) with the sequence *ABAB*… . Inter–layer contacts are formed by CaO_6 coordination polyhedra

Selected interatomic distances are listed in *Appendix 57*. The P—O bond lengths within the phosphate tetrahedra range from 1.509(2) Å to 1.584(2) Å. O—P—O angles vary from 106.15(12)° to 112.2(5)°. Bond lengths (B—O) and bond angles (O—B—O) within the hydrogenborate tetrahedra range from 1.449(4) Å to 1.478(4) Å (with shorter B—OH bonds) and 104.3(2)° to 112.4(3)°, respectively. Bond distances (P—O, B—O) and bond angles (O—P—O, O—B—O) within the oligomeric units are similar to related borophosphates [12, 29]. The cobalt coordination octahedra share a common edge to form dimers $[Co_2O_8(H_2O)_2]$ with Co—Co distances of 3.1667(4) Å. The dimers are connected to six PO_4 tetrahedra, two $(HO)BO_3$ tetrahedra and two coordinating water molecules. Co—O distances and O—Co—O angles in the Co coordination octahedra range from 2.038(3) Å to 2.160(2) Å and 83.31(9)° to 174.08(9)°, respectively. Calcium is found to be hexacoordinated with distances Ca—O between 2.338(2) Å and 2.403(2) Å. The proton H9 is attached to O9 with *d*(O9—H9) = 0.83(6) Å and *d*(O9—H9···O5; O9···O5) = 2.778(1) Å. The protons H10A and H10B are connnected to O10 (aqua ligand) with *d*(O10—H10A = 0.79(3) Å; O10—H10B = 0.78(3) Å; O10—H10A···O8; O10···O8 = 2.748(1) Å; O10—H10B···O5; O10···O5 = 2.815(1) Å). The protons of the crystal water, H11A and H11B, are attached to O11 with distances O11—H11A = 0.81(3) Å and O11—H11B = 0.78(3) Å, respectively. The angles H10A—O10—H10B and H11A—O11—H11B are 103(6)° and 117(7)°, respectively.

3.3.5 $M1^{II}_{0.5}M2^{II}(H_2O)_2[BP_2O_8]\cdot H_2O$ ($M1^{II}_{0.5}$ = Ca, Sr, Ba; $M2^{II}$ = Fe, Co, Ni)

3.3.5.1 Synthesis

A large variety of cations M^I, M^{II} and M^{III} (M^I = Li–Cs; M^{II} = Mn–Zn; M^{III} = Fe, Sc, In) and their combinations are known to balance the three negative charges per formula unit of the helical anion $^1{}_\infty[BP_2O_8]^{3-}$.

Single crystals of $M1^{II}_{0.5}M2^{II}(H_2O)_2[BP_2O_8]\cdot H_2O$ ($M1^{II}_{0.5}$ = Ca, Sr, Ba; $M2^{II}$ = Fe, Co, Ni) were prepared by mild hydrothermal synthesis. The reaction mixtures (see *Table 3.9*) were homogenized in 10 ml of water and acidified with 1 ml HCl (37 %). The water was evaporated slowly to form a gel which was then treated hydrothermally at 170 ºC.

Table 3.9: *Experimental conditions for the preparation of $M1^{II}_{0.5}M2^{II}(H_2O)_2[BP_2O_8]\cdot H_2O$ ($M1^{II}$ = Ca, Sr, Ba; $M2^{II}$ = Fe, Co, Ni) at 170 ºC*

Compound	Chemicals used	Molar Ratio	Weight (g)	Reaction Conditions
	$Ca(OH)_2$	1	0.7453	pH = 1
$Ca_{0.5}Fe$	$FeCl_2\cdot 4H_2O$	2	1.0005	Filling 30%
	B_2O_3	2	0.7003	V = 20 ml
	H_3PO_4	6	3.4793	10 days
	$Ca(OH)_2$	1	0.2974	pH = 1
$Ca_{0.5}Co$	$Co(CH_3COO)_2\cdot 4H_2O$	1	1.0009	Filling 40%
	B_2O_3	2	0.5590	V = 20 ml
	H_3PO_4	6	2.7771	7 days
	$Ca(OH)_2$	1	0.2480	pH = 1
$Ca_{0.5}Ni$	NiO	1	0.2500	Filling 30%
	B_2O_3	4	0.4606	V = 10 ml
	H_3PO_4	6	2.3153	8 days
	$Sr(OH)_2\cdot H_2O$	0.25	0.2216	pH = 1
$Sr_{0.5}Co$	CoO	1	0.2500	Filling 30%
	B_2O_3	2	0.4645	V = 10 ml
	H_3PO_4	6	2.3078	8 days
	$Ba(OH)_2\cdot 8H_2O$	0.5	1.3151	pH = 1
$Ba_{0.5}Fe$	$FeC_2O_4\cdot 2H_2O$	1	1.5003	Filling 50%
	B_2O_3	2	1.1610	V = 20 ml
	H_3PO_4	6	5.7677	8 days
	$Ba(OH)_2\cdot 8H_2O$	1	1.2665	pH = 1
$Ba_{0.5}Co$	$Co(CH_3COO)_2\cdot 4H_2O$	1	1.0008	Filling 40%
	B_2O_3	2	0.5590	V = 20 ml
	H_3PO_4	6	2.7771	7 days
	$Ba(OH)_2\cdot 8H_2O$	0.25	0.2639	pH = 1
$Ba_{0.5}Ni$	NiO	1	0.2500	Filling 30%
	B_2O_3	2	0.4660	V = 10 ml
	H_3PO_4	6	2.3153	6 days

The reaction products were cooled down to ambient temperature and were separated by vacuum filtration. The colorless bipyramids of $Ca_{0.5}Fe(H_2O)_2[BP_2O_8]\cdot H_2O$ and $Ba_{0.5}Fe(H_2O)_2[BP_2O_8]\cdot H_2O$, the violet bipyramids of $Ca_{0.5}Co(H_2O)_2[BP_2O_8]\cdot H_2O$, $Sr_{0.5}Co(H_2O)_2[BP_2O_8]\cdot H_2O$ and $Ba_{0.5}Co(H_2O)_2[BP_2O_8]\cdot H_2O$), and the yellow bipyramids of $Ca_{0.5}Ni(H_2O)_2[BP_2O_8]\cdot H_2O$ and $Ba_{0.5}Ni(H_2O)_2[BP_2O_8]\cdot H_2O$ were

washed with hot water / acetone and filtered before they were dried in air at 60 ºC. SEM micrographs of the obtained crystals are shown in *Figure 3.53* and *Figure 3.54*. Phase purities for the reaction products were checked using powder X–ray diffraction. The cobalt containing compounds were obtained as phase pure reaction products (*Figure 3.55* to *Figure 3.57*).

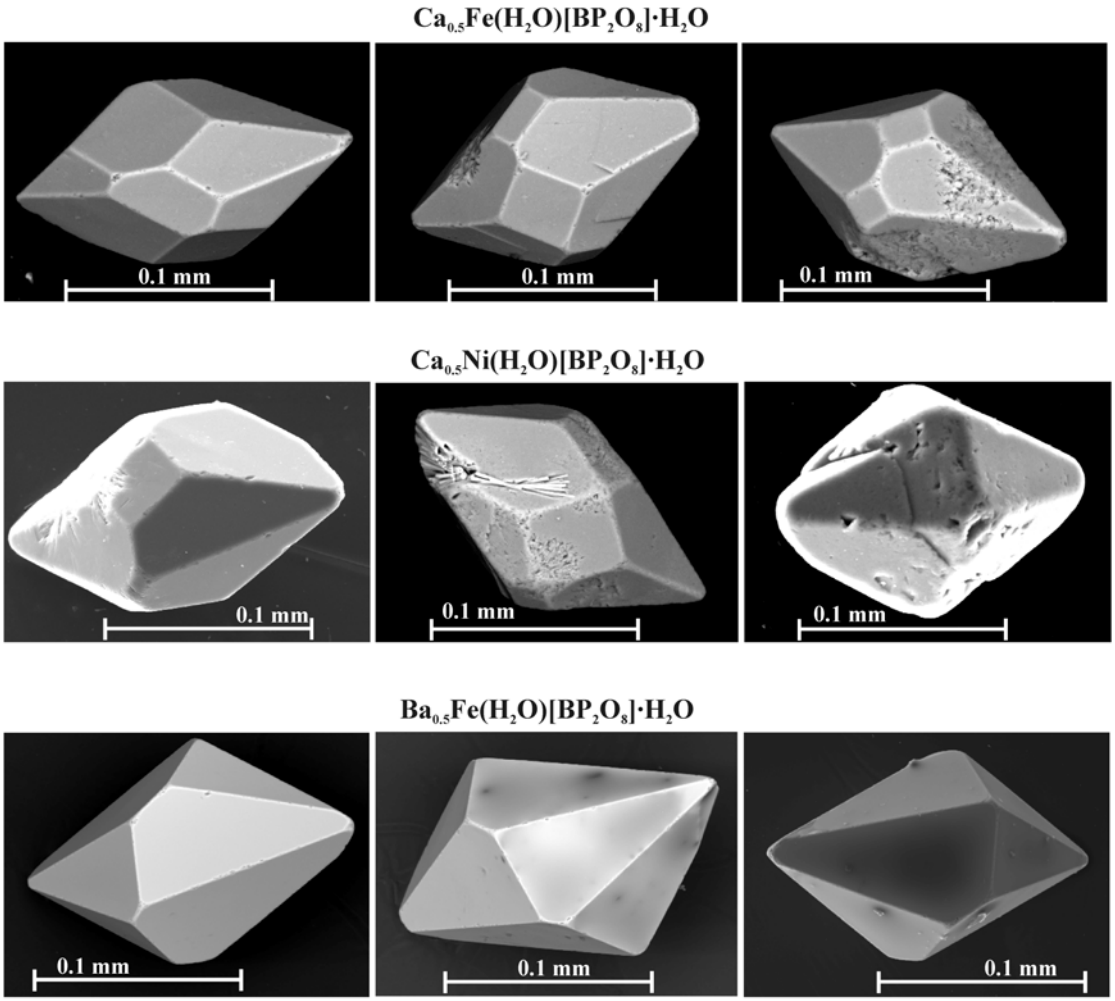

Figure 3.53: *SEM images of single crystals of $M1^{II}_{0.5}M2^{II}(H_2O)_2[BP_2O_8]\cdot H_2O$ ($M1^{II}$ = Ca, Ba; $M2^{II}$ = Fe, Ni) which shows no superstructure.*

The results of the chemical analyses of $Ca_{0.5}Co(H_2O)_2[BP_2O_8]\cdot H_2O$, $Sr_{0.5}Co(H_2O)_2[BP_2O_8]\cdot H_2O$, $Ba_{0.5}Co(H_2O)_2[BP_2O_8]\cdot H_2O$ are given in *Table 3.10*. The elements calcium, strontium, barium, cobalt, boron and phosphorus were analyzed using ICP–OES, while the hot extraction method was applied for hydrogen. The molar ratio of the products Ca : Co : B : P = 0.52 : 1 : 1.02 : 2.04, Sr : Co : B : P =

0.49 : 1 : 1.01 : 2 and Ba : Co : B : P = 0.46 : 1 : 1.03 : 1.99 is in accordance with the chemical formula obtained from the single–crystal structure refinements. Except for boron and hydrogen the presence of the elements were additionally confirmed by EDX measurements.

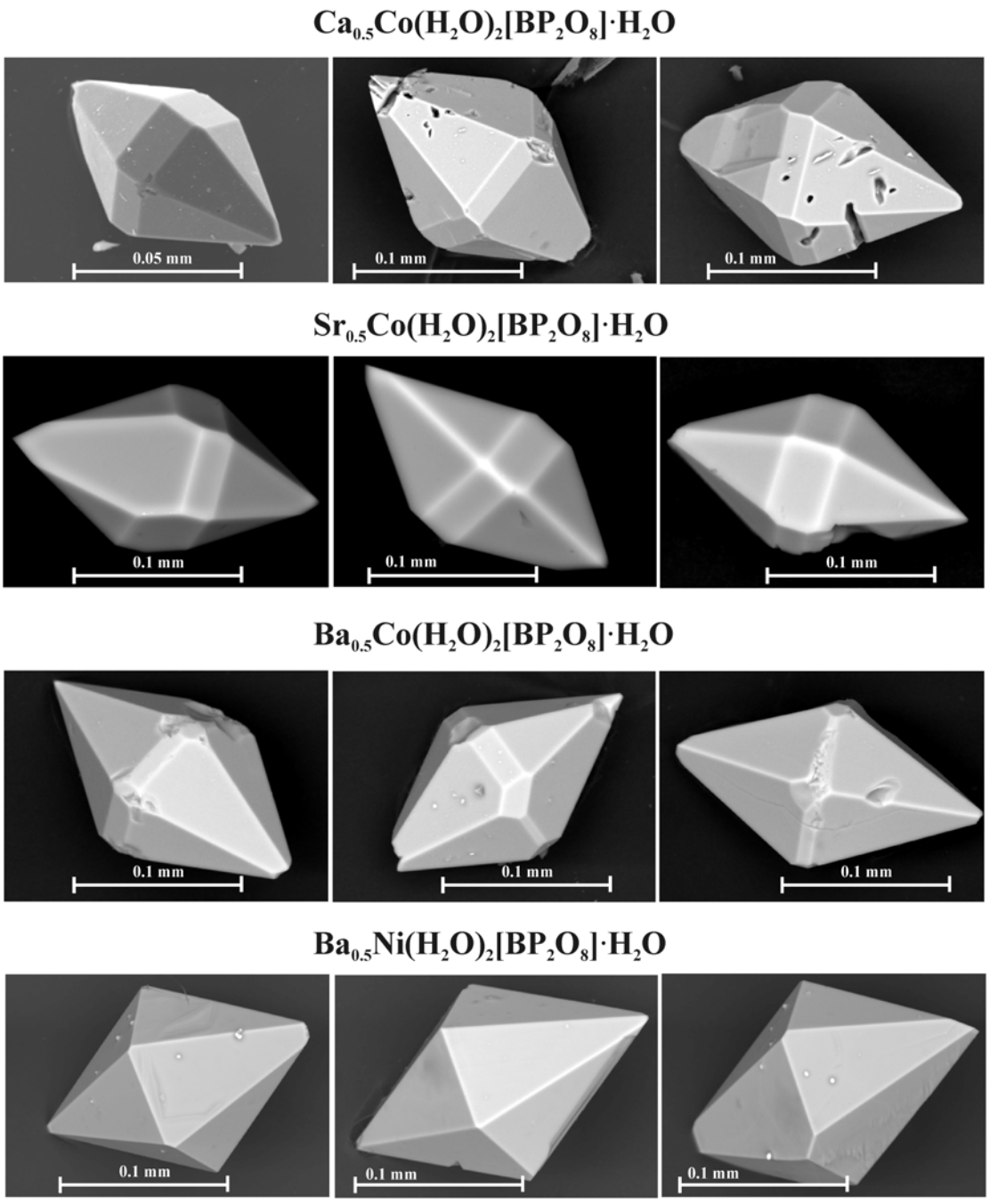

Figure 3.54: *SEM images of single crystals of $M1^{II}_{0.5}M2^{II}(H_2O)_2[BP_2O_8]\cdot H_2O$ ($M1^{II}$ = Ca, Sr, Ba; $M2^{II}$ = Co, Ni).*

Table 3.10: *Results of chemical analyses of $MI^{II}_{0.5}Co(H_2O)_2[BP_2O_8]\cdot H_2O$ (MI^{II} = Ca, Sr, Ba)*

Element	Observed (e.s.d.) weight %	Calculated weight %
Ca	6.13(2)	6.0
Co	17.22(5)	17.65
B	3.25(1)	3.23
P	18.48(8)	18.55
O	44.53(2)	52.72
H	1.80(4)	1.81
Sr	11.93(11)	12.25
Co	16.16(17)	16.48
B	3.02(2)	3.02
P	17.05(20)	17.32
O	44.8(5)	49.22
H	1.73(1)	1.69
Ba	17.31(2)	17.92
Co	15.81(8)	15.41
B	3.01(2)	2.82
P	16.40(10)	16.20
O	38.5(2)	46.04
H	1.46(4)	1.58

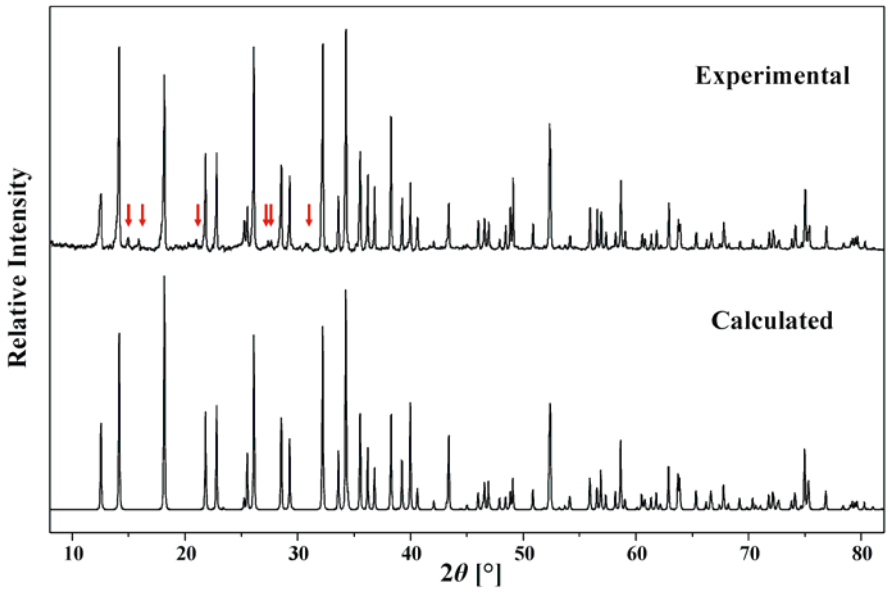

Figure 3.55: *Observed (background subtracted) and calculated (substructure) powder X–ray diffraction patterns of $Ca_{0.5}Co(H_2O)_2[BP_2O_8]\cdot H_2O$. Observed superstructure reflections are marked by red arrows (Co $K_{\alpha 1}$–radiation).*

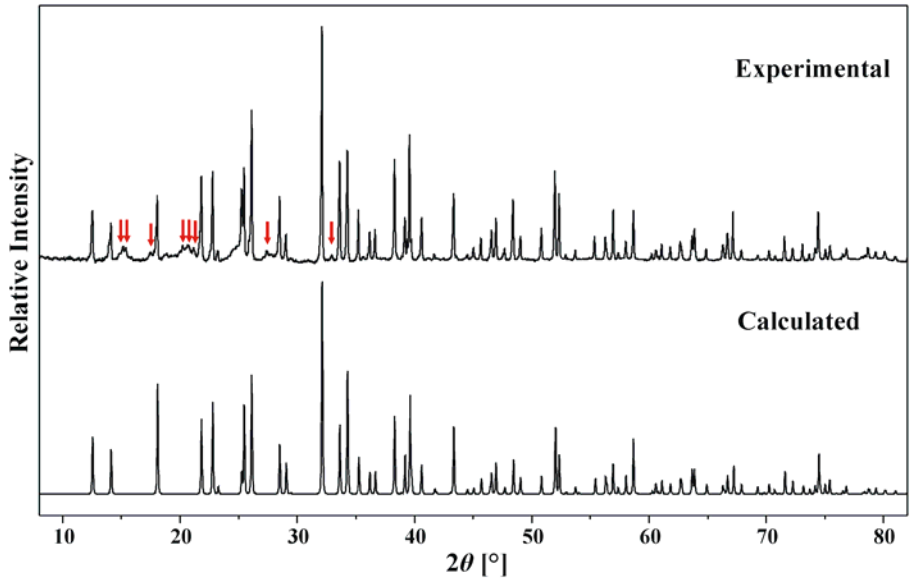

Figure 3.56: *Observed (background subtracted) and calculated (substructure) powder X–ray diffraction patterns of $Sr_{0.5}Co(H_2O)_2[BP_2O_8]\cdot H_2O$. Observed superstructure reflections are marked by red arrows (Co $K_{\alpha 1}$–radiation).*

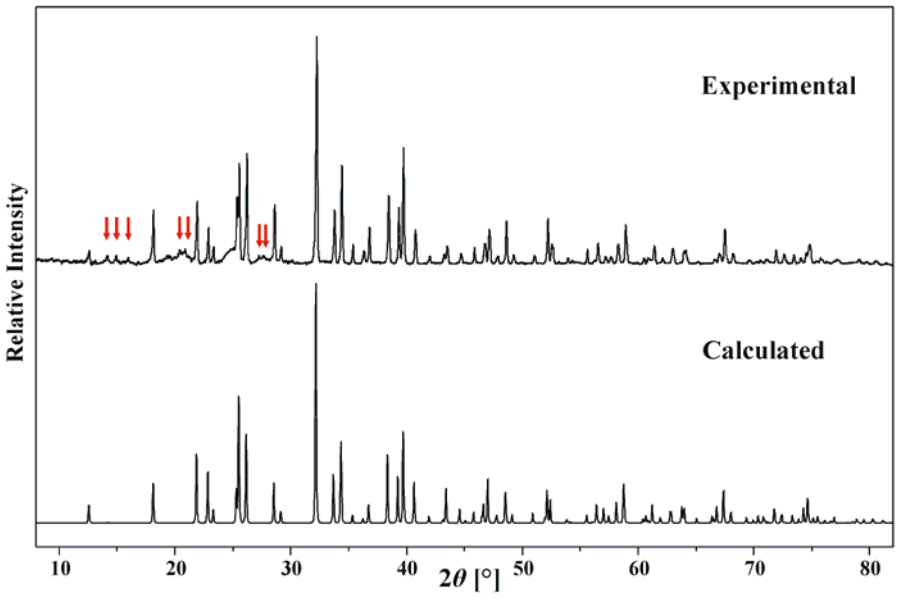

Figure 3.57: *Observed (background subtracted) and calculated (substructure) powder X–ray diffraction patterns of $Ba_{0.5}Co(H_2O)_2[BP_2O_8]\cdot H_2O$. Observed superstructure reflections are marked by red arrows (Co $K_{\alpha 1}$–radiation)*

3.3.5.2 Crystal Structure Determination

Suitable hexagonal bipyramidal single crystals were selected for X–ray investigations. The Laue method was used to check the quality of the single crystals. The intensity data were collected only for appropriate individuals. The crystal structures of $Ca_{0.5}Fe(H_2O)_2[BP_2O_8]\cdot H_2O$ and $Ca_{0.5}Ni(H_2O)_2[BP_2O_8]\cdot H_2O$ were solved in the space groups $P6_522$ (No.179) (a = 9.5091(4) Å, c = 15.734(1) Å, Z = 6) and $P6_122$ (No.178) (a = 9.3715(3) Å, c = 15.7261(6) Å, Z = 6) of the hexagonal system by direct methods. Subsequent Fourier difference analyses were used to locate all the atoms. The occupancy of the Ca site was refined without any restrains. In the final refinement cycles the occupancy was fixed to 0.25. The positions of the hydrogen atoms close to O5 (coordinating water) were located in a Fourier difference maps. Their coordinates and isotropic displacement parameters were refined without any restraints. For the oxygen atom of the hydrate water (O6), a split model was assumed with occupancy factor of 0.5 [67, 69, 73, 111]. The corresponding hydrogen atoms could not be localized. However, only lattice parameters were determined for $Ba_{0.5}Fe(H_2O)_2[BP_2O_8]\cdot H_2O$ (a = 9.4447(3) Å, c = 15.7337(9) Å) due to the bad quality of the investigated crystal.

From the obtained single crystal X–ray diffraction data including superstructure reflections, it was not possible to develop an appropriate structural model for the compounds $M1^{II}_{0.5}M2^{II}(H_2O)_2[BP_2O_8]\cdot H_2O$ ($M1^{II}$ = Ca, Sr, Ba; $M2^{II}$ = Co, Ni). Lattice parameters with $\sqrt{3}\,a$ (in comparison with the $M^{I}M^{II}(H_2O)_2[BP_2O_8]\cdot H_2O$, M^{I} = Li – Cs; Mn – Zn) were observed for $Ca_{0.5}Co(H_2O)_2[BP_2O_8]\cdot H_2O$ (a = 16.3724(5) Å, c = 15.6980(7) Å) and $Sr_{0.5}Co(H_2O)_2[BP_2O_8]\cdot H_2O$ (a = 15.8287(8) Å, c = 15.8287(8) Å) while the c axes remained unchanged. The superstructure reflections suggested that the unit cell must be magnified by the factor 3 ($a' = 2a + b$, $b' = -a + b$, c′ = c). $Ba_{0.5}Co(H_2O)_2[BP_2O_8]\cdot H_2O$ (a = 18.8665(5) Å, c = 31.5967(15 Å) is also affected by a superstructure with doubled a and c axis. In all the investigated cases the supercell was transformed into the subcell and the crystal structures were solved in the hexagonal space groups $P6_522$ (No.179) (a = 9.4526(3) Å, c = 15.6980(7) Å for $Ca_{0.5}Co$, a = 9.4434(3) Å, c = 15.8287(8) Å for $Sr_{0.5}Co$ and a = 9.4333(3) Å, c = 15.7984(8) Å for $Ba_{0.5}Co$) by direct methods. The handedness (6_1 or 6_5) was assessed on the basis of the Flack x parameter of the investigated individuals. The protons bound to hydrate water could not be determined from Fourier difference maps.

For $Ba_{0.5}Ni(H_2O)_2[BP_2O_8]\cdot H_2O$ (a = 16.11 Å, c = 15.81 Å), only the supercell ($\sqrt{3}\,a$, c) was determined (no complete data collection). The presence of additional structural reflections (marked by red arrows) on the basis of powder X–ray examinations are shown in *Figure 3.55* to *Figure 3.57*. The problem of finding the proper structural model has already been explained for $M^{I}_{x}M^{II}_{y}(H_2O)_2[BP_2O_8]\cdot zH_2O$ (M^{I}_{x} = Rb, Cs; M^{II}_{y} = Mg, Mn, Fe, Co) [42] and $M1^{II}_{0.5}Mg(H_2O)_2[BP_2O_8]\cdot H_2O$ ($M1^{II}_{0.5}$ = Ca, Sr, Ba) compounds [45]. The lattice parameters of the supercell and subcell for all compounds are listed in *Table 3.11*.

It seems that the crystal morphology (*Figure 3.53* and *Figure 3.54*) corresponds with the "kind of superstructure". The morphology of the crystals presented in *Figure 3.53* are clearly non-centrosymmetric and they do not show superstructure reflections where as in *Figure 3.54* an additional face grows between two bipyramidal faces which show superstructure. This may be a hint to identify the handedness of the crystals (L or R) from the morphology.

The crystallographic data and refinement parameters for all compounds are summarized in *Appendix 58* to *Appendix 64*. The final fractional atomic coordinates, equivalent / isotropic and anisotropic displacement parameter factors are given in *Appendix 65* to *Appendix 74.*

Table 3.11: *Space group and lattice parameters of $M1^{II}_{0.5}M2^{II}(H_2O)_2[BP_2O_8]\cdot H_2O$ ($M1^{II}$ = Ca, Sr, Ba; $M2^{II}$ = Fe, Co, Ni).*

	Space group	a (Å)	c (Å)	a (Å)	c (Å)
		Sub cell		Super cell	
$Ca_{0.5}Fe$	$P6_522$ (No.179)	9.5091(4)	15.734(1)		
$Ca_{0.5}Ni$	$P6_122$ (No.178)	9.3715(3)	15.7261(6)		
$Ba_{0.5}Fe$[a]		9.4447(3)	15.7337(9)		
$Ca_{0.5}Co$	$P6_522$ (No.179)	9.4526(3)	15.6980(7)	16.3724(5)	15.6980(7)
$Sr_{0.5}Co$	$P6_522$ (No.179)	9.4434(3)	15.8287(8)	16.3564(5)	15.8287(8)
$Ba_{0.5}Co$	$P6_522$ (No.179)	9.4333(3)	15.7984(8)	18.8665(5)	31.5967(15)
$Ba_{0.5}Ni$[a]				16.11	15.81

[a] only the lattice parameters were determined on a single crystal diffractometer; no complete data collection

3.3.5.3 Crystal Structure Description

The anionic partial structure of helical borophosphates contains one–dimensional infinite loop–branched borophosphate helices, $^{1}_{\infty}[BP_2O_8]^{3-}$, which are wound around a

left– or right–handed six–fold screw axis (6_1 or 6_5 helix) built of alternatively borate and phosphate tetrahedra (*Figure 3.58*). The borate groups share all their oxygen apices with the neighbouring four phosphate tetrahedra. The phosphate tetrahedra are connected only to two BO_4 units. The resulting structural motif can be described as a spiral ribbon of four–membered rings of tetrahedra in which PO_4 and BO_4 groups alternate. The phosphate groups occupy the borders of the ribbons with two terminal oxygen atoms as shown in *Figure 3.58*. The chiral architecture is closely related to Chiral Zinc Phosphate–topology [42, 137, 138], which has been previously observed in the crystal structure of $NaZnPO_4 \cdot H_2O$ [137] and its cobalt substituted variant (tetrahedral frameworks) [139]. In comparison to these crystal structures, boron in the borophosphate helices replaces the position of Zn1 in $NaZnPO_4 \cdot H_2O$.

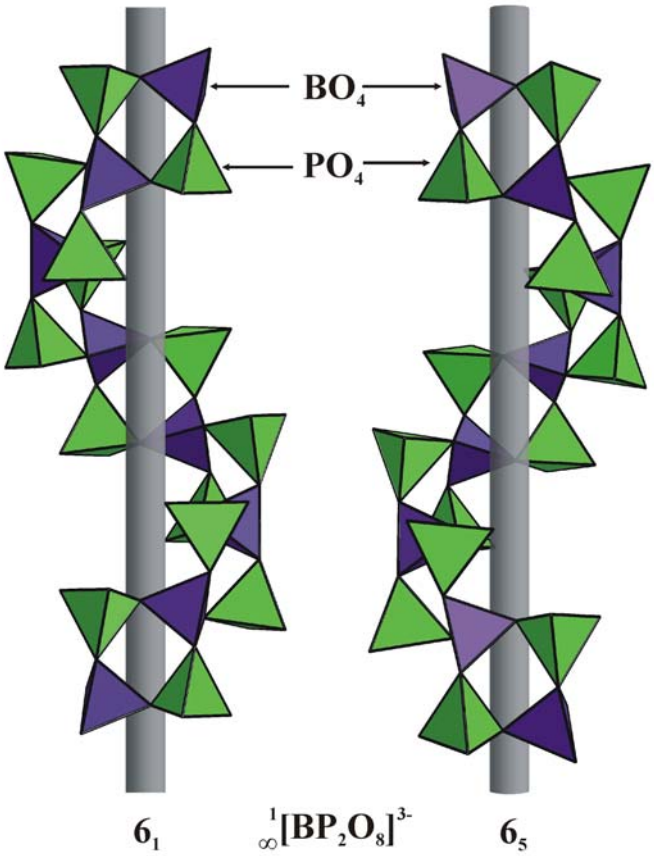

Figure 3.58: *Anionic partial structures, $^1_\infty[BP_2O_8]^{3-}$, in the crystal structure of $M1^{II}_{0.5}M2^{II}(H_2O)_2[BP_2O_8] \cdot H_2O$ ($M1^{II}_{0.5}$ = Ca, Sr, Ba; $M2^{II}$ = Fe, Co, Ni) built of four–membered rings of tetrahedra in which BO_4 and PO_4 are alternate and forming a spiral ribbon (6_1 or 6_5 helix).*

The crystal structure of $M1^{II}_{0.5}M2^{II}(H_2O)_2[BP_2O_8]\cdot H_2O$ ($M1^{II}_{0.5}$ = Ca, Sr, Ba; $M2^{II}$ = Fe, Co, Ni) is shown in *Figure 3.59*. Helical chains $^1_\infty[BP_2O_8]^{3-}$, running along [001], are placed on the edges of the hexagonal unit cell and are interconnected *via* $M2^{II}O_4(OH_2)_2$ ($M2^{II}$ = Fe, Co, Ni) coordination octahedra. The hydrate water is located within the helical channels.

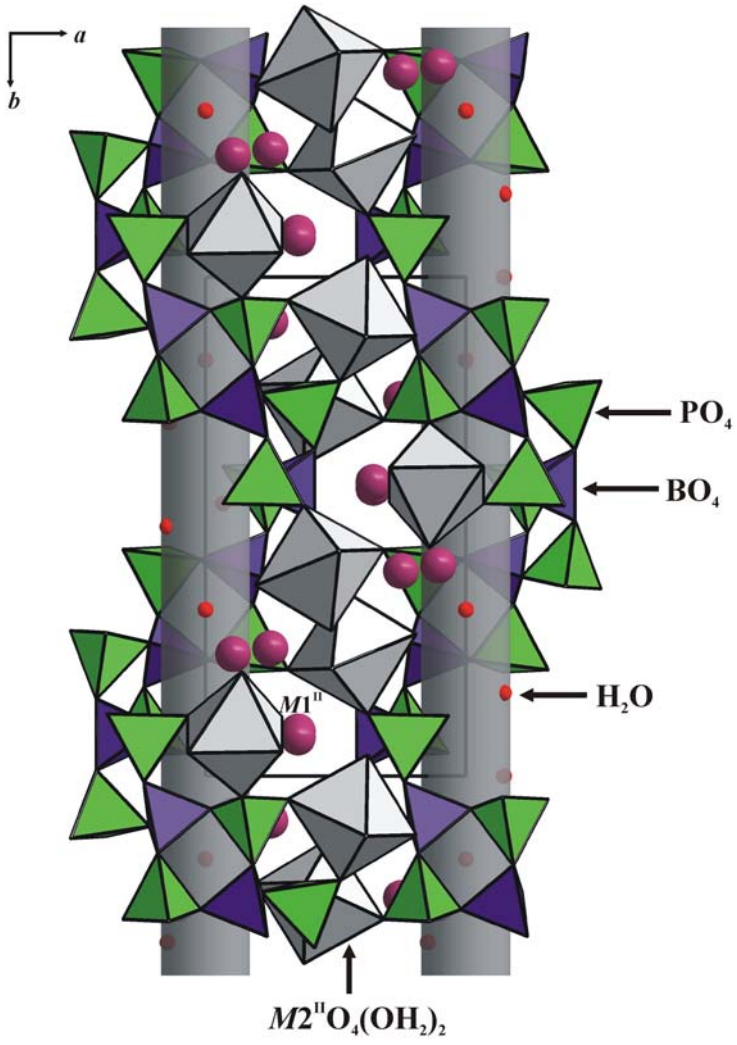

Figure 3.59: *Crystal structure $M1^{II}_{0.5}M2^{II}(H_2O)_2[BP_2O_8]\cdot H_2O$ ($M1^{II}_{0.5}$ = Ca, Sr, Ba; $M2^{II}$ = Fe, Co, Ni). Helical chains $^1_\infty[BP_2O_8]^{3-}$, running along [001] and interconnected via $M2^{II}O_4(OH_2)_2$ coordination octahedra (protons are omitted for clarity). The position of the $M1^{II}$ site is only 25 % occupied. The hydrate water (red spheres) is located within the helical channels (indicated as grey tubes). The unit cell is outlined.*

$M2^{II}$ is six–fold coordinated by four oxygen atoms originating from phosphate groups and two water molecules. The helices, $^1_\infty[BP_2O_8]^{3-}$, are connected *via* $M2^{II}O_4(OH_2)_2$ ($M2^{II}$ = Fe, Co, Ni) coordination octahedra and the free threads of the helices are

quarterly (25 %) occupied by $M1^{II}$($M1^{II}$ = Ca, Sr) which are fixed by an irregular surroundings of oxygen atoms from the adjacent phosphate groups (*Figure 3.59*). The arrangement of helices can be illustrated as a dense packing of rods (*Figure 3.60*) and the location of the hydrate water (O6) could be located inside the channels.

In the refined crystal structure (substructure) of $M1^{II}_{0.5}M2^{II}(H_2O)_2[BP_2O_8]\cdot H_2O$ ($M1^{II}_{0.5}$ = Ca, Sr, Ba; $M2^{II}$ = Fe, Co, Ni), the B—O distances and the O—B—O angles for the borate tetrahedron for all the compounds range from 1.452(3) Å to 1.481(5) Å and 101.6(4)° to 114.3(3)°, respectively. Similarly, the P—O distances and the O—P—O angles are in the range of 1.500(3) Å to 1.571(4) Å and 105.66(14)° to 116.05(11)°, respectively. The metal atoms ($M2^{II}$) are six–fold coordinated by oxygen and distances $d(M2^{II}—O)$ are in between 2.052(2) Å and 2.280(4) Å. Calcium is seven–fold coordinated (see *Figure 3.69*) by oxygen with distances d(Ca—O) = 2.38(2) – 2.674(19) Å in case of $Ca_{0.5}Fe$, d(Ca—O) = 2.210(5) – 2.654(4) Å in case of $Ca_{0.5}Co$ and d(Ca—O) = 2.328(17) – 2.718(5) Å for $Ca_{0.5}Ni$.

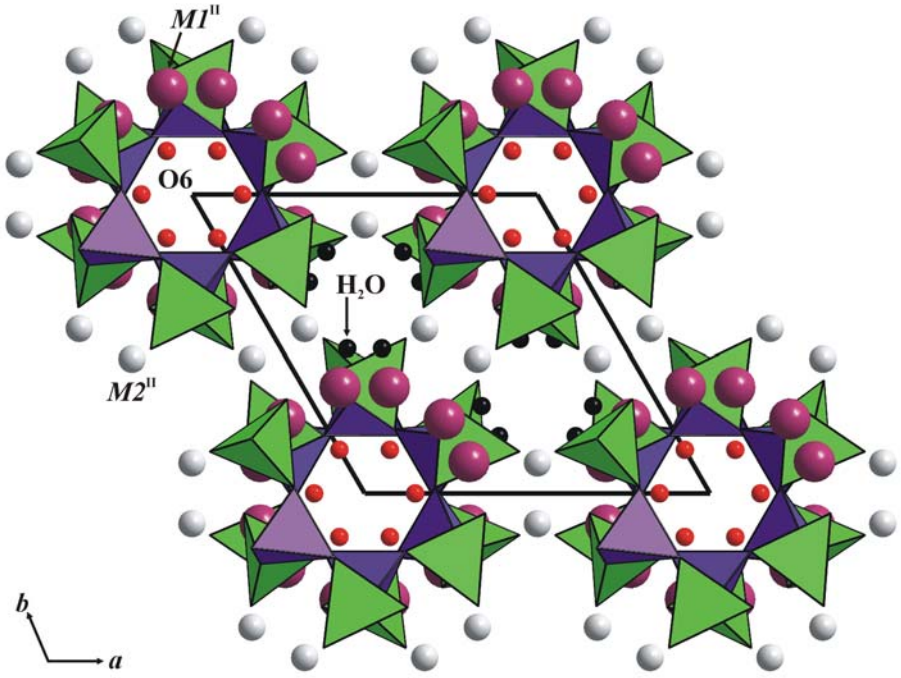

Figure 3.60: *Crystal structure of $M1^{II}_{0.5}M2^{II}(H_2O)_2[BP_2O_8]\cdot H_2O$ ($M1^{II}_{0.5}$ = Ca, $M2^{II}$ = Fe, Ni) along [001], illustrating the arrangement of the chains in a dense rod–packing motif and the hydrate water (O6, red spheres) could be located within the helical channels. The oxygen of the coordination water (H_2O) attached to $M2^{II}$ is shown as black spheres.*

Sr and Ba in the crystal structure of $Sr_{0.5}Co(H_2O)_2[BP_2O_8]\cdot H_2O$ and $Ba_{0.5}Co(H_2O)_2[BP_2O_8]\cdot H_2O$ are nine–fold coordinated (see *Figure 3.69*) by oxygen with distances *d*(Sr—O) = 2.349(6) – 3.303(4) Å and *d*(Ba—O) = 2.295(14) – 3.133(15) Å), respectively. In the crystal structures of $Ca_{0.5}Fe(H_2O)_2[BP_2O_8]\cdot H_2O$), and $Ca_{0.5}Ni(H_2O)_2[BP_2O_8]\cdot H_2O$, the protons H5A and H5B are attached to O5 (aqua ligand) with distances *d*(O5—H5A) = 0.80(5) Å, *d*(O5—H5A···O1) = 2.758(1) Å , and *d*(O5—H5B) = 0.82(4) Å, *d*(O5—H5B···O4) = 2.813(1) Å) for $Ca_{0.5}Fe(H_2O)_2[BP_2O_8]\cdot H_2O$) and distances *d*(O5—H5A) = 0.87(4) Å; *d*(O5—H5B) = 0.79(4) Å; *d*(O5—H5A···O4) = 2.796(1) Å; *d*(O5—H5B···O1) = 2.729(1) Å) for $Ca_{0.5}Ni(H_2O)_2[BP_2O_8]\cdot H_2O$), respectively.

Selected bond lengths and bond angles of $M1^{II}_{0.5}M2^{II}(H_2O)_2[BP_2O_8]\cdot H_2O$ ($M1^{II}_{0.5}$ = Ca, Sr, Ba; $M2^{II}$ = Fe, Co, Ni) are listed in *Appendix 75* to *Appendix 79*.

3.3.5.4 Thermal Analysis

The thermal properties of $M1^{II}_{0.5}Co(H_2O)_2[BP_2O_8]\cdot H_2O$ ($M1^{II}_{0.5}$ = Ca, Sr, Ba) were analyzed by thermogravimetric (TG) and difference thermal analyses (DTA) with heating and cooling rates of 5 K / min up to 1000 ºC in a continuous argon gas flow.

Previously, it has been reported that the compounds $NaZn(H_2O)_2[BP_2O_8]\cdot H_2O$ [88] and $Fe(H_2O)_2[BP_2O_8]\cdot H_2O$ [68] show two step mass loss releasing 2 mol of water (coordination) per formula unit in the first step. In contrast to that, the compound $Sc(H_2O)_2[BP_2O_8]\cdot H_2O$ [67] first releases the 1 mol of water (hydrate) per molecule per formula unit upon thermal treatment till 250 ºC.

The dehydration of $M1^{II}_{0.5}M2^{II}(H_2O)_2[BP_2O_8]\cdot H_2O$ ($M1^{II}_{0.5}$ = Ca, Sr, Ba; $M2^{II}$ = Co) is a two step process (*Figure 3.61*). In the first step (100 – 250 ºC) 2 mol of water are released (as reported for $NaZn(H_2O)_2[BP_2O_8]\cdot H_2O$ [88] and $Fe(H_2O)_2[BP_2O_8]\cdot H_2O$) [68]. The last mol of water is lost at 250 – 750 ºC (*Figure 3.61*). Further studies to investigate the release of water (coordination or hydrate) after the first step were not carried out.

Simultaneously recorded DTA traces for heating and cooling are shown in *Figure 3.62*. The main mass loss of $M1^{II}_{0.5}Co(H_2O)_2[BP_2O_8]\cdot H_2O$ ($M1^{II}_{0.5}$ = Ca, Sr, Ba) is accompanied by broad endothermic ($Ca_{0.5}Co$: 214 ºC, 258 ºC; $Sr_{0.5}Co$: 224 ºC; $Ba_{0.5}Co$: 204 ºC) and exothermic effects ($Ca_{0.5}Co$: 690 ºC; $Sr_{0.5}Co$: 397 ºC and 696 ºC ; $Ba_{0.5}Co$: 722 ºC). During cooling an exothermic peak at 941 ºC ($Ca_{0.5}Co$) and at 950 ºC ($Sr_{0.5}Co$) is observed.

After the DTA / TG runs, the products were analyzed by powder X–ray diffraction showing unidentified diffraction patterns along with BPO_4 [140]. The powder patterns could not be indexed. Details concerning thermal effects and decomposition products are summarized in *Table 3.12*.

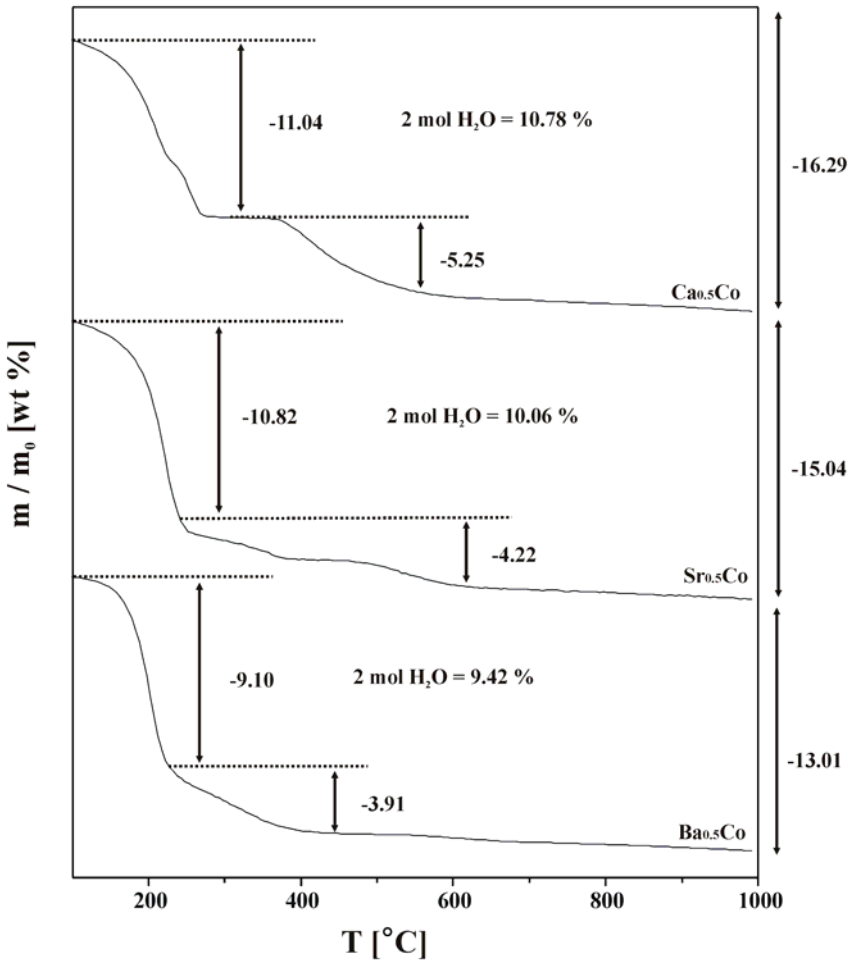

Figure 3.61: *Thermogravimetric curves of $M1^{II}_{0.5}Co(H_2O)_2[BP_2O_8]\cdot H_2O$ ($M1^{II}_{0.5}$ = Ca, Sr, Ba) recorded with heating rates of 5 K / min. The mass loss (weight %) is given at the right.*

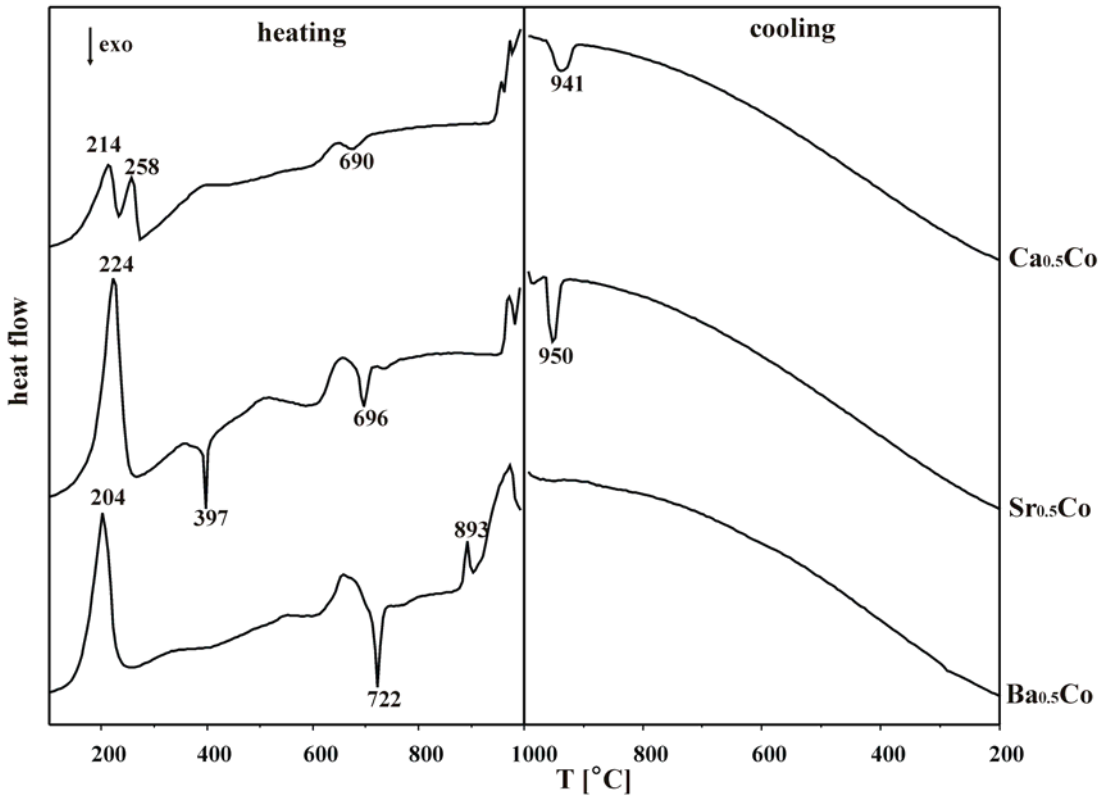

Figure 3.62: *DTA traces during thermal decomposition of $MI^{II}_{0.5}Co(H_2O)_2[BP_2O_8]\cdot H_2O$ ($MI^{II}_{0.5}$ = Ca, Sr, Ba) recorded for the heating (left) and the cooling segment (right) (rate ± 5 °C / min).*

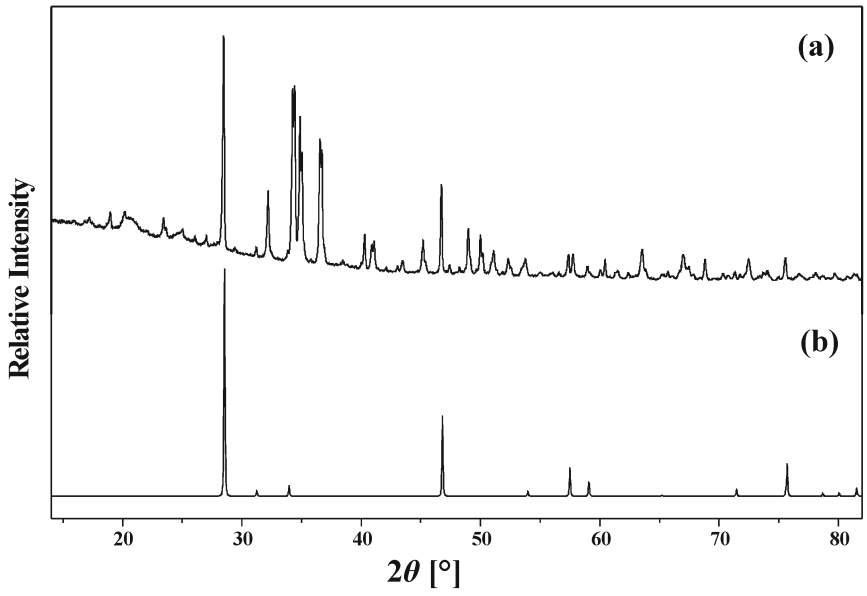

Figure 3.63: *Powder X–ray diffraction patterns of (a) the decomposition product of $Ca_{0.5}Co(H_2O)_2[BP_2O_8]\cdot H_2O$ after heating to 1000 °C, and (b) compared with the calculated powder diffraction pattern of α–BPO_4 [140] (Co $K_{\alpha 1}$–radiation)*

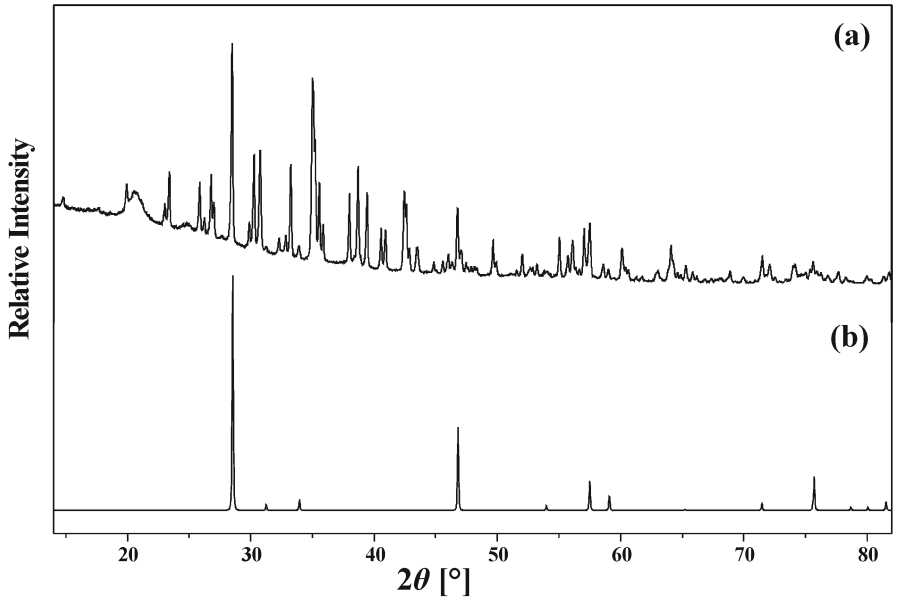

Figure 3.64: *Powder X–ray diffraction pattern of (a) the decomposition product of $Sr_{0.5}Co(H_2O)_2[BP_2O_8]\cdot H_2O$ heated to 1000 °C, and (b) the calculated powder diffraction pattern of α–BPO_4 [140] (Co $K_{\alpha 1}$–radiation)*

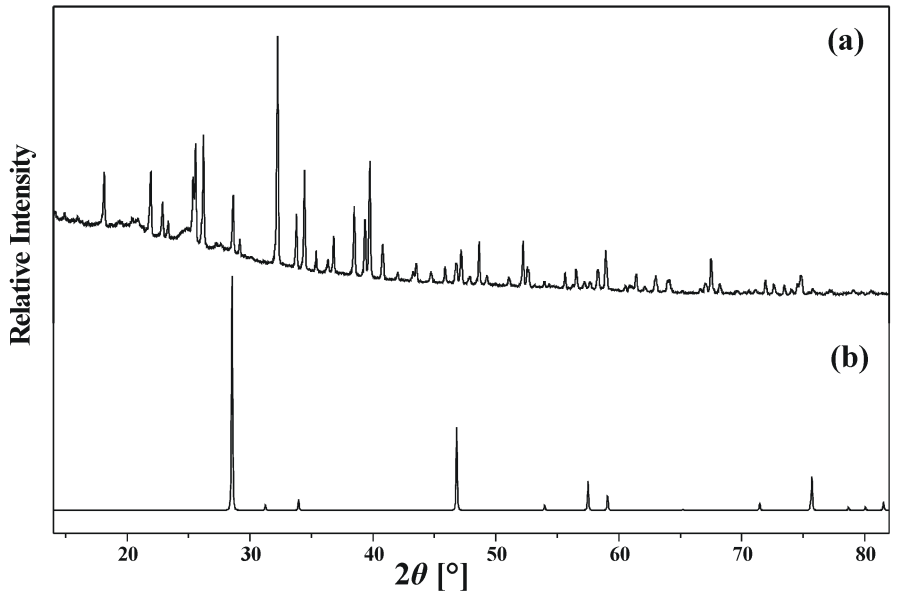

Figure 3.65: *Powder X–ray diffraction pattern of (a) the decomposition product of $Ba_{0.5}Co(H_2O)_2[BP_2O_8]\cdot H_2O$ heated to 1000 °C, and (b) the calculated powder diffraction pattern of (α–BPO_4 [140] (Co $K_{\alpha 1}$–radiation)*

Table 3.12: *Thermal analyses of $M1^{II}_{0.5}Co(H_2O)_2[BP_2O_8]\cdot H_2O$ ($M1^{II}_{0.5}$ = Ca, Sr, Ba)*

Compound	Mol. Wt.	Expt. mass loss (wt %)	Calc. mass loss (wt %)	Decomposition product
$Ca_{0.5}Co$	333.77	16.29	16.17 ($3 \times H_2O$)	α–BPO_4 [140] + Unidentified
$Sr_{0.5}Co$	357.52	15.04	15.12 ($3 \times H_2O$)	α–BPO_4 [140] + Unidentified
$Ba_{0.5}Co$	382.36	13.01	14.13 ($3 \times H_2O$)	α–BPO_4 [140] + Unidentified

3.3.5.5 Magnetic Susceptibility

Magnetic susceptibility measurements of $M1^{II}_{0.5}Co(H_2O)_2[BP_2O_8]\cdot H_2O$ ($M1^{II}_{0.5}$ = Ca, Sr, Ba) were performed on powdered samples in the temperature range of 1.8 – 400 K with an applied field of 1 Tesla. Within the range of 40 – 400 K the temperature dependent magnetic susceptibility of $M1^{II}_{0.5}Co(H_2O)_2[BP_2O_8]\cdot H_2O$ ($M1^{II}_{0.5}$ = Ca, Sr, Ba) can be described by a Curie–Weiss law with 6.12 μ_B (θ = –4.8 K) for $Ca_{0.5}Co(H_2O)_2[BP_2O_8]\cdot H_2O$, 6.02 μ_B (θ = –8.4 K) for $Sr_{0.5}Co(H_2O)_2[BP_2O_8]\cdot H_2O$ and 6.15 μ_B (θ = –7.1 K) for $Ca_{0.5}Co(H_2O)_2[BP_2O_8]\cdot H_2O$. The effective magnetic moment derived from the measurement was found to be very high with the expected value of 4.7 – 5.2 μ_B in the octahedral coordination and for d^7 ions (Co^{2+}). The higher magnetic moment was due to the contributions from unidentified magnetic impurities which hide the genuine magnetic behavior.

3.3.6 Discussion

This section consists of four parts. The first part discusses the anionic partial structures of $[BP_2O_7(OH)_3]^{4-}$ and $[BP_2O_8(OH)_2]^{5-}$. The second part, the anion $[B_2P_4O_{16}(OH)_2]^{8-}$ and the new dimer $CoO_3O_{2/2}(H_2O)$. In the third part, the significant differences in the crystal structures and coordination of $M1^{II}$ in $M1^{II}_{0.5}M2^{II}(H_2O)_2[BP_2O_8]\cdot H_2O$ ($M1^{II}_{0.5}$ = Ca, Sr, Ba; $M2^{II}$ = Fe, Co, Ni) are given. Finally, an overview on tetrahedral borophosphates possessing the molar composition B : P = 1 : 2 is described.

Anion $[BP_2O_7(OH)_3]^{4-}$ and $[BP_2O_8(OH)_2]^{5-}$:

The anion $[BP_2O_7(OH)_3]^{4-}$ is a tetrahedral triple, built from a central $(HO)_2BO_2$ tetrahedron sharing common vertices with two $(H_{0.5})OPO_3$ tetrahedra (*Figure 3.42a*).

However, the anion $[BP_2O_8(OH)_2]^{5-}$, built from a central $(HO)_2BO_2$ tetrahedron sharing common vertices with two PO_4 tetrahedra (*Figure 3.48a*).

With the exception of $Mg_2[BP_2O_7(OH)_3]$ (triclinic, space group *P*1) [141] all borophosphates containing the unbranched tetrahedral triple $[BP_2O_7(OH)_3]^{4-}$ are isotypic and crystallize in the space group *C*2/*c* (No. 15) (*Figure 3.66b*) independently whether the charge of the borophosphate anion is balanced by one monovalent cation together with a trivalent cation ($M^IM^{III}[BP_2O_7(OH)_3]$ where M^I = Na, K; M^{III} = Al, V, Fe, Ga, In) [48, 49, 107, 108, 133, 134, 141] or by two different divalent cations ($CaM2^{II}[BP_2O_7(OH)_3]$ where $M2^{II}$ = Fe, Ni). In this regard $SrFe[BP_2O_8(OH)_2]$ represents the first compound belonging to this family of borophosphates where the charge of the borophosphate anion is compensated by a divalent cation together with a trivalent cation (triclinic, space group $P\bar{1}$).

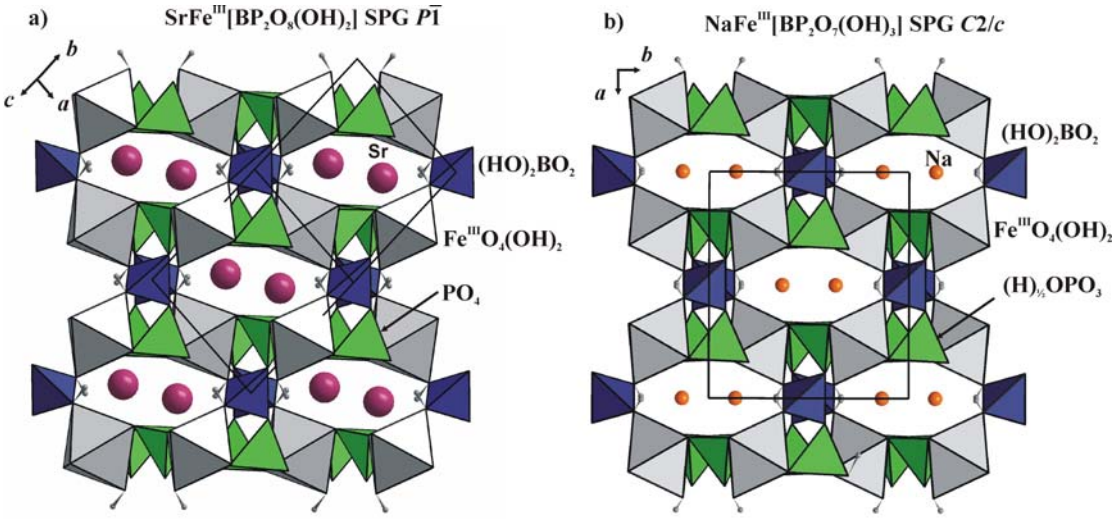

Figure 3.66: *Crystal structures of (a) $SrFe[BP_2O_8(OH)_2]$ viewed along [011] and (b) $NaFe[BP_2O_7(OH)_3]$ [48] viewed along [001]. Octahedra and tetrahedra form a similar three–dimensional framework which contains elliptical channels. The unit cell is outlined.*

However, as shown in *Figure 3.66* both structure types are closely related. The metrical transformation of the triclinic unit cell into the pseudo monoclinic *C*–centered cell by applying the matrix (1 –1 0, 1 1 0, 0 1 1) leads to doubling of the cell volume (V = 730.15(1) Å^3) and comparable lattice parameters (a = 10.3201(1) Å, b = 8.3090(1) Å, c = 9.5065(1) Å, β = 116.402(1)°) as reported for the compounds adopting the space group *C*2/*c*. The main local structural difference between the two structure types shown in *Figure 3.66* is the position and the coordination sphere of the

cations. In the crystal structure of $NaFe^{III}[BP_2O_7(OH)_3]$ sodium is situated on a special Wyckoff position (4*e*) and is eightfold coordinated by oxygen (*d*(Na—O) = 2.516(2) – 2.660(2) Å) whereas in the crystal structure of $SrFe[BP_2O_8(OH)_2]$ the Sr ion resides on a general Wyckoff position (2*i*) which is surrounded by ten oxygen atoms. Interestingly, in the third structure type observed for $Mg_2[BP_2O_7(OH)_3]$ the Mg ion on this site is only six–fold coordinated which suggests a certain flexibility of the framework built up of the borophosphate oligomers and octahedra. The same observation was made for the family of helical borophosphates [29] where a wide variety of cations can compensate for the negative charge of the anionic partial structure and for a Mn –organo –templated structures [142].

Anion $[B_2P_4O_{16}(OH)_2]^{8-}$ and the dimer $CoO_3O_{2/2}(H_2O)$:

The $[B_2P_4O_{16}(OH)_2]^{8-}$ anion comprises of open–branched four–membered rings, which are formed by alternating $(HO)BO_3$ and PO_4 sharing common apices with two additional PO_4 tetrahedra (*Figure 3.45a*). Generally, the condensation of the borophosphate anions, $[B_2P_4O_{16}(OH)_2]^{8-}$, with $M2^{II}O_5(OH)$ or $M^{III}O_5(OH)$ ($M2^{II}$ = Mn, Fe, Co, Ni, Zn; M^{III} = Fe, Sc, In) coordination octahedra *via* common corners results in an overall three–dimensional framework which contains channels extending along [100] as shown in *Figure 3.67a*.

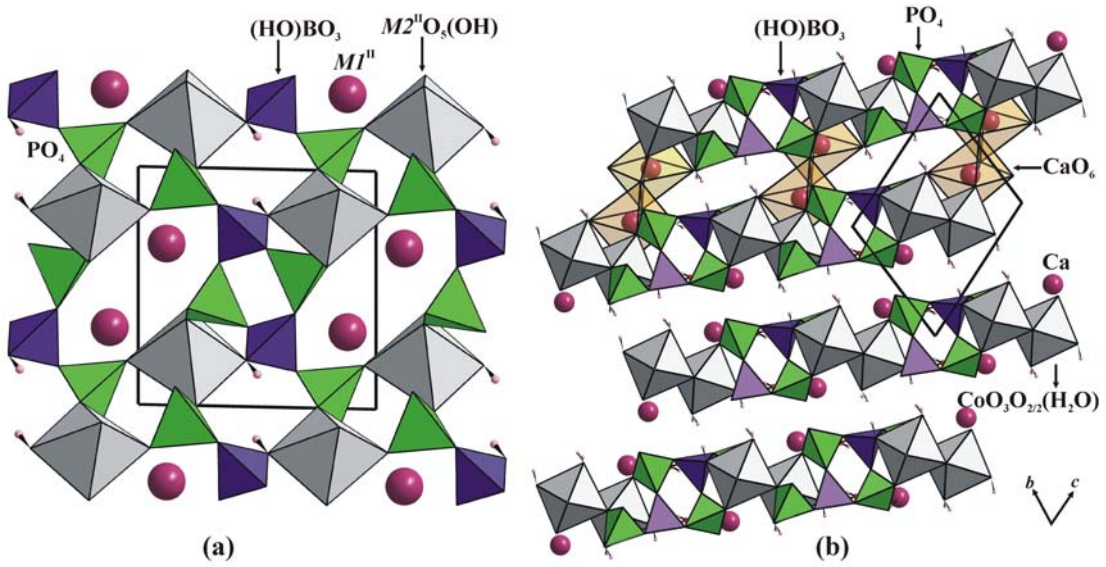

Figure 3.67: *The crystal structure of (a) $M1^{II}M2^{II}[BP_2O_8(OH)]$ ($M1^{II}$ = Ba; $M2^{II}$ = Fe, Co) (view along [100]) and (b) $CaCo(H_2O)[BP_2O_8(OH)]\cdot H_2O$ viewed along [100]. The unit cell is outlined.*

The cross sections of the channels are defined by eight–membered rings consisting of two $M2^{II}$ or M^{III} coordination octahedra, four phosphate tetrahedra and two hydrogenborate groups. The M^{I} or $M1^{II}$ (M^{I} = K, Rb, Cs; $M1^{II}$ = Ca, Ba) ions reside within the channels. However, although being a member of the same family ($[B_2P_4O_{16}(OH)_2]^{8-}$) the crystal structure of $CaCo(H_2O)[BP_2O_8(OH)]\cdot H_2O$ shows a different structural feature. The $[B_2P_4O_{16}(OH)_2]^{8-}$ anion interconnects with dimers of coordination octahedra $CoO_3O_{2/2}(H_2O)$ results in layers along [011] (*Figure 3.67b*) with the sequence *ABAB*…. Inter–layer contacts are formed by CaO_6 coordination polyhedra. This is the first example of $M1^{II}M2^{II}$ borophosphates representing a two–dimensional layered arrangement

Generally, isolated monomeric coordination metal octahedra have been observed for all *3d* transition metal containing borophosphates. However, there are four different types of arrangements of coordination octahedra found in cobalt containing borophosphates so far (*Figure 3.68*) [57, 61, 79].

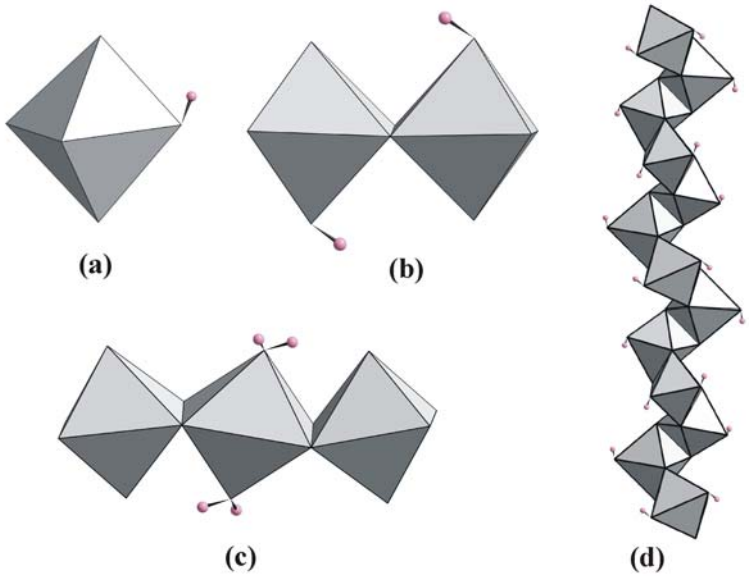

Figure 3.68: *Arrangements of cobalt octahedra observed in cobalt (II) containing borophosphates: (a) monomeric $CoO_5(OH)$ coordination octahedron; (b) dimeric units $Co_2O_8(OH)_2$ formed by two $CoO_3O_{2/2}(OH)$ octahedra; (c) trimeric units $Co_3O_{12}(H_2O)_2$ formed by $CoO_{4/2}(H_2O)_2$ octahedra connected via two opposite edges of $CoO_4O_{2/2}$ octahedra; (d) one–dimensional infinite chains, which built from $CoO_{4/2}(OH)_2$ coordination octahedra by sharing common edges (protons are shown as small pink spheres).*

Monomeric $CoO_5(OH)$ coordination octahedra (*Figure 3.68a*) in $BaCo[BP_2O_8(OH)]$, dimeric units $Co_2O_8(OH)_2$ formed by two $CoO_3O_{2/2}(OH)$ octahedra (*Figure 3.68b*) in $NaCo[BP_2O_7(OH)_2]$ [57], trimeric units $Co_3O_{12}(H_2O)_2$ formed by $CoO_{4/2}(H_2O)_2$ octahedra connected *via* two opposite edges of a $CoO_4O_{2/2}$ octahedra (*Figure 3.68c*) in $Rb_2Co_3(H_2O)_2[B_4P_6O_{24}(OH)_2]$ [79], and one–dimensional infinite chains, which are built from $CoO_{4/2}(OH)_2$ coordination octahedra by sharing common edges (*Figure 3.68d)* in $Co[BPO_4(OH)_2]$ [61]. The $CaCo(H_2O)[BP_2O_8(OH)]\cdot H_2O$ contains the dimers of $Co_2O_8(H_2O)_2$ formed by two $CoO_3O_{2/2}(H_2O)$ octahedra as shown in *Figure 3.51*.

Helical anion $^1_\infty[BP_2O_8]^{3-}$:

All helical borophosphates $M1^{II}_{0.5}M2^{II}(H_2O)_2[BP_2O_8]\cdot H_2O$ ($M1^{II}_{0.5}$ = Ca, Sr, Ba; $M2^{II}$ = Fe, Co, Ni) comprise of one dimensional infinite loop–branched borophosphate helices, $^1_\infty[BP_2O_8]^{3-}$, built of alternatively borate and phosphate tetrahedra (*Figure 3.58*). Helical borophosphates emerge to be the largest group of compounds among the borophosphates. The group of compounds with $^1_\infty[BP_2O_8]^{3-}$ helical chain anions has been synthesized in combination with different cations M^IM^{II} and M^{III} (M^I = Li, Na, K; M^{II} = Mg, Mn, Fe, Co, Ni, Zn; M^{III} = Sc, In, Fe). The systematic investigation on borophosphate systems with transition metals (Fe, Co, Ni) and alkaline–earth metals led to the formation of $M1^{II}_{0.5}M2^{II}(H_2O)_2[BP_2O_8]\cdot H_2O$ ($M1^{II}_{0.5}$ = Ca, Sr, Ba; $M2^{II}$ = Fe, Co, Ni). Due to their flexibility, the helical chains ($^1_\infty[BP_2O_8]^{3-}$) can host different cations and, thus, the number of compounds with this kind of anionic partial structure is comparatively large.

An observation was made on the substructures of magnesium [45] and cobalt compounds. In the refined substructure of $M1^{II}_{0.5}Mg(H_2O)_2[BP_2O_8]\cdot H_2O$ ($M1^{II}_{0.5}$ = Ca, Sr, Ba) the $M1^{II}$ cations are 25 % (¼) occupied and have higher numbers of coordination oxygen atoms and water molecules (crystal water O6 and coordination water O2) in the coordination sphere. The same situation is true for $M1^{II}_{0.5}Co(H_2O)_2[BP_2O_8]\cdot H_2O$ ($M1^{II}_{0.5}$ = Ca, Sr, Ba) (*Figure 3.69*).

Calcium ion in both $Ca_{0.5}Mg(H_2O)_2[BP_2O_8]\cdot H_2O$ and $Ca_{0.5}Co(H_2O)_2[BP_2O_8]\cdot H_2O$ was found to be seven–fold coordinated by two oxygen and five water molecules with distances d(Ca—O) = 2.210(4) Å to 2.681(4) Å for $Ca_{0.5}Mg$ and d(Ca—O) = 2.210(5) Å to 2.654(4) Å (next neighbouring oxygen atom is at 3.24 Å) for $Ca_{0.5}Co$, respectively. The distances of calcium to the neighbouring oxygen atoms are

comparable with the corresponding distances of $Ca[BPO_5]$ [11] in which calcium is ten–fold coordinated by oxygen. In case of $Sr_{0.5}Mg(H_2O)_2[BP_2O_8]\cdot H_2O$, the strontium ion was found to be eight–fold coordinated by three oxygen atoms and five water molecules (d(Sr—O) = 2.348(3) Å to 3.017(2) Å) whereas in $Sr_{0.5}Co(H_2O)_2[BP_2O_8]\cdot H_2O$, the strontium was nine–fold coordinated by four oxygen atoms and five water molecules with distances d(Sr—O) = 2.349(6) Å to 3.303(2) Å (next neighbouring oxygen atom is at 3.66 Å). The distances of Sr in both compounds are similar to the compound $Sr_6[BP_4O_{16}][PO_4]$ [143] (d(Sr—O) = 2.42 Å to 3.17 Å, ten–fold coordinated).

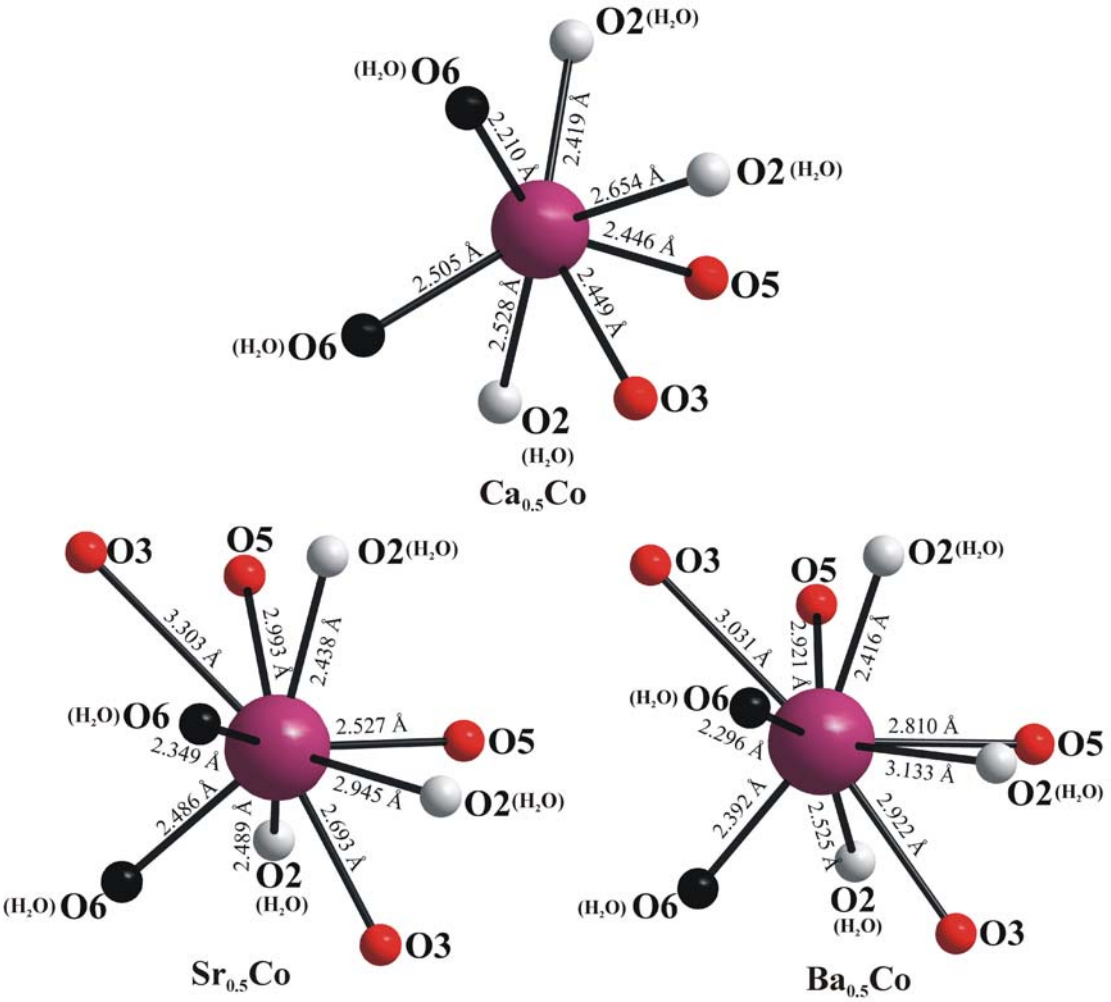

Figure 3.69: *Coordination environments of calcium, strontium and barium (violet spheres) in the refined substructure of $M1^{II}_{0.5}Co(H_2O)_2[BP_2O_8]\cdot H_2O$ ($M1^{II}_{0.5}$ = Ca, Sr, Ba). The black (O6) and gray spheres (O2) indicate the oxygens of the crystal water and coordination water, respectively.*

Similarly, the barium ion in $Ba_{0.5}Mg(H_2O)_2[BP_2O_8]\cdot H_2O$ was ten–fold coordinated by four oxygen atoms and six water molecules (d(Ba—O) = 2.362(5) Å to 3.2976(2) Å) but $Ba_{0.5}Co(H_2O)_2[BP_2O_8]\cdot H_2O$ has the coordination number nine for barium with four oxygen and five water molecules with distances d(Ba—O) = 2.295(1) Å to 3.133(1) Å (next neighbouring oxygen atom is at 3.37 Å). The barium distances in the compound $Ba_3[BP_3O_{12}]$ [11] (d(Ba—O) = 2.630 Å to 3.090 Å, eight–fold coordinated) are comparable with both $Sr_{0.5}Mg(H_2O)_2[BP_2O_8]\cdot H_2O$ and $Sr_{0.5}Co(H_2O)_2[BP_2O_8]\cdot H_2O$.

Significant difference between the position of the $M1^{II}$ ions (Wyckoff position 12c) and crystal water (Wyckoff position 6a) were observed in the crystal structure of $M1^{II}_{0.5}Co(H_2O)_2[BP_2O_8]\cdot H_2O$ ($M1^{II}_{0.5}$ = Ca, Sr, Ba). The $M1^{II}$ ions ($M1^{II}$ = Ca, Sr, Ba) have different size and the coordination in the crystal structure. The shortest distances between the ($M1^{II}$) positions are well explained by increasing ionic radius [122]. The neighbouring $M1^{II}$ positions of the calcium are 1.3571(1) Å apart whereas the distance between two strontium are 0.7672(1) Å. The distance between two barium ions were found to be 0.2406(1) Å. This indicates that higher the number of coordination (with increasing ionic radii) closer the positions of the $M1^{II}$ ions as shown in *Figure 3.70*.

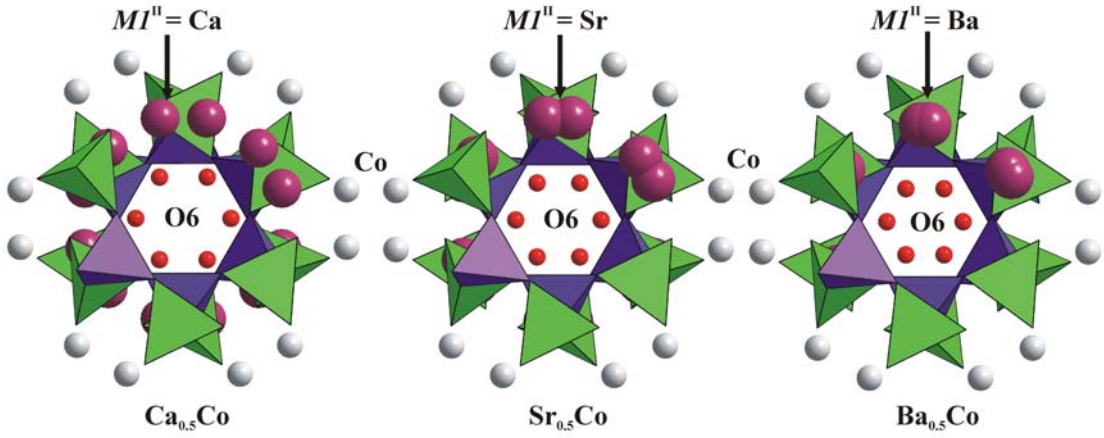

Figure 3.70: *A view of helical borophosphates $M1^{II}_{0.5}Co(H_2O)_2[BP_2O_8]\cdot H_2O$ ($M1^{II}_{0.5}$ = Ca, Sr, Ba) along [001]. With increasing ionic radii the distance between the $M1^{II}_{0.5}$ cation (¼ occupations) decreases.*

Tetrahedral borophosphates with B : P = 1 : 2:

The largest group of tetrahedral borophosphates possesses a molar composition B : P = 1 : 2 comprising a variety of complex anions ranging from simple oligomers to

layers [29]. The only 3D network with B : P = 1 : 2 is present in the crystal structure of $M^{I}[BeBP_2O_8]{\cdot}xH_2O$ (M^{I} = Na^+, K^+, NH_4^+), which contains additional tetrahedral building units (BeO_4) and is therefore classified by definition as a berylloborophosphate [144]. Focusing on $M1^{II}M2^{II}$ borophosphates ($M1^{II}$= Ca, Ba; $M2^{II}$ = Fe, Ni and $M1^{II}$ =Ba; $M2^{II}$ = Co) with B : P = 1 : 2, only three different types of anionic partial structures are realized so far: $[BP_2O_7(OH)_3]^{4-}$ $[BP_2O_8(OH)]^{4-}$ and $[BP_2O_8]^{3-}$. The simplest fundamental building block (FBB) with B : P = 1 : 2 is a unbranched tetrahedral triple, $[BP_2O_7(OH)_3]^{4-}$, built up by a central ($(HO)_2BO_2$) tetrahedra sharing two common corners with two ($H_{1/2}$)OPO_3 tetrahedra (*Figure 3.71a*) [48]. By condensation of two FBBs, an open–branched hexamer is formed which is $[B_2P_4O_{16}(OH)_2]^{8-}$, formed by alternating ($(HO)BO_3$) and PO_4 tetrahedra sharing common corners with two PO_4 branches (*Figure 3.71b*) [48]. These anions condense together to form helical chains, $^1{}_\infty[BP_2O_8]^{3-}$, comprises of distorted BO_4 and PO_4 tetrahedra alternatively (*Figure 3.71c*) [69].

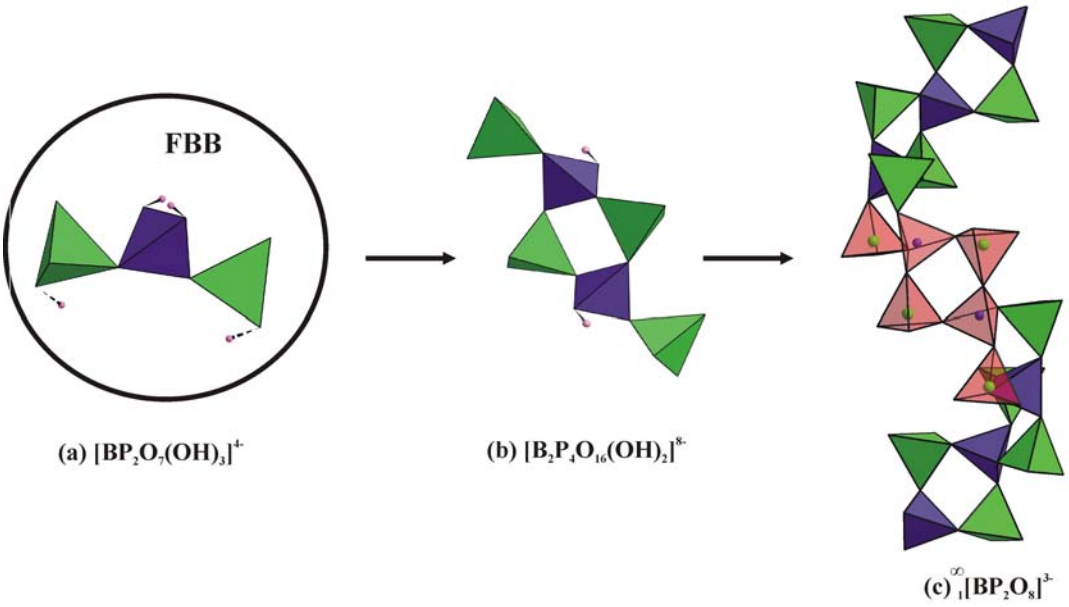

Figure 3.71: *Assembly of helical chain from fundamental building units with B : P = 1 : 2 (green: PO_4 tetrahedra; blue: BO_4 tetrahedra; pink spheres: protons). (a) $[BP_2O_7(OH)_3]^{4-}$, built up by a central $(HO)_2BO_2$ tetrahedron sharing two common corners with two PO_4 tetrahedra, (b) $[B_2P_4O_{16}(OH)_2]^{8-}$, formed by alternating $(HO)BO_3$) and PO_4 tetrahedra sharing common corners with two PO_4 branches, (c) $^1{}_\infty[BP_2O_8]^{3-}$, comprises of distorted BO_4 and PO_4 tetrahedra alternatively. The helical chains $^1{}_\infty[BP_2O_8]^{3-}$ which are built up by $[B_2P_4O_{16}(OH)_2]^{8-}$ tetrahedral units are shown by color red.*

In conclusion, several borophosphates were synthesized containing alkaline–earth and transition metals. It was evidenced that depending upon the shape and size of the $M1^{II}$ ion it is possible to control the shape and size of cavities or channels in the framework structures. The crystal structure of $CaCo(H_2O)[BP_2O_8(OH)]\cdot H_2O$ showed the first example of $M1^{II}M2^{II}$ borophosphates representing a two–dimensional layered arrangement. In addition, the first divalent–trivalent borophosphate $SrFe[BP_2O_8(OH)_2]$ was synthesized.

3.4 Layered borophosphates

This chapter deals with one of the few examples of borophosphates containing layered anionic partial structures (6^3 net topology). Details on synthesis, crystal structure, thermal and physical properties of 3 new members containing transition metal cations are given. Furthermore, the formation of a solid solution series containing two transition metal ions is described for this structure type. Topologies and directedness (upward or downward direction of a tetrahedron) of these layered borophosphates are compared with those of phosphates and silicates.

3.4.1 $M^{II}(H_2O)_2[B_2P_2O_8(OH)_2]\cdot H_2O$ (M^{II} = Fe, Co, Ni)

3.4.1.1 Synthesis

Single crystals of $M^{II}(H_2O)_2[B_2P_2O_8(OH)_2]\cdot H_2O$ (M^{II} = Fe, Co, Ni) (*Figure 3.72*) were obtained under hydrothermal conditions from the corresponding aqueous solutions of iron (II) oxalate, cobalt (II) carbonate, nickel (II) oxide, boron oxide, phosphoric acid and distilled water.

Transparent colorless single crystals of $Fe(H_2O)_2[B_2P_2O_8(OH)_2]\cdot H_2O$ were prepared from a mixture of 1.0003 g $FeC_2O_4\cdot 2H_2O$, 0.7740 g B_2O_3 and 3.8451 g H_3PO_4 (molar ratio Fe : B : P = 1 : 2 : 6). 5 ml of water were added (pH = 1) and the mixture was transferred to a 20 ml Teflon–lined autoclave (filling degree 40 %), which was then heated at 170 ºC for 7 days. Violet single crystals of $Co(H_2O)_2[B_2P_2O_8(OH)_2]\cdot H_2O$ were synthesized from a mixture of 0.5002 g $CoCO_3$, 0.5853 g B_2O_3 and 2.9078 g H_3PO_4 (molar ratio Co : B : P = 1 : 2 : 6). 10 ml of water were added and the pH value of the solution was found to be 1. The reaction mixture was then transferred into a 10 ml Teflon–lined autoclave (filling degree 30 %) and heated under autogenous pressure at 170 ºC for 10 days. Greenish single crystals of $Ni(H_2O)_2[B_2P_2O_8(OH)_2]\cdot H_2O$ were obtained from 0.2501 g NiO, 0.4660 g B_2O_3, 2.3153 g H_3PO_4 (molar ratio Ni : B : P = 1 : 2 : 6). 10 ml of water were added and the mixture (pH =1) was filled into a 20 ml Teflon–lined autoclave and treated at 170 ºC for 7 days. In each case the reaction product was separated by vacuum filtration, washed with hot water, filtered and washed again with acetone and finally dried at 60 ºC in air. The single crystals of all the compounds prepared were of dimensions ranging from 0.1 mm to 0.5 mm (*Figure 3.72*).

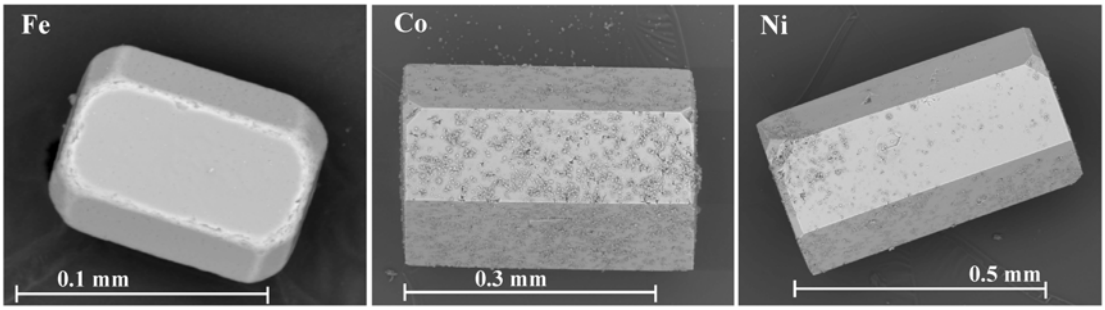

Figure 3.72: *SEM images of single crystals of $M^{II}(H_2O)_2[B_2P_2O_8(OH)_2].H_2O$ (M^{II} = Fe, Co, Ni)*

Remarkable changes in the crystal habit were observed during the synthesis of $M^{II}(H_2O)_2[B_2P_2O_8(OH)_2]\cdot H_2O$ (M^{II} = Fe, Co, Ni). SEM image of single crystal of $Ni(H_2O)_2[B_2P_2O_8(OH)_2]\cdot H_2O$ with traces of alkali–metals present is shown in *Figure 3.73a*. Synthesis with the absence of alkali–metals lead to a change in the crystal habit by reducing of the number of faces in direction of the more simple prismatic morphology (*Figure 3.73b*).

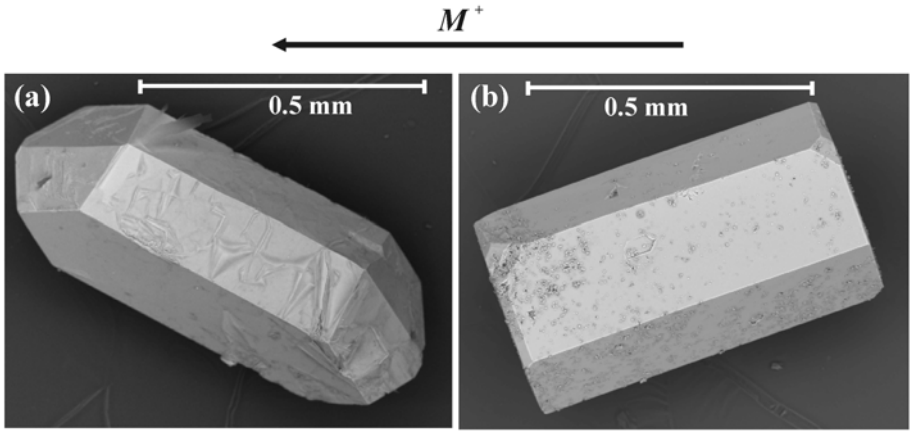

Figure 3.73: *(a) SEM image of single crystal of $Ni(H_2O)_2[B_2P_2O_8(OH)_2]\cdot H_2O$ with traces of alkali–metals present (b) Synthesis with the absence of alkali–metals lead to a change in the crystal habit by reducing of the number of faces in direction of the more simple prismatic morphology.*

The observed powder XRD patterns are found to be in agreement with the calculated ones generated on the basis of single–crystal structure data, proving the phase purity of the synthesized products (*Figure 3.74* to *Figure 3.76*).

The results of chemical analyses are given in *Table 3.13*. The chemical composition of $M^{II}(H_2O)_2[B_2P_2O_8(OH)_2]\cdot H_2O$ (M^{II} = Fe, Co, Ni) was confirmed by ICP–OES, while the hot extraction method was applied for analyzing the hydrogen content. The oxygen value determined was too low as the oxygen of the H_2O molecules is detected incompletely by the hot extraction method. The obtained (experimental) molar compositions for $M^{II}(H_2O)_2[B_2P_2O_8(OH)_2]\cdot H_2O$ (M^{II} = Fe, Co, Ni) were found to be Fe : P : B = 1 : 1.98 : 2.1, Co : P : B = 1 : 1.91 : 1.84, and Ni : P : B = 1 : 1.95 : 1.91 (wt %) and are in good agreement with the chemical formula obtained from the single crystal structure refinements Fe : P : B = Co : P : B = Ni : P : B = 1 : 2 : 2, evidencing that pure products were yielded.

EDX analyses were also used to determine the elements present semi–quantitatively (Fe : P = Co : P = Ni : P ≈ 1 : 2). Infrared spectra were recorded and the absorption band at 1628 cm^{-1} (H_2O deformation) and 3594 cm^{-1} (O—H stretching) clearly indicates the presence of water in the crystal structures (see *Appendix 5.4.4*).

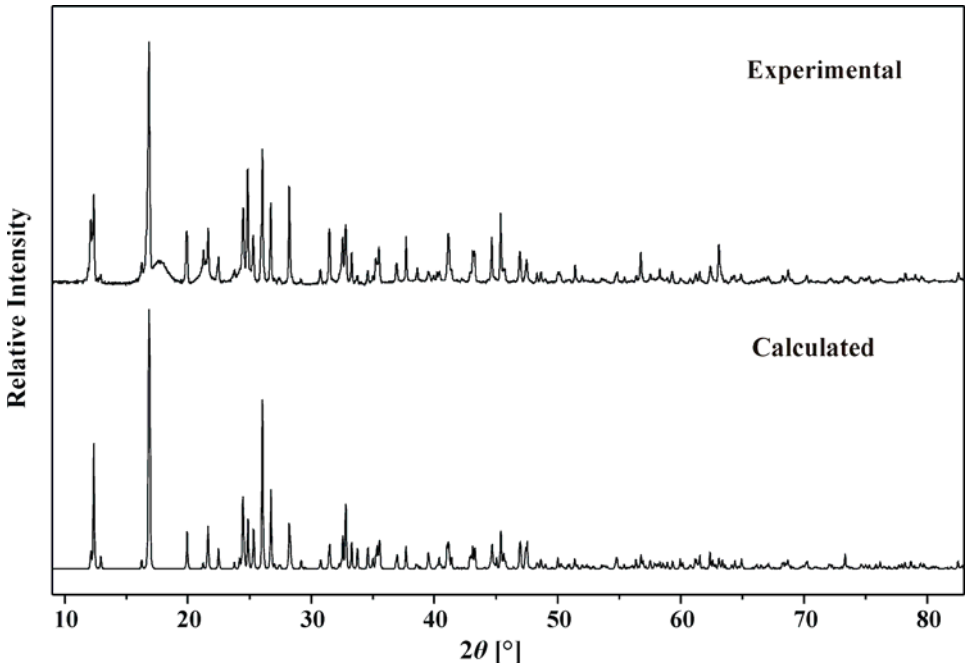

Figure 3.74: *Observed (background subtracted) and calculated powder X–ray diffraction patterns of $Fe(H_2O)_2[B_2P_2O_8(OH)_2]\cdot H_2O$ (Co $K_{\alpha 1}$–radiation)*

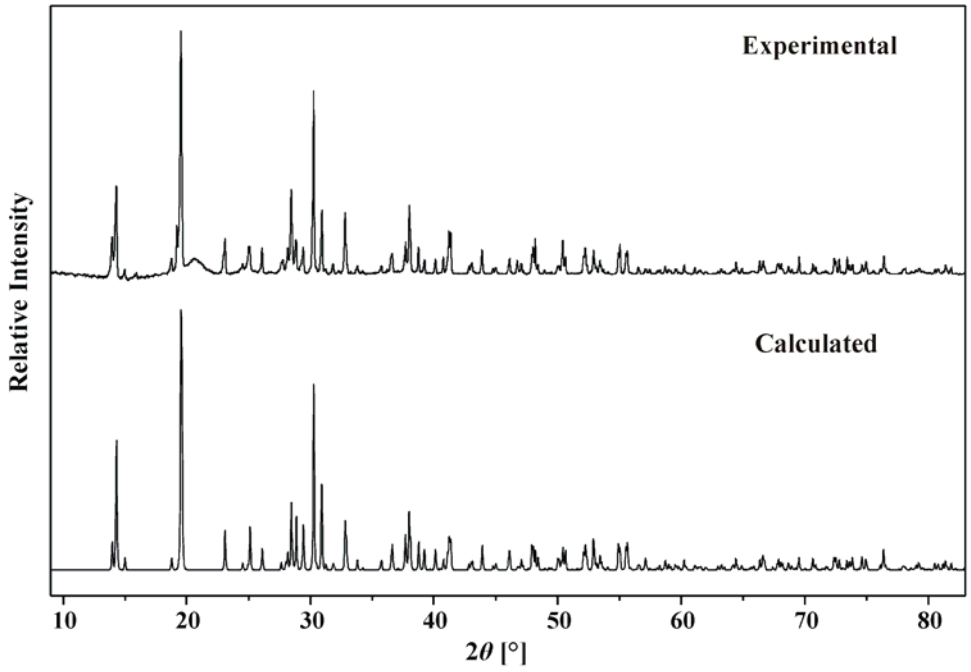

Figure 3.75: *Observed (background subtracted) and calculated powder X–ray diffraction patterns of* $Co(H_2O)_2[B_2P_2O_8(OH)_2]\cdot H_2O$ *(Co* $K_{\alpha 1}$*–radiation)*

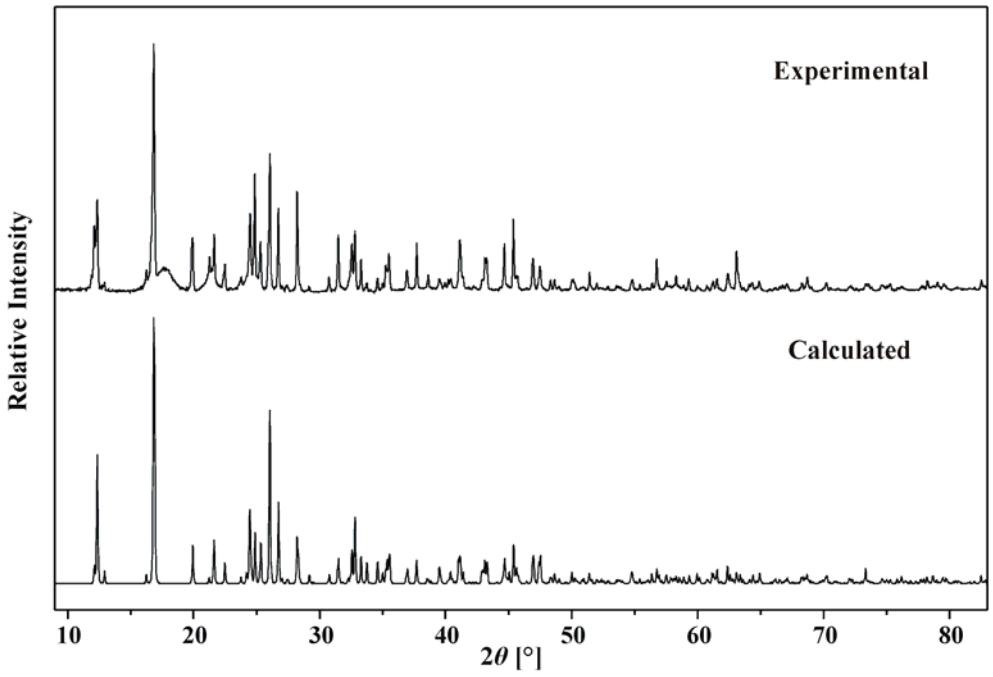

Figure 3.76: *Observed (background subtracted) and calculated powder X–ray diffraction patterns of* $Ni(H_2O)_2[B_2P_2O_8(OH)_2]\cdot H_2O$ *(Cu* $K_{\alpha 1}$*–radiation)*

Table 3.13: *Chemical analyses of $M^{II}(H_2O)_2[B_2P_2O_8(OH)_2]\cdot H_2O$ (M^{II} = Fe, Co, Ni)*

Element	Observed (e.s.d.) weight %	Calculated weight %
Fe	14.73(8)	15.80
B	5.65(4)	6.12
P	18.21(14)	17.53
O	51.37(86)	58.35
H	2. 37(2)	1.71
Co	16.24(20)	16.53
B	6.08(5)	6.06
P	16.82(3)	17.37
O	38.25(2)	58.34
H	1.36(2)	1.70
Ni	16.68(6)	16.47
B	5.97(1)	6.07
P	16.76(4)	17.39
O	51.1(2)	58.38
H	2.14(2)	1.70

3.4.1.2 Crystal Structure Determination

Single crystals of $M^{II}(H_2O)_2[B_2P_2O_8(OH)_2]\cdot H_2O$ (M^{II} = Fe, Co, Ni) were selected under a light microscope and mounted on the tip of a glass capillary and the X–ray data were collected at a temperature of 293 K. All crystal structures were solved by direct methods. The crystal structures of $M^{II}(H_2O)_2[B_2P_2O_8(OH)_2]\cdot H_2O$ (M^{II} = Fe, Co, Ni) were solved in the monoclinic space group $P2_1/c$ (No. 14) (see *Table 3.14*).

Table 3.14: *Space group and lattice parameters of $M^{II}(H_2O)_2[B_2P_2O_8(OH)_2]\cdot H_2O$ (M^{II} = Fe, Co, Ni)*

	Space group	*a* (Å)	*b* (Å)	*c* (Å)	*ß*	*Z*
Fe	$P2_1/c$ (No. 14)	7.7449(4)	14.7900(10)	8.2429(6)	90.304(4)	2
Co	$P2_1/c$ (No. 14)	7.7408(4)	14.6975(5)	8.2219(4)	90.26(4)	2
Ni	$P2_1/c$ (No. 14))	7.7389(7)	14.5735(11)	8.2060(4)	90.30(4)	2

All framework atoms Fe, Co, Ni, P, B and O could be unambiguously located. The H atoms of the water molecules were subsequently located from the difference Fourier maps. The positions of the H atoms were found to be close to O9 to O13 and the positional coordinates could be refined as free variables. For the final anisotropic refinement steps the displacement parameters of the H atoms were restrained to 1.5 U_{iso} of the oxygen atoms to which they are attached. The crystal structure of $Co(H_2O)_2[B_2P_2O_8(OH)_2]\cdot H_2O$ was refined as twin with *a* as the twin axis (matrix 100, 0–10, 00–1). The twin law was determined by the program PLATON [P6].

The crystallographic data, refinement parameters, the final fractional atomic coordinates and equivalent / isotropic and anisotropic displacement factors for all the compounds under investigation are listed in *Appendix 80* to *Appendix 88*.

3.4.1.3 Crystal Structure Description

The crystal structure of $M^{II}(H_2O)_2[B_2P_2O_8(OH)_2]\cdot H_2O$ (M^{II} = Fe, Co, Ni) contains a corrugated layered anionic partial structure, which is rare in the field of borophosphates (*Figure 3.77*) [145].

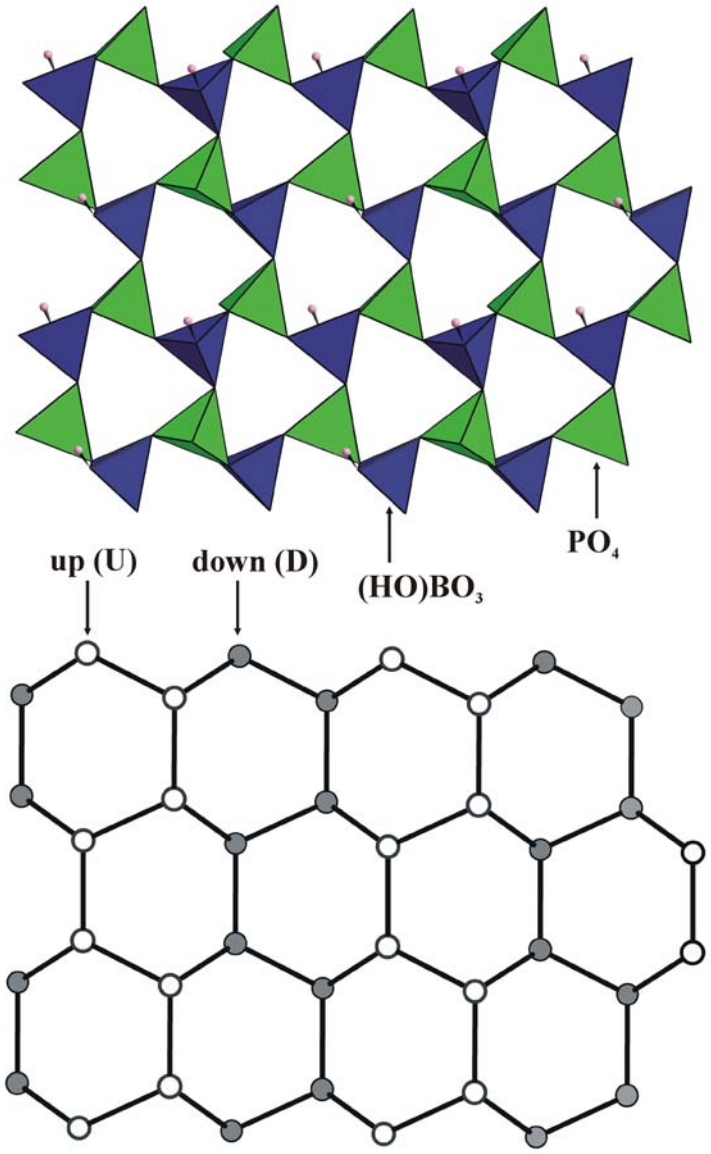

Figure 3.77: *6^3 nets of alternating PO_4 and $(HO)BO_3$ units forming the anionic partial structure (top) of $M^{II}(H_2O)_2[B_2P_2O_8(OH)_2]\cdot H_2O$ (M^{II} = Fe, Co, Ni). In each six–membered ring (bottom) four tetrahedra are pointing in one direction (gray spheres) and two in the opposite direction (white spheres) with respect to the borophosphate layer.*

It comprises a two–dimensional arrangement of distorted phosphate (PO_4) and hydrogenborate ($(OH)BO_3$) groups that are connected in an alternating fashion *via* common corners. This arrangement of tetrahedra is described as a wavy 6^3 net in the field of silicate structural chemistry [78, 146]. The topology of the layers and the directedness of their tetrahedra can be easily and very clearly visualized. In each six–membered ring of the layer two adjacent tetrahedra are pointing in one direction (U or D), the remaining four tetrahedra point in the opposite direction (*Figure 3.77* bottom). The coordination of the metal atoms (M^{II} = Fe, Co, Ni) with hydrogenborate and phosphate tetrahedra is shown in *Figure 3.78*.

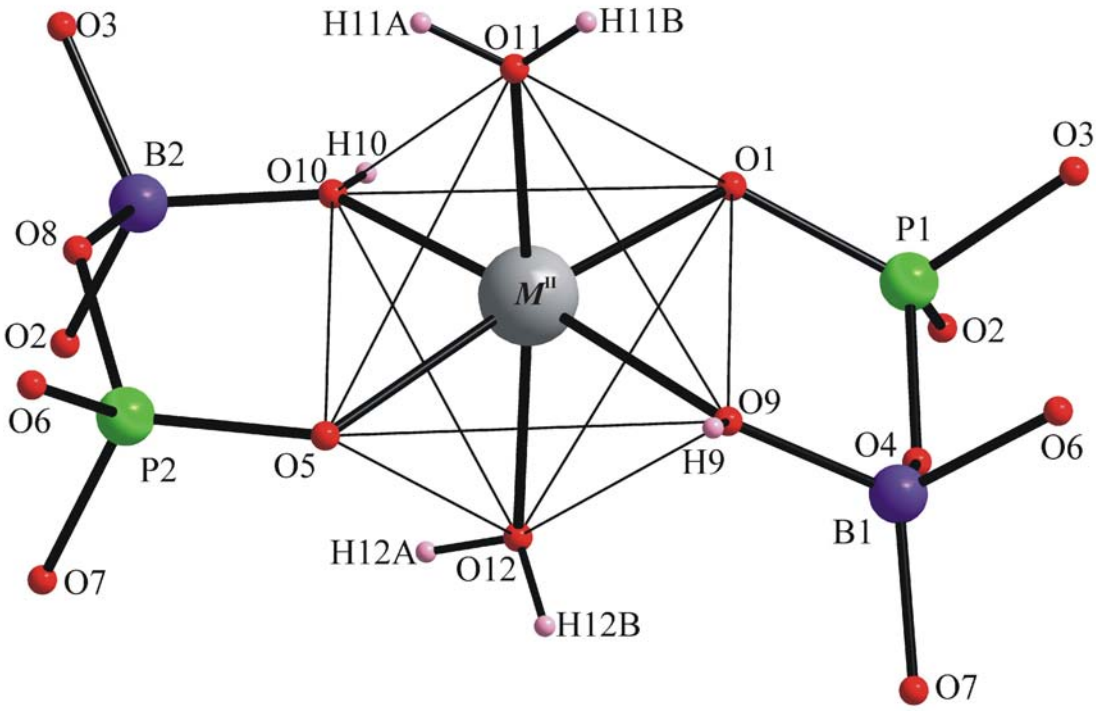

Figure 3.78: *Octahedral coordination of M^{II} in the crystal structure of $M^{II}(H_2O)_2[B_2P_2O_8(OH)_2]\cdot H_2O$ (M^{II} = Fe, Co, Ni). The equatorial positions are occupied by oxygen atoms originating from hydrogenborate and phosphate tetrahedra. The two water molecules coordinated to the apical vertices of the octahedron (aqua–ligands).*

The M^{II}–octahedra (M^{II} = Fe, Co, Ni) interconnect the corrugated layers of wavy the 6^3 wavy nets of tetrahedra to form an overall three–dimensional framework which contains channels running along [100] (*Figure 3.79*). The cross sections of the channels are defined by ten–membered polyhedral rings consisting of two M^{II}–octahedra, four phosphate tetrahedra and four hydrogenborate groups. Crystal water is

located within the channels. Furthermore, also six–membered polyhedral rings are present in the crystal structure consisting of two M^{II}–octahedra, two phosphate tetrahedra and two hydrogenborate tetrahedra. The framework topology is shown in *Figure 3.80*.

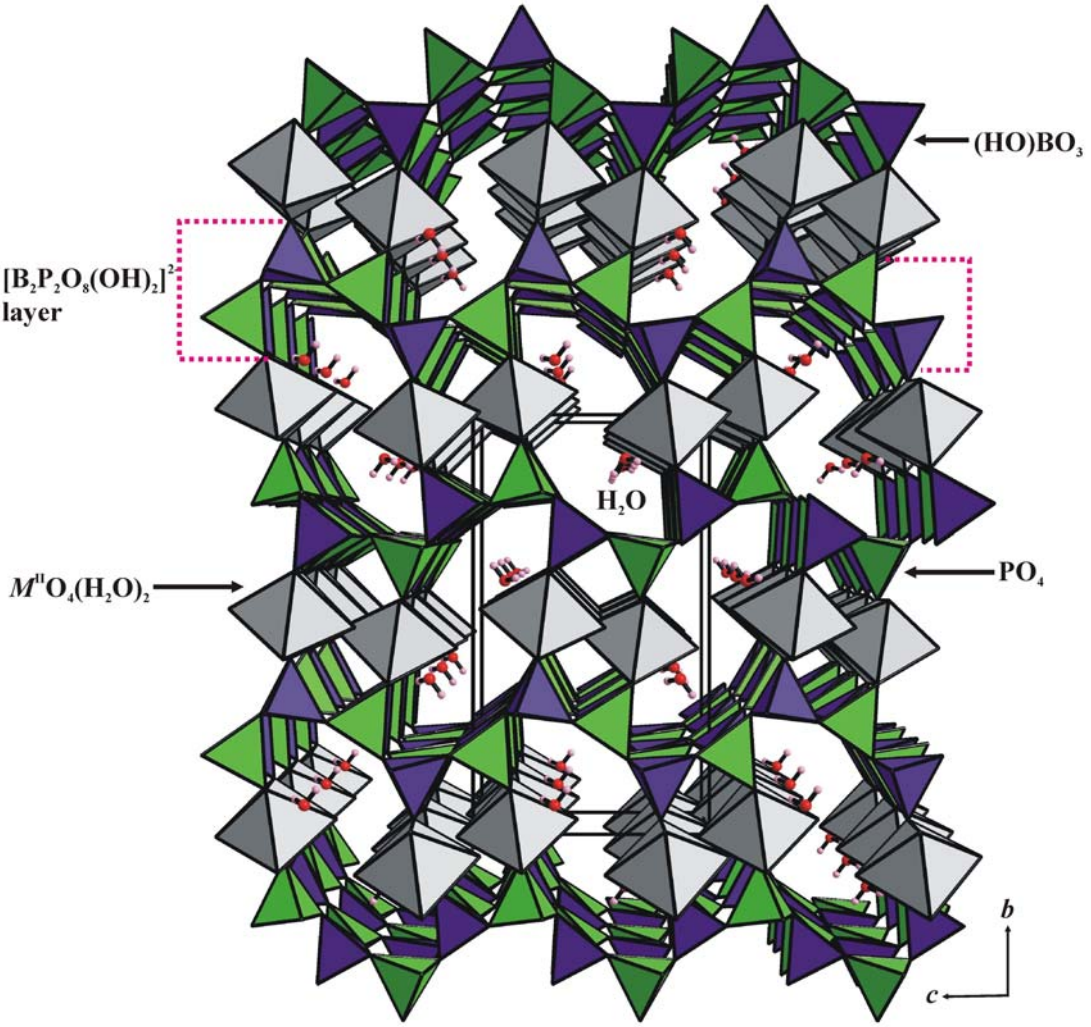

Figure 3.79: *Crystal structure of $M^{II}(H_2O)_2[B_2P_2O_8(OH)_2]\cdot H_2O$($M^{II}$ = Fe, Co, Ni): The M^{II} coordination octahedra are connected to the borophosphate layers to form a three–dimensional framework (aqua–ligands at $M^{II}(H_2O)_2$ are omitted for clarity). The unit cell is outlined.*

In case of $Fe(H_2O)_2[B_2P_2O_8(OH)_2]\cdot H_2O$, the B—O bond distance in the hydrogen borate groups range from 1.438(3) Å to 1.485(3) Å of which the B—OH bonds are the shortest (1.438(3) Å and 1.446(3) Å). The O—B—O angles have values between 106.02(19)° and 113.1(2)°. In the phosphate groups the P—O bond distances range from 1.5014(18) Å to 1.5445(18) Å and the O—P—O angles vary between

105.44(9)° and 113.68(10)°. In case of $Co(H_2O)_2[B_2P_2O_8(OH)_2]\cdot H_2O$, the B—O bond distances are in the range of 1.445(2) Å to 1.479(3) Å. The notably shorter bond distances again are observed for B—OH (1.445(2) Å and 1.446(2) Å). The O—B—O angles vary between 105.64(15)° and 113.54(17)°. In the phosphate groups the P—O bond distances and the O—P—O angles vary from 1.5017(18) Å to 1.5460(15) Å and 105.44(9)° to 113.77(10)°, respectively.

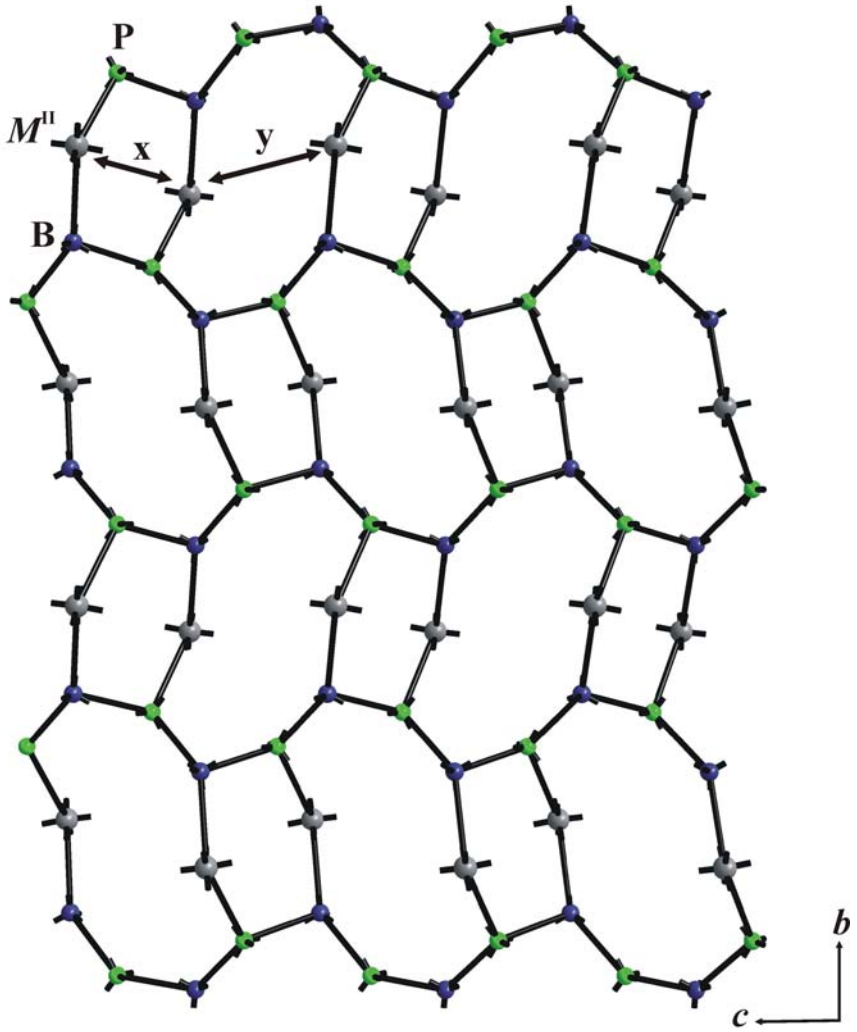

Figure 3.80: *View of the 6– and the 10–membered polyhedral rings present in the crystal structure of $M^{II}(H_2O)_2[B_2P_2O_8(OH)_2]\cdot H_2O$ (M^{II} = Fe, Co, Ni). Crystal water is located within the 10–membered polyhedral rings. x and y are the shortest M^{II}—M^{II} contacts in the 6– and the 10–membered polyhedral rings (5.23 Å and 6.36 Å for Fe, 5.19 Å and 6. 36 Å for Co, 5.15 Å and 6. 41 Å for Ni)*

In case of $Ni(H_2O)_2[B_2P_2O_8(OH)_2]\cdot H_2O$, the B—O bond distances and the O—B—O angles vary between 1.445(4) Å to 1.449(3) Å and 105.9(2)° to 113.8(2)° and the shortest distances (1.445(4) Å and 1.449(4) Å) were observed for B—OH. The P—O bond distances and the O—P—O angles for the phosphate groups vary from 1.4990(2) Å to 1.5470(2) Å and 105.46(11)° to 113.69(12)°, respectively. The bond distances and the bond angles of the phosphate tetrahedra and the hydrogenborate groups are in well accordance with the trends observed in pure borates and phosphates [101, 147].

The metal atoms (M^{II} = Fe, Co, Ni) were found to be six–fold coordinated by two oxygen atoms, two OH—groups and two water molecules (*Figure 3.78*). The oxo– and the protonated oxo– ligands originate from two hydrogenborate and two phosphate units and are located on the equatorial positions of the distorted octahedra with almost equal distances (d(Fe—O = 2.1211(19) Å – 2.1385(19) Å, d(Co—O = 2.0931(16) Å – 2.1130(16) Å, d(Ni—O = 2.0510(2) Å – 2.0780(2) Å)). The apical positions are occupied by water molecules with Fe—OH_2 distances of 2.0780(2) Å and 2.2220(2) Å, Co—OH_2 distances of 2.0460(2) Å and 2.1853(18) Å, and Ni—OH_2 distances of 2.0300(3) Å and 2.1200(2) Å, respectively. The angles between ligands on adjacent corners have values between 83.30° and 94.22(9)° for O—Fe—O, 83.57° and 94.75° for O—Co—O, 86.16(10)° and 93.65(9)° for O—Ni—O, respectively. The shortest M^{II}—M^{II} distances (labeled x in *Figure 3.80*) are 5.23 Å (Fe—Fe), 5.19 Å (Co—Co) and 5.15 Å (Ni—Ni) for the six–membered rings and 6.36 Å, 6.36 Å and 6.41 Å for the ten–membered rings (labeled y in *Figure 3.80*). The cell volumes of $M^{II}(H_2O)_2[B_2P_2O_8(OH)_2]\cdot H_2O$ (M^{II} = Fe, Co, Ni) decrease in the sequence Fe (944.19(11) $Å^3$) → Co (935.40(7) $Å^3$) → Ni (925.48(12) $Å^3$).

Selected interatomic distances and bond angles of $Fe(H_2O)_2[B_2P_2O_8(OH)_2]\cdot H_2O$, $Co(H_2O)_2[B_2P_2O_8(OH)_2]\cdot H_2O$, and $Ni(H_2O)_2[B_2P_2O_8(OH)_2]\cdot H_2O$ are listed in *Appendix 89* and *Appendix 90*.

3.4.1.4 Thermal Analysis

Simultaneous constant rate thermogravimetry (TG) and difference thermal analysis (DTA) of $M^{II}(H_2O)_2[B_2P_2O_8(OH)_2]\cdot H_2O$ (M^{II} = Fe, Co, Ni) were carried out. The samples dried at 60 ºC were placed in an open crucible and then heated with 5 K / min to 1000 ºC in a continuous argon gas flow. For the examination of the rehydration behavior $Ni(H_2O)_2[B_2P_2O_8(OH)_2]\cdot H_2O$ was heated with 5 K / min to 250 ºC in the

thermobalance, then subjected for one day to atmospheric moisture and reheated again. The same compound was also investigated by a thermobalance coupled to a mass spectrometer in order to identify the evolved gases. All TG curves were corrected by subtraction of a blank run and all the products obtained were examined by powder XRD.

The TG curves of $M^{II}(H_2O)_2[B_2P_2O_8(OH)_2]\cdot H_2O$ (M^{II} = Fe, Co, Ni) are shown in *Figure 3.81*. The main mass loss is observed between 100 ºC and 430 ºC without well resolved steps. Further heating results in a continuous mass loss which is finished between 530 ºC and 630 ºC depending on the metal cation. The overall mass loss for all compounds is smaller than the expected one for the release of 4 mole water per formula $M^{II}(H_2O)_2[B_2P_2O_8(OH)_2]\cdot H_2O$ (Fe: calc –20.4 wt % / exp –18.4 wt %, Co: calc –20.1 wt % / exp –9.3 wt %, Ni: calc –20.1 wt % / exp –19.6 wt %).

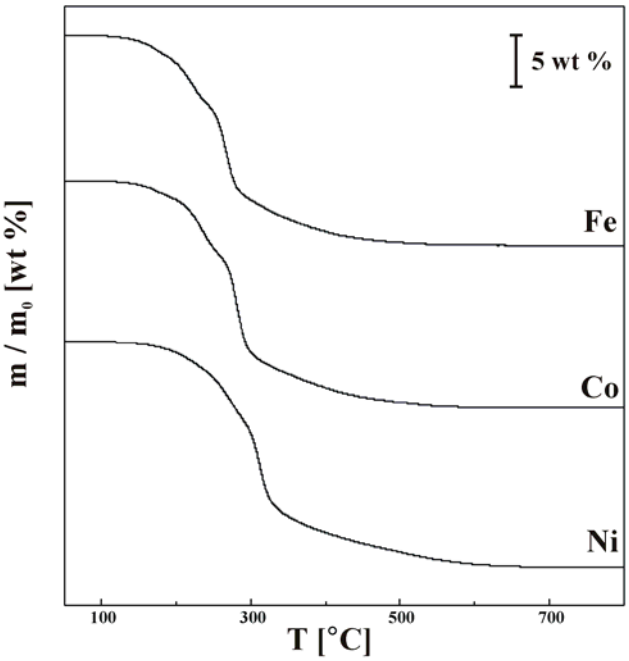

Figure 3.81: *Thermogravimetric curves of $M^{II}(H_2O)_2[B_2P_2O_8(OH)_2]\cdot H_2O$ (M^{II} = Fe, Co, Ni) with a heating rate of 5 K / min.*

Figure 3.82 shows the simultaneously recorded DTA traces for the heating and segments. The main mass loss is accompanied by a broad endothermic effect with three distinct maxima. The position of the strongest peak shifts to higher temperatures in the sequence Fe → Co → Ni. After the main decomposition process all samples show exothermic effects in the range between 530 ºC and 730 ºC which may indicate

crystallization of amorphous decomposition products. For the iron containing compound two endothermic peaks are observed at 890 ºC and 930 ºC and during cooling two exothermic peaks at 960 ºC and 890 ºC are detected. This can be interpreted as a (partial) melting crystallization process within the sample. The decomposition product of $Co(H_2O)_2[B_2P_2O_8(OH)_2]\cdot H_2O$ exhibits a small exothermic peak at 290 ºC during cooling which is close to the reported temperature for the phase transition of α–$Co_2P_2O_7$ [148]. The products identified by powder XRD in all cases after thermal treatment correspond to pyrophosphates $M^{II}P_2O_7$ (γ, α, σ) [149-151] and α–BPO_4 [140] besides unassigned reflection patterns (*Figure 3.83* to *Figure 3.85*). The overall mass loss and the decomposition products are listed in *Table 3.15*.

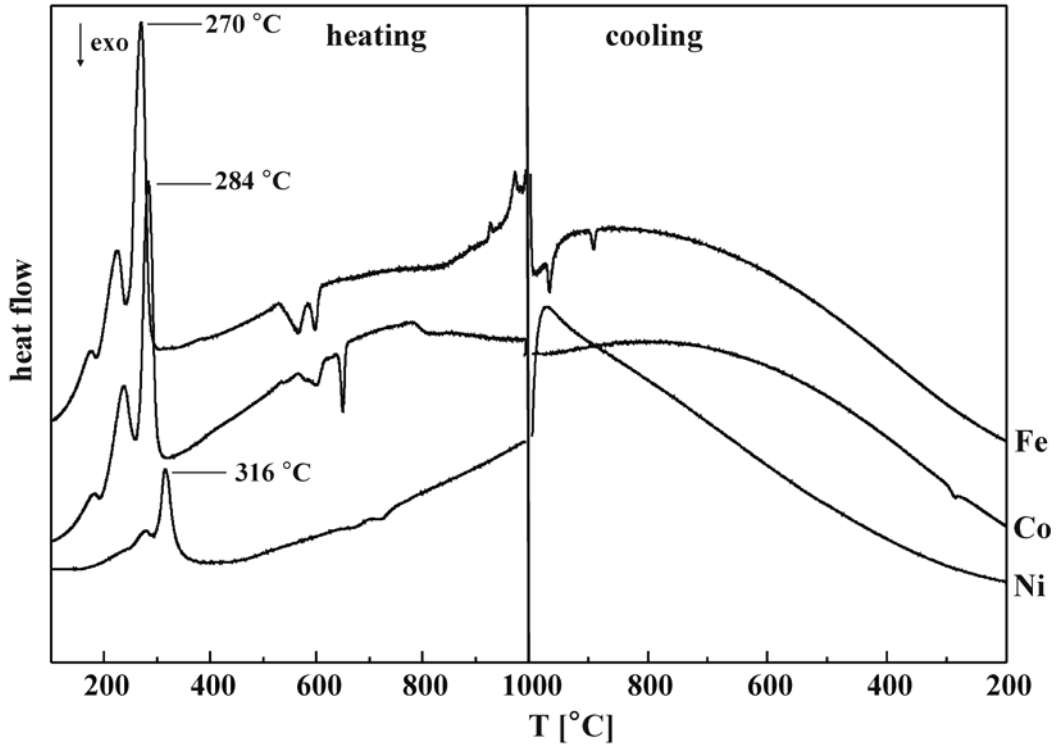

Figure 3.82: *DTA traces for the thermal decomposition of $M^{II}(H_2O)_2[B_2P_2O_8(OH)_2]\cdot H_2O$ (M^{II} = Fe, Co, Ni) recorded for the heating (left) and cooling (right) segment (rate ± 5 K / min).*

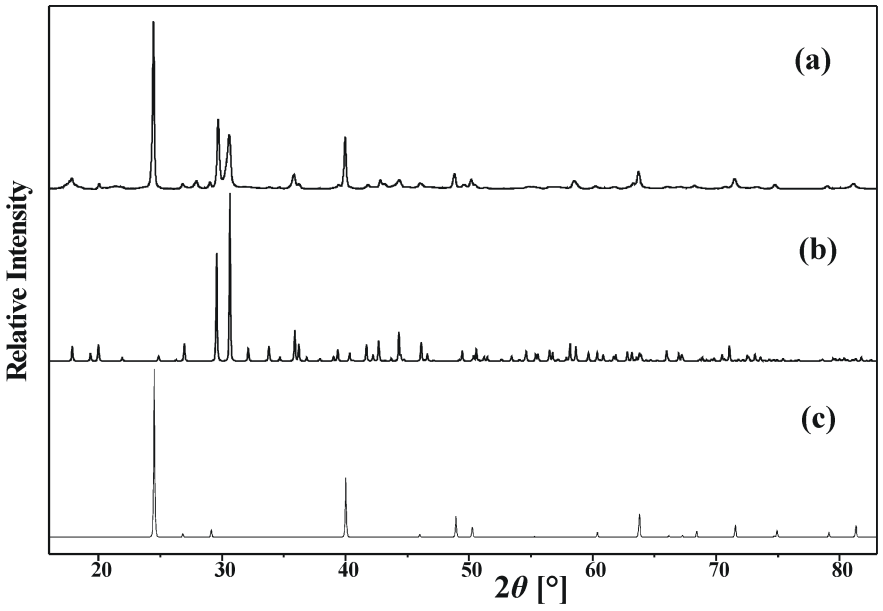

Figure 3.83: *Powder X–ray diffraction pattern of (a) the decomposition product of $Fe(H_2O)_2[B_2P_2O_8(OH)_2]\cdot H_2O$ heated to 1000 °C, compared with the calculated powder diffraction pattern of (b) γ–$Fe_2P_2O_7$ [151] and (c) α–BPO_4 [140] (Co $K_{\alpha 1}$–radiation)*

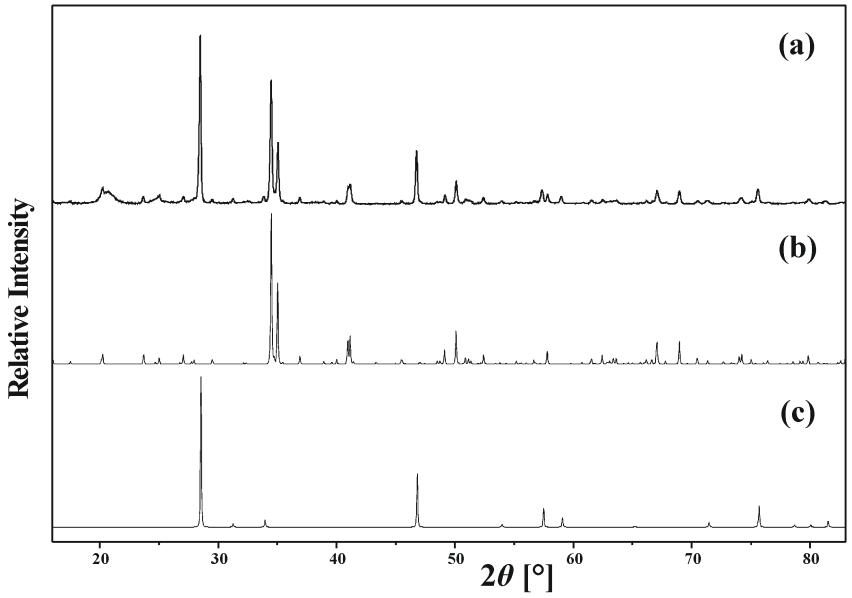

Figure 3.84: *Powder X–ray diffraction pattern of (a) the decomposition product of $Co(H_2O)_2[B_2P_2O_8(OH)_2]\cdot H_2O$ heated to 1000 °C, compared with the calculated powder diffraction pattern of (b) α–$Co_2P_2O_7$ [149] and (c) α–BPO_4 [140] (Co $K_{\alpha 1}$–radiation)*

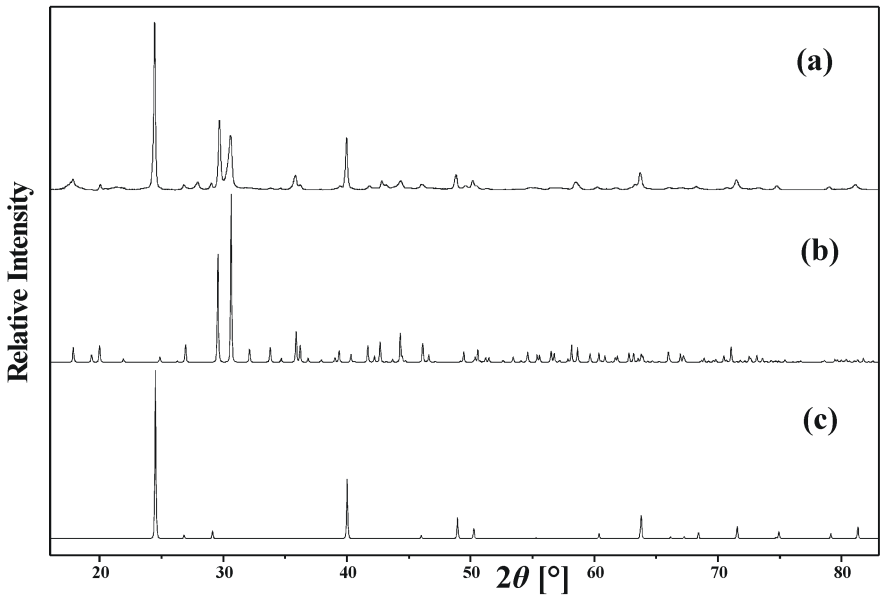

Figure 3.85: *Powder X–ray diffraction pattern of (a) the decomposition product of* $Ni(H_2O)_2[B_2P_2O_8(OH)_2]\cdot H_2O$ *heated to 1000 °C, compared with the calculated powder diffraction pattern of (b)* σ*–*$Ni_2P_2O_7$ *[150] and (c)* α*–*BPO_4 *[140] (Co* $K_{\alpha 1}$*–radiation)*

The de–rehydration behavior was studied due to the presence of two chemically different types of water (water of coordination, crystal water) in the crystal structures as observed for helical borophosphates [67, 68]. The result of a de–rehydration experiment of $Ni(H_2O)_2[B_2P_2O_8(OH)_2]\cdot H_2O$ is shown in *Figure 3.86*. After the first heating to 250 ºC a mass loss of 5.6 wt % (approximately 1.1 mol H_2O) is observed connected with an endothermic peak. After exposure to atmospheric moisture a weight gain of only 0.4 wt % is observed. Consequently, neither a significant mass loss nor an endothermic peak is detected during the second heating proving that the recovery of the hydrated phase was not obtained by exposing the sample of the dehydration phase to moisture.

The powder X–ray analyses of the dehydrated products indicated minor changes in the peak position of the starting compound and the presence of additional peaks which may suggest that the sample starts to decompose at 250 ºC. $Fe(H_2O)_2[B_2P_2O_8(OH)_2]\cdot H_2O$ and $Co(H_2O)_2[B_2P_2O_8(OH)_2]\cdot H_2O$ follow the same trend up to 250 ºC as observed for $Ni(H_2O)_2[B_2P_2O_8(OH)_2]\cdot H_2O$. The non–reversibility of the dehydration was also reported for the isotypic compound $Cu(H_2O)_2[B_2P_2O_8(OH)_2]\cdot H_2O$ [77].

The evolved gases during the decomposition of $Ni(H_2O)_2[B_2P_2O_8(OH)_2]\cdot H_2O$ were analyzed by mass spectrometry (*Figure 3.86*). Only water was detected during heating to 1000 ºC. The intensity of the signal is in accordance with the rate of the mass loss.

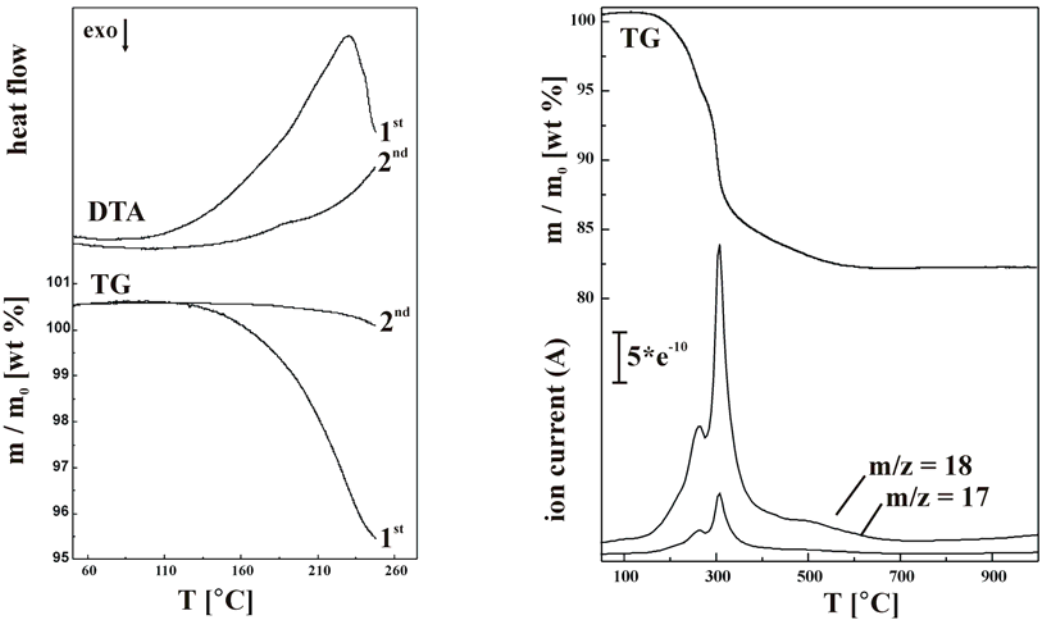

Figure 3.86: *TG and DTA traces for $Ni(H_2O)_2[B_2P_2O_8(OH)_2]\cdot H_2O$ (Figure left) when heated for the first time to 250 ºC and when reheated after the exposure to humid air. TG and DTA traces (m / z = 17, 18) for $Ni(H_2O)_2[B_2P_2O_8(OH)_2]\cdot H_2O$ (Figure right) when heated for the first time to 250 ºC and when reheated after the exposure to humid air.*

Table 3.15: *Thermal analyses of $M^{II}(H_2O)_2[B_2P_2O_8(OH)_2]\cdot H_2O$ (M^{II} = Fe, Co, Ni)*

Compound	Mol. Wt.	Expt. mass loss (wt%)	Calculated (wt%)	Decomposition product
Fe	249.79	20.4	18.4 ($4 \times H_2O$)	γ–$Fe_2P_2O_7$ [151] + α–BPO_4 [140]
Co	276.02	20.1	19.3 ($4 \times H_2O$)	α–$Co_2P_2O_7$ [149] + α–BPO_4 [140]
Ni	322.38	20.1	19.6 ($4 \times H_2O$)	σ–$Ni_2P_2O_7$ [150] + α–BPO_4 [140]

3.4.1.5 Magnetic susceptibility

The temperature–dependent magnetic susceptibility in a static magnetic field of 1 Tesla is shown in *Figure 3.87* for the compounds $M^{II}(H_2O)_2[B_2P_2O_8(OH)_2]\cdot H_2O$ (M^{II} = Fe, Ni).

The magnetic susceptibility was fitted in the range from 40 K to 400 K with a Curie–Weiss law including one parameter for the temperature–independent magnetism. The Curie constants C and the Weiss temperatures θ are: 3.345 cm^3 K / mol and 2.7 K for the Fe– compound, and 1.172 cm^3 K / mol and 0.62 K for the Ni– compound. These values are typical for isolated *3d* transition element ions in high–spin configuration. The magnetic behavior below 40 K indicates zero–field splitting and / or high–spin to low–spin transition. In contrast to $Cu(H_2O)_2[B_2P_2O_8(OH)_2]\cdot H_2O$ (θ = 27.77 K) [77] no ferrimagnetic ordering was observed in the examined temperature range. $Co(H_2O)_2[B_2P_2O_8(OH)_2]\cdot H_2O$ samples revealed contributions from unknown magnetic impurities which hide their genuine magnetic behavior.

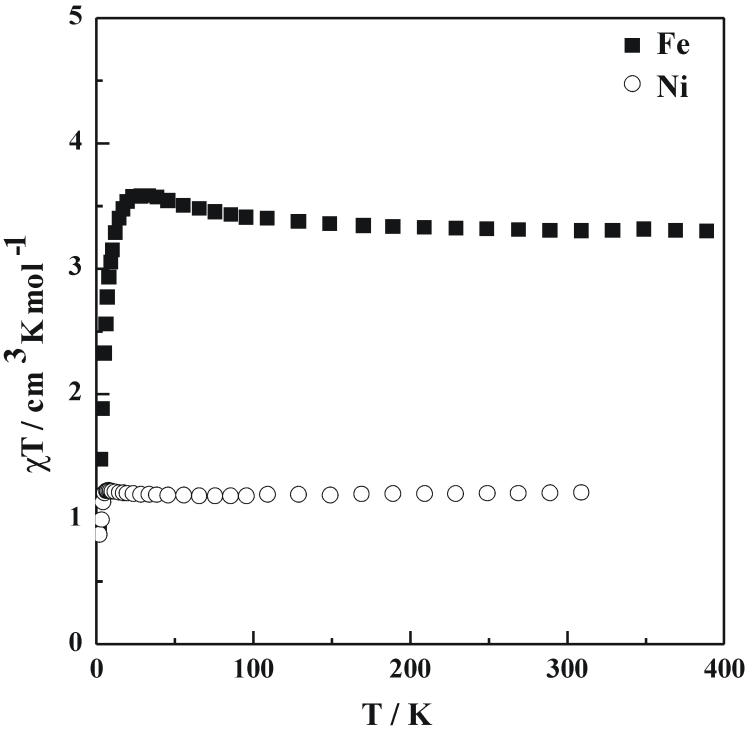

Figure 3.87: *Magnetic susceptibility of $M^{II}(H_2O)_2[B_2P_2O_8(OH)_2]\cdot H_2O$ (M^{II} = Fe, Ni) as a function of temperature.*

3.4.2 Discussion

Foremost, the topology and the directedness of the layers of the wavy 6^3 nets of tetrahedra observed in phosphates and silicates are described. The comparison of $M^{II}(H_2O)_2[BP_2O_8(OH)_2]\cdot H_2O$ (M^{II} = Fe, Co, Ni) (SPG: $P2_1/c$) is made with $Cu(H_2O)_2[B_2P_2O_8(OH)_2]\cdot H_2O$ (SPG: *Pbca*) [77]. Finally, correlation of substituted

phases of the two different transition metals with the pure transition metal compounds is discussed.

Topology and the directedness:

The topology of the layers and the directedness of their tetrahedra can be easily and very clearly visualized (*Figure 3.88*). Layered building units have proven to be suitable not only for describing the frameworks, but also for predicting unknown ones [146]. The term "Directedness" can either be upwards (U) or downwards (D), depending on the tetrahedra which point away from, and those which point towards the interior of the layer formed by the tetrahedra.

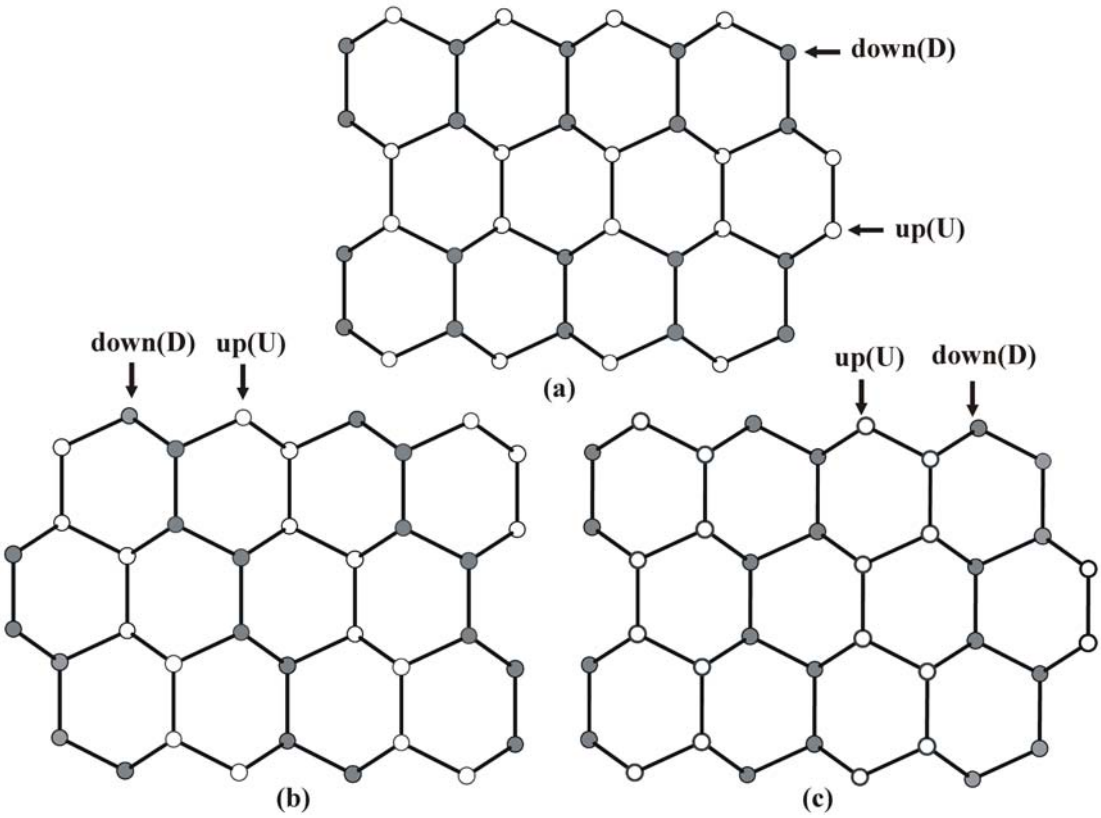

Figure 3.88: *Layered anionic partial structures in (a) δ–$Na_2Si_2O_5$ [152] (b) $[C_{10}N_2H_{10}][ZnCl(HPO_4)_2]$ [153] and (c) $M^{II}(H_2O)_2[B_2P_2O_8(OH)_2]\cdot H_2O$ (M^{II} = Fe, Co, Ni) revealing 6^3 topologies with different tetrahedral sequences (directedness, upwards and downwards).*

The schematic diagram of $^2{}_\infty[B_2P_2O_8(OH)_2]^{2-}$ anion is shown in *Figure 3.88c*. In each six–membered ring of the layer two adjacent tetrahedra are pointing in one direction (U or D), the remaining four in the opposite one. Anionic partial structures of single

layers with 6^3 net topology have already been observed previously in $[C_{10}N_2H_{10}][ZnCl(HPO_4)_2]$ [40] and in δ–$Na_2Si_2O_5$ [152]. In the six–membered ring of $[C_{10}N_2H_{10}][ZnCl(HPO_4)_2]$ (*Figure 3.88b*), three tetrahedra point in the same, the remaining three in the opposite direction whereas in δ–$Na_2Si_2O_5$ *(Figure 3.88a*), four tetrahedra are pointing in one direction and the remaining in the opposite direction. In silicates, these layer types are based on the periodicity of the fundamental chain from which the layer can be generated by successive linking. Only unbranched zweier, dreier, vierer, fünfer and sechser single layers have been discovered till date [146]. The anionic partial structure of $M^{II}(H_2O)_2[B_2P_2O_8(OH)_2]\cdot H_2O$ (M^{II} = Fe, Ni) is represented as vierer– single layer on the basis of silicate structural chemistry [146].

Comparision with $Cu(H_2O)_2[BP_2O_8(OH)_2]\cdot H_2O$:

The compounds $M^{II}(H_2O)_2[BP_2O_8(OH)_2]\cdot H_2O$ (M^{II} = Fe, Co, Ni) crystallize in the same space group (SPG: $P2_1/c$) as observed for $Mg(H_2O)_2[B_2P_2O_8(OH)_2]\cdot H_2O$ [78]. Comparing the situation with $Cu(H_2O)_2[B_2P_2O_8(OH)_2]\cdot H_2O$ (SPG: *Pbca*) [77], the main structural difference is observed concerning the coordination polyhedron around the transition metal. As known for many other compounds Cu^{2+} (d^9) prefers a strongly distorted six–fold coordination sphere. Hence, in $Cu(H_2O)_2[B_2P_2O_8(OH)_2]\cdot H_2O$ [77] four short equatorial distances ranging from 1.943 Å to 1.954 Å and two significantly longer ones to the water molecules (2.532 Å) are present.

$M^{II}(H_2O)_2[B_2P_2O_8(OH)_2]\cdot H_2O$ (M^{II} = $Ni_{0.5}Co_{0.5}$, $Ni_{0.8}Zn_{0.2}$, $Ni_{0.5}Mg_{0.5}$):

Substituted phases of two different transition metal ions $Ni_{0.5}Co_{0.5}(H_2O)_2[B_2P_2O_8(OH)_2]\cdot H_2O$, $Ni_{0.8}Zn_{0.2}(H_2O)_2[B_2P_2O_8(OH)_2]\cdot H_2O$ and $Ni_{0.5}Mg_{0.5}(H_2O)_2[B_2P_2O_8(OH)_2]\cdot H_2O$ were also realized for this structure type similar to $Mg_{1-x}Co_x(H_2O)_2[B_2P_2O_8(OH)_2]\cdot H_2O$ ($x \approx 0.25$) [78]. The crystal structures were solved in the monoclinic space group $P2_1/c$ (No. 14) and the cell parameters are given in *Table 3.16*. Crystallographic data, refinement parameters, the final fractional atomic coordinates and equivalent / isotropic and anisotropic displacement factors for all the compounds under discussion are listed in *Appendix 91* to *Appendix 93* and *Appendix 94* to *Appendix 99*. Interatomic distances and bond angles are given in *Appendix 100* and *Appendix 101*.

Chemical analyses of the powdered samples dissolved in acids comprised a ratio of Ni : Co = 0.5 : 0.5, Ni : Mg = 0.8 : 0.2 and Ni : Mg = 0.5 : 0.5 which was also supported by EDX analyses (Ni : Co = 0.5 : 0.5, Ni : Mg = 0.8 : 0.2 and Ni : Mg = 0.5 : 0.5). The composition of Co, Ni, Zn and Mg was fixed from results obtained from the EDX and the chemical analyses.

Table 3.16: *Lattice parameters of $M^{II}(H_2O)_2[B_2P_2O_8(OH)_2]\cdot H_2O$ (M^{II} = $Ni_{0.5}Co_{0.5}$, $Ni_{0.8}Zn_{0.2}$, $Ni_{0.5}Mg_{0.5}$)*

	a (Å)	*b* (Å)	*c* (Å)	*β*	*Z*
$Ni_{0.5}Co_{0.5}$	7.7411(7)	14.6307(9)	8.2146(4)	90.248(3)	2
$Ni_{0.8}Zn_{0.2}$	7.7411(5)	14.5893(10)	8.2928(7)	90.257(4)	2
$Ni_{0.5}Mg_{0.5}$	7.7389(5)	14.5735(9)	8.2060(4)	90.254(3)	2

The relation between unit cell volume verses mole fraction (Zen's law) of the substituted phases are compared with the "end" members is shown in *Figure 3.89a – Figure 3.89c*. The compounds $Ni_xCo_{1-x}(H_2O)_2[B_2P_2O_8(OH)_2]\cdot H_2O$ (x = 0, 0.5, 1) and $Ni_xZn_{1-x}(H_2O)_2[B_2P_2O_8(OH)_2]\cdot H_2O$ (x = 0.8, 1) (although pure zinc compound has not been reported yet) show linear dependence whereas the compound $Ni_xMg_{1-x}(H_2O)_2$ $[B_2P_2O_8(OH)_2]$ H_2O (x = 0, 0.5, 1) shows non–linear dependence. The same situation is true for the correlation between unit cell volume and mean cationic radius [122] (Shannon 1976) of the transition metal cations (*Figure 3.89d*).

From *Figure 3.89,* it is clear that there is a chance to synthesize a complete series for the transition metals containing $Ni_xCo_{1-x}(H_2O)_2[B_2P_2O_8(OH)_2]\cdot H_2O$ (x = 0 – 1) and $Ni_xZn_{1-x}(H_2O)_2[B_2P_2O_8(OH)_2]\cdot H_2O$ (x = 0 – 1) but the preliminary result show a significant divergence for the transition metal and the alkaline–earth metal containing $Ni_xMg_{1-x}(H_2O)_2$ $[B_2P_2O_8(OH)_2]$ H_2O (x = 0 – 1).

Thermochemical properties of $M^{II}(H_2O)_2[B_2P_2O_8(OH)_2]\cdot H_2O$ (M^{II} = $Ni_{0.5}Co_{0.5}$, $Ni_{0.8}Zn_{0.2}$, $Ni_{0.5}Mg_{0.5}$) were investigated by simultaneous constant rate thermogravimetry (TG) with heating and cooling rates of 5 K / min up to 1000 ºC in a continuous argon gas flow. The overall mass loss of the compounds was comparable with the expected one for the release of 4 mole water per formula ($Ni_{0.5}Co_{0.5}$: calc – 20.1 wt % / exp –19.8 wt %, $Ni_{0.8}Zn_{0.2}$: calc –20.0 wt % / exp –18.4 wt %). The products identified by powder XRD after thermal treatment corresponds to their pyrophosphates and α–BPO_4. IR spectra showed characteristic absorption bands in the range of 3000 – 3600 cm^{-1} confirming the presence of O—H groups.

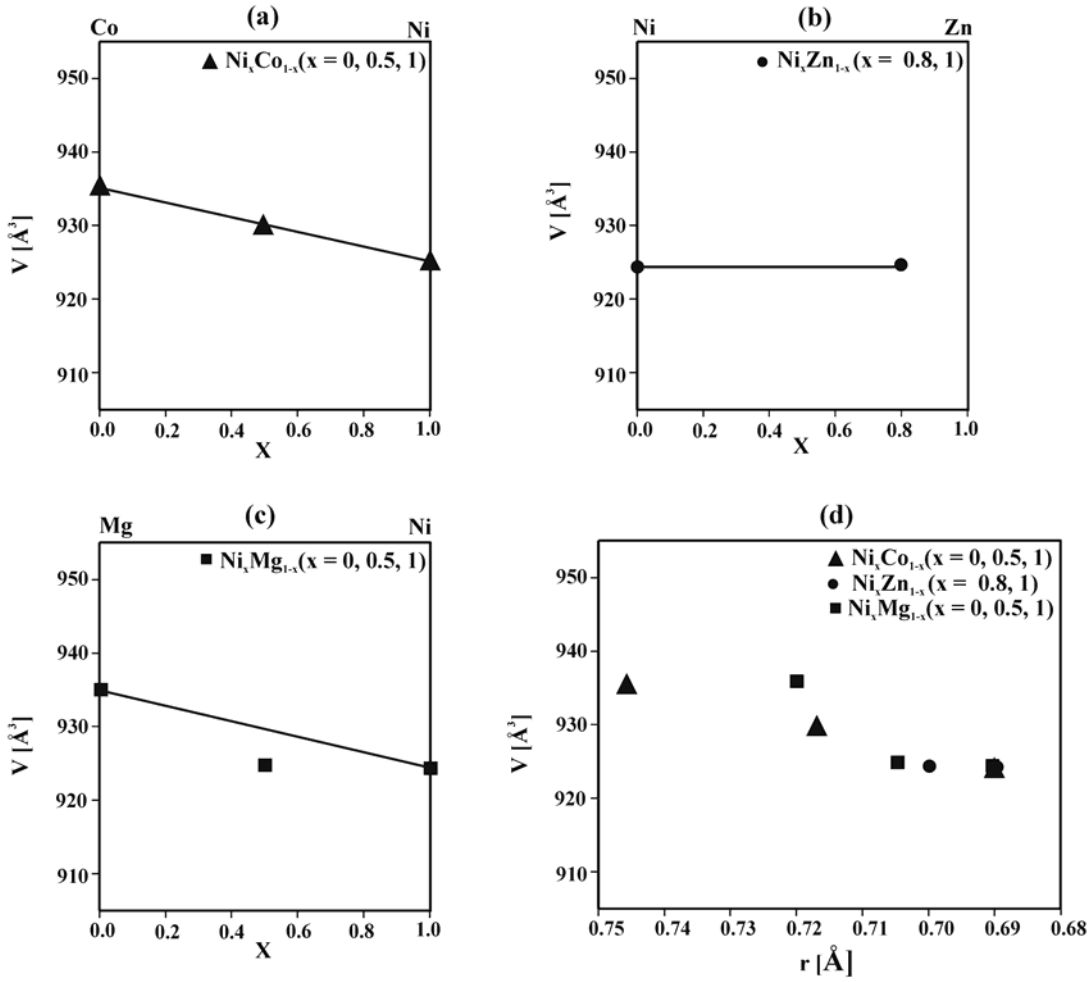

Figure 3.89*: Relation between unit cell volume V verses mole fraction X (Zen's law) of (a) $Ni_xCo_{1-x}(H_2O)_2[B_2P_2O_8(OH)_2]\cdot H_2O$ (x =0, 0.5, 1) and (b) $Ni_xZn_{1-x}(H_2O)_2[B_2P_2O_8(OH)_2]\cdot H_2O$ (x = 0.8, 1) show linear dependence whereas (c) $Ni_xMg_{1-x}(H_2O)_2[B_2P_2O_8(OH)_2]\cdot H_2O$ (x = 0, 0.5, 1) shows non–linear dependence. The correlation between unit cell volume and mean cation radius [122] (Shannon 1976) of the transition metal cations are shown in (d).*

3.5 Mixed Transition Metal Phosphates and Borophosphates

In this chapter the results obtained during the synthesis of transition metal borophosphates are presented. First, the preparation and characterization of the mixed transition metal borophosphates and phosphates are reported and the complex anionic partial structures and their arrangements in the crystal structure are described. Further on, a brief description of the thermal and magnetic behavior of these compounds is given.

3.5.1 $FeCo(H_2O)[BP_3O_9(OH)_4]$ and $Fe_{1.3}Co_{0.7}[P_2O_7]\cdot 2H_2O$

3.5.1.1 Synthesis

Single crystals of $FeCo(H_2O)[BP_3O_9(OH)_4]$ and $Fe_{1.3}Co_{0.7}[P_2O_7]\cdot 2H_2O$ were obtained under mild hydrothermal conditions.

$FeCo(H_2O)[BP_3O_9(OH)_4]$: Single crystals were prepared from a mixture of 0.5006 g $FeC_2O_4\cdot 2H_2O$, 0.3305 g $CoCO_3$, 0.3437 g H_3BO_3 and 1.9225 g H_3PO_4 in the molar ratio Fe : Co : B : P = 1 : 2 : 2 : 6. 10 ml of deionized water was added and stirred at 100 ºC. During stirring, 2 ml HCl (37 %) were added to adjust the pH value to 1. The mixture was then filled into a 10 ml Teflon–lined autoclave (filling degree 30 %) and heated at 170 ºC under autogenous pressure for 8 days.

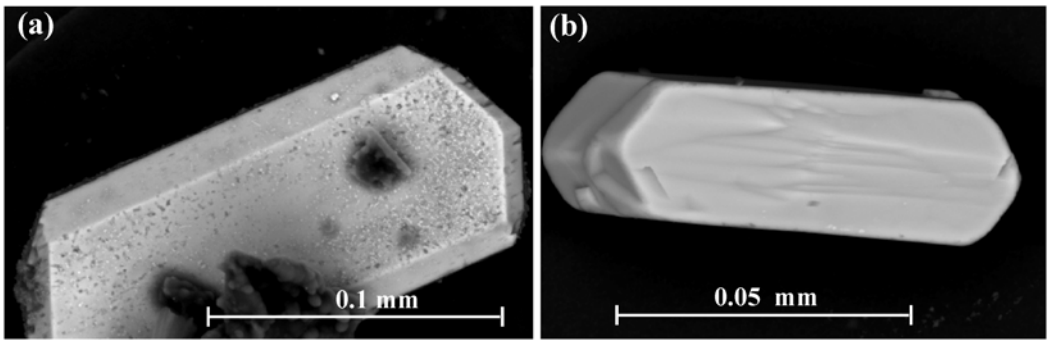

Figure 3.90: *SEM images of single crystals of (a) $FeCo(H_2O)[BP_3O_9(OH)_4]$ and (b) $Fe_{1.3}Co_{0.7}[P_2O_7]\cdot 2H_2O$*

$Fe_{1.3}Co_{0.7}[P_2O_7]\cdot 2H_2O$: Single crystals were synthesized using a mixture of 1.0007 g $Co(CH_3COO)_2\cdot 4H_2O$, 1.4444 g $FeC_2O_4\cdot 2H_2O$ and 2.7771 g H_3PO_4 (85 %) in the

molar ratio Fe : Co : P = 1 : 2 : 6. 10 ml of deionized water were added followed by 1 ml HCl (37 %) to adjust the pH value to 1. The mixture was then filled into a 10 ml Teflon–lined autoclave (filling degree 30%) and heated at 170 ºC under autogenous pressure for 7 days.

The resulting products in each case were filtered off, washed with deionized water / acetone and dried at 60 ºC in air. The pink crystals obtained were up to 0.2 mm in length. SEM micrographs of $FeCo(H_2O)[BP_3O_9(OH)_4]$ and $Fe_{1.3}Co_{0.7}[P_2O_7]\cdot 2H_2O$ are shown in *Figure 3.90*. The phase purity of the reaction products was checked using powder X–ray diffraction. The observed powder pattern fits quite well with the calculated powder pattern (*Figure 3.91* and *Figure 3.92*).

The results of the chemical analyses are given in *Table 3.17*. The elements iron, cobalt, boron and phosphorus were analyzed using ICP–OES. Hydrogen was analyzed by the hot extraction method. Except boron and hydrogen the elements were confirmed by EDX measurements (Fe : Co : P ≈ 1 : 1 : 3; Fe : Co : P ≈ 1.3 : 0.7 : 2). Infrared spectra were consistent with the presence of —OH groups (see *Appendix 5.4.5*)

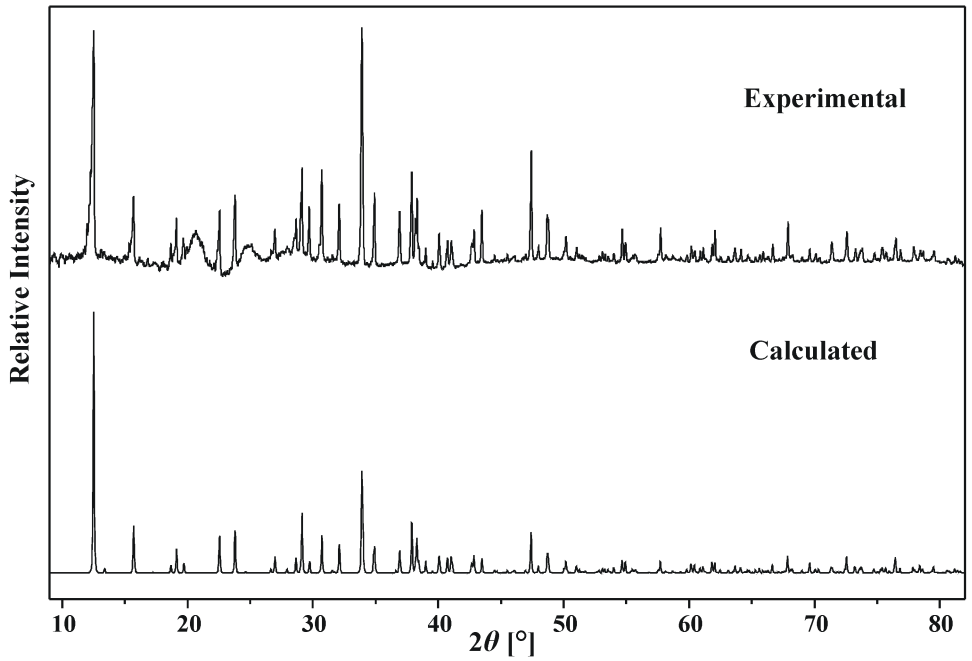

Figure 3.91: *Observed (background subtracted) and calculated powder X–ray diffraction patterns of* $FeCo(H_2O)[BP_3O_9(OH)_4]$ *(Co* $K_{\alpha 1}$*–radiation)*

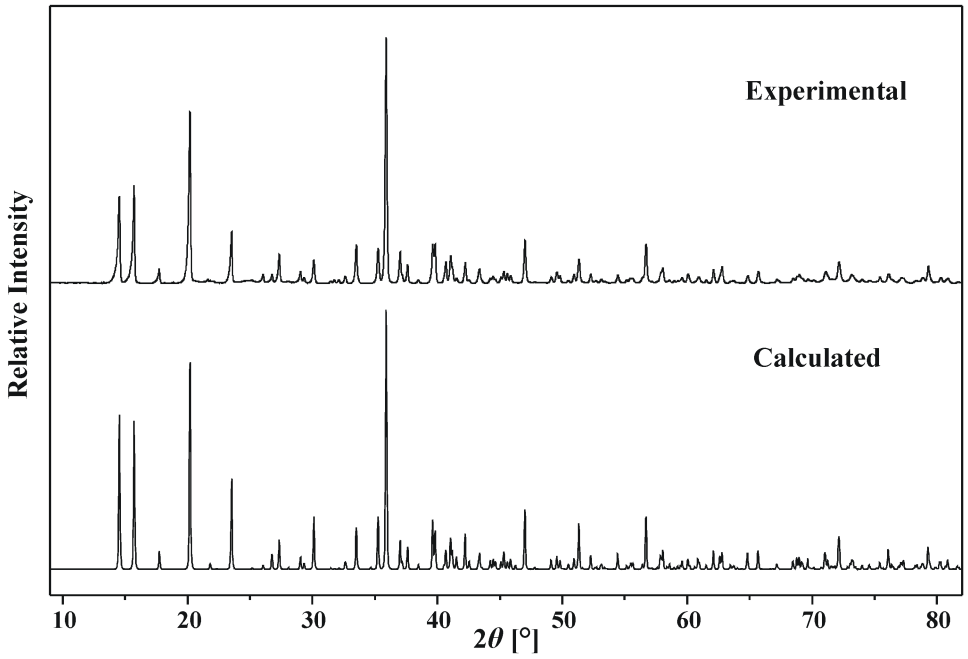

Figure 3.92: *Observed (background subtracted) and calculated powder X–ray diffraction patterns of* $Fe_{1.3}Co_{0.7}[P_2O_7]\cdot 2H_2O$ *(Co* $K_{\alpha 1}$*–radiation)*

Table 3.17: *Results of chemical analyses of* $FeCo(H_2O)[BP_3O_9(OH)_4]$ *and* $Fe_{1.3}Co_{0.7}[P_2O_7]\cdot 2H_2O$

Element	Observed (e.s.d.) weight %	Calculated weight %
Fe	10.78(02)	12.45
Co	13.96(02)	13.14
B	2.33(03)	2.41
P	18.98(08)	20.72
O	45.45(25)	49.94
H	1.39(02)	1.35
Fe	23.93(21)	22.41
Co	11.06(08)	12.73
P	18.71(17)	19.12
O	44.25(30)	46.46
H	2.30(07)	1.24

3.5.1.2 Crystal Structure Determination

$FeCo(H_2O)[BP_3O_9(OH)_4]$: A suitable single crystal was selected. The X–ray data were collected with long and short exposure times in order to obtain accurate intensities of strong and weak reflections. The crystal structure of $FeCo(H_2O)[BP_3O_9(OH)_4]$ was solved in the orthorhombic space group $P2_12_12_1$ (No. 19) (a = 7.1353(4) Å, b = 8.6742(4) Å, c = 16.4052(7) Å, Z = 2) by direct methods. With this step the atomic positions of the Fe, Co, P and most of the oxygen atoms were localized already. The remaining atomic sites were located during least squares refinements from the difference Fourier maps. Hydrogen atoms were found close to O8, O11, O12, O13 and O14, the coordinates and displacement parameters could be refined as free variables. The composition of Fe and Co (Fe : Co = 1 : 1) was fixed from EDX and chemical analyses. The Flack parameter x indicated the presence of racemic twinning. The refinement of the atomic coordinates and anisotropic thermal parameters led to reliability factors R1 = 0.027 and wR2 = 0.062 ($I > 2\sigma$ (I)) considering 2843 independent reflections.

$Fe_{1.3}Co_{0.7}[P_2O_7]\cdot 2H_2O$: A suitable but rather small single crystal was selected for single crystal XRD analysis. The data were collected and the structure was solved in the monoclinic space group $P2_1/n$ (No.14) (a = 6.3868(5) Å, b = 14.1318(11) Å, c = 7.4051(8) Å, β = 95.148(5)º, Z = 4) by direct methods. The positions of Fe, Co, P, and O could be unambiguously located. The position of the protons could be located in the difference Fourier maps (close to O5 and O9), and their coordinates were refined as free variables. The Fe : Co (Fe : Co = 1.3 : 0.7) ratio was fixed from EDX analyses. The refinement of the atomic coordinates and anisotropic thermal parameters led to reliability factors R1 = 0.040 and wR2 = 0.092 ($I > 2\sigma$ (I)) considering 1551 independent reflections.

The crystallographic data and refinement parameters of $FeCo(H_2O)[BP_3O_9(OH)_4]$ and $Fe_{1.3}Co_{0.7}[P_2O_7]\cdot 2H_2O$ are summarized in *Appendix 102* and *Appendix 103*. The final fractional atomic coordinates, equivalent / isotropic and anisotropic displacement factors are enlisted in *Appendix 104 to Appendix 107*.

3.5.1.3 Crystal Structure Description

$FeCo(H_2O)[BP_3O_9(OH)_4]$: The crystals structure of $FeCo(H_2O)[BP_3O_9(OH)_4]$ is an isotype of $Mg_2(H_2O)[BP_3O_9(OH)_4]$ [145]. The anionic partial structure,

$[BP_3O_9(OH)_4]^{4-}$, represents an open–branched tetramer built from a central hydrogenborate tetrahedron ($(HO)BO_3$) sharing common O–corners with one hydrogenphosphate ($(HO)PO_3$), one dihydrogenphosphate ($(HO)_2PO_2$), and one phosphate tetrahedron (PO_4) as shown in *Figure 3.93*.

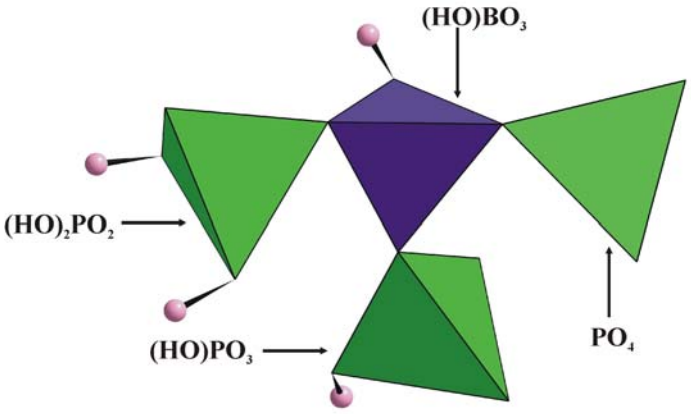

Figure 3.93: *Anionic partial structure of $FeCo(H_2O)[BP_3O_9(OH)_4]$: an open–branched tetramer built from a central $(HO)BO_3$ group sharing common O– corners with one $(HO)_2PO_2$, one $(HO)PO_3$, and one PO_4 tetrahedron.*

Both crystallographically independent M^{II} sites (M^{II} = $Fe_{0.5}Co_{0.5}$) are six–fold coordinated with five oxygen atoms and one OH–group ($M^{II}O_5(OH)$) and five oxygen atoms and one water molecule ($M^{II}O_5(H_2O)$), respectively. The resulting $M^{II}O_5(OH)$ and $M^{II}O_5(OH_2)$ coordination octahedra are alternatively connected *via* common edges to form infinite zigzag chains running along [010] as shown in *Figure 3.94a*.
Each bend of the octahedral chain $M^{II}O_5(OH)$ and $M^{II}O_5(OH_2)$ octahedra are bridged with the central borate group and the branching $(HO)PO_3$ and PO_4 units (intrastrand connection, *Figure 3.94b*) of borophosphate anion. The $(HO)_2PO_2$ groups, which are not involved in the intrastrand connection are linked to neighbouring chains (interstrand connection) at the concatenating edge of the M^{II} coordination octahedra (*Figure 3.94c*). Thus, each $[BP_3O_9(OH)_4]^{4-}$ is connected to three chain entities and every oxygen which is part of a shared edge in the 1D infinite octahedral arrangement is threefold bounded to two M^{II} and one phosphorus atom. A view along [010] (*Figure 3.95*) shows the resulting 3D arrangement in which the octahedra form a hexagonal rod–packing arrangement interconnected by the borophosphate anions.

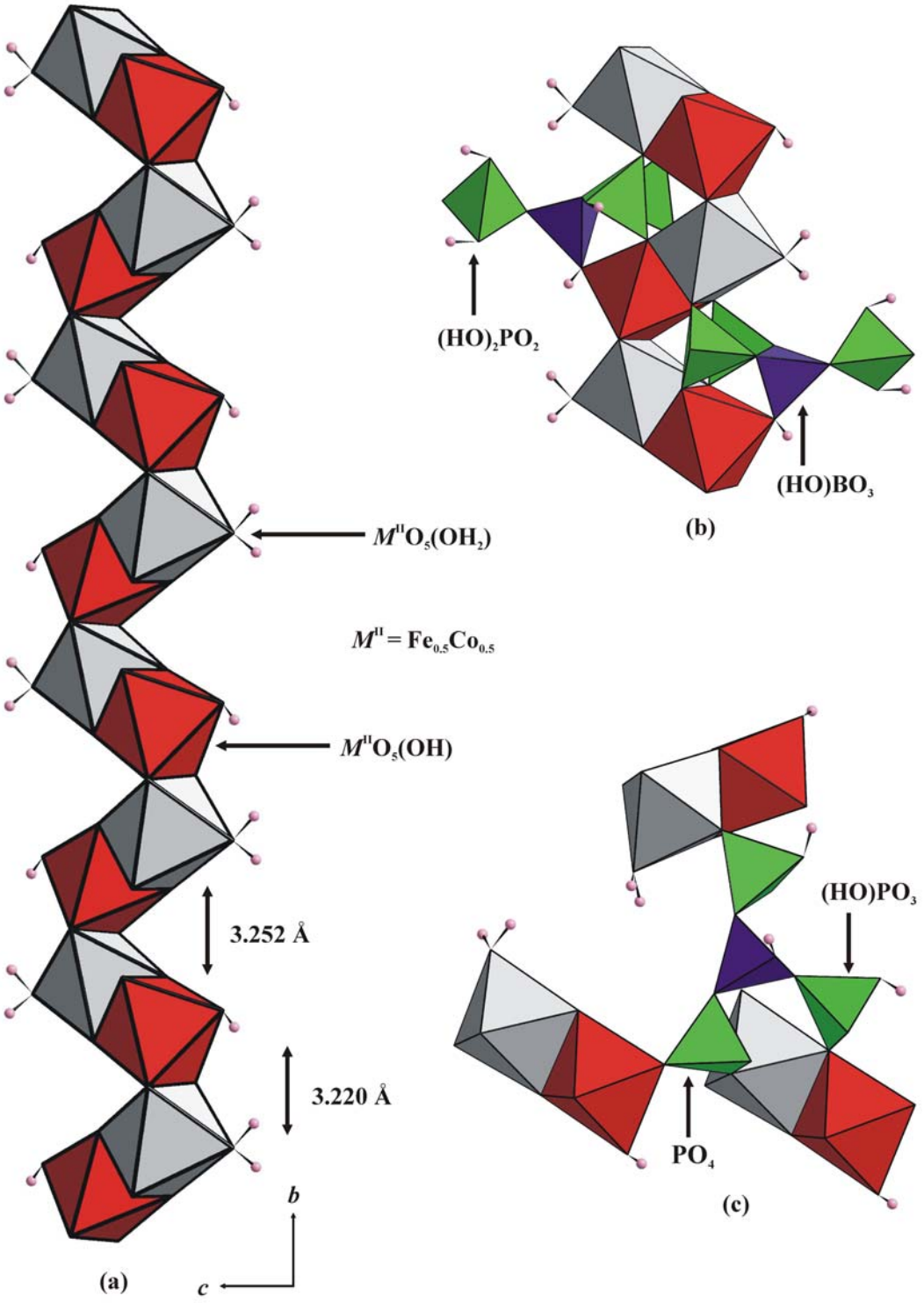

Figure 3.94: *(a) Corrugated chain of alternating edge–sharing $M^{II}O_5(OH)$ and $M^{II}O_5(H_2O)$ octahedra ($M^{II} = Fe_{0.5}Co_{0.5}$) running along [010]. (b) borophosphate anions coordinating the M^{II} centers along the chain with the central hydrogenborate, hydrogenphosphate ($(HO)PO_3$) and phosphate (PO_4) units (intrastrand connection) and (c) two adjacent octahedral chains linked to the complex polyanion via dihydrogenphosphate ($(HO)_2PO_2$) and phosphate tetrahedra (PO_4) (interstrand connection).*

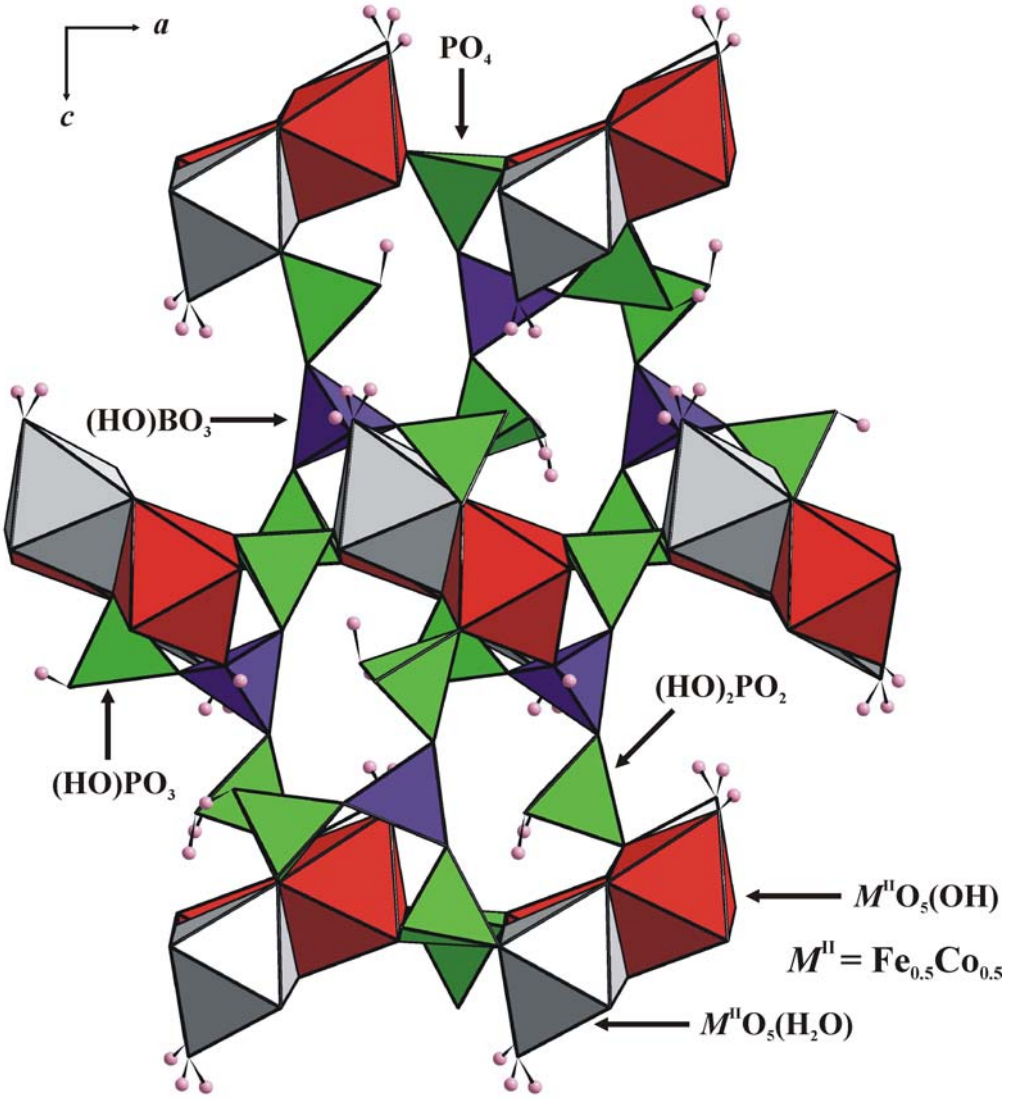

Figure 3.95: *3D arrangement of polyhedra in the crystal structure of $FeCo(H_2O)[BP_3O_9(OH)_4]$ viewed along [010]. Each chain of octahedra is surrounded by six neighbouring chains (hexagonal rod–packing), interconnected by the borophosphate tetramers.*

Selected bond lengths and bond angles of the crystal structures of $FeCo(H_2O)[BP_3O_9(OH)_4]$ are enlisted in *Appendix 108*. B—O distances and O—B—O angles range from 1.440(4) Å to 1.477(4) Å and 102.2(2)° to 112.4(2)°, respectively. In the (hydrogen) phosphate groups the P—O distances and the O—P—O angles are found in the range from 1.509(2) Å to 1.573(3) Å and 101.55(11)° to 113.12(11)°, respectively. While for the borate unit the distance B—OH = 1.440(4) Å is significantly short, two long P—OH distances are found in the $(HO)PO_3$ and $(HO)_2PO_2$ groups (1.573(2) Å and 1.559(2) Å) and a shorter one for the second

hydroxy group of the $(HO)_2PO_2$ unit (1.537(2) Å) which is involved in a hydrogen bond to the PO_4 unit (d(O11—H11···O2) = 2.507(1) Å).

The M^{II}—O distances range from 2.082(2) Å to 2.213(2) Å and rather short bonds are observed for $d(M^{II}—OH)$ = 2.099(2) Å and $d(M^{II}—OH_2)$ = 2.093(2) Å. O—M^{II}—O angles within the octahedra have values between 79.32(8)° and 179.72(9)°. $M^{II}\cdots M^{II}$ distances along the chain alternate between 3.220(3) Å and 3.252(3) Å (*Figure 3.94a*). Hydrogen bonds are formed between the dihydrogenphosphate groups and the phosphate groups. The relatively long O—H and short H···O distances d(O11—H11) = 1.15(6) Å, d(H11···O2) = 1.363(2) Å) as well as the angle O11—H11···O2 = 173.07(4)° indicate a strong hydrogen bond interaction in which the proton is clearly directed towards the acceptor oxygen.

$Fe_{1.3}Co_{0.7}[P_2O_7]\cdot 2H_2O$: The crystal structure of $Fe_{1.3}Co_{0.7}[P_2O_7]\cdot 2H_2O$ belongs to the isotypic series $M^{II}[X_2O_7]\cdot 2H_2O$ (M^{II} = Mg, Mn, Co, Fe and X = P, As) [145, 154-156]. The anionic partial structure, $[P_2O_7]^{2-}$, comprises of two phosphate tetrahedra sharing a common O–corner as shown in *Figure 3.97*.

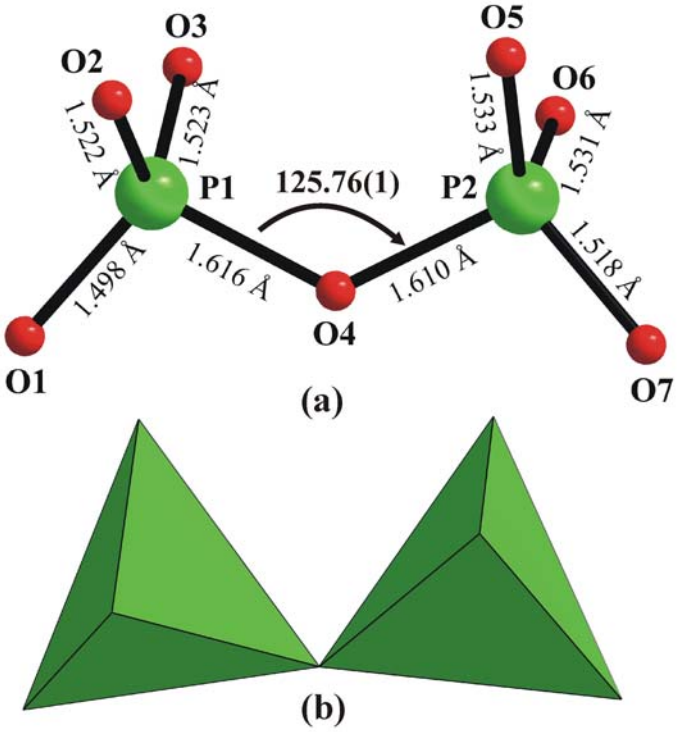

Figure 3.96: *(a) The diphosphate anion, $[P_2O_7]^{4-}$ viewed approximately perpendicular to the P1 / O4 / P2 plane (P1—O4—P2 = 125.76°), (b) Polyhedral representation.*

The two crystallographically independent phosphorus sites are tetrahedrally bound to oxygen atoms and share a common vertex (O4) to form the diphosphate group. The confirmation of the diphosphate anion is close to eclipsed and exhibits a bent angle P—O—P of 125.76(1)°. P—O distances for the terminal oxygen atoms range from 1.498(3) Å to 1.532(3) Å, those to the bridging oxygen atom are longer (1.615(3) Å and 1.611(3) Å) and the O—P—O angles range from 104.15(17)° to 114.71(18) (comparable to other iron diphosphates), respectively.

Edge–sharing ($FeO_5(H_2O)$) and mixed iron / cobalt coordination octahedra, ($Fe_{0.3}Co_{0.7}O_5(H_2O)$), form infinite chains running along [010] (*Figure 3.97a*), which are connected *via* diphosphate anions. The remaining (free) octahedral positions at Fe and $Fe_{0.3}Co_{0.7}$ are occupied by coordination water. The three–dimensional arrangement of polyhedra in the crystal structure of $Fe_{1.3}Co_{0.7}[P_2O_7]\cdot 2H_2O$ is shown in *Figure 3.97b* and cavities running along [100]. The protons of the aqua–ligands all point into a common channel as shown in *Figure 3.98*.

Selected bond lengths and bond angles in the crystal structure of $Fe_{1.3}Co_{0.7}[P_2O_7]\cdot 2H_2O$ are given in *Appendix 109*. The iron and the mixed cobalt / iron sites are in octahedral coordination by one water molecule and five oxygen atoms of diphosphate groups. Fe—O distances range from 2.078(3) Å to 2.171(3) Å and the O—Fe—O angles have values between 81.90(11)° and 173.36(15)°. $Fe_{0.3}Co_{0.7}$—O distances range from 2.022(3) Å to 2.195(3) Å and the O—$Fe_{0.3}Co_{0.7}$—O angles have values between 81.19(11)° and 173.95(12)°. The two aqua–ligands consist of the protons H8A and H8B attached to O8 at $Fe_{0.3}Co_{0.7}O_5(H_2O)$ and the protons H9A and H9B attached to O9 at $FeO_5(H_2O)$ (*d*(O8—H8A) = 0.82(7) Å, *d*(O8—H8B) = 0.81(9) Å; *d*(O9—H9A) = 0.70(15) Å, *d*(O9—H9) = 0.73(10) Å). These values are in good agreement with those reported for a series of iron (II) phosphate hydrates and iron diphosphates [101]. Distances Fe···($Co_{0.7}Fe_{0.3}$) along the chain are 3.207(2) Å and 3.260(2) Å, respectively.

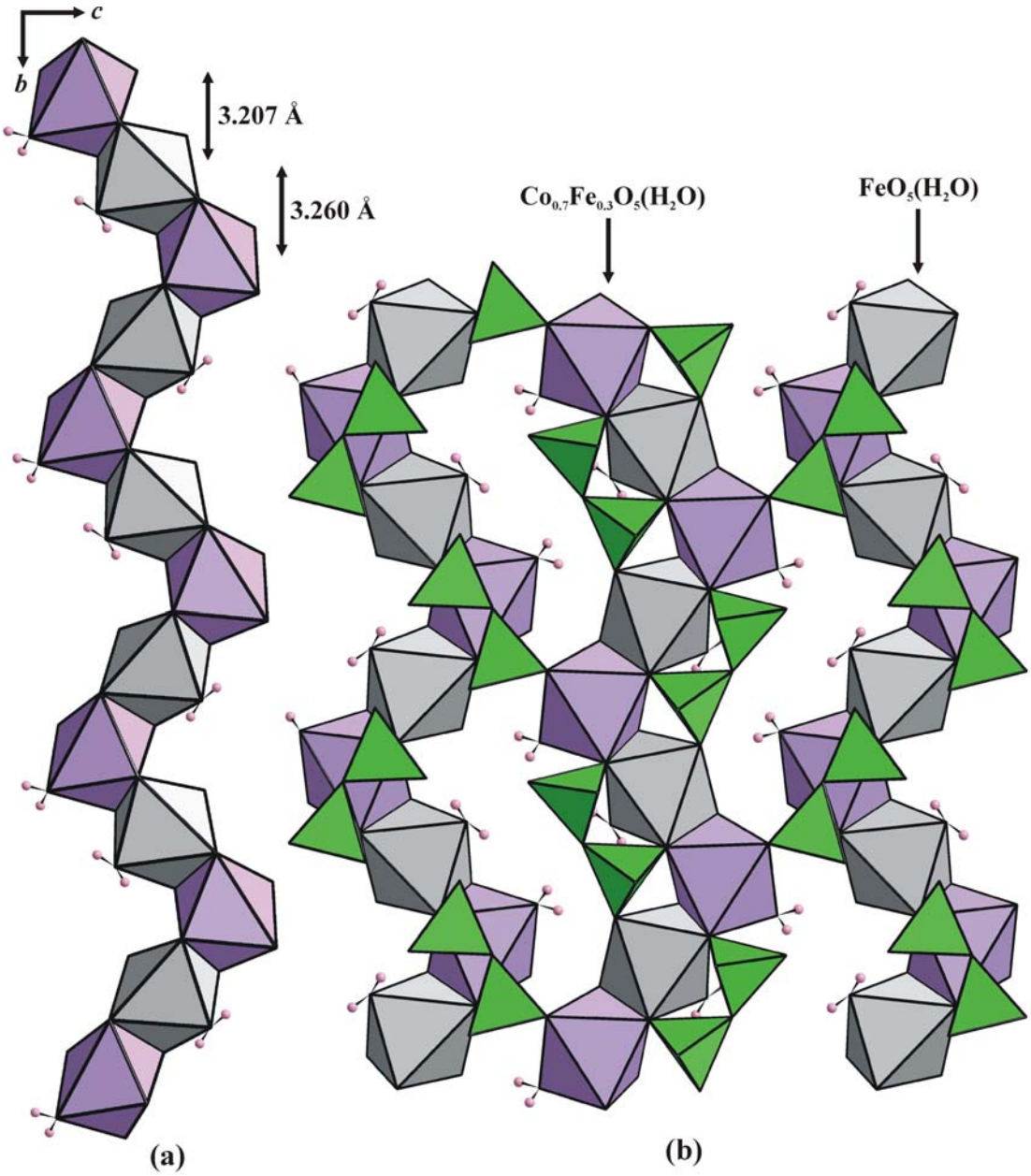

Figure 3.97: *(a) Edge–sharing coordination octahedra $FeO_5(H_2O)$ and $Co_{0.7}Fe_{0.3}O_5(H_2O)$, forming an infinite chain. Distances $Fe\cdots(Co_{0.7}Fe_{0.3})$ along the chain are 3.207(2) Å and 3.260(2) Å, respectively. (b) 3D arrangement of polyhedra in the crystal structure of $Fe_{1.3}Co_{0.3}[P_2O_7]\cdot 2H_2O$. The octahedral chains are inter–connected by bridging diphosphate groups.*

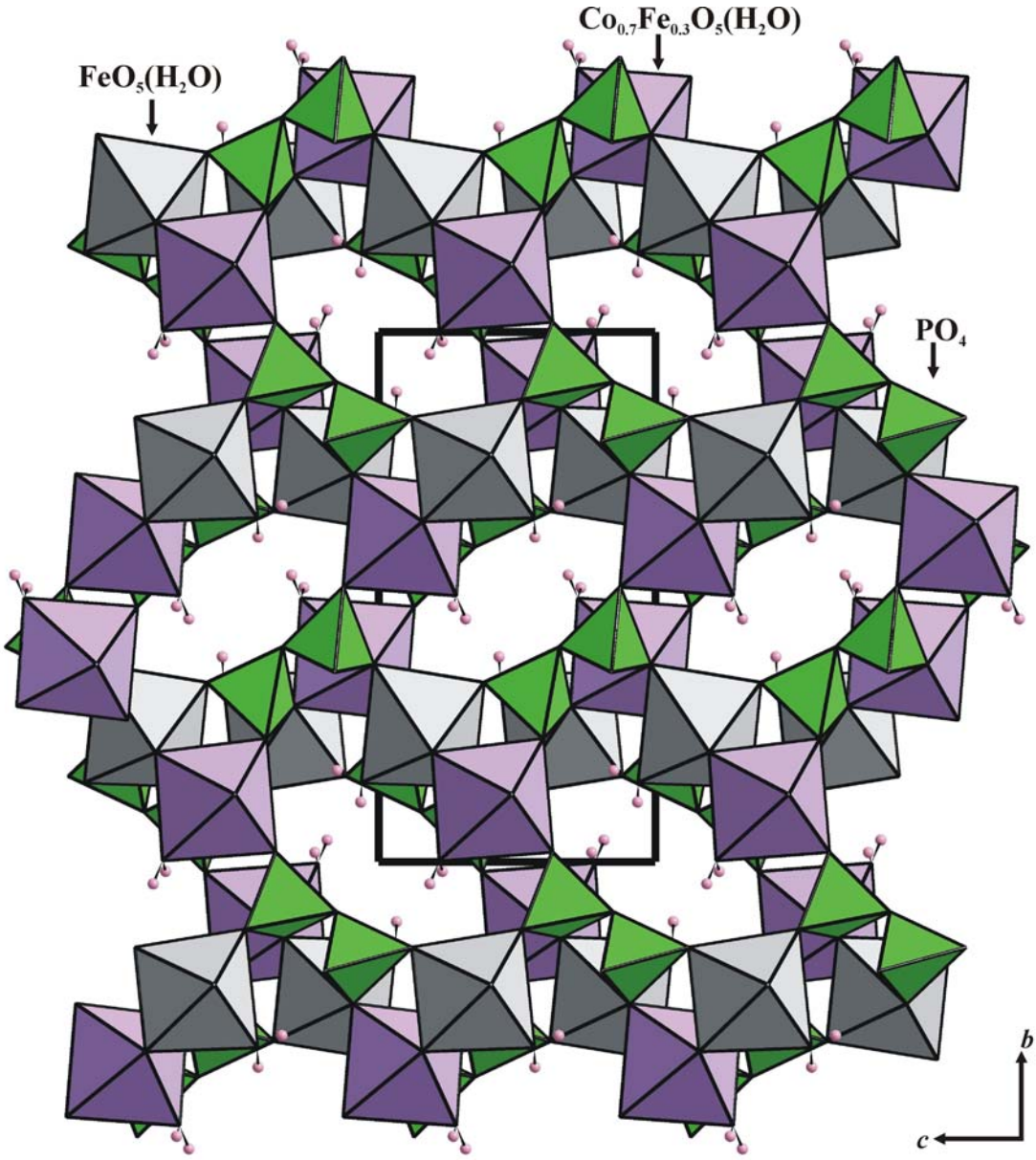

Figure 3.98: *Crystal structure of $Fe_{1.3}Co_{0.7}[P_2O_7]\cdot 2H_2O$ with channels running along [100]. The protons of the aqua–ligands point into common channels. The unit cell is outlined.*

3.5.1.4 Thermal Analysis

Simultaneous constant rate thermogravimetry (TG) and difference thermal analysis (DTA) of $FeCo(H_2O)[BP_3O_9(OH)_4]$ and $Fe_{1.3}Co_{0.7}[P_2O_7]\cdot 2H_2O$ were carried out on samples dried at 60 ºC. The samples are placed in an open crucible and heated with rate of 5 K / min to 1000 ºC in a continuous argon gas flow.

The TG curve of $FeCo(H_2O)[BP_3O_9(OH)_4]$ (*Figure 3.99*) shows a two step mass loss which is not well resolved. The mass loss slowly starts at 140 ºC and drops drastically

at 330 ºC. The overall mass loss is observed to be 13.1 %, which is slightly higher than the loss of three water molecules per formula unit (3 × H_2O, 1 mol H_2O = 4.01 wt %, calculated). Endothermic effects with discrete maxima at 161 ºC and 365 ºC were observed. In addition, at higher temperatures, two small exothermic effects appeared at 577 ºC and 657 ºC. After DTA / TG investigations, the pink product was investigated by powder X–ray diffraction (*Figure 3.101*). The pattern was indexed and identified as a mixture of the pyrophosphate α–$Co_2P_2O_7$ [157] (from the lattice parameters) and α–BPO_4 [140] (*Table 3.2*).

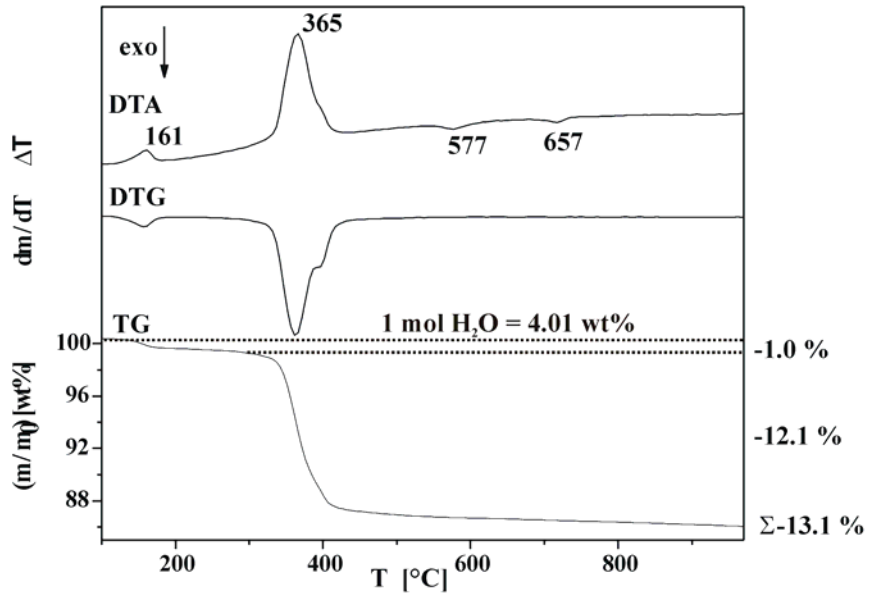

Figure 3.99: *Simultaneous thermogravimetry (TG) and difference thermal analysis (DTA) of $FeCo(H_2O)[BP_3O_9(OH)_4]$ as well as the first derivative (DTG) of the TG trace. The measured mass loss is given on the bottom right (1 mol H_2O = 4.01 weight %).*

The TG curve of $Fe_{1.3}Co_{0.7}[P_2O_7]\cdot 2H_2O$ (*Figure 3.100*) shows one step mass loss. The mass loss starts at 280 °C with an overall loss of 12.11 %, which is close to the calculated loss of two molecules of water per formula unit (2 × H_2O, 1 mol H_2O = 5.55 wt %, calculated). An endothermic peak appears at maxima 451 °C coinciding with the mass loss. After thermal treatment, the pink product was analyzed by powder X–ray diffraction (*Figure 3.102*). The lattice parameters obtained from the powder pattern showed the presence of the pyrophosphate α–$Co_2P_2O_7$ [157] (*Table 3.2*).

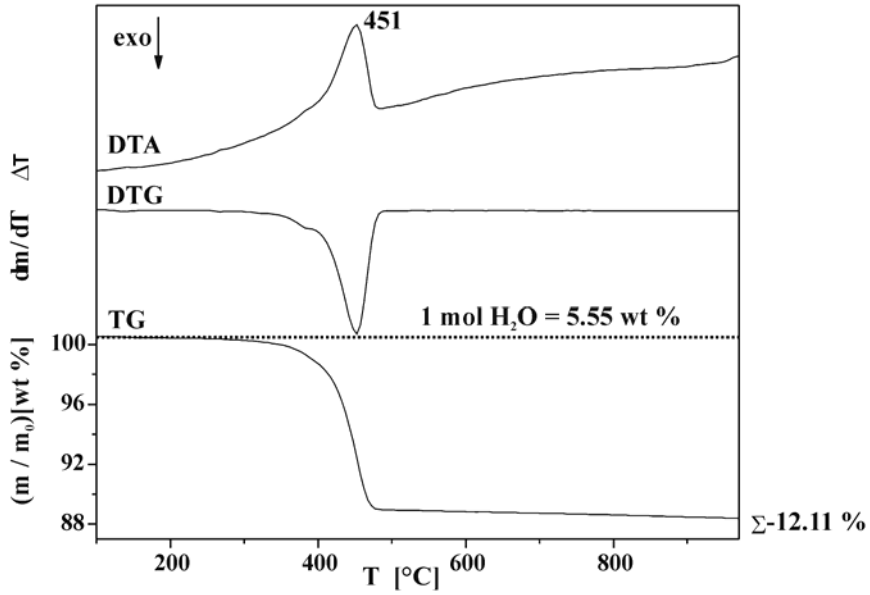

Figure 3.100: *Simultaneous thermogravimetry (TG) and difference thermal analysis (DTA) of* $Fe_{1.3}Co_{0.7}[P_2O_7]\cdot 2H_2O$ *as well as the first derivative (DTG) of the TG trace. The measured mass loss is given on the bottom right (1 mol* H_2O *= 5.55 weight %).*

Table 3.18: *Details of thermal analyses of* $FeCo(H_2O)[BP_3O_9(OH)_4]$ *and* $Fe_{1.3}Co_{0.3}[P_2O_7]\cdot 2H_2O$

Compound	Mol. Wt.	Expt. mass loss wt %	Calc. mass loss wt %	Decomposition product
FeCo	448.52	13.09	12.03 ($3 \times H_2O$)	α–$Co_2P_2O_7$ [157] + α–BPO_4 [140]
$Fe_{1.3}Co_{0.7}$	323.82	12.11	11.10 ($2 \times H_2O$)	α–$Co_2P_2O_7$ [157]

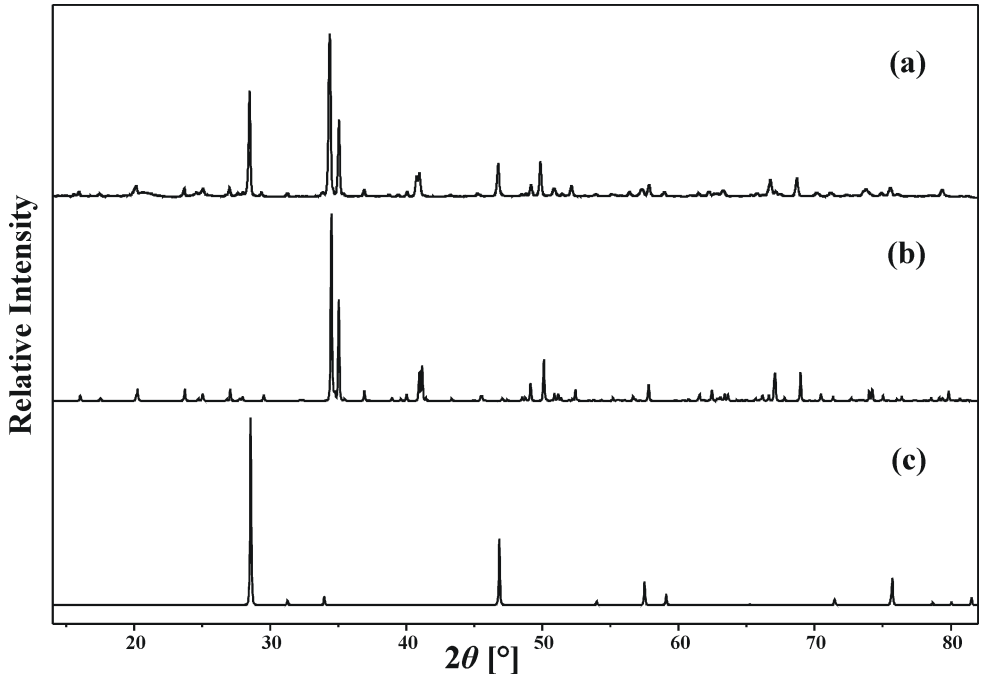

Figure 3.101: *Powder X–ray diffraction pattern of (a) the decomposition product of $FeCo(H_2O)[BP_3O_9(OH)_4]$ after heating to 1000 °C (background subtracted), compared with the calculated powder diffraction pattern of (b) α–$Co_2P_2O_7$ [157] and (c) α–BPO_4 [140] (Co $K_{\alpha 1}$–radiation).*

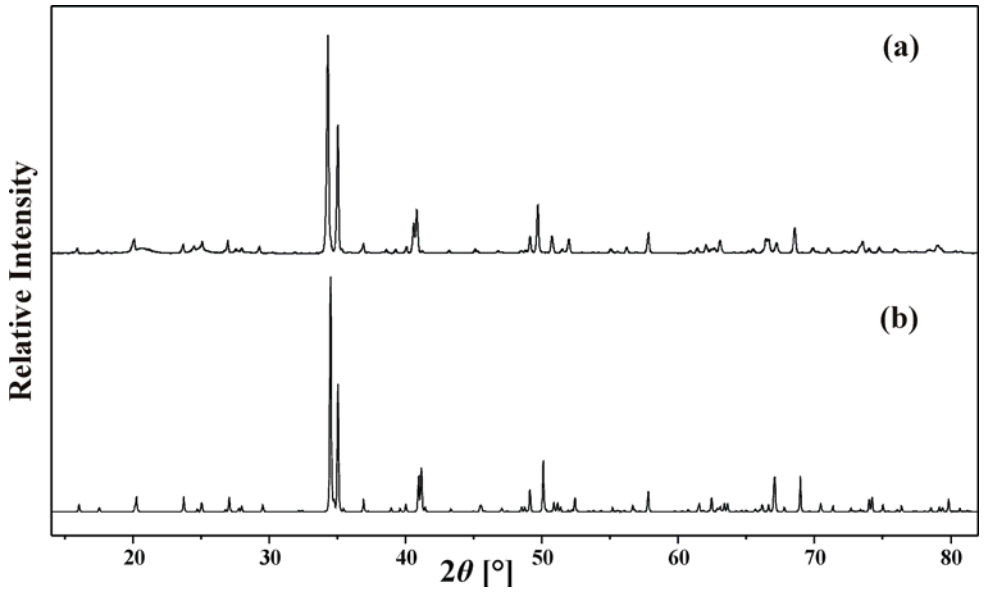

Figure 3.102: *Powder X–ray diffraction pattern of (a) the decomposition product of $Fe_{1.3}Co_{0.7}[P_2O_7]\cdot 2H_2O$ after heating to 1000 °C (background subtracted), compared with the calculated powder diffraction pattern of (b) α–$Co_2P_2O_7$ [157] (Co $K_{\alpha 1}$–radiation).*

3.5.1.5 Magnetic Susceptibility

The temperature–dependent magnetic susceptibility of both, $FeCo(H_2O)[BP_3O_9(OH)_4]$ and $Fe_{1.3}Co_{0.7}[P_2O_7]\cdot 2H_2O$, were measured in a static magnetic field of 1 Tesla. The magnetic susceptibility follows a Curie–Weiss law at temperatures above 40 K with μ_{eff} = 8.4 μB / $Fe^{2+}Co^{2+}$ and θ = −7.5 K for $FeCo(H_2O)[BP_3O_9(OH)_4]$ and μ_{eff} = 8.1 μB / $Fe^{2+}Co^{2+}$and θ = −5.1 K for $Fe_{1.3}Co_{0.3}[P_2O_7]\cdot 2H_2O$. The effective magnetic moments were found to be too high compared to an expected value of 4.7 – 5.2 μ_B in the octahedral coordination of Fe^{II} and Co^{II} ions. The higher magnetic moment was due to the contributions from unidentified magnetic impurities which hide the genuine magnetic behavior of $FeCo(H_2O)[BP_3O_9(OH)_4]$ and $Fe_{1.3}Co_{0.7}[P_2O_7]\cdot 2H_2O$.

3.5.2 Discussion

This section consists of two parts. The fist part deals with the anionic partial structure of $FeCo(H_2O)[BP_3O_9(OH)_4]$ and $Fe_{1.3}Co_{0.7}[P_2O_7]\cdot 2H_2O$ in detail. While, the second part compares the octahedral chains of these borophosphates to the octahedral arrangements in $M^{II}H_2P_2O_7$ (M^{II} = Co, Ni) [158] and $M^{II}[BPO_4(OH)_2]$ (M^{II} = Mn, Fe, Co) [61].

The anionic partial structure of $FeCo(H_2O)[BP_3O_9(OH)_4]$ comprises of corner sharing $[BP_3O_9(OH)_4]^{4-}$ anion. In terms of silicate structural chemistry, the complex anion, $[BP_3O_9(OH)_4]^{4-}$, is denoted as an open–branched tetramer [146]. The $[BP_3O_9(OH)_4]^{4-}$ may either exist as an isolated anion (*Figure 3.103a*) or as the Fundamental Building Block (FBB) of borophosphate partial structures with larger extension (*Figure 3.103b*). As the borate tetrahedron comprises only an unshared oxygen atom, the dimensionality of the borophosphates formed is limited due to the avoidance of P—O—P bonds. There are only limited numbers of tetrahedral borophosphates known till now with B : P = 1 : 3 (*Table 3.19*) [53, 54, 145, 159, 160]. The anions of $(NH_4)_4Mn_9[BP_3O_{11}(OH)_2]_2[HPO_4]_2[PO_4]_2$ and $Mg(H_2O)_2[BP_3O_9(OH)_4]$ are open–branched tetramers whereas the anions of $[Co(en)_3][V_3BP_3O_{19}][H_2PO_4]\cdot 4H_2O$, $[Co(en)_3][enH_2][VBP_3O_{19}]\cdot 4.5H_2O$ and $[Co(en)_3][V_3BP_3O_{19}][H_2PO_4]\cdot 4H_2O$ form clusters with vanadium [53, 159, 160]. The open–branched single chains were observed for $M^{II}_3[BP_3O_{12}]$ (M^{II}_3 = Ba, Pb) and $K_3[BP_3O_9(OH)_3]$ [11, 30, 161].

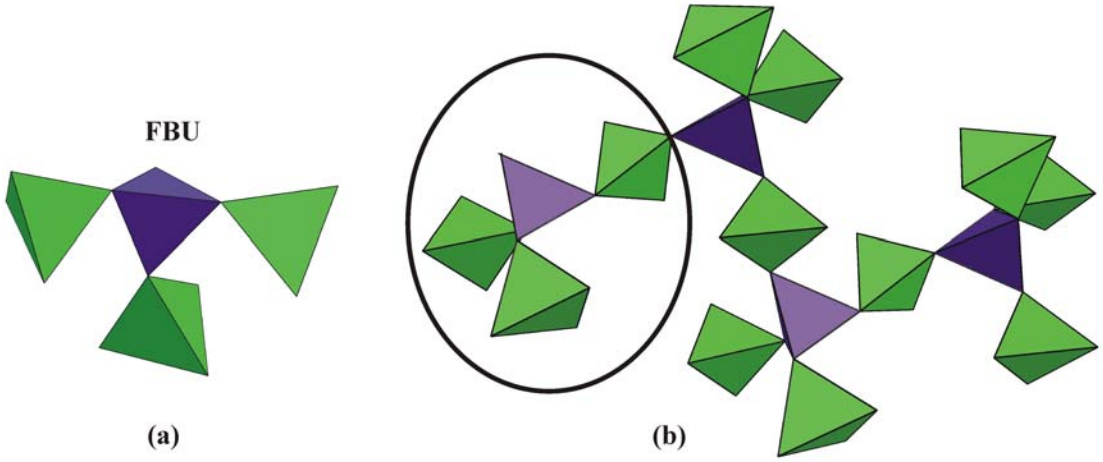

Figure 3.103: *Interconnection of (a) open–branched tetramers (fundamental building unit) forming (b) an open–branched single chain as observed in borophosphates with B : P = 1: 3 (protons omitted).*

Table 3.19: *Tetrahedral borophosphates with B: P = 1: 3*

Compound	Space group
Open–branched tetramer	
$(NH_4)_5[V_3BP_3O_{19}]\cdot H_2O$	$P\bar{1}$ (No.2) [53]
$[Co(en)_3][enH_2][VBP_3O_{19}]\cdot 4.5H_2O$	$P2_1/c$ (No.14) [159]
$[Co(en)_3][V_3BP_3O_{19}][H_2PO_4]\cdot 4H_2O$	$C2/c$ (No. 15) [160]
$(NH_4)_4Mn_9[BP_3O_{11}(OH)_2]_2[HPO_4]_2[PO_4]_2$	$C2/c$ (No. 15) [54]
$Mg(H_2O)_2[BP_3O_9(OH)_4]$	$P2_12_12_1$ (No. 19) [145]
Open–branched single chains	
$M^{II}_3[BP_3O_{12}]$	
M^{II} = Ba	*Ibca* (No. 73) [11]
M^{II} = Pb	*Pbca* (No. 61) [161]
$K_3[BP_3O_9(OH)_3]$	$C2/c$ (No. 15) [30]

The anionic partial structure of $Fe_{1.3}Co_{0.7}[P_2O_7]\cdot 2H_2O$ is a diphosphate composed of two corner–sharing tetrahedra constituting the largest family of condensed phosphates. In the crystal chemistry of diphosphates many aspects of the geometrical configuration of this anion are discussed, with the P—O—P angle and the relative orientation of the two PO_4 tetrahedra being the main aspects. A terminology has been developed in order to distinguish between “eclipsed” or “staggered” confirmations [162]. Diphosphates have been the subject of hundreds of investigations containing M^{I}, M^{II}, M^{III}, $M^{I}M^{III}$, $M^{I}M^{II}$, $M^{II}M^{III}$, M^{IV} or even higher–valance cations [162].

A large number of divalent (M^{II}) metal diphosphates have been investigated during the past four decades because of their potential use as fertilizers. The divalent metal

diphosphates were classified into three groups, namely, (1) anhydrous divalent cation diphosphates ($M^{II}[P_2O_7]$; M^{II} = Mg–Ba, Mn–Zn) (2) anhydrous mixed divalent cation diphosphates ($M1^{II}M2^{II}[P_2O_7]$; $M1^{II}$ = Mg–Ba, $M2^{II}$ = Mn–Zn, Pb), and (3) hydrated divalent cation diphosphates ($M^{II}[P_2O_7]\cdot 2H_2O$; M^{II} = Mg, Mn–Co). Our systematic investigations on transition metal diphosphates led into the formation of the first hydrated mixed divalent cation diphosphate $Fe_{1.3}Co_{0.7}[P_2O_7]\cdot 2H_2O$.

The crystal structure of both, $FeCo(H_2O)[BP_3O_9(OH)_4]$ and $Fe_{1.3}Co_{0.7}[P_2O_7]\cdot 2H_2O$, contains octahedral zigzag chains, which are interconnected by the respective tetrahedral anions. The octahedral chains in these crystal structures are closely related to the octahedral arrangements in $M^{II}H_2P_2O_7$ (M^{II} = Co, Ni) [158] and $M^{II}[BPO_4(OH)_2]$ (M^{II} = Mn, Fe, Co) [61]. The compounds $M^{II}H_2P_2O_7$ (M^{II} = Co, Ni) exhibit a field-induced metamagnetic behavior from an antiferromagnetic state to a ferromagnetic state and are considered as quasi-one-dimensional systems. The compounds $M^{II}[BPO_4(OH)_2]$ (M^{II} = Mn, Fe, Co, Ni) [158] indicate a low-dimensional antiferromagnetic correlation of the M^{II} ions by dominant exchange interactions within the one–dimensional octahedral chain structure [61]. Therefore, due to the similar structural features, $FeCo(H_2O)[BP_3O_9(OH)_4]$ and $Fe_{1.3}Co_{0.7}[P_2O_7]\cdot 2H_2O$ may exhibit interesting magnetic properties.

4 Conclusions and Outlook

In this chapter the results obtained from syntheses, crystal structure investigations and properties of selected transition metal (Sc, Fe, Co, Ni) borophosphates are summarized. Furthermore, a brief conclusion is presented.

4.1 Summary and Conclusions

Objective 1: During the investigation of borophosphates containing alkali–metals and scandium, the following three compounds were prepared and structurally characterized:

Compound	Space group	Anionic partial structure
$KSc[BP_2O_8(OH)]$ **$RbSc[BP_2O_8(OH)]$**	$P\bar{1}$ (No. 2)	 $[B_2P_4O_{16}(OH)_2]^{8-}$
$CsSc[B_2P_3O_{11}(OH)_3]$	*Pnna* (No. 52)	 $[B_2P_3O_{11}(OH)_3]^{4-}$
		New borophosphate anion

The anionic partial structure of $M^{I}Sc[BP_2O_8(OH)]$ (M^{I} = K, Rb) consists of the well known open–branched four–membered rings of alternating borate and phosphate tetrahedra (a loop–branched hexamer with B : P = 1 : 2). The anionic partial structure of $CsSc[B_2P_3O_{11}(OH)_3]$ represents the new type of oligomer containing boron in three– and four– fold coordination (B : P = 2 : 3). This is also the first time that a BO_3 group is not only linked to borate species but also to a phosphate tetrahedron. This kind of oligomer was already predicted for borates but was never observed [1, 2]. By this, $CsSc[B_2P_3O_{11}(OH)_3]$ is a special compound with regard to the structural building principles of borates and borophosphates. The significant differences in the crystal structures of $M^{I}Sc[BP_2O_8(OH)]$ (M^{I} = K, Rb) and $CsSc[B_2P_3O_{11}(OH)_3]$ may be due to

the higher coordination number of cesium. Thermal treatment (up to 1000 ºC) of these compounds resulted in white crystalline products containing new phases with unknown crystal structures.

The overall investigations evidenced that it is possible to synthesize alkali–metal scandium borophosphates with framework structures as observed for other trivalent metal cations (Fe, In, Ga, Al, V) [63-65, 103, 107, 109, 133, 134]. Thermal analyses of the compounds revealed that they may be used as precursors for new borophosphates.

During our extensive investigation of alkali–metal scandium borophosphates various preparative parameters (filling degree, pH, the temperature, time, B : P ratio) were changed. Besides the discovery of alkali–metal scandium borophosphates, five new alkali–metal scandium hydrogenphosphates were synthesized and structurally characterized:

Compound	Space group	Crystal structure
$Li_2Sc[(PO_4)(HPO_4)]$	$P12_1/n1$ (no. 14)	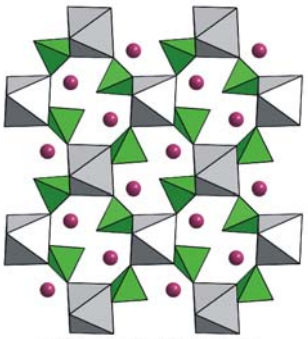 $Li_2Sc[(PO_4)(HPO_4)]$
$KSc(HPO_4)_2$	*Pnma* (No. 64)	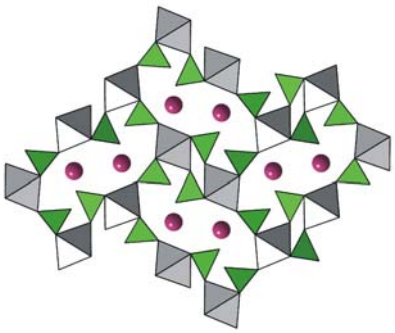 $KSc(HPO_4)$ **New structure type**

$RbSc(HPO_4)_2$ **$CsSc(HPO_4)_2$** **$NH_4Sc(HPO_4)_2$**	$P2_1/c$ (No. 14)	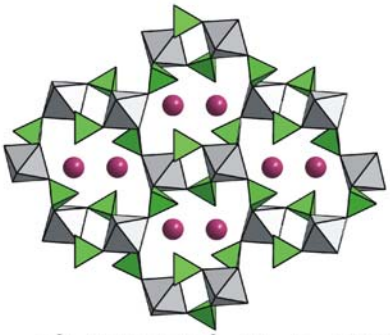 $M^{I}Sc(HPO_4)$ (M^{I} = Rb, Cs, NH_4)

It was already predicted by *Riou* [96] that open framework scandium phosphates should be isotypes of the respective indium phosphates. It was also stated that there should be a whole family of scandium hydrogenphosphates as we were able to confirm with the five novel compounds. Our systematic study reveals the structural changes of the anionic partial frameworks with increasing ionic radii of the alkali–metal ion. With respect to the M—T connections (M = six coordinated central metal atom, T = four coordinated phosphorus atom) the channel size increases from 8–membered rings in $Li_2Sc[(PO_4)(HPO_4)]$ to 12–membered rings in $M^{I}Sc(HPO_4)_2$ (M^{I} = K, Rb, Cs, NH_4). $KSc(HPO_4)_2$ exhibits a new structure type in the family of monohydrogenphosphates with the general formula $M^{I}M^{III}(HPO_4)_2$. This provides further evidence that scandium is a suitable element for the synthesis of framework structures with different channel sizes. The observation that in analogy to $M^{I}Sc(HPO_4)_2$ (M^{I} = Rb, Cs, NH_4) a compound exists where the M^{I} site is replaced by H_3O^{+} gives rise to the hope that ion exchange properties could be of interest in this class of compounds [93]. In addition, the possible existence of further modifications (as reported for the element–combinations RbV, NH_4V, RbFe, and CsIn) should be investigated by thermoanalytical and X–ray methods.

Objective 2: The extensive studies on borophosphate containing the transition metals Fe, Co, Ni together with alkaline earth–metals (Mg, Ca, Sr, Ba) led to the preparation of 13 compounds containing the combination of two different divalent $M1^{II}M2^{II}$ ions.

Compound	Space group	Anionic partial structure
$CaFe[BP_2O_7(OH)_3]$ **$CaNi[BP_2O_7(OH)_3]$**	$C2/c$ (No. 15)	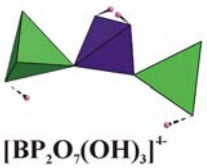 $[BP_2O_7(OH)_3]^{+}$

$BaFe[BP_2O_8(OH)]$
$BaCo[BP_2O_8(OH)]$

$P\bar{1}$ (No. 2)

$SrFe[BP_2O_8(OH)_2]$

$P\bar{1}$ (No. 2)

First $M^{II}M^{III}$ borophosphate

$CaCo(H_2O)[BP_2O_8(OH)]\cdot H_2O$

$P\bar{1}$ (No. 2)

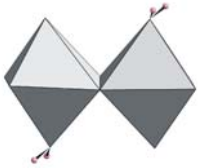

New cobalt dimer with layered structure

$Ca_{0.5}Fe(H_2O)_2[BP_2O_8]\cdot H_2O$ $P6_522$ (No. 179)
$Ca_{0.5}Co(H_2O)_2[BP_2O_8]\cdot H_2O$ $P6_522$ (No.179)
$Ca_{0.5}Ni(H_2O)_2[BP_2O_8]\cdot H_2O$ $P6_122$ (No. 178)
$Sr_{0.5}Co(H_2O)_2[BP_2O_8]\cdot H_2O$ $P6_122$ (No. 178)
$Ba_{0.5}Fe(H_2O)_2[BP_2O_8]\cdot H_2O$ —
$Ba_{0.5}Co(H_2O)_2[BP_2O_8]\cdot H_2O$ $P6_522$ (No.179)
$Ba_{0.5}Ni(H_2O)_2[BP_2O_8]\cdot H_2O$ —

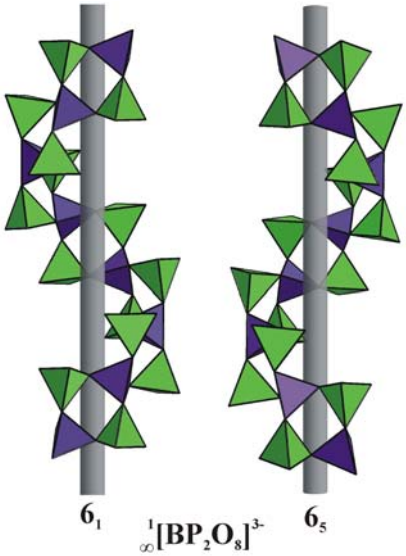

The anionic partial structure of $CaM2^{II}[BP_2O_7(OH)_3]$ ($M2^{II}$ = Fe, Ni) consists of a tetrahedral triple $[BP_2O_7(OH)_3]^{4-}$, built from a central $(HO)_2BO_2$ tetrahedron sharing common vertices with two $(H_{0.5})OPO_3$ tetrahedra. The complex anions in the crystal structure of $BaM2^{II}[BP_2O_8(OH)]$ ($M2^{II}$ = Fe, Co) comprises open–branched four–

membered rings, $[B_2P_4O_{16}(OH)_2]^{8-}$, which are formed by alternating $(HO)BO_3$ and PO_4 tetrahedra sharing common corners with two additional PO_4 branches. The interconnection of these complex anions with $M2^{II}$ coordination octahedra ($M2^{II}$ = Fe, Co, Ni) by sharing common corners results in overall three–dimensional frameworks which contain channels filled with the $M1^{II}$ ions ($M1^{II}$ = Ca, Ba). The anionic partial structure of $SrFe[BP_2O_8(OH)_2]$ is built from a central $(HO)_2BO_2$ tetrahedron sharing common vertices with two PO_4 tetrahedra. Surprisingly, $SrFe[BP_2O_8(OH)_2]$ represents the first example in the structural chemistry of borophosphates where the charge of the anionic partial structure is balanced by a divalent and a trivalent species ($M^{II}M^{III}$). Although being a member of the $M1^{II}M2^{II}[BP_2O_8(OH)]$ family the crystal structure of $CaCo(H_2O)[BP_2O_8(OH)]\cdot H_2O$ is different. Interestingly, this is the first case in the borophosphate structural chemistry where dimers of cobalt coordination octahedra together with borophosphate oligomers form a (two–dimensional) layered structure.

The helical borophosphates $M1^{II}_{0.5}M2^{II}(H_2O)_2[BP_2O_8]\cdot H_2O$ ($M1^{II}_{0.5}$ = Ca, Sr, Ba; $M2^{II}$ = Fe, Co, Ni) contain one–dimensional infinite loop–branched borophosphate helices built of alternatively distorted borate and phosphate tetrahedra. Up to now, the group of compounds with $^1_\infty[BP_2O_8]^{3-}$ helical chain anions has been synthesized only in combination with different cations M^IM^{II} and M^{III} (M^I = Li, Na, K; M^{II} = Mg, Mn, Fe, Co, Ni, Zn; M^{III} = Sc, In, Fe). The systematic investigation on helical borophosphates of transition metals (Fe, Co, Ni) and alkaline–earth metals showed that it is also possible to accommodate divalent metal cations within the structure without disturbing the anionic partial structure. It was not possible to find the completely ordered structural model [45] for the compounds $M1^{II}_{0.5}M2^{II}(H_2O)_2[BP_2O_8]\cdot H_2O$ ($M1^{II}_{0.5}$ = Ca, Sr, Ba; $M2^{II}$ = Co) but the substructure presented shows good agreement with the ordered known helical borophosphate compounds. Interestingly, it was also possible to judge the "kind of superstructure" against the crystal morphology.

In conclusion, several borophosphates containing alkaline earth– and transition metals (B : P = 1 : 2) have been synthesized which are isotypic to the borophosphates containing alkali– and transition metals [48, 63-65, 67, 69, 88]. This proved that it is possible to replace alkali–metal ions by alkaline–earth metal ions and still retain the crystal structures. Nevertheless, beside several isotypic structures, a new type of layered structure and the first $M1^{II}M2^{III}$ borophosphate could also be obtained. This

shows that it is also possible to find new type of crystal structures besides the isotypic ones.

Objective 3: Syntheses of one of the few examples of borophosphates containing layered anionic partial structures (6^3 net topology) containing transition metal cations (Fe, Co, Ni) was realized with 6 isotypic compounds.

Compound	Space group	Anionic partial structure
$Fe(H_2O)_2[B_2P_2O_8(OH)_2]\cdot H_2O$ **$Co(H_2O)_2[B_2P_2O_8(OH)_2]\cdot H_2O$** **$Ni(H_2O)_2[B_2P_2O_8(OH)_2]\cdot H_2O$** **$Ni_{0.5}Co_{0.5}(H_2O)_2[B_2P_2O_8(OH)_2]\cdot H_2O$** **$Ni_{0.8}Zn_{0.2}(H_2O)_2[B_2P_2O_8(OH)_2]\cdot H_2O$** **$Ni_{0.5}Mg_{0.5}(H_2O)_2[B_2P_2O_8(OH)_2]\cdot H_2O$**	$P2_1/c$ (No. 14)	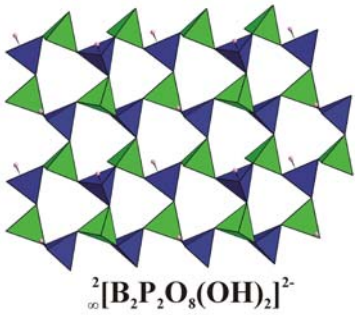 $^2_\infty[B_2P_2O_8(OH)_2]^{2-}$ **Layered borophosphates**

The compounds $M^{II}(H_2O)_2[B_2P_2O_8(OH)_2]\cdot H_2O$ (M^{II} = Fe, Co, Ni) adopt the structure type of $Mg(H_2O)_2[B_2P_2O_8(OH)_2]\cdot H_2O$ [93, 145] characterized by a two–dimensional borophosphate anion. Substitution on the transition metal sites was shown to be possible ($Ni_{0.5}Co_{0.5}$) for this structure type. With the synthesis of $Ni_{0.8}Zn_{0.2}(H_2O)_2[B_2P_2O_8(OH)_2]\cdot H_2O$ and $Ni_{0.5}Mg_{0.5}(H_2O)_2[B_2P_2O_8(OH)_2]\cdot H_2O$ it was also proved that magnetically diluted samples can be prepared in analogy to $Mg_{1-x}Co_x(H_2O)_2[B_2P_2O_8(OH)_2]\cdot H_2O$ ($x \approx 0.25$) [78]. The thermal stability of these compounds is very similar with a slight shift to higher decomposition temperatures for $Ni_{0.5}Mg_{0.5}(H_2O)_2[B_2P_2O_8(OH)_2]\cdot H_2O$. In contrast to other borophosphates such as $M^IM^{II}(H_2O)_2[BP_2O_8]\cdot H_2O$ and $M^{III}(H_2O)_2[BP_2O_8]\cdot H_2O$, it is not possible to rehydrate partially dehydrated samples even though the crystal structure may suggest this property. This shows that the aqua–ligands significantly contribute to the stability of the structure. The magnetic behavior of $M^{II}(H_2O)_2[B_2P_2O_8(OH)_2]\cdot H_2O$ (M^{II} = Fe, Ni) corresponds well with separated *3d* ions without strong magnetic interactions down to 1.8 K. Quite surprising was the remarkable change in the crystal habit that was observed during the synthesis upon addition of alkali–metal cations. Syntheses with the absence of alkali–metals lead to a change in the crystal habit by reducing of the number of faces in direction of the more simple prismatic morphology.

Our research on borophosphates containing mixed transition metals led to the preparation of a borophosphate and a phosphate.

Compound	Space group	Anionic partial structure
$FeCo(H_2O)[BP_3O_9(OH)_4]$	$P2_12_12_1$ (No. 19)	 $[BP_3O_9(OH)]^+$
$Fe_{1.3}Co_{0.7}[P_2O_7]\cdot 2H_2O$	$P2_1/n$ (No.14)	 $[P_2O_7]^{4+}$ **First hydrated mixed divalent cation diphosphate**

The anionic partial structure of $FeCo(H_2O)[BP_3O_9(OH)_4]$ is an open–branched tetramer built from $(HO)BO_3$ sharing common O–corners with one $(HO)PO_3$, one $(HO)_2PO_2$ and one PO_4 group. The crystal structure is an isotype to $Mg_2(H_2O)[BP_3O_9(OH)_4]$ [145]. $Fe_{1.3}Co_{0.7}[P_2O_7]\cdot 2H_2O$ contains the diphosphate composed of two corner–sharing tetrahedra (isotypic to $M^{II}[X_2O_7]\cdot 2H_2O$ (M^{II} = Mg, Mn, Co, Fe and X = P, As) [145, 154-156]. However, the crystal structure of both, $FeCo(H_2O)[BP_3O_9(OH)_4]$ and $Fe_{1.3}Co_{0.7}[P_2O_7]\cdot 2H_2O$, contains octahedral zigzag chains, which are interconnected by the respective tetrahedral anions. The octahedral chains in these crystal structures are closely related to the octahedral arrangements in $M^{II}H_2P_2O_7$ (M^{II} = Co, Ni) [158] which exhibit a field-induced metamagnetic behavior from an antiferromagnetic state to a ferromagnetic state and to $M^{II}[BPO_4(OH)_2]$ (M^{II} = Mn, Fe, Co) [61] which indicate a low-dimensional antiferromagnetic correlation of the M^{II} ions by dominant exchange interactions within the one–dimensional octahedral chain structure. Therefore, due to the similar structural features, $FeCo(H_2O)[BP_3O_9(OH)_4]$ and $Fe_{1.3}Co_{0.7}[P_2O_7]\cdot 2H_2O$ may exhibit interesting magnetic properties. Thermal investigation revealed that both compounds are stable until 300 ºC and transform into pyrophosphates at higher temperatures. $Fe_{1.3}Co_{0.7}[P_2O_7]\cdot 2H_2O$ represents the first hydrated mixed divalent cation diphosphate.

4.2 Outlook

The main aim of the presented work was to synthesize and structurally characterize newly selected *3d* transition metal (Sc, Fe, Co, Ni) borophosphates. The study focused on producing a variety of borophosphates with unique connection patterns. During our investigations, the following aspects seemed worth studying in the future.

The first scandium borophosphate was synthesized exhibiting remarkable thermal properties. Investigation of borophosphates containing alkali–metals and scandium led to numerous borophosphates and hydrogenphosphates. Alkali–metal scandium borophosphates revealed that they may be used as precursors for new borophosphates upon thermal treatment. Alkali–metal scandium hydrogenphosphates may show existence of polymorphism upon thermal treatment (extreme temperature range) and may show ion exchange properties.

The catalytic properties of transition metal phosphates are well known and they are widely used for the selective oxidation of organic compounds. Due to the close structural relation of borophosphates and phosphates and probably different catalytic properties depending on the B : P ratio, the development of transition metal borophosphates towards new heterogeneous catalysts is proposed.

Systematic investigations on borophosphates containing alkaline–earth and transition metals (AE–T^{II} and AE–T^{III}) with Fe, Co and Ni have proved that it is possible to replace alkali–metal ions by alkaline–earth metal ions and still retain the crystal structures. Also, new types of crystal structures besides the isotypic ones were realized for these systems. In continuation of this research, the emphasis will be given to the syntheses, structural characterization and study of the properties of new borophosphates containing alkaline–earth and *3d* transition metals (Sc–Zn) and transition metals of higher oxidation number (T^{IV}… etc).

All the above mentioned compound preparation will be conducted by different synthetic techniques (hydrothermal, solvothermal, higher temperature, flux and micro-wave assisted) with different reaction conditions (the temperature, the time, the molar composition, the pH of the medium and the degree of filling).

5 Appendix

5.1 Chemicals Used

Appendix 1: Chemicals used for the synthesis of borophosphates and phosphates

Chemicals	Company	Quality
Iron(II)oxalate Dihydrate, $FeC_2O_4 \cdot 2H_2O$	Alfa Aesar	99.999%
Cobalt(II)acetate Tetrahydrate, $Co(C_2H_3O_2)_2 \cdot 4H_2O$	Alfa Aesar	99%
Cobalt(II)carbonate, $CoCO_3$	Alfa Aesar	99.5%
Cobalt(II)oxide, CoO	Alfa Aesar	95%
Nickel(II)oxalate Dihydrate, $NiC_2O_4 \cdot 2H_2O$	Alfa Aesar	99%
Nickel(II)oxide, NiO	Alfa Aesar	99%
Nickel(II)dichloride Hexahydrate, $NiCl_2 \cdot 6H_2O$	Merck	98%
Zinc(II)oxide, ZnO	Merck	99%
Discandiumtrioxide, Sc_2O_3	Abcr	99.9%
Diindiumtrioxide, In_2O_3	Alfa Aesar	99.9%
Dilithiumtetraborate, $Li_2B_4O_7$	Aldrich	95%
Disodiumetetraborate Decahydrate, $Na_2B_4O_7 \cdot 10H_2O$	Riedel-De Haen	99.5%
Disodiumhydrogenphosphate Dihydrate, $Na_2HPO_4 \cdot 2H_2O$	Riedel-De Haen	99.5%
Dipotassiumtetraborate Tetrahydrate, $K_2B_4O_7 \cdot 4H_2O$	Riedel-De Haen	99%
Dipotassiumhydrogenphosphate, K_2HPO_4	Merck	99%
Rubidiumhydroxide, RbOH	Alfa Aesar	99%
Cesiumhydroxide, CsOH	Alfa Aesar	99.9%
Diammoniumhydrogenphosphate, $(NH_4)_2HPO_4$	Merck	98%
Magnesiumhydroxide, $Mg(OH)_2$	Merck	98%
Calciumhydroxide, $Ca(OH)_2$	Aldrich	98%
Strontiumhydroxide Octahydrate, $Sr(OH)_2 \cdot 8H_2O$	Aldrich	98%
Bariumhydroxide Octahydrate, $Ba(OH)_2 \cdot 8H_2O$	Merck	98%
Boric Acid, H_3BO_3	Alfa Aesar	99.9%
Diborotrioxide, B_2O_3	Chempur	99.99%
Phosphoric Acid, H_3PO_4	Merck	85%
Diphosphoruspentoxide, P_2O_5	Roth	98.5%

5.2 Crystallographic Tables

5.2.1 $M^{I}Sc[BP_2O_8(OH)]$ (M^{I} = K, Rb)

Appendix 2: *$KSc[BP_2O_8(OH)]$: Crystallographic data and refinement parameters*

Crystallographic data

Formula weight (g / mol)	301.82
Dimensions of the crystal (mm^3)	0.125 × 0.075 × 0.060
Crystal color and habit	transparent, colorless block
Temperature of measurement (K)	293
Crystal system	triclinic
Space group	$P\bar{1}$ (No.2)
Unit cell parameters	a = 5.2696(2) Å α = 88.22(1)° b = 8.2739(8) Å β = 79.701(6)° c = 8.3890(5) Å γ = 86.67(1)°
Cell volume ($Å^3$)	359.2
Formula units Z	2
Calculated density, ρ_{calc} (g / cm^3)	2.791

Data collection and refinement parameters

Diffractometer	RIGAKU AFC7 CCD, MoK_α–radiation (λ = 0.7107 Å), Graphite monochromator
Absorption coefficient, μ (MoK_α), mm^{-1}	2.077
Scan type	φ / ω
2θ range (°)	4.94 – 63.06
Limiting indices	$-7 \le h \le 7$, $-10 \le k \le 10$, $-12 \le l \le 12$
Total data collected	6078
Unique data	1918
R(int)	0.023
Observed data, $I > 2\sigma(I)$	1783
Paramenter refined	131
F(000)	296
Goodness–of–fit (on F^2)	1.158
R1/wR2, $I > 2\sigma(I)$	0.031 / 0.071
R1/wR2, all data	0.034 / 0.074
Residual electron density (max. / min.) ($eÅ^{-3}$)	0.611 / –0.595

Appendix 3: *$RbSc[BP_2O_8(OH)]$: Crystallographic data and refinement parameters*

Crystallographic data

Formula weight (g / mol)	348.19
Dimensions of the crystal (mm^3)	0.065 × 0.140 × 0.175
Crystal color and habit	transparent, colorless block
Temperature of measurement (K)	293
Crystal system	triclinic
Space group	$P\bar{1}$ (No.2)
Unit cell parameters	a = 5.3296(2) Å α = 87.27(1)° b = 8.3919(8) Å β = 80.124(6)° c = 8.4319(5) Å γ = 86.60(1)°
Cell volume ($Å^3$)	370.6
Formula units Z	2
Calculated density, ρ_{calc} (g / cm^3)	3.120

Data collection and refinement parameters

Diffractometer	RIGAKU AFC7 CCD, MoK_α–radiation (λ = 0.7107 Å), Graphite monochromator
Absorption coefficient, μ (MoK_α), mm^{-1}	7.976
Scan type	φ / ω
2θ range (°)	4.86 – 63.42
Limiting indices	$-7 \le h \le 7$, $-12 \le k \le 9$, $-11 \le l \le 11$
Total data collected	6669
Unique data	2013
R(int)	0.022
Observed data, $I > 2\sigma$	1927
Paramenter refined	131
F(000)	332
Goodness–of–fit (on F^2)	1.144
R1/wR2, $I > 2\sigma$ (I)	0.023 / 0.065
R1/wR2, all data	0.025 / 0.066
Residual electron density (max. / min.) ($eÅ^{-3}$)	0.481 / –0.949

Appendix 4: *$KSc[BP_2O_8(OH)]$: Atomic coordinates and equivalent / isotropic displacement parameters ($Å^2$)*

Atom	Site	*x*	*y*	*z*	U_{eq} / U_{iso}
K	2*i*	0.7204(1)	0.3218(1)	0.1195(1)	0.020(1)
Sc	2*i*	0.2765(1)	0.1963(1)	0.8035(1)	0.008(1)
P1	2*i*	0.1945(1)	0.5751(1)	0.2999(1)	0.008(1)
P2	2*i*	0.2132(1)	0.0613(1)	0.1923(1)	0.008(1)
B	2*i*	0.1138(5)	0.2692(3)	0.4414(3)	0.011(1)
O1	2*i*	0.0283(3)	0.4084(2)	0.7925(2)	0.012(1)
O2	2*i*	0.0364(3)	0.1521(2)	0.3357(2)	0.012(1)
O3	2*i*	0.0626(3)	0.9219(2)	0.1540(2)	0.012(1)
O4	2*i*	0.1269(3)	0.6659(2)	0.4623(2)	0.013(1)
O5	2*i*	0.2649(3)	0.1822(2)	0.0498(2)	0.013(1)
O6	2*i*	0.2592(3)	0.3953(2)	0.3406(2)	0.012(1)
O7	2*i*	0.2848(3)	0.1947(2)	0.5463(2)	0.014(1)
O8	2*i*	0.4411(3)	0.6363(2)	0.2021(2)	0.011(1)
O9	2*i*	0.4686(3)	0.0053(2)	0.2445(2)	0.014(1)
H7	2*i*	0.40(1)	0.138(6)	0.499(6)	0.07(2)*

* refined with isotropic displacement parameter

Appendix 5: *$KSc[BP_2O_8(OH)]$: Anisotropic displacement parameters U_{ij} ($Å^2 \times 10^3$). The anisotropic displacement factor exponent takes the form: $-2\pi [h^2a^{*2}U_{11} + \cdots + 2hka^*b^* U_{12}]$*

Atom	U_{11}	U_{22}	U_{33}	U_{23}	U_{13}	U_{12}
K	14(1)	21(1)	24(1)	–1(1)	–2(1)	0(1)
Sc	7(1)	9(1)	9(1)	1(1)	–2(1)	0(1)
P1	7(1)	8(1)	9(1)	0(1)	–1(1)	0(1)
P2	7(1)	8(1)	9(1)	0(1)	–2(1)	0(1)
B	10(1)	11(1)	10(1)	–1(1)	–1(1)	3(1)
O1	11(1)	10(1)	15(1)	–1(1)	–4(1)	0(1)
O2	11(1)	12(1)	12(1)	–3(1)	0(1)	0(1)
O3	11(1)	10(1)	14(1)	–2(1)	–2(1)	–4(1)
O4	10(1)	15(1)	11(1)	–4(1)	0(1)	2(1)
O5	16(1)	14(1)	10(1)	2(1)	–3(1)	–5(1)
O6	11(1)	8(1)	14(1)	1(1)	1(1)	1(1)
O7	15(1)	17(1)	9(1)	2(1)	–2(1)	6(1)
O8	8(1)	12(1)	13(1)	0(1)	0(1)	–2(1)
O9	10(1)	13(1)	19(1)	–2(1)	–7(1)	2(1)

Appendix 6: *$RbSc[BP_2O_8(OH)]$: Atomic coordinates and equivalent / isotropic displacement parameters ($Å^2$)*

Atom	Site	*x*	*y*	*z*	U_{eq} / U_{iso}
Rb	2*i*	0.7218(1)	0.3259(1)	0.1212(1)	0.015(1)
Sc	2*i*	0.2797(1)	0.1919(1)	0.8002(1)	0.006(1)
P1	2*i*	0.1920(1)	0.5820(1)	0.3046(1)	0.006(1)
P2	2*i*	0.2117(1)	0.0628(1)	0.1937(1)	0.005(1)
B	2*i*	0.1165(5)	0.2739(3)	0.4387(3)	0.007(1)
O1	2*i*	0.0283(3)	0.3981(2)	0.7891(2)	0.009(1)
O2	2*i*	0.0458(3)	0.1585(2)	0.3325(2)	0.010(1)
O3	2*i*	0.0512(3)	0.9294(2)	0.1617(2)	0.010(1)
O4	2*i*	0.1238(3)	0.6658(2)	0.4675(2)	0.010(1)
O5	2*i*	0.2675(3)	0.1774(2)	0.0466(2)	0.011(1)
O6	2*i*	0.2549(3)	0.4022(2)	0.3407(2)	0.011(1)
O7	2*i*	0.2865(4)	0.1987(2)	0.5436(2)	0.012(1)
O8	2*i*	0.4365(3)	0.6443(2)	0.2108(2)	0.009(1)
O9	2*i*	0.4621(3)	0.0036(2)	0.2474(2)	0.011(1)
H7	2*i*	0.389(9)	0.147(6)	0.500(7)	0.08(2)*

* refined with isotropic displacement parameter

Appendix 7: *$RbSc[BP_2O_8(OH)]$: Anisotropic displacement parameters U_{ij} ($Å^2 \times 10^3$). The anisotropic displacement factor exponent takes the form: $-2\pi [h^2a^{*2}U_{11} + \cdots + 2hka^*b^* U_{12}]$*

Atom	U_{11}	U_{22}	U_{33}	U_{23}	U_{13}	U_{12}
Rb	8(1)	16(1)	22(1)	0(1)	–4(1)	–1(1)
Sc	2(1)	6(1)	11(1)	1(1)	–3(1)	–1(1)
P1	2(1)	5(1)	11(1)	1(1)	–1(1)	–1(1)
P2	2(1)	4(1)	11(1)	0(1)	–3(1)	–1(1)
B	8(1)	5(2)	11(1)	0(1)	–2(1)	–1(1)
O1	3(1)	7(1)	18(1)	0(1)	–5(1)	–1(1)
O2	7(1)	9(1)	15(1)	–3(1)	–1(1)	0(1)
O3	6(1)	9(1)	18(1)	0(1)	–3(1)	–5(1)
O4	5(1)	13(1)	13(1)	–2(1)	–2(1)	0(1)
O5	9(1)	11(1)	14(1)	1(1)	–5(1)	–5(1)
O6	8 (1)	6(1)	18(1)	2(1)	0(1)	0(1)
O7	11(1)	15(1)	12(1)	1(1)	–3(1)	4(1)
O8	3(1)	9(1)	15(1)	1(1)	–1(1)	–3(1)
O9	6(1)	9(1)	19(1)	–1(1)	–7(1)	1(1)

Appendix 8: *$KSc[BP_2O_8(OH)]$: Selected interatomic distances (Å) and angles (°)*

Atom contact	Distance	Atom contact	Distance
K—O6	2.8291(16)	P1—O8	1.5124(16)
K—O1[a]	2.8419(17)	P1—O1[f]	1.5165(16)
K—O5	2.8822(17)	P1—O6	1.5478(17)
K—O2[b]	2.9461(17)	P1—O4	1.5512(17)
K—O8	2.9525(18)		
K—O8[c]	2.9758(17)	P2—O3[i]	1.5112(16)
K—O5[b]	2.9939(18)	P2—O9	1.5309(16)
K—O1[d]	3.0155(17)	P2—O5	1.5317(17)
K—O9	3.0742(18)	P2—O2	1.5661(17)
K—O3[c]	3.1181(18)		
		B—O2	1.457(3)
Sc—O5[e]	2.0556(16)	B—O4[f]	1.460(3)
Sc—O3[f]	2.0571(16)	B—O7	1.467(3)
Sc—O9[g]	2.0826(17)	B—O6	1.482(3)
Sc—O8[a]	2.0844(16)		
Sc—O1	2.1361(17)	O7—H7	0.80(1)
Sc—O7	2.1503(17)	O7—H7···O9	3.000(1)

Atoms	Angle	Atoms	Angle
O5[e]—Sc—O3[f]	86.64(7)	O8—P1—O1[f]	112.25(9)
O5[e]—Sc—O9[g]	94.39(7)	O8—P1—O6	105.36(9)
O3[f]—Sc—O9[g]	98.13(7)	O1[f]—P1—O4	111.13(9)
O5[e]—Sc—O8[a]	86.33(7)	O8—P1—O4	109.50(9)
O3[f]—Sc—O8[a]	164.53(7)	O1[f]—P1—O4	110.86(9)
O3[f]—Sc—O8[a]	96.13(7)	O4—P1—O6	107.49(9)
O5[e]—Sc—O1	98.92(7)		
O3[f]—Sc—O1	84.14(6)	O3[i]—P2—O9	112.73(10)
O9[g]—Sc—O1	166.62(7)	O3[i]—P2—O5	111.90(9)
O8[a]—Sc—O1	83.36(6)	O9—P2—O5	109.55(9)
O5[e]—Sc—O7	176.33(7)	O3[i]—P2—O2	106.02(9)
O3[f]—Sc—O7	91.00(7)	O9—P2—O2	109.05(9)
O9[g]—Sc—O7	83.15(7)	O5—P2—O2	107.36(10)
O8[a]—Sc—O7	96.62(7)		
O1—Sc—O7	83.62(6)	O2—B—O6	109.04(18)
		O4[f]—B—O6	112.64(19)
O2—B—O4[f]	105.20(18)	O7—B—O6	107.14(18)
O2—B—O7	112.1(2)		
O4[f]—B—O7	110.78(18)	O7—H7···O9	133.20(1)

Symmetry transformation used to generate equivalent atoms: [a] $-x+1, -y+1, -z+1$; [b] $x+1, y, z$; [c] $-x+1, -y+1, -z$; [d] $x+1, y, z-1$; [e] $x, y, z+1$; [f] $-x, -y+1, -z+1$; [g] $-x+1, -y, -z+1$; [i] $x-1, y, z+1$.

Appendix 9: *$RbSc[BP_2O_8(OH)]$: Selected interatomic distances (Å) and angles (°)*

Atom contact	Distance	Atom contact	Distance
Rb—O6	2.8937(18)	P1—O8	1.5117(17)
Rb—O1[a]	2.9311(18)	P1—O1[e]	1.5208(18)
Rb—O2[b]	2.9425(18)	P1—O4	1.5507(19)
Rb—O5	2.9607(18)	P1—O6	1.5531(19)
Rb—O1[c]	3.0436(18)		
Rb—O8[d]	3.0540(18)	P2—O3[h]	1.5097(18)
Rb—O8	3.0564(19)	P2—O9	1.5294(18)
Rb—O5[b]	3.0697(19)	P2—O5	1.5317(18)
Rb—O9	3.1665(19)	P2—O2	1.5641(19)
Rb—O3[d]	3.3061(19)		
		B—O2	1.458(3)
Sc—O3[e]	2.0583(18)	B—O4[e]	1.461(3)
Sc—O5[f]	2.0648(18)	B—O7	1.468(3)
Sc—O9[g]	2.0861(19)	B—O6	1.479(3)
Sc—O8[a]	2.0908(18)		
Sc—O1	2.1333(18)	O7—H7	0.61(1)
Sc—O7	2.1565(19)	O7—H7···O9	3.033(1)

Atoms	Angle	Atoms	Angle
O3[e]—Sc—O5[f]	87.48(7)	O8—P1—O1[e]	112.62(10)
O3[e]—Sc—O9[g]	98.12(8)	O8—P1—O4	109.58(10)
O5[f]—Sc—O9[g]	95.24(8)	O1[e]—P1—O4	110.77(10)
O3[e]—Sc—O8[a]	167.06(8)	O8—P1—O6	105.12(10)
O5[f]—Sc—O8[a]	87.32(7)	O1[e]—P1—O6	110.45(10)
O9[g]—Sc—O8[a]	94.16(7)	O4—P1—O6	108.07(10)
O3[e]—Sc—O1	84.02(7)		
O5[e]—Sc—O1	98.09(8)	O3[h]—P2—O9	113.41(11)
O9[g]—Sc—O1	166.59(7)	O3[h]—P2—O5	111.38(10)
O8[a]—Sc—O1	84.99(7)	O9—P2—O5	109.60(10)
O3[e]—Sc—O7	90.81(7)	O3[h]—P2—O2	105.81(10)
O5[f]—Sc—O7	177.94(8)	O9—P2—O2	108.80(10)
O9[g]—Sc—O7	83.87(7)	O5—P2—O2	107.59(10)
O8[a]—Sc—O7	94.59(7)		
O1—Sc—O7	82.86(7)	O2—B—O6	109.39(19)
		O4[e]—B—O6	112.0(2)
O2—B—O4[e]	105.39(19)	O7—B—O6	107.7(2)
O2—B—O7	111.1(2)		
O4[e]—B—O7	111.28(19)	O7—H7···O9	136.60(1)

Symmetry transformation used to generate equivalent atoms: [a] $-x+1, -y+1, -z+1$; [b] $x+1, y, z$; [c] $x+1, y, z-1$; [d] $-x+1, -y+1, -z$; [e] $-x, -y+1, -z+1$; [f] $x, y, z+1$; [g] $-x+1, -y, -z+1$; [h] $x, y-1, z$.

5.2.2 $CsSc[B_2P_3O_{11}(OH)_3]$

Appendix 10: *$CsSc[B_2P_3O_{11}(OH)_3]$: Crystallographic data and refinement parameters*

Crystallographic data

Formula weight (g / mol)	519.42
Dimensions of the crystal (mm^3)	0.2 × 0.1 × 0.4
Crystal color and habit	transparent, colorless block
Crystal system	orthorhombic
Space group	*Pnna* (No. 52)
Unit cell parameters	a = 13.0529(15) Å b = 18.3403(17) Å c = 10.3838(12) Å
Cell volume ($Å^3$)	3485.8(5)
Formula units Z	8
Calculated density, ρ_{calc} (g / cm^3)	2.773

Data collection and refinement parameters

Diffractometer	RIGAKU AFC7 CCD, MoK_α–radiation (λ = 0.7107 Å), Graphite monochromator
Absorption coefficient, μ (MoK_α), mm^{-1}	3.94
Scan type	φ / ω
2θ range (°)	6 – 61.82
Limiting indices	$-18 \le h \le 15$, $-11 \le k \le 11$, $-14 \le l \le 9$
Total data collected	10581
Unique data	1676
R(int)	0.038
Observed data $I > 2\sigma$	1521
Paramenter refined	190
F(000)	1968
Goodness–of–fit (on F^2)	1.111
R_1/wR_2, $I > 2\sigma$ (I)	0.044 / 0.115
R_1/wR_2, all data	0.049 / 0.121
Residual electron density (max. / min.) ($eÅ^{-3}$)	1.363 / –1.488

Appendix 11: *$CsSc[B_2P_3O_{11}(OH)_3]$: Atomic coordinates and equivalent / isotropic displacement parameters ($Å^2$)*

Atom	Site	*x*	*y*	*z*	U_{eq}/U_{iso}
Cs	8*e*	–0.3610(1)	–0.3839(1)	0.6086(1)	0.038(1)
Sc	8*e*	–0.6143(1)	–0.2316(1)	0.5021(1)	0.015(1)
P1	8*e*	–0.5650(1)	–0.1326(1)	0.2194(1)	0.016(1)
P2	8*e*	–0.1592(1)	–0.1316(1)	0.2282(1)	0.015(1)
P3	8*e*	–0.3639(1)	–0.1895(2)	0.5005(1)	0.017(1)
B1	8*e*	–0.3642(4)	–0.1180(5)	0.2718(6)	0.015(3)
B2	8*e*	–0.3708(4)	–0.0464(7)	0.4782(7)	0.019(3)
O1	8*e*	–0.3673(3)	–0.1092(3)	0.5543(4)	0.021(2)
O2	8*e*	–0.2688(2)	–0.2258(3)	0.5493(3)	0.021(1)
O3	8*e*	–0.0945(3)	–0.0646(3)	0.1828(3)	0.023(1)
O4	8*e*	–0.2714(2)	–0.1135(3)	0.1918(3)	0.021(1)
O5	8*e*	–0.3608(2)	–0.1828(3)	0.3527(4)	0.016(2)
O6	8*e*	–0.4582(2)	–0.2286(3)	0.5463(3)	0.022(1)
O7	8*e*	–0.1233(3)	–0.1943(3)	0.1504(4)	0.025(2)
O8	8*e*	–0.1466(2)	–0.1397(3)	0.3732(3)	0.018(2)
O9	8*e*	–0.3722(2)	–0.0507(3)	0.3474(4)	0.020(2)
O10	8*e*	–0.6182(3)	–0.0555(3)	0.2133(4)	0.025(2)
O11	8*e*	–0.4506(2)	–0.1218(2)	0.1825(3)	0.018(1)
O12	8*e*	–0.5766(2)	–0.1603(3)	0.3543(3)	0.021(1)
O13	8*e*	–0.6130(3)	–0.1776(3)	0.1163(3)	0.022(2)
O14	8*e*	–0.3727(3)	0.0179(4)	0.5396(4)	0.032(2)
H3	8*e*	–0.1034	–0.0326	0.2270	0.028*
H10	8*e*	–0.6188	–0.0405	0.2923	0.029*
H14	8*e*	–0.3730	0.505	0.4854	0.039*

* U_{iso} values of the hydrogen atoms were kept at 1.2 U_{eq} of the oxygen atoms to which they are attached.

Appendix 12: *$CsSc[B_2P_3O_{11}(OH)_3]$: Anisotropic displacement parameters U_{ij} ($Å^2 \times 10^3$). The anisotropic displacement factor exponent takes the form: $-2\pi [h^2a^{*2}U_{11} + \cdots + 2hka^*b^* U_{12}]$.*

Atom	U_{11}	U_{22}	U_{33}	U_{23}	U_{13}	U_{12}
Cs	34(1)	44(1)	36(1)	12(1)	–1(1)	–3(1)
Sc	10(1)	24(2)	11(1)	0(1)	0(1)	–1(1)
P1	13(1)	23(2)	11(1)	0(1)	–1(1)	0(1)
P2	13(1)	22(2)	10(1)	–1(1)	1(1)	0(1)
P3	10(1)	28(3)	12(1)	3(1)	0(1)	1(1)
B1	12(2)	22(10)	10(3)	–1(4)	–2(2)	–3(3)
B2	20(3)	14(11)	22(3)	0(5)	–1(2)	2(3)
O1	32(2)	13(6)	17(2)	–3(3)	0(1)	4(2)
O2	9(1)	31(4)	22(2)	11(2)	0(1)	0(2)
O3	26(2)	26(5)	17(1)	–2(2)	3(1)	–3(2)
O4	13(2)	35(4)	14(2)	4(2)	2(1)	1(2)
O5	19(2)	15(5)	14(2)	–2(2)	–1(1)	2(2)
O6	8(1)	36(4)	22(2)	5(2)	–2(1)	–1(2)
O7	32(2)	27(5)	16(2)	–3(2)	3(2)	6(2)
O8	16(2)	27(5)	11(2)	0(2)	–2(1)	–1(2)
O9	28(2)	19(5)	14(2)	3(3)	1(1)	0(2)
O10	31(2)	24(5)	19(2)	2(2)	–1(1)	7(2)
O11	12(2)	28(4)	14(2)	5(2)	–2(1)	–1(2)
O12	17(2)	28(4)	18(2)	6(2)	2(1)	–1(2)
O13	24(2)	24(5)	19(2)	–10(2)	–6(1)	0(2)
O14	60(3)	16(6)	21(2)	–7(3)	4(2)	3(3)

Appendix 13: *$CsSc[B_2P_3O_{11}(OH)_3]$: Selected interatomic distances (Å) and angles (°) (The P—O and B—O distances are given in Table 3.4)*

Atom contact	Distance	Atom contact	Distance
Cs—O11[b]	3.242(3)	Sc—O7[a]	2.058(5)
Cs—O3[a]	3.284(4)	Sc—O13[b]	2.070(5)
Cs—O4[b]	3.331(3)	Sc—O12	2.075(4)
Cs—O10[e]	3.341(5)	Sc—O2[c]	2.089(3)
Cs—O13[f]	3.428(4)	Sc—O6	2.089(3)
Cs—O1[d]	3.504(4)	Sc—O8[c]	2.166(5)
Cs—O10[f]	3.530(4)		
Cs—O7[a]	3.739(4)	O3—H3	0.755(1)
		O3—H3···O9	2.754(1)
O10—H10	0.865(1)	O14—H14	0.821(1)
O10—H10···O14	2.659(1)	O14—H14···O8	2.836(1)

Atoms	Angle	Atoms	Angle
O7[a]—Sc—O13[b]	85.0(2)	O7—P2—O8	115.3(3)
O7[a]—Sc—O12	169.48(14)	O7—P2—O4	109.4(2)
O13[b]—Sc—O12	93.77(18)	O8—P2—O4	111.40(19)
O7[a]—Sc—O2[c]	99.77(16)	O7—P2—O3	106.0(3)
O13[b]—Sc—O2[c]	84.10(16)	O8—P2—O3	108.5(3)
O12—Sc—O2[c]	90.48(15)	O4—P2—O3	105.7(2)
O7[a]—Sc—O6	84.72(15)		
O13[b]—Sc—O6	98.23(17)	O2—P3—O6	111.1(3)
O12—Sc—O6	85.12(14)	O2—P3—O5	110.5(2)
O2[c]—Sc—O6	175.1(2)	O6—P3—O5	112.1(2)
O7[a]—Sc—O8[c]	93.12(18)	O2—P3—O1	108.6(2)
O13[b]—Sc—O8[c]	169.20(14)	O6—P3—O1	108.1(2)
O12—Sc—O8[c]	90.0(2)	O5—P3—O1	106.3(3)
O2[c]—Sc—O8[c]	85.74(15)		
O6—Sc—O8[c]	92.18(15)	O5—B1—O11	110.5(6)
		O5—B1—O9	112.3(5)
O13—P1—O12	116.2(3)	O11—B1—O9	108.9(5)
O13—P1—O11	107.3(2)	O5—B1—O4	110.3(5)
O12—P1—O11	111.73(19)	O11—B1—O4	106.3(4)
O13—P1—O10	106.5(3)	O9—B1—O4	108.3(6)
O12—P1—O10	107.3(2)		
O11—P1—O10	107.4(2)	O3—H3—O9	178.65(1)
		O10—H10···O14	174.04(1)
		O14—H···O8	169.16(1)

Symmetry transformation used to generate equivalent atoms: [a] x–1/2, –y–1/2, z+1/2; [b] x, –y–1/2, –z+1/2; [c] x–1/2, y, –z+1; [d] x, –y–1/2, –z+3/2; [e] –x–1, y–1/2, z+1/2; [f] x+1/2, –y–1/2, z+1/2.

5.2.3 $Li_2Sc[(PO_4)(HPO_4)]$ and $M^{I}Sc(HPO_4)_2$ (M^{I} = K, Rb, Cs, NH_4)

Appendix 14: *$Li_2Sc[(PO_4)(HPO_4)]$: Crystallographic data and refinement parameters*

Crystallographic data

Formula weight (g / mol)	249.79
Dimensions of the crystal (mm^3)	0.04 × 0.04 × 0.08
Crystal color and habit	transparent, colorless prism
Temperature of measurement (K)	293
Crystal system	monoclinic
Space group	$P2_1/n$ (No. 14)
Unit cell parameters	a = 4.8582(12) Å b = 8.1887(12) Å β =104.111(7)° c = 7.6683(18) Å
Cell volume ($Å^3$)	296.2
Formula units Z	2
Calculated density, ρ_{calc} (g / cm^3)	2.801

Data collection and refinement parameters

Diffractometer	RIGAKU AFC7 CCD, MoK_α–radiation (λ = 0.7107 Å), Graphite monochromator
Absorption coefficient, μ (MoK_α), mm^{-1}	1.786
Scan type	φ / ω
2θ range (°)	3.7 – 59.95
Limiting indices	$-6 \le h \le 4$, $-11 \le k \le 11$, $-10 \le l \le 8$
Total data collected	2222
Unique data	841
R(int)	0.030
Observed data, $I > 2\sigma$	743
Paramenter refined	61
F(000)	244
Goodness–of–fit (on F^2)	1.070
R1/wR2, $I > 2\sigma$ (I)	0.038 / 0.083
R1/wR2, all data	0.045 / 0.088
Residual electron density (max. / min.) ($eÅ^{-3}$)	0.631 / –0.549

Appendix 15: *$KSc(HPO_4)_2$: Crystallographic data and refinement parameters*

Crystallographic data

Formula weight (g / mol)	276.02
Dimensions of the crystal (mm^3)	0.045 × 0.05 × 0.26
Crystal color and habit	transparent, colorless needle
Temperature of measurement (K)	293
Crystal system	orthorhombic
Space group	*Pnma* (No. 62)
Unit cell parameters	a = 14.5095(2) Å b = 5.4260(4) Å c = 8.4882(5) Å
Cell volume ($Å^3$)	668.26
Formula units Z	4
Calculated density, ρ_{calc} (g / cm^3)	2.74

Data collection and refinement parameters

Diffractometer	RIGAKU AFC7 CCD, MoK_α–radiation (λ = 0.7107 Å), Graphite monochromator
Absorption coefficient, μ (MoK_α), mm^{-1}	2.21
Scan type	φ / ω
2θ range (°)	2.4 – 56
Limiting indices	$-22 \le h \le 16$, $-8 \le k \le 6$, $-12 \le l \le 12$
Total data collected	6779
Unique data	1332
R(int)	0.022
Observed data, $I > 2\sigma$	1263
Paramenter refined	70
F(000)	272
Goodness–of–fit (on F^2)	1.233
R1/wR2, $I > 2\sigma$ (I)	0.045 / 0.105
R1/wR2, all data	0.047 / 0.109
Residual electron density (max. / min.) ($eÅ^{-3}$)	0.969 / –1.161

Appendix 16: *$RbSc(HPO_4)_2$: Crystallographic data and refinement parameters*

Crystallographic data

Formula weight (g / mol)	322.38
Dimensions of the crystal (mm^3)	0.025 × 0.04 × 0.1
Crystal color and habit	transparent, colorless needle
Temperature of measurement (K)	293
Crystal system	monoclinic
Space group	$P2_1/c$ (No. 14)
Unit cell parameters	a = 5.3214(6) Å b = 8.9221(7) Å β = 94.967(5)° c = 14.7579(12) Å
Cell volume ($Å^3$)	698.04
Formula units Z	4
Calculated density, ρ_{calc} (g / cm^3)	3.07

Data collection and refinement parameters

Diffractometer	RIGAKU AFC7 CCD, MoK_α–radiation (λ = 0.7107 Å), Graphite monochromator
Absorption coefficient, μ (MoK_α), mm^{-1}	8.45
Scan type	φ / ω
2θ range (°)	2.67 – 63.4
Limiting indices	$-7 \le h \le 7$, $-12 \le k \le 12$, $-12 \le l \le 12$
Total data collected	7962
Unique data	7960
Observed data, $I > 2\sigma$	6533
Paramenter refined	111
F(000)	137
Goodness–of–fit (on F^2)	1.047
R1/wR2, $I > 2\sigma$ (I)	0.059 / 0.160[a]
R1/wR2, all data	0.075 / 0.180[a]
Residual electron density (max. / min.) ($eÅ^{-3}$)	1.502 / –1.393

[a] refined as twin

Appendix 17: *$CsSc(HPO_4)_2$: Crystallographic data and refinement parameters*

Crystallographic data

Formula weight (g / mol)	369.83
Dimensions of the crystal (mm^3)	0.09 × 0.04 × 0.4
Crystal color and habit	transparent, colorless needle
Temperature of measurement (K)	293
Crystal system	monoclinic
Space group	$P2_1/c$ (No. 14)
Unit cell parameters	a = 5.3639(4) Å b = 9.1604(6) Å β = 93.7278(44)° c = 14.7052(10) Å
Cell volume ($Å^3$)	721.01
Formula units Z	4
Calculated density, ρ_{calc} (g / cm^3)	3.41

Data collection and refinement parameters

Diffractometer	RIGAKU AFC7 CCD, MoK_α–radiation (λ = 0.7107 Å), Graphite monochromator
Absorption coefficient, μ (MoK_α), mm^{-1}	6.45
Scan type	φ / ω
2θ range (°)	2.22 – 63.2
Limiting indices	$-7 \le h \le 7$, $-9 \le k \le 13$, $-21 \le l \le 21$
Total data collected	6185
Unique data	1926
R(int)	0.019
Observed data, $I > 2\sigma$	1773
Paramenter refined	117
F(000)	344
Goodness–of–fit (on F^2)	1.111
R1/wR2, $I > 2\sigma$ (I)	0.035 / 0.068
R1/wR2, all data	0.040 / 0.071
Residual electron density (max. / min.) ($eÅ^{-3}$)	1.102 / –1.532

Appendix 18: *$NH_4Sc(HPO_4)_2$: Crystallographic data and refinement parameters*

Crystallographic data

Formula weight (g / mol)	498.83
Dimensions of the crystal (mm^3)	0.025 × 0.065 × 0.075
Crystal color and habit	transparent, colorless needle
Temperature of measurement (K)	293
Crystal system	monoclinic
Space group	$P2_1/c$ (No. 14)
Unit cell parameters	a = 5.3211(5) Å b = 8.8660(7) Å β = 95.266(4)° c = 14.7909(12) Å
Cell volume ($Å^3$)	694.84
Formula units Z	4
Calculated density, ρ_{calc} (g / cm^3)	2.44

Data collection and refinement parameters

Diffractometer	RIGAKU AFC7 CCD, MoK_α–radiation (λ = 0.7107 Å), Graphite monochromator
Absorption coefficient, μ (MoK_α), mm^{-1}	1.53
Scan type	φ / ω
2θ range (°)	2.68 – 63.26
Limiting indices	$-7 \le h \le 6$, $-12 \le k \le 12$, $-21 \le l \le 21$
Total data collected	7912
Unique data	7912
Observed data, $I > 2\sigma$	5752
Paramenter refined	111
F(000)	490
Goodness–of–fit (on F^2)	1.068
R1/wR2, $I > 2\sigma$ (I)	0.092 / 0.242[a]
R1/wR2, all data	0.116 / 0.286[a]
Residual electron density (max. / min.) ($eÅ^{-3}$)	2.736 / –1.259

[a] refined as twin

Appendix 19: *$Li_2Sc[(PO_4)(HPO_4)]$: Atomic coordinates and equivalent / isotropic displacement parameters ($Å^2$)*

Atom	Site	*x*	*y*	*z*	U_{eq}
Li	4*e*	0.8910(13)	0.3661(7)	0.3416(8)	0.022(1)
Sc	2*b*	0	0	1/2	0.009(1)
P	4*e*	0.3626(2)	0.1524(1)	0.2280(1)	0.009(1)
O1	4*e*	0.1402(4)	0.1766(2)	0.3367(3)	0.012(1)
O2	4*e*	0.4831(4)	0.3150(2)	0.1831(3)	0.013(1)
O3	4*e*	0.6026(4)	0.0437(3)	0.3326(3)	0.013(1)
O4	4*e*	0.2375(5)	0.0633(3)	0.0478(3)	0.015(1)

Appendix 20: *$KSc(HPO_4)_2$: Atomic coordinates and equivalent / isotropic displacement parameters ($Å^2$)*

Atom	Site	*x*	*y*	*z*	U_{eq} / U_{iso}
K	4*c*	0.3800(1)	1/4	0.4668(1)	0.031(1)
Sc	4*c*	0.1234(1)	1/4	0.3310(1)	0.010(1)
P1	4*c*	0.0158(1)	1/4	0.7060(1)	0.010(1)
P2	4*c*	0.2824(1)	1/4	0.0230(1)	0.010(1)
O1	8*d*	0.0345(2)	0.5206(3)	0.2389(2)	0.015(1)
O2	4*c*	0.0364(2)	1/4	0.5307(3)	0.016(1)
O3	4*c*	0.1107(2)	1/4	0.8007(3)	0.020(1)
O4	4*c*	0.1965(2)	1/4	0.1234(3)	0.017(1)
O5	8*d*	0.2110(1)	0.5181(4)	0.4241(2)	0.020(1)
O6	4*c*	0.3656(2)	1/4	0.1436(3)	0.023(1)
H6	4*c*	0.4120(30)	1/4	0.1110(70)	0.034*

* refined with isotropic displacement parameter

Appendix 21: *$RbSc(HPO_4)_2$: Atomic coordinates and equivalent / isotropic displacement parameters ($Å^2$)*

Atom	Site	*x*	*y*	*z*	U_{eq}
Rb	4*e*	0.2742(1)	0.4994(1)	0.1134(1)	0.033(1)
Sc	4*e*	0.2578(1)	0.0377(1)	0.1500(1)	0.013(1)
P1	4*e*	0.7241(2)	0.8406(1)	0.0613(1)	0.013(1)
P2	4*e*	0.2198(2)	0.7613(1)	0.3108(1)	0.013(1)
O1	4*e*	0.9143(5)	0.9522(3)	0.1010(2)	0.020(1)
O2	4*e*	0.7420(5)	0.8169(3)	–0.0396(2)	0.017(1)
O3	4*e*	0.4553(5)	0.8786(3)	0.0822(2)	0.019(1)
O4	4*e*	0.2106(5)	0.1801(3)	0.3961(2)	0.022(1)
O5	4*e*	0.2625(5)	0.9121(3)	0.2684(2)	0.018(1)
O6	4*e*	0.4180(5)	0.6485(3)	0.2922(2)	0.017(1)
O7	4*e*	–0.0459(5)	0.7025(3)	0.2840(2)	0.016(1)
O8	4*e*	0.2389(5)	0.8006(3)	0.4169(2)	0.019(1)

Appendix 22: *$CsSc(HPO_4)_2$: Atomic coordinates and equivalent / isotropic displacement parameters (in $Å^2$)*

Atom	Site	*x*	*y*	*z*	U_{eq} / U_{iso}
Cs	4*e*	0.2655(1	0.4991(1)	0.1096(1)	0.022(1)
Sc	4*e*	0.2499(1)	0.0364(1)	0.1515(1)	0.009(1)
P1	4*e*	0.7218(2)	0.8467(1)	0.0617(1)	0.008(1)
P2	4*e*	0.2296(2)	0.7561(1)	0.3091(1)	0.008(1)
O1	4*e*	0.9100(5)	0.9531(3)	0.1035(2)	0.017(1)
O2	4*e*	0.7458(5)	0.8247(3)	–0.0394(2)	0.012(1)
O3	4*e*	0.4544(5)	0.8844(3)	0.0821(2)	0.014(1)
O4	4*e*	0.2193(5)	0.1894(3)	0.3955(2)	0.017(1)
O5	4*e*	0.2614(5)	0.9052(3)	0.2672(2)	0.013(1)
O6	4*e*	0.4402(5)	0.6517(3)	0.2912(2)	0.014(1)
O7	4*e*	–0.0271(5)	0.6921(3)	0.2811(2)	0.012(1)
O8	4*e*	0.2382(5)	0.7920(3)	0.4156(2)	0.014(1)
H4	4*e*	0.187(12)	0.195(7)	0.345(3)	0.051(1)*
H8	4*e*	0.248(12)	0.728(5)	0.441(4)	0.05(2)*

* refined with isotropic displacement parameter

Appendix 23: *$NH_4Sc(HPO_4)_2$: Atomic coordinates and equivalent / isotropic displacement parameters ($Å^2$)*

Atom	Site	*x*	*y*	*z*	U_{eq}
N	4*e*	0.2744(7)	0.4974(5)	0.1118(3)	0.045(1)
Sc	4*e*	0.2595(1)	0.0370(1)	0.1496(1)	0.024(1)
P1	4*e*	0.7249(2)	0.8386(1)	0.0601(1)	0.024(1)
P2	4*e*	0.2184(2)	0.7594(1)	0.3097(1)	0.024(1)
O1	4*e*	0.9152(5)	0.9524(3)	0.0988(2)	0.032(1)
O2	4*e*	0.7398(5)	0.8116(3)	–0.0408(2)	0.028(1)
O3	4*e*	0.4574(4)	0.8770(3)	0.0795(2)	0.027(1)
O4	4*e*	0.2104(5)	0.1787(3)	0.3939(2)	0.034(1)
O5	4*e*	0.2668(5)	0.9088(3)	0.2657(2)	0.030(1)
O6	4*e*	0.4143(5)	0.6426(3)	0.2923(2)	0.027(1)
O7	4*e*	–0.0496(5)	0.7024(3)	0.2831(2)	0.027(1)
O8	4*e*	0.2382(5)	0.7997(3)	0.4151(2)	0.031(1)

Appendix 24: *$Li_2Sc[(PO_4)(HPO_4)]$: Anisotropic displacement parameters U_{ij} ($Å^2 \times 10^3$). The anisotropic displacement factor exponent takes the form: $-2\pi [h^2a^{*2}U_{11} + \cdots + 2hka^*b^* U_{12}]$.*

Atom	U_{11}	U_{22}	U_{33}	U_{23}	U_{13}	U_{12}
Li	30(3)	19(2)	18(3)	5(2)	9(2)	7(2)
Sc	10(1)	9(1)	9(1)	0(1)	2(1)	1(1)
P	8(1)	9(1)	8(1)	1(1)	2(1)	0(1)
O1	13(1)	12(1)	14(1)	2(1)	6(1)	2(1)
O2	15(1)	11(1)	14(1)	3(1)	5(1)	–2(1)
O3	10(1)	13(1)	14(1)	2(1)	1(1)	3(1)
O4	14(1)	22(1)	9(1)	–4(1)	3(1)	–7(1)

Appendix 25: *$KSc(HPO_4)_2$: Anisotropic displacement parameters U_{ij} ($Å^2 \times 10^3$). The anisotropic displacement factor exponent takes the form: $-2\pi [h^2a^{*2}U_{11} + \cdots + 2hka^*b^* U_{12}]$.*

Atom	U_{11}	U_{22}	U_{33}	U_{23}	U_{13}	U_{12}
K	26(1)	40(1)	26(1)	0	–7(1)	0
Sc	11(1)	9(1)	11(1)	0	1(1)	0
P1	11(1)	9(1)	11(1)	0	0(1)	0
P2	10(1)	9(1)	12(1)	0	1(1)	0
O1	18(1)	14(1)	14(1)	1(1)	1(1)	5(1)
O2	18(1)	14(1)	15(1)	0	5(1)	0
O3	14(1)	23(1)	24(1)	0	–7(1)	0
O4	15(1)	22(1)	15(1)	0	6(1)	0
O5	19(1)	16(1)	26(1)	–9(1)	–2(1)	–4(1)
O6	14(1)	31(1)	22(1)	0	–4(1)	0

Appendix 26: *$RbSc(HPO_4)_2$: Anisotropic displacement parameters U_{ij} ($Å^2 \times 10^3$). The anisotropic displacement factor exponent takes the form: $-2\pi [h^2a^{*2}U_{11} + \cdots + 2hka^*b^* U_{12}]$.*

Atom	U_{11}	U_{22}	U_{33}	U_{23}	U_{13}	U_{12}
Rb	29(1)	31(1)	39(1)	–5(1)	–3(1)	5(1)
Sc	14(1)	13(1)	11(1)	–1(1)	2(1)	0(1)
P1	14(1)	13(1)	12(1)	–1(1)	2(1)	–1(1)
P2	11(1)	13(1)	13(1)	1(1)	1(1)	–1(1)
O1	16(1)	22(2)	23(1)	–1(1)	4(1)	–2(1)
O2	20(1)	16(1)	15(1)	0(1)	6(1)	–4(1)
O3	16(1)	17(1)	26(1)	–5(1)	8(1)	0(1)
O4	31(2)	13(1)	23(1)	–4(1)	5(1)	–4(1)
O5	21(1)	16(1)	18(1)	4(1)	1(1)	–5(1)
O6	16(1)	16(1)	18(1)	1(1)	–4(1)	5(1)
O7	14(1)	16(1)	19(1)	6(1)	–2(1)	0(1)
O8	22(1)	21(1)	14(1)	–4(1)	4(1)	–2(1)

Appendix 27: *$CsSc(HPO_4)_2$: Anisotropic displacement parameters U_{ij} ($Å^2 \times 10^3$). The anisotropic displacement factor exponent takes the form: $-2\pi [h^2a^{*2}U_{11} + \cdots + 2hka^*b^* U_{12}]$.*

Atom	U_{11}	U_{22}	U_{33}	U_{23}	U_{13}	U_{12}
Cs	18(1)	22(1)	27(1)	–4(1)	–3(1)	3(1)
Sc	7(1)	9(1)	9(1)	–1(1)	0(1)	0(1)
P1	8(1)	8(1)	9(1)	–1(1)	1(1)	0(1)
P2	7(1)	8(1)	9(1)	1(1)	0(1)	–1(1)
O1	11(1)	19(1)	18(1)	–6(1)	–2(1)	–4(1)
O2	16(1)	13(1)	8(1)	–1(1)	1(1)	0(1)
O3	10(1)	12(1)	19(1)	–4(1)	4(1)	2(1)
O4	21(2)	13(1)	16(1)	–2(1)	–1(1)	–5(1)
O5	15(1)	11(1)	13(1)	5(1)	0(1)	–3(1)
O6	9(1)	16(1)	15(1)	2(1)	1(1)	3(1)
O7	9(1)	12(1)	12(1)	3(1)	0(1)	–2(1)
O8	16(1)	16(1)	9(1)	0(1)	2(1)	–1(1)

Appendix 28: *$NH_4Sc(HPO_4)_2$: Anisotropic displacement parameters U_{ij} ($Å^2 \times 10^3$). The anisotropic displacement factor exponent takes the form: $-2\pi [h^2a^{*2}U_{11} + \cdots + 2hka^*b^* U_{12}]$*

Atom	U_{11}	U_{22}	U_{33}	U_{23}	U_{13}	U_{12}
N	39(2)	51(2)	45(2)	–2(2)	0(2)	5(2)
Sc	23(1)	26(1)	24(1)	0(1)	2(1)	0(1)
P1	23(1)	25(1)	23(1)	–2(1)	2(1)	0(1)
P2	23(1)	25(1)	25(1)	2(1)	3(1)	–1(1)
O1	27(1)	37(2)	30(1)	–10(1)	0(1)	–4(1)
O2	31(1)	30(1)	23(1)	–2(1)	1(1)	1(1)
O3	20(1)	28(1)	34(1)	–5(1)	4(1)	2(1)
O4	39(2)	29(1)	34(1)	–1(1)	5(1)	–4(1)
O5	29(1)	30(1)	30(2)	5(1)	6(1)	–3(1)
O6	26(1)	28(1)	28(1)	0(1)	3(1)	2(1)
O7	26(1)	26(1)	29(1)	4(1)	0(1)	–3(1)
O8	29(1)	37(2)	28(1)	0(1)	1(1)	1(1)

Appendix 29: *$Li_2Sc[(PO_4)(HPO_4)]$: Selected interatomic distances (Å) and angles (°)*

Atom contact	Distance	Atom contact	Distance
Li—O1[f]	1.976(1)	Sc—O3[a]	2.073(2)
Li—O3[g]	1.981(1)	Sc—O3[b]	2.073(2)
Li—O4[h]	1.991(2)	Sc—O2[c]	2.082(2)
Li—O2	2.099(2)	Sc—O2[d]	2.082(2)
Li—O4[g]	2.418(2)	Sc—O1	2.131(2)
		Sc—O1[e]	2.131(2)
P—O2	1.529(2)		
P—O1	1.530(2)		
P—O3	1.530(2)		
P—O4	1.550(2)		

Atoms	Angle	Atoms	Angle
O3[a]—Sc—O3[b]	180.0	O3[b]—Sc—O1[e]	95.65(8)
O3[a]—Sc—O2[c]	83.81(8)	O2[c]—Sc—O1[e]	91.59(8)
O3[b]—Sc—O2[c]	96.19(8)	O2[d]—Sc—O1[e]	88.41(8)
O3[a]—Sc—O2[d]	96.19(8)	O1—Sc—O1[e]	180.0
O3[b]—Sc—O2[d]	83.81(8)		
O2[c]—Sc—O2[d]	180.0	O2—P—O3	109.98(12)
O3[a]—Sc—O1	95.65(8)	O2—P—O1	111.68(12)
O3[b]—Sc—O1	84.35(8)	O3—P—O1	109.81(12)
O2[c]—Sc—O1	88.41(8)	O2—P—O4	107.39(12)
O2[d]—Sc—O1	91.59(8)	O3—P—O4	106.04(12)
O3[a]—Sc—O1[e]	84.35(8)	O1—P—O4	111.78(12)

Symmetry transformation used to generate equivalent atoms: [a] $-x+1, -y, -z+1$; [b] $x-1, y, z$; [c] $x-1/2, -y+1/2, z+1/2$; [d] $-x+1/2, y-1/2, -z+1/2$; [e] $-x, -y, -z+1$; [f] $x+1, y, z$; [g] $-x+3/2, y+1/2, -z+1/2$; [h] $x+1/2, -y+1/2, z+1/2$.

Appendix 30: *$KSc(HPO_4)_2$: Selected interatomic distances (Å) and angles (°)*

Atom contact	Distance	Atom contact	Distance
K—O5[a]	2.874(2)	P2—O4	1.510(2)
K—O5	2.874(2)	P2—O5[e]	1.5161(19)
K—O1[b]	2.9024(19)	P2—O5[b]	1.5161(19)
K—O1[c]	2.9024(19)	P2—O6	1.583(3)
K—O3[d]	3.0604(14)		
K—O3[e]	3.0604(14)	Sc—O4	2.056(2)
K—O1[f]	3.198(2)	Sc—O5	2.0865(18)
K—O1[g]	3.198(2)	Sc—O5[a]	2.0865(18)
K—O4[b]	3.2185(15)	Sc—O1[a]	2.1052(17)
K—O4[h]	3.2185(15)	Sc—O1	2.1052(17)
		Sc—O2	2.113(2)
P1—O1[c]	1.5170(18)		
P1—O1[d]	1.5170(18)	O6—H6	0.74(4)
P1—O2	1.518(2)	O6—H6···O2	2.887(1)
P1—O3	1.593(3)		

Atoms	Angle	Atoms	Angle
O4—Sc—O5	90.62(8)	O1[c]—P1—O1[d]	110.25(14)
O4—Sc—O5[a]	90.62(8)	O1[c]—P1—O2	113.38(8)
O5—Sc—O5[a]	88.40(11)	O1[c]—P1—O2	113.38(8)
O4—Sc—O1[a]	89.86(7)	O1[c]—P1—O3	105.09(9)
O5—Sc—O1[a]	179.52(8)	O1[c]—P1—O3	105.09(9)
O5[a]—Sc—O1[a]	91.57(8)	O2—P1—O3	108.96(15)
O4—Sc—O1	89.86(7)		
O5—Sc—O1	91.57(8)	O4—P2—O5[e]	111.43(9)
O5[a]—Sc—O1	179.52(8)	O4—P2—O5[b]	111.43(9)
O1[a]—Sc—O1	88.46(10)	O5[e]—P2—O5[b]	112.21(16)
O4—Sc—O2	174.34(10)	O4—P2—O6	105.35(15)
O5—Sc—O2	93.44(8)	O5[e]—P2—O6	108.03(10)
O5[a]—Sc—O2	93.44(8)	O5[b]—P2—O6	108.03(10)
O1[a]—Sc—O2	86.08(7)		
O1—Sc—O2	86.08(7)	O6—H6···O2	168.77(1)

Symmetry transformation used to generate equivalent atoms: [a] *x*, *–y*+1/2, *z*; [b] *–x*+1/2, *–y*+1, *z*–1/2; [c] *–x*, *y*–1/2, *–z*+1; [d] *–x*, *–y*+1, *–z*+1; [e] *–x*+1/2, *y*–1/2, *z*–1/2; [f] x+1/2, y, –z+1/2; [g] x+1/2, –y+1/2, –z+1/2; [h] –x+1/2, –y, z+1/2

Appendix 31: *$RbSc(HPO_4)_2$: Selected interatomic distances (Å) and angles (°)*

Atom contact	Distance	Atom contact	Distance
Rb—O6	2.995(3)	P2—O6	1.500(3)
Rb—O5[a]	2.997(2)	P2—O5	1.509(3)
Rb—O2[b]	3.024(3)	P2—O7	1.527(3)
Rb—O4[c]	3.035(3)	P2—O8	1.600(3)
Rb—O4[d]	3.194(3)		
Rb—O8[a]	3.203(3)		
Rb—O8[e]	3.254(3)		
Rb—O7[e]	3.332(3)	Sc—O1[g]	2.053(3)
Rb—O8[f]	3.397(3)	Sc—O5[h]	2.074(2)
Rb—O5[e]	3.559(3)	Sc—O3[h]	2.075(3)
Rb—O3	3.559(3)	Sc—O2[b]	2.083(3)
		Sc—O6[a]	2.104(3)
P1—O1	1.503(3)	Sc—O7[e]	2.139(3)
P1—O2	1.516(3)		
P1—O3	1.527(3)		
P1—O4[d]	1.590(3)		

Atoms	Angle	Atoms	Angle
O1[g]—Sc—O5[h]	92.38(11)	O1—P1—O2	112.19(15)
O1[g]—Sc—O3[h]	92.81(11)	O1—P1—O3	112.65(15)
O5[h]—Sc—O3[h]	93.87(11)	O2—P1—O3	111.65(15)
O1[g]—Sc—O2[b]	90.94(11)	O1—P1—O4[d]	109.05(16)
O5[h]—Sc—O2[b]	174.11(11)	O2—P1—O4[d]	103.45(15)
O3[h]—Sc—O2[b]	90.81(11)	O3—P1—O4[d]	107.29(16)
O1[g]—Sc—O6[a]	172.26(11)		
O5[h]—Sc—O6[a]	87.86(10)	O6—P2—O5	112.90(16)
O3[h]—Sc—O6[a]	94.90(11)	O6—P2—O7	111.85(15)
O2[b]—Sc—O6[a]	88.19(10)	O5—P2—O7	111.62(15)
O1[g]—Sc—O7[e]	85.81(11)	O6—P2—O8	109.87(15)
O5[h]—Sc—O7[e]	87.48(10)	O5—P2—O8	102.14(15)
O3[h]—Sc—O7[e]	178.11(10)	O7—P2—O8	107.91(15)
O2[b]—Sc—O7[e]	87.92(10)		
O6[a]—Sc—O7[e]	86.47(10)		

Symmetry transformation used to generate equivalent atoms: [a] $-x+1, y-1/2, -z+1/2$; [b] $-x+1, -y+1, -z$; [c] $-x, y+1/2, -z+1/2$; [d] $-x+1, y+1/2, -z+1/2$; [e] $-x, y-1/2, -z+1/2$; [f] x, $-y+3/2, z-1/2$; [g] $x-1, y-1, z$; [h] $x, y-1, z$.

Appendix 32: *$CsSc(HPO_4)_2$: Selected interatomic distances (Å) and angles (°)*

Atom contact	Distance	Atom contact	Distance
Cs—O6	3.105(3)	P2—O6	1.511(3)
Cs—O4[a]	3.129(3)	P2—O5	1.516(3)
Cs—O2[b]	3.138(3)	P2—O7	1.529(2)
Cs—O5[c]	3.141(2)	P2—O8	1.595(3)
Cs—O4[d]	3.272(3)		
Cs—O8[e]	3.298(3)	Sc—O1[h]	2.058(2)
Cs—O8[c]	3.306(3)	Sc—O3[i]	2.080(3)
Cs—O8[f]	3.431(3)	Sc—O5[i]	2.081(2)
Cs—O7[e]	3.521(3)	Sc—O2[b]	2.085(3)
Cs—O7	3.529(2)	Sc—O6[c]	2.099(2)
Cs—O5[e]	3.560(3)	Sc—O7[e]	2.144(2)
Cs—O4[g]	3.580(3)		
		O4—H4	0.76(4)
P1—O1	1.507(3)	O4—H4···O7	2.737(1)
P1—O2	1.514(2)		
P1—O3	1.525(3)	O8—H8	0.71(4)
P1—O4[d]	1.593(3)	O8—H8···O3	3.100(1)

Atoms	Angle	Atoms	Angle
O1[h]—Sc—O3[i]	93.82(10)	O1—P1 —O2	112.92(15)
O1[h]—Sc—O5[i]	92.57(10)	O1—P1—O3	112.78(15)
O3[i]—Sc—O5[i]	91.48(10)	O2—P1—O3	111.46(14)
O1[h]—Sc—O2[b]	90.57(11)	O1—P1—O4[d]	108.37(15)
O3[i]—Sc—O2[b]	89.32(10)	O2—P1—O4[d]	103.71(15)
O5[i]—Sc—O2[b]	176.70(10)	O3—P1—O4[d]	106.97(15)
O1[h]—Sc—O6[c]	169.93(11)		
O3[i]—Sc—O6[c]	96.08(10)	O5—P2—O6	113.18(15)
O5[i]—Sc—O6[c]	89.02(10)	O5—P2—O7	111.13(14)
O2[b]—Sc—O6[c]	87.71(10)	O6—P2—O7	112.27(15)
O1[i]—Sc—O7[e]	84.07(10)	O5—P2—O8	102.32(15)
O3[i]—Sc—O7[e]	177.65(10)	O6—P2—O8	109.15(14)
O5[i]—Sc—O7[e]	89.66(10)	O7—P2—O8	108.21(14)
O2[b]—Sc—O7[e]	89.66(10)		
O6[c]—Sc—O7[e]	85.99(10)	O4—H4···O7	167.03(1)
		O8—H8···O3	143.52(1)

Symmetry transformation used to generate equivalent atoms: [a] $-x, y+1/2, -z+1/2$; [b] $-x+1, -y+1, -z$; [c] $-x+1, y-1/2, -z+1/2$; [d] $-x+1, y+1/2, -z+1/2$; [e] $-x, y-1/2, -z+1/2$; [f] $x, -y+3/2, z-1/2$; [g] $x, -y+1/2, z-1/2$; [h] $x-1, y-1, z$; [i] $x, y-1, z$.

Appendix 33: *$NH_4Sc(HPO_4)_2$: Selected interatomic distances (Å) and angles (°)*

Atom contact	Distance	Atom contact	Distance
Sc—O5^{e}	2.057(3)	P1—O1	1.505(3)
Sc—O1^{b}	2.057(3)	P1—O3	1.516(3)
Sc—O6^{c}	2.087(3)	P1—O2	1.520(3)
Sc—O3^{a}	2.097(3)	P1—O4^{f}	1.597(3)
Sc—O2^{d}	2.097(3)		
Sc—O7^{e}	2.143(3)	P2—O6	1.508(3)
		P2—O5	1.509(3)
		P2—O7	1.530(3)
		P2—O8	1.592(3)

Atoms	Angle	Atoms	Angle
O5^{a}—Sc—O1^{b}	92.98(11)	O1—P1—O3	112.82(15)
O5^{a}—Sc—O6^{c}	87.30(11)	O1—P1—O2	112.65(16)
O1^{b}—Sc—O6^{c}	173.43(11)	O3—P1—O2	110.86(15)
O5^{a}—Sc—O3^{a}	93.85(11)	O1—P1—O4^{f}	108.78(16)
O1^{b}—Sc—O3^{a}	92.49(10)	O3—P1—O4^{f}	106.73(15)
O6^{c}—Sc—O3^{a}	94.04(10)	O2—P1—O4^{f}	104.45(16)
O5^{a}—Sc—O2^{d}	173.63(11)		
O1^{b}—Sc—O2^{d}	90.96(11)	O6—P2—O5	112.39(15)
O6^{c}—Sc—O2^{d}	88.21(10)	O6—P2—O7	111.83(15)
O3^{a}—Sc—O2^{d}	90.97(11)	O5—P2—O7	111.77(15)
O5^{a}—Sc—O7^{e}	87.76(10)	O6—P2—O8	109.69(15)
O1^{b}—Sc—O7^{e}	86.26(11)	O5—P2—O8	103.07(16)
O6^{c}—Sc—O7^{e}	87.19(10)	O7—P2—O8	107.62(15)
O3^{a}—Sc—O7^{e}	178.01(11)		
O2^{d}—Sc—O7^{e}	87.51(10)		

Symmetry transformation used to generate equivalent atoms: ^{a} x, y–1, z; ^{b} x–1, y–1, z; ^{c} –x+1, y–1/2, –z+1/2; ^{d} –x+1, –y+1, –z; ^{e} –x, y–1/2, –z+1/2; ^{f} –x+1, y+1/2, –z+1/2.

5.2.4 Ca$M2^{II}$[$BP_2O_7(OH)_3$] ($M2^{II}$ = Fe, Ni)

Appendix 34: *$CaFe[BP_2O_7(OH)_3]$: Crystallographic data and refinement parameters*

Crystallographic data

Formula weight (g / mol)	331.70
Dimensions of the crystal (mm^3)	0.125 × 0.075 × 0.060
Crystal color and habit	colorless, platy
Temperature of measurement (K)	293
Crystal system	monoclinic
Space group	*C*1 2/*c*1 (No.15)
Unit cell parameters	*a* = 10.2332(15) Å *b* = 8.2391(8) Å β = 117.069(6)° *c* = 9.1587(12) Å
Cell volume ($Å^3$)	687.61
Formula units *Z*	4
Calculated density, ρ_{calc} (g / cm^3)	3.204

Data collection and refinement parameters

Diffractometer	RIGAKU AFC7 CCD, MoK_α–radiation (λ = 0.7107 Å), Graphite monochromator
Absorption coefficient, μ (MoK_α), mm^{-1}	3.452
Scan type	φ / ω
2θ range (°)	6.66 – 65.16
Limiting indices	$-14 \le h \le 13$, $-9 \le k \le 12$, $-13 \le l \le 13$
Total data collected	3650
Unique data	1166
R(int)	0.016
Observed data, $I > 2\sigma$	1120
Paramenter refined	75
F(000)	656
Goodness–of–fit (on F^2)	1.122
R1/wR2, $I > 2\sigma$ (*I*)	0.024 / 0.062
R1/wR2, all data	0.026 / 0.064
Residual electron density (max. / min.) ($eÅ^{-3}$)	0.667 / –0.630

Appendix 35: *$CaNi[BP_2O_7(OH)_3]$: Crystallographic data and refinement parameters*

Crystallographic data

Formula weight (g / mol)	334.56
Dimensions of the crystal (mm^3)	0.12 × 0.11 × 0.05
Crystal color and habit	green, platy
Temperature of measurement (K)	293
Crystal system	monoclinic
Space group	*C*1 2/*c*1 (No.15)
Unit cell parameters	*a* = 10.2515(9) Å *b* = 8.3364(5) Å β = 116.34(4)° *c* = 9.1752(13) Å
Cell volume ($Å^3$)	702.70
Formula units *Z*	4
Calculated density, ρ_{calc} (g / cm^3)	3.162

Data collection and refinement parameters

Diffractometer	RIGAKU AFC7 CCD, MoK_α–radiation Graphite monochromator
Absorption coefficient, μ (MoK_α), mm^{-1}	3.992
Scan type	φ / ω
2θ range (°)	6.60 – 67.42
Limiting indices	$-15 \le h \le 15$, $-11 \le k \le 12$, $-9 \le l \le 13$
Total data collected	4130
Unique data	1111
R(int)	0.022
Observed data, $I > 2\sigma$	1120
Paramenter refined	76
F(000)	664
Goodness–of–fit (on F^2)	1.114
R1/wR2, $I > 2\sigma$ (*I*)	0.027 / 0.075
R1/wR2, all data	0.029 / 0.076
Residual electron density (max. / min.) ($eÅ^{-3}$)	0.838 / –0.630

Appendix 36: *$CaFe[BP_2O_7(OH)_3]$: Atomic coordinates and equivalent / isotropic displacement parameters ($Å^2$)*

Atom	Site	*x*	*y*	*z*	U_{eq} / U_{iso}
Ca	4*e*	0	0.1494(1)	1/4	0.010(1)
Fe	4*c*	1/4	1/4	0	0.006(1)
P	8*f*	0.2862(1)	0.4341(1)	0.3256(1)	0.006(1)
B	4*e*	0	0.5270(3)	1/4	0.007(1)
O1	8*f*	0.1342(1)	0.1856(2)	0.5390(2)	0.011(1)
O2	8*f*	0.3260(1)	0.4123(2)	0.1843(2)	0.008(1)
O3	8*f*	0.1763(1)	0.1125(2)	0.1214(2)	0.009(1)
O4	8*f*	0.1159(1)	0.4127(2)	0.2592(2)	0.008(1)
O5	8*f*	0.4437(1)	0.1260(2)	0.1015(2)	0.008(1)
H5	8*f*	0.5090(40)	0.1760(40)	0.940(40)	0.023(8)*

* refined with isotropic displacement parameter

Appendix 37: *$CaNi[BP_2O_7(OH)_3]$: Atomic coordinates and equivalent / isotropic displacement parameters ($Å^2$)*

Atom	Site	*x*	*y*	*z*	U_{eq} / U_{iso}
Ca	4*e*	0	0.1328(1)	1/4	0.016(1)
Ni	4*c*	1/4	1/4	0	0.009(1)
P	8*f*	0.2838(1)	0.4352(1)	0.3256(1)	0.009(1)
B	4*e*	0	0.05261(3)	1/4	0.009(1)
O1	8*f*	0.1154(1)	0.4117(2)	0.2573(2)	0.011(1)
O2	8*f*	0.1526(2)	0.1867(2)	0.5317(2)	0.020(1)
O3	8*f*	0.1676(1)	0.1049(2)	0.1163(2)	0.009(1)
O4	8*f*	0.3346(1)	0.3997(2)	0.1977(2)	0.016(1)
O5	8*f*	0.4446(1)	0.1195(2)	0.1021(2)	0.014(1)
H2	4*d*	1/4	1/4	1/2	0.4(1)*
H5	8*f*	0.505(5)	0.168(5)	0.094(5)	0.05(1)*

* refined with isotropic displacement parameter

Appendix 38: *$CaFe[BP_2O_7(OH)_3]$: Anisotropic displacement parameters U_{ij} ($Å^2 \times 10^3$). The anisotropic displacement factor exponent takes the form: $-2\pi [h^2a^{*2}U_{11} + \cdots + 2hka^*b^* U_{12}]$.*

Atom	U_{11}	U_{22}	U_{33}	U_{23}	U_{13}	U_{12}
Ca	121)	9(1)	11(1)	0	6(1)	0
Fe	7(1)	5(1)	6(1)	1(1)	3(1)	0(1)
P	5(1)	6(1)	6(1)	–1(1)	3(1)	0(1)
B	6(1)	5(1)	9(1)	0	3(1)	0
O1	11(1)	12(1)	9(1)	3(1)	3(1)	3(1)
O2	10(1)	9(1)	8(1)	–2(1)	6(1)	–2(1)
O3	9(1)	8(1)	11(1)	3(1)	6(1)	2(1)
O4	6(2)	7(1)	11(1)	–1(1)	4(1)	0(1)
O5	7(1)	10(1)	8(1)	3(1)	3(1)	1(1)

Appendix 39: *$CaNi[BP_2O_7(OH)_3]$: Anisotropic displacement parameters U_{ij} ($Å^2 \times 10^3$). The anisotropic displacement factor exponent takes the form: $-2\pi [h^2a^{*2}U_{11} + \cdots + 2hka^*b^* U_{12}]$.*

Atom	U_{11}	U_{22}	U_{33}	U_{23}	U_{13}	U_{12}
Ca	20(2)	14(2)	20(2)	0	13(1)	0
Ni	11(1)	7(1)	9(1)	0(1)	5(1)	0(1)
P	9(1)	7(1)	11(1)	–1(1)	4(1)	0(1)
B	9(1)	7(1)	9(1)	0	4(1)	0
O1	9(1)	9(2)	16(1)	–1(1)	6(1)	1(1)
O2	16(1)	16(1)	18(1)	7(1)	0(1)	–2(1)
O3	14(1)	9(1)	18(1)	5(1)	10(1)	3(1)
O4	16(2)	17(1)	20(1)	–10(1)	12(1)	–6(1)
O5	13(1)	13(1)	16(2)	6(1)	7(1)	2(1)

Appendix 40: *$CaFe[BP_2O_7(OH)_3]$: Selected interatomic distances (Å) and angles (°)*

Atom contact	Distance	Atom contact	Distance
Ca—O1	2.3814(13)	Fe—O3	2.0556(16)
Ca—O1[a]	2.3814(13)	Fe—O3[d]	2.0571(16)
Ca—O4	2.4550(13)	Fe—O2	2.0826(17)
Ca—O4[a]	2.4550(13)	Fe—O2[d]	2.0844(16)
Ca—O2[b]	2.5245(13)	Fe—O5[d]	2.1361(17)
Ca—O2[c]	2.5245(13)	Fe—O5	2.1503(17)
Ca—O3[a]	2.5821(13)		
Ca—O3	2.5821(13)	B—O5[f]	1.4606(18)
		B—O5[g]	1.4606(18)
P—O1	1.5014(13)	B—O4[a]	1.486(2)
P—O2[e]	1.5348(13)	B—O4	1.486(2)
P—O3	1.5408(13)		
P—O4[f]	1.5725(13)	O5—H5	0.82(3)
		O5—H5···O1	2.748(1)

Atoms	Angle	Atoms	Angle
O3[d]—Fe—O3	180.00(5)	O1[e]—P—O2	111.56(8)
O3[d]—Fe—O2	89.42(5)	O1[e]—P—O3[f]	113.75(7)
O3—Fe—O2	90.58(5)	O2—P—O3[f]	104.65(7)
O3[d]—Fe—O2[d]	90.58(5)	O1[e]—P—O4	109.60(7)
O3—Fe—O2[d]	89.42(5)	O2—P—O4	109.48(7)
O2—Fe—O2[d]	180.00(5)	O3[f]—P—O4	107.60(7)
O3[d]—Fe—O5[d]	89.83(5)		
O3—Fe—O5[d]	90.17(5)	O5[f]—B—O5[g]	112.10(19)
O2—Fe—O5[d]	88.52(5)	O5[f]—B—O4[b]	111.90(7)
O2[d]—Fe—O5[d]	91.48(5)	O5[g]—B—O4[a]	109.56(7)
O3[d]—Fe—O5	90.17(5)	O5[f]—B—O4	109.56(7)
O3—Fe—O5	89.83(5)	O5[g]—B—O4	111.90(7)
O2—Fe—O5	91.48(5)	O4[a]—B—O4	101.35(18)
O2[d]—Fe—O5	88.52(5)		
O5[d]—Fe—O5	180.00(6)	O5—H5···O1	168.76(1)

Symmetry transformation used to generate equivalent atoms: [a] –x, y, –z+1/2; [b] x–1/2, y–1/2, z; [c] –x+1/2, y–1/2, –z+1/2; [d] –x+1/2, –y+1/2, –z; [e] –x+1/2, –y+1/2, –z+1; [f] –x+1/2, y+1/2, –z+1/2; [g] x–1/2, y+1/2, z.

Appendix 41: *$CaNi[BP_2O_7(OH)_3]$: Selected interatomic distances (Å) and angles (°)*

Atom contact	Distance	Atom contact	Distance
Ca—O2	2.3960(18)	Ni—O3	2.0284(13)
Ca—O2[a]	2.3960(18)	Ni—O3[d]	2.0284(13)
Ca—O4[b]	2.4816(14)	Ni—O4[d]	2.0504(14)
Ca—O4[c]	2.4816(14)	Ni—O4	2.0504(14)
Ca—O3[a]	2.5265(14)	Ni—O5[d]	2.0931(14)
Ca—O3	2.5265(14)	Ni—O5	2.0931(14)
Ca—O1	2.5961(13)		
Ca—O1[a]	2.5961(13)	B—O5[e]	1.4447(19)
		B—O5[g]	1.4447(19)
P—O4	1.5096(15)	B—O1[a]	1.498(2)
P—O3[e]	1.5161(13)	B—O1	1.498(2)
P—O2[f]	1.5538(15)		
P—O1	1.5655(13)	O2—H2	1.2713(15)
		O2—H2···O2	2.542(1)
		O5—H5···O2	0.77(4)
		O5—H5···O2	2.966(1)

Atoms	Angle	Atoms	Angle
O3—Ni—O3[d]	180.00(8)	O4—P—O3[e]	106.46(8)
O3—Ni—O4[d]	89.48(6)	O4—P—O2[f]	111.52(9)
O3[d]—Ni—O4[d]	90.52(6)	O3[e]—P—O2[f]	111.38(8)
O3—Ni—O4	90.52(6)	O4—P—O1	111.32(8)
O3[d]—Ni—O4	89.48(6)	O3[e]—P—O1	112.91(7)
O4[d]—Ni—O4	180.008)	O2[f]—P—O1	103.38(8)
O3—Ni—O5[d]	90.50(5)		
O3[d]—Ni—O5[d]	89.50(5)	O5[e]—B—O5[g]	114.7(2)
O4[d]—Ni—O5[d]	88.58(7)	O5[e]—B—O1[a]	111.03(8)
O4—Ni—O5[e]	91.42(7)	O5[g]—B—O1[a]	109.14(8)
O3—Ni—O5	89.50(5)	O5[e]—B—O1	109.14(8)
O3[d]—Ni—O5	90.50(5)	O5[g]—B—O1	111.03(8)
O4[d]—Ni—O5	91.42(7)	O1[a]—B—O1	100.93(17)
O4—Ni—O5	88.58(7)		
O5[d]—Ni—O5	180.00(6)	O2—H2···O2	180
		O5—H5···O2	171.35(1)

Symmetry transformation used to generate equivalent atoms: [a] –x, y, –z+1/2; [b] x–1/2, y–1/2, z; [c] –x+1/2, y–1/2, –z+1/2; [d] –x+1/2, –y+1/2, –z; [e] –x+1/2, y+1/2, –z+1/2; [f] –x+1/2, –y+1/2, –z+1; [g] x–1/2, y+1/2, z.

5.2.5 Ba$M2^{II}$[BP_2O_8(OH)] ($M2^{II}$ = Fe, Co)

Appendix 42: *$BaFe[BP_2O_8(OH)]$: Crystallographic data and refinement parameters*

Crystallographic data

Formula weight (g / mol)	410.95
Dimensions of the crystal (mm^3)	0.04 × 0.125 × 0.125
Crystal color and habit	colorless, platy
Temperature of measurement (K)	293
Crystal system	triclinic
Space group	$P\bar{1}$ (No.2)
Unit cell parameters	a = 5.3393(4) Å α = 89.047(15)° b = 8.0179(9) Å β = 79.211(12)° c = 8.3443(10) Å γ = 87.446(14)°
Cell volume ($Å^3$)	350.54
Formula units Z	2
Calculated density, ρ_{calc} (g / cm^3)	3.893

Data collection and refinement parameters

Diffractometer	RIGAKU AFC7 CCD, MoK_α–radiation (λ = 0.7107 Å), Graphite monochromator
Absorption coefficient, μ (MoK_α), mm^{-1}	8.136
Scan type	φ / ω
2θ range (°)	4.96 – 66.18
Limiting indices	$-8 \le h \le 8$, $-12 \le k \le 12$, $-12 \le l \le 12$
Total data collected	6869
Unique data	2252
R(int)	0.022
Observed data, $I > 2\sigma$	2119
Paramenter refined	128
F(000)	380
Goodness–of–fit (on F^2)	1.129
R1/wR2, $I > 2\sigma$ (I)	0.034 / 0.083
R1/wR2, all data	0.036 / 0.086
Residual electron density (max. / min.) ($eÅ^{-3}$)	2.537 / –2.772

Appendix 43: *$BaCo[BP_2O_8(OH)]$: Crystallographic data and refinement parameters*

Crystallographic data

Formula weight (g / mol)	414.03
Dimensions of the crystal (mm^3)	0.04 × 0.7 × 0.20
Crystal color and habit	pink, platy
Temperature of measurement (K)	293
Crystal system	triclinic
Space group	$P\bar{1}$ (No.2)
Unit cell parameters	a = 5.3147(3) Å α = 88.634(14)° b = 7.9926(8) Å β = 79.461(10)° c = 8.2936(8) Å γ = 87.139(13)°
Cell volume ($Å^3$)	345.88
Formula units Z	2
Calculated density, ρ_{calc} (g / cm^3)	3.975

Data collection and refinement parameters

Diffractometer	RIGAKU AFC7 CCD, MoK_α–radiation (λ = 0.7107 Å), Graphite monochromator
Absorption coefficient, μ (MoK_α), mm^{-1}	8.546
Scan type	φ / ω
2θ range (°)	5 – 64.08
Limiting indices	$-7 \le h \le 7$, $-11 \le k \le 11$, $-12 \le l \le 12$
Total data collected	6311
Unique data	2173
R(int)	0.021
Observed data, $I > 2\sigma$	2079
Paramenter refined	132
F(000)	382
Goodness–of–fit (on F^2)	1.179
R1/wR2, $I > 2\sigma$ (I)	0.028 / 0.067
R1/wR2, all data	0.030 / 0.068
Residual electron density (max. / min.) ($eÅ^{-3}$)	1.948 / –1.940

Appendix 44: *$BaFe[BP_2O_8(OH)]$: Atomic coordinates and equivalent / isotropic displacement parameters ($Å^2$)*

Atom	Site	*x*	*y*	*z*	U_{eq}
Ba	2*i*	0.7225(1)	0.3104(1)	0.1156(1)	0.010(1)
Fe	2*i*	0.2716(1)	0.2000(1)	0.8021(1)	0.008(1)
P1	2*i*	0.1999(2)	0.5667(1)	0.3018(1)	0.007(1)
P2	2*i*	0.2224(2)	0.0603(1)	0.1835(1)	0.007(1)
B	2*i*	0.1100(8)	0.2542(5)	0.4524(5)	0.009(1)
O1	2*i*	0.4467(5)	0.6191(3)	0.1941(4)	0.010(1)
O2	2*i*	0.0175(5)	0.4310(3)	0.7931(4)	0.010(1)
O3	2*i*	0.1343(5)	0.6750(3)	0.4568(4)	0.011(1)
O4	2*i*	0.2657(5)	0.3860(3)	0.3598(4)	0.012(1)
O5	2*i*	0.0911(5)	0.9110(3)	0.1347(4)	0.011(1)
O6	2*i*	0.4838(5)	0.0200(3)	0.2261(4)	0.012(1)
O7	2*i*	0.2456(6)	0.2023(3)	0.0560(4)	0.011(1)
O8	2*i*	0.0333(5)	0.1370(3)	0.3373(4)	0.009(1)
O9	2*i*	0.2648(6)	0.1702(4)	0.5562(4)	0.013(1)

Appendix 45: *$BaCo[BP_2O_8(OH)]$: Atomic coordinates and equivalent / isotropic displacement parameters ($Å^2$)*

Atom	Site	*x*	*y*	*z*	U_{eq}
Ba	2*i*	0.7234(1)	0.3108(1)	0.1159(1)	0.009(1)
Co	2*i*	0.2706(1)	0.2004(1)	0.8029(1)	0.007(1)
P1	2*i*	0.2013(2)	0.0568(1)	0.3018(1)	0.006(1)
P2	2*i*	0.2247(2)	0.0594(1)	0.1823(1)	0.006(1)
B	2*i*	0.1112(7)	0.2538(5)	0.4529(5)	0.008(1)
O1	2*i*	0.4489(5)	0.6200(3)	0.1944(3)	0.009(1)
O2	2*i*	0.0175(5)	0.4292(3)	0.7935(3)	0.010(1)
O3	2*i*	0.1344(5)	0.6754(3)	0.4575(3)	0.009(1)
O4	2*i*	0.2685(5)	0.3861(3)	0.3599(3)	0.010(1)
O5	2*i*	0.0913(5)	0.9113(3)	0.1346(3)	0.009(1)
O6	2*i*	0.4891(5)	0.0181(3)	0.2230(3)	0.011(1)
O7	2*i*	0.2454(5)	0.2041(3)	0.0546(3)	0.010(1)
O8	2*i*	0.0381(5)	0.1354(3)	0.3380(3)	0.009(1)
O9	2*i*	0.2672(5)	0.1704(4)	0.5590(3)	0.012(1)

Appendix 46: *$BaFe[BP_2O_8(OH)]$: Anisotropic displacement parameters U_{ij} ($Å^2 \times 10^3$). The anisotropic displacement factor exponent takes the form: $-2\pi [h^2a^{*2}U_{11} + \cdots + 2hka^*b^* U_{12}]$.*

Atom	U_{11}	U_{22}	U_{33}	U_{23}	U_{13}	U_{12}
Ba	9(1)	9(1)	13(1)	–2(1)	1(1)	–2(1)
Fe	9(1)	7(1)	8(1)	0(1)	0(1)	–2(1)
P1	7(1)	5(1)	7(1)	–1(1)	2(1)	–2(1)
P2	7(1)	5(1)	7(1)	0(1)	1(1)	–2(1)
B	11(2)	6(1)	8(2)	–1(1)	2(1)	–1(1)
O1	7(1)	8(1)	13(1)	1(1)	3(1)	–2(1)
O2	8(1)	10(1)	13(1)	–2(1)	–2(1)	–2(1)
O3	11(1)	10(1)	10(1)	–4(1)	1(1)	–1(1)
O4	10(1)	8(1)	15(1)	2(1)	2(1)	–3(1)
O5	12(1)	9(1)	11(1)	–2(1)	1(1)	–4(1)
O6	10(1)	9(1)	18(1)	–1(1)	–3(1)	–1(1)
O7	15(1)	7(1)	10(1)	3(1)	–1(1)	–5(1)
O8	10(1)	9(1)	9(1)	–3(1)	1(1)	–2(1)
O9	15(1)	13(1)	9(2)	2(1)	–1(1)	2(1)

Appendix 47: *$BaCo[BP_2O_8(OH)]$: Anisotropic displacement parameters U_{ij} ($Å^2 \times 10^3$). The anisotropic displacement factor exponent takes the form: $-2\pi [h^2a^{*2}U_{11} + \cdots + 2hka^*b^* U_{12}]$.*

Atom	U_{11}	U_{22}	U_{33}	U_{23}	U_{13}	U_{12}
Ba	6(1)	10(1)	12(1)	0	–1(1)	0(1)
Co	6(1)	9(1)	7(1)	1(1)	–2(1)	0(1)
P1	4(1)	7(1)	7(1)	1(1)	–1(1)	0(1)
P2	4(1)	7(1)	7(1)	1(1)	–2(1)	–1(1)
B	7(2)	8(2)	8(1)	1(1)	0(1)	–1(1)
O1	6(1)	8(1)	12(1)	2(1)	1(1)	–2(1)
O2	7(1)	12(1)	13(1)	0(1)	–5(1)	–1(1)
O3	5(1)	12(1)	10(1)	–2(1)	0(1)	0(1)
O4	8(1)	10(1)	12(1)	4(1)	–1(1)	0(1)
O5	8(1)	10(1)	10(1)	–1(1)	–2(1)	–2(1)
O6	6(1)	12(1)	14(1)	0(1)	–4(1)	2(1)
O7	11(1)	12(1)	8(1)	3(1)	–3(1)	–1(1)
O8	7(1)	11(1)	9(1)	0(1)	0(1)	–1(1)
O9	12(1)	13(1)	11(1)	2(1)	–4(1)	4(1)

Appendix 48: *$BaFe[BP_2O_8(OH)]$: Selected interatomic distances (Å) and angles (°)*

Atom contact	Distance	Atom contact	Distance
Ba—O2[a]	2.741(3)	Fe—O9	2.077(3)
Ba—O6	2.766(3)	Fe—O7[e]	2.098(3)
Ba—O5[b]	2.774(3)	Fe—O6[f]	2.137(3)
Ba—O7[c]	2.842(3)	Fe—O5[g]	2.140(3)
Ba—O1	2.844(3)	Fe—O1[a]	2.140(3)
Ba—O7	2.858(3)	Fe—O2	2.255(3)
Ba—O4	2.918(3)		
Ba—O1[b]	2.932(3)	P2—O5[h]	1.512(3)
Ba—O8[c]	2.995(3)	P2—O6	1.523(3)
Ba—O2[d]	3.020(3)	P2—O7	1.538(3)
		P2—O8	1.590(3)
P1—O1	1.521(3)	B—O9	1.445(5)
P1—O2[g]	1.522(3)	B—O3[g]	1.475(5)
P1—O3	1.546(3)	B—O8	1.478(5)
P1—O4	1.566(3)	B—O4	1.489(5)

Atoms	Angle	Atoms	Angle
O9—Fe—O7[e]	172.13(12)	O1—P1—O2[g]	111.22(17)
O9—Fe—O6[f]	84.73(12)	O1—P1—O3	110.95(16)
O7[e]—Fe—O6[f]	93.05(12)	O2[g]—P1—O3	112.14(16)
O9—Fe—O5[g]	90.12(12)	O1—P1—O4	103.93(15)
O7[e]—Fe—O5[g]	82.81(12)	O2[g]—P1—O4	111.68(16)
O6[f]—Fe—O5[g]	99.83(11)	O3—P1—O4	106.54(17)
O9—Fe—O1[a]	104.49(12)		
O7[e]—Fe—O1[a]	83.30(11)	O5[h]—P2—O6	114.59(16)
O6[f]—Fe—O1[a]	98.81(11)	O5[h]—P2—O7	113.15(17)
O5[g]—Fe—O1[a]	157.26(11)	O6—P2—O7	108.96(17)
O9—Fe—O2	87.18(11)	O5[h]—P2—O8	105.38(16)
O7[e]—Fe—O2	95.10(11)	O6—P2—O8	110.13(17)
O6[f]—Fe—O2	171.85(12)	O7—P2—O8	104.04(16)
O5[g]—Fe—O2	81.14(10)		
O1[a]—Fe—O2	82.26(10)		
O9—B—O3[g]	113.2(3)	O9—B—O4	107.3(3)
O9—B—O8	111.4(3)	O3[g]—B—O4	111.3(3)
O3[g]—B—O8	104.0(3)	O8—B—O4	109.7(3)

Symmetry transformation used to generate equivalent atoms: [a] –x+1 –y+1, –z+1; [b] –x+1, –y+1, –z; [c] x+1, y, z; [d] x+1, y, z–1; [e] x, y, z+1; [f] –x+1, –y, –z+1; [g] –x, –y+1, –z+1; [h] x, y–1, z.

Appendix 49: *$BaCo[BP_2O_8(OH)]$: Selected interatomic distances (Å) and angles (°)*

Atom contact	Distance	Atom contact	Distance
Ba—O2[a]	2.742(3)	Co—O9	2.046(3)
Ba—O6	2.757(3)	Co—O7[e]	2.068(3)
Ba—O5[b]	2.773(3)	Co—O6[f]	2.104(3)
Ba—O7[c]	2.820(3)	Co—O1[a]	2.124(3)
Ba—O1	2.833(3)	Co—O5[g]	2.133(3)
Ba—O7	2.855(3)	Co—O2	2.224(3)
Ba—O4	2.903(3)		
Ba—O1[b]	2.917(3)	P2—O5[h]	1.506(3)
Ba—O8[c]	2.988(3)	P2—O6	1.523(3)
Ba—O2[d]	2.998(3)	P2—O7	1.544(3)
		P2—O8	1.590(3)
P1—O1	1.518(3)	B—O9	1.446(5)
P1—O2[g]	1.520(3)	B—O3[g]	1.472(4)
P1—O3	1.544(3)	B—O8	1.473(5)
P1—O4	1.566(3)	B—O4	1.492(5)

Atoms	Angle	Atoms	Angle
O9—Co—O7[e]	172.62(12)	O1—P1—O2[g]	111.56(15)
O9—Co—O6[f]	84.24(11)	O1—P1—O3	111.26(15)
O7[e]—Co—O6[f]	93.31(11)	O2[g]—P1—O3	111.94(15)
O9—Co—O1[a]	104.07(11)	O1—P1—O4	103.57(15)
O7[e]—Co—O1[a]	83.18(11)	O2[g]—P1—O4	111.43(15)
O6[f]—Co—O1[a]	99.12(10)	O3—P1—O4	106.68(15)
O9—Co—O5[g]	90.34(11)		
O7[e]—Co—O5[g]	83.17(10)	O5[h]—P2—O6	114.82(15)
O6[f]—Co—O5[g]	99.19(11)	O5[h]—P2—O7	113.47(15)
O5[g]—Co—O1[a]	157.70(10)	O6—P2—O7	108.67(15)
O9—Co—O2	87.89(10)	O5[h]—P2—O8	105.20(15)
O7[e]—Co—O2	94.55(10)	O6—P2—O8	110.13(14)
O6[f]—Co—O2	172.12(10)	O7—P2—O8	103.90(15)
O1[a]—Co—O2	82.36(10)		
O5[g]—Co—O2	81.25(10)		
O9—B—O3[g]	113.1(3)	O9—B—O4	106.8(3)
O9—B—O8	111.1(3)	O3[g]—B—O4	111.5(3)
O3[g]—B—O8	104.4(3)	O8—B—O4	109.9(3)

Symmetry transformation used to generate equivalent atoms: [a] –x+1 –y+1,-z+1; [b] –x+1, –y+1, –z; [c] x+1, y, z; [d] x+1, y, z–1;, [e] x, y, z+1; [f] –x+1, –y, –z+1; [g] –x, –y+1, –z+1; [h] x, y–1, z.

5.2.6 $SrFe^{III}[BP_2O_8(OH)_2]$

Appendix 50: *$SrFe[BP_2O_8(OH)_2]$: Crystallographic data and refinement parameters*

Crystallographic data

Formula weight (g / mol)	379.24
Dimensions of the crystal (mm^3)	0.015 × 0.065 × 0.075
Crystal color and habit	colorless, prism
Temperature of measurement (K)	293
Crystal system	triclinic
Space group	$P\bar{1}$ (No.2)
Unit cell parameters	a = 6.6704(12)Å α = 109.829(5)° b = 6.6927(13) Å β = 102.068(6)° c = 9.3891(19) Å γ = 103.151(3)°
Cell volume ($Å^3$)	364.74
Formula units Z	2
Calculated density, ρ_{calc} (g / cm^3)	3.453

Data collection and refinement parameters

Diffractometer	RIGAKU AFC7 CCD, MoK_α–radiation (λ = 0.7107 Å), Graphite monochromator
Absorption coefficient, μ (MoK_α), mm^{-1}	9.784
Scan type	φ / ω
2θ range (°)	4.86 – 64.78
Limiting indices	$-6 \le h \le 9$, $-10 \le k \le 10$, $-14 \le l \le 11$
Total data collected	4464
Unique data	2244
R(int)	0.025
Observed data, $I > 2\sigma$	1905
Paramenter refined	146
F(000)	364
Goodness–of–fit (on F^2)	1.075
R1/wR2, $I > 2\sigma$ (I)	0.040 / 0.101
R1/wR2, all data	0.047 / 0.105
Residual electron density (max. / min.) ($eÅ^{-3}$)	1.446 / –2.526

Appendix 51: *$SrFe[BP_2O_2(OH)_2]$: Atomic coordinates and equivalent / isotropic displacement parameters ($Å^2$)*

Atom	Site	*x*	*y*	*z*	U_{eq} / U_{iso}
Sr	2*i*	0.3347(1)	0.1049(1)	0.7101(1)	0.013(1)
Fe1	1*c*	0	1/2	0	0.008(1)
Fe2	1*h*	1/2	1/2	1/2	0.008(1)
P1	2*i*	0.3513(2)	0.6253(2)	0.8346(1)	0.008(1)
P2	2*i*	0.2026(2)	0.9556(2)	0.3189(1)	0.008(1)
B	2*i*	0.0299(6)	0.2743(6)	0.2491(5)	0.007(1)
O1	2*i*	0.4356(4)	0.4918(4)	0.7105(3)	0.012(1)
O2	2*i*	0.2250(4)	0.4639(4)	0.8928(3)	0.010(1)
O3	2*i*	0.5385(4)	0.8203(5)	0.9736(3)	0.015(1)
O4	2*i*	0.2021(4)	0.7394(4)	0.7635(3)	0.011(1)
O5	2*i*	0.1098(5)	0.8589(5)	0.4248(3)	0.015(1)
O6	2*i*	0.4224(4)	0.1391(4)	0.4082(3)	0.014(1)
O7	2*i*	0.2300(4)	0.7714(4)	0.1796(3)	0.011(1)
O8	2*i*	0.0324(4)	0.0521(4)	0.2463(3)	0.011(1)
O9	2*i*	0.0721(5)	0.2929(5)	0.1048(3)	0.012(1)
O10	2*i*	0.1733(4)	0.4544(4)	0.3946(3)	0.011(1)
H9	2*i*	0.188(9)	0.254(9)	0.092(7)	0.022(1)*
H10	2*i*	0.158(8)	0.606(9)	0.418(7)	0.020(1)*

* refined with isotropic displacement parameter

Appendix 52: *$SrFe[BP_2O_2(OH)_2]$: Anisotropic displacement parameters U_{ij} ($Å^2 \times 10^3$). The anisotropic displacement factor exponent takes the form: $-2\pi [h^2a^{*2}U_{11} + \cdots + 2hka^*b^* U_{12}]$.*

Atom	U_{11}	U_{22}	U_{33}	U_{23}	U_{13}	U_{12}
Sr	13(1)	9(1)	15(1)	4(1)	6(1)	2(1)
Fe1	8(1)	7(1)	8(1)	3(1)	4(1)	1(1)
Fe2	8(1)	7(1)	8(1)	2(1)	3(1)	1(1)
P1	8(1)	7(1)	9(1)	3(1)	4(1)	2(1)
P2	8(2)	7(2)	8(1)	2(1)	3(1)	2(1)
B	7(2)	6(2)	9(1)	3(1)	2(1)	2(1)
O1	17(1)	12(1)	13(1)	7(1)	9(1)	7(1)
O2	12(1)	10(1)	12(1)	5(1)	8(1)	3(1)
O3	13(1)	10(1)	14(1)	2(1)	–2(1)	–1(1)
O4	9(1)	11(1)	16(1)	7(1)	4(1)	3(1)
O5	19(1)	15(1)	13(1)	8(1)	7(1)	5(1)
O6	10(1)	9(1)	16(1)	0(1)	0(1)	1(1)
O7	11(1)	10(1)	9(1)	1(1)	3(1)	2(1)
O8	10(1)	8(1)	14(1)	5(1)	4(1)	3(1)
O9	15(1)	14(1)	13(1)	8(1)	8(1)	8(1)
O10	9(1)	9(1)	11(1)	1(1)	1(1)	2(1)

Appendix 53: *$SrFe[BP_2O_7(OH)_2]$: Selected interatomic distances (Å) and angles (°) in*

Atom contact	Distance	Atom contact	Distance
Sr—O5[a]	2.518(3)	Fe2—O10[d]	2.101(3)
Sr—O1	2.521(3)	Fe2—O10	2.101(3)
Sr—O8[b]	2.609(3)	Fe2—O1	2.124(3)
Sr—O4[a]	2.655(3)	Fe2—O1[d]	2.124(3)
Sr—O6[c]	2.693(3)	Fe2—O6	2.163(3)
Sr—O7[d]	2.694(3)	Fe2—O6[d]	2.163(3)
Sr—O3[e]	2.745(3)		
Sr—O2	2.789(3)	P1—O1	1.506(3)
Sr—O5[f]	3.069(3)	P1—O2	1.534(3)
Sr—O6	3.082(3)	P1—O3	1.545(3)
		P1—O4	1.560(3)
Fe1—O2[g]	1.989(2)		
Fe1—O2[f]	1.989(2)	P2—O5	1.517(3)
Fe1—O7[h]	2.017(3)	P2—O6[i]	1.526(3)
Fe1—O7	2.017(3)	P2—O7	1.540(3)
Fe1—O9	2.038(3)	P2—O8[i]	1.575(3)
Fe1—O9[h]	2.038(3)		
		B—O10	1.430(4)
O9—H9	0.89(6)	B—O9	1.479(5)
O9—H9···O1	3.106(3)	B—O8	1.483(4)
		B—O4[f]	1.506(5)
O10—H10	1.00(5)		
O10—H10···O5	2.764(1)		

Atoms	Angle	Atoms	Angle
O7[g]—Fe1—O2[f]	180.0(2)	O10[d]—Fe—O10	180.0
O2[g]—Fe1—O7[h]	92.60(11)	O10[d]—Fe—O1	89.20(10)
O2[f]—Fe1—O7[h]	87.40(11)	O10—Fe—O1	90.80(10)
O2[g]—Fe1—O7	87.40(11)	O10[d]—Fe—O1[d]	90.80(10)
O2[f]—Fe1—O7	92.60(11)	O10—Fe—O1[d]	89.20(10)
O7[h]—Fe1—O7	180.00(16)	O1—Fe—O1[d]	180.000(1)
O2[g]—Fe1—O9	90.48(11)	O10[d]—Fe—O6	91.07(10)
O7[f]—Fe1—O9	89.52(11)	O10—Fe—O6	88.93(10)
O7[h]—Fe1—O9	88.14(11)	O1—Fe—O6	88.13(11)
O7—Fe1—O9	91.86(11)	O1[d]—Fe—O6	91.87(11)
O2[g]—Fe1—O9[h]	89.52(11)	O10[d]—Fe—O6[d]	88.93(10)
O2[f]—Fe1—O9[h]	90.48(11)	O10—Fe—O6[d]	91.07(10)
O7[h]—Fe1—O9[h]	91.86(11)	O1—Fe—O6[d]	91.87(11)
O7—Fe1—O9[h]	88.14(11)	O1[d]—Fe—O6[d]	88.13(11)
O9—Fe1—O9[h]	180.0	O6—Fe—O6[d]	180.00(17)
O1—P1—O2	107.87(15)	O5—P2—O6[i]	114.59(16)
O1—P1—O3	111.05(16)	O5—P2—O7	113.15(17)
O2—P1—O3	111.48(16)	O6[i]—P2—O7	108.96(17)
O1—P1—O4	110.64(15)	O5—P2—O8[i]	105.38(16)
O2—P1—O4	110.54(15)	O6[i]—P2—O8[i]	110.13(17)
O3—P1—O4	105.29(15)	O7—P2—O8[i]	104.04(16)

O10—B—O9	113.7(3)	O10—B—O4[f]	110.4(3)
O10—B—O8	112.0(3)	O9—B—O4[f]	108.5(3)
O9—B—O8	109.3(3)	O8—B—O4[f]	102.3(3)
O9—H9···O1	169.26(1)	O10—H10···O5	170.30(1)

Symmetry transformation used to generate equivalent atoms: [a] x, y –1, z; [b] –x, –y, –z+1; [c] –x+1, –y, –z+1; [d] –x+1, –y+1, –z+1; [e] –x+1, –y+1, –z+2; [f] –x, –y+1, –z+1; [g] x, y, z –1; [h] –x, –y+1, –z; [i] x, y+1, z.

5.2.7 $CaCo(H_2O)[BP_2O_8(OH)]\cdot H_2O$

Appendix 54: *$CaCo(H_2O)[BP_2O_8(OH)]\cdot H_2O$: Crystallographic data and refinement parameters*

Crystallographic data

Formula weight (g / mol)	350.28
Dimensions of the crystal (mm^3)	0.030 × 0.130 × 0.130
Crystal color and habit	pink, platelet
Temperature of measurement (K)	293
Crystal system	triclinic
Space group	$P\bar{1}$ (No.2)
Unit cell parameters	a = 6.5793(3) Å α = 68.785(7)° b = 7.8320(1) Å β = 82.719(10)° c = 8.8172(1) Å γ = 73.985(9)°
Cell volume ($Å^3$)	406.93
Formula units Z	2
Calculated density, ρ_{calc} (g / cm^3)	2.859

Data collection and refinement parameters

Diffractometer	RIGAKU AFC7 CCD, MoK_α–radiation (λ = 0.7107 Å), Graphite monochromator
Absorption coefficient, μ (MoK_α), mm^{-1}	3.188
Scan type	φ / ω
2θ range (°)	4.96 – 60
Limiting indices	$-6 \le h \le 9$, $-10 \le k \le 10$, $-12 \le l \le 12$
Total data collected	6609
Unique data	2261
R(int)	0.025
Observed data, $I > 2\sigma$	2079
Paramenter refined	161
F(000)	345
Goodness–of–fit (on F^2)	1.160
R1/wR2, $I > 2\sigma$ (I)	0.043 / 0.107
R1/wR2, all data	0.046 / 0.112
Residual electron density (max. / min.) ($eÅ^{-3}$)	0.869 / –1.214

Appendix 55: *$CaCo(H_2O)[BP_2O_8(OH)]\cdot H_2O$: Atomic coordinates and equivalent / isotropic displacement parameters ($Å^2$)*

Atom	Site	*x*	*y*	*z*	U_{eq} / U_{iso}
Ca	2*i*	0.0861(1	0.5499(1)	0.1603(1)	0.016(1)
Co	2*i*	0.3193(1)	0.6760(1)	0.4074(1)	0.013 (1)
P1	2*i*	0.5640(1)	0.7114(1)	0.0661(1)	0.011 (1)
P2	2*i*	0.2080(1)	0.2634(1)	0.5499(1)	0.011(1)
B	2*i*	0.4657(5)	0.0171(5)	–0.2111(4)	0.012(1)
O1	2*i*	0.7626(4)	0.5653(3)	0.0507(3)	0.017(1)
O2	2*i*	0.3959(4)	0.6310(3)	0.1819(3)	0.014(1)
O3	2*i*	0.3658(3)	0.1462(3)	–0.1207(3)	0.013(1)
O4	2*i*	0.4662(4)	0.8215(3)	–0.1057(3)	0.015(1)
O5	2*i*	0.1780(4)	0.2631(3)	0.3823(3)	0.016(1)
O6	2*i*	–0.0027(3)	0.3107(3)	0.6385(3)	0.016(1)
O7	2*i*	0.3483(4)	0.3925(3)	0.5453(3)	0.015(1)
O8	2*i*	0.3291(4)	0.0558(3)	–0.3465(3)	0.014(1)
O9	2*i*	0.3237(4)	0.9610(3)	0.2695(3)	0.014(1)
O10	2*i*	0.2460(5)	0.7520(5)	0.6095(4)	0.031(1)
O11	2*i*	0.0336(5)	0.8347(5)	–0.0657(4)	0.039(1)
H9	2*i*	0.269(10)	0.043(9)	0.311(8)	0.022(1)*
H10A	2*i*	0.293(9)	0.830(7)	0.620(8)	0.047(1)*
H10B	2*i*	0.126(5)	0.784(9)	0.629(8)	0.047(1)*
H11A	2*i*	0.139(7)	0.869(9)	–0.109(7)	0.059(1)*
H11A	2*i*	–0.076(6)	0.905(8)	–0.095(8)	0.059(1)*

* refined with isotropic displacement parameter. The U_{iso} value of H10A, H10B, H11A and H11B were kept at 1.5 U_{eq} of the O10 and O11 atom to which they are attached.

Appendix 56: *$CaCo(H_2O)[BP_2O_8(OH)]\cdot H_2O$: Anisotropic displacement parameters U_{ij} ($Å^2 \times 10^3$). The anisotropic displacement factor exponent takes the form: $-2\pi [h^2a^{*2}U_{11} + \cdots + 2hka^*b^* U_{12}]$.*

Atom	U_{11}	U_{22}	U_{33}	U_{23}	U_{13}	U_{12}
Ca	12(1)	12(1)	13(1)	–1(1)	–1(1)	–4(1)
Co	16(1)	19(1)	13(1)	–4(1)	–1(1)	–5(1)
P1	10(1)	10(1)	11(1)	–1(1)	–1(1)	–3(1)
P2	10(1)	10(1)	11(1)	–1(1)	–1(1)	–3(1)
B	12(1)	13(1)	12(1)	–2(1)	–1(1)	–4(1)
O1	14(1)	14(1)	24(1)	–6(1)	–1(1)	–3(1)
O2	15(1)	16(1)	12(1)	–3(1)	2(1)	–8(1)
O3	14(1)	13(1)	14(1)	–5(1)	–1(1)	–5(1)
O4	20(1)	13(1)	10(1)	1(1)	–2(1)	–8(1)
O5	19(1)	17(1)	13(1)	–5(1)	–4(1)	–2(1)
O6	11(1)	19(1)	15(1)	–4(1)	0(1)	–3(1)
O7	14(1)	11(1)	18(1)	–1(1)	–1(1)	–6(1)
O8	16(1)	10(1)	14(1)	–1(1)	–6(1)	–3(1)
O9	13(1)	11(1)	16(1)	–2(1)	0(1)	–3(1)
O10	38(2)	35(2)	33(2)	–21(1)	18(1)	–23(1)
O11	16(1)	42(1)	39(1)	11(1)	–3(1)	–7(1)

Appendix 57: *$CaCo(H_2O)[BP_2O_8(OH)]\cdot H_2O$: Selected interatomic distances (Å) and angles (°)*

Atom contact	Distance	Atom contact	Distance
Ca—O6[a]	2.338(2)	P1—O1	1.509(2)
Ca—O2	2.344(2)	P1—O2	1.515(2)
Ca—O1[c]	2.349(3)	P1—O3[e]	1.555(2)
Ca—O11	2.366(3)	P1—O4	1.564(2)
Ca—O5	2.368(2)		
Ca—O1[d]	2.403(2)	P2—O5	1.516(2)
		P2—O6	1.523(2)
Co—O10	2.038(3)	P2—O7	1.534(2)
Co—O7	2.078(2)	P2—O8[f]	1.584(2)
Co—O2	2.119(2)		
Co—O9	2.127(2)	B—O9[f]	1.449(4)
Co—O6[a]	2.140(2)	B—O3	1.475(4)
Co—O7[b]	2.160(2)	B—O4	1.476(4)
		B—O8	1.478(4)
O9—H9	0.83(6)		
O9—H9···O5	2.778(1)	O11—H11A	0.81(3)
		O11—H11A···O4	2.801(1)
O10—H10A	0.79(3)	O11—H11B	0.78(3)
O10—H10A···O8	2.748(1)	O11—H11B···O5	2.868(1)
O10—H10B	0.78(3)		
O10—H10B···O5	2.815(1)		

Atoms	Angle	Atoms	Angle
O10—Fe—O7	91.63(11)	O1—P1—O2	114.39(14)
O10—Fe—O2	173.19(11)	O1—P1—O3[e]	106.44(13)
O7—Fe—O2	95.13(9)	O2—P1—O3[e]	111.09(13)
O10—Fe—O9	88.52(11)	O1—P1—O4	108.87(14)
O7—Fe—O9	174.08(9)	O2—P1—O4	108.11(13)
O2—Fe—O9	84.68(9)	O3[e]—P1—O4	107.75(12)
O10—Fe—O6[a]	96.26(12)		
O7—Fe—O6[a]	87.39(9)	O5—P2—O6	111.86(13)
O2—Fe—O6[a]	84.79(9)	O5—P2—O7	112.58(14)
O9—Fe—O6[a]	98.47(9)	O6—P2—O7	111.33(13)
O10—Fe—O7[b]	89.87(12)	O5—P2—O8[f]	107.41(13)
O7—Fe—O7[b]	83.31(9)	O6—P2—O8[f]	107.10(13)
O2—Fe—O7[b]	90.20(9)	O7—P2—O8[f]	106.15(12)
O9—Fe—O7[b]	90.77(9)		
O6[a]—Fe—O7[b]	169.01(9)	O9[e]—B—O3	110.5(2)
		O9[e]—B—O4	112.4(3)
O9—H9···O5	169.16(1)	O3—B—O4	109.0(3)
O10—H10A···O8	164.67(1)	O9[e]—B—O8	111.6(3)
O10—H10B···O5	143.53(1)	O3—B—O8	108.8(2)
O11—H11A···O4	146.84(1)	O4—B—O8	104.3(2)
O11—H11B···O5	151.10(1)		

Symmetry transformation used to generate equivalent atoms: [a] –x, –y+1, –z+1; [b] –x+1, –y+1, –z+1; [c] –x+1, –y+1, –z; [d] x–1, y, z; [e] –x+1, –y+2, –z; [f] x, y–1, z+1.

5.2.8 $M1^{II}_{0.5}M2^{II}(H_2O)_2[BP_2O_8]\cdot H_2O$ ($M1^{II}_{0.5}$ = Ca, Sr, Ba; $M2^{II}$ = Fe, Co, Ni)

Appendix 58: *$Ca_{0.5}Fe(H_2O)_2[BP_2O_8]\cdot H_2O$: Crystallographic data and refinement parameters*

Crystallographic data

Formula weight (g / mol)	333.35
Dimensions of the crystal (mm^3)	0.025 × 0.025 × 0.065
Crystal color and habit	colorless, hexagonal bipyramid
Temperature of measurement (K)	293
Crystal system	hexagonal
Space group	$P6_522$ (No.179)
Unit cell parameters	a = 9.5091(4) Å c = 15.734(1) Å
Cell volume ($Å^3$)	1232.12
Formula units Z	6
Calculated density, ρ_{calc} (g / cm^3)	2.674

Data collection and refinement parameters

Diffractometer	RIGAKU AFC7 CCD, MoK_α–radiation (λ = 0.7107 Å), Graphite monochromator
Absorption coefficient, μ (MoK_α), mm^{-1}	2.592
Scan type	φ / ω
2θ range (°)	4.94 – 56.02
Limiting indices	$-10 \le h \le 12$, $-12 \le k \le 10$, $-20 \le l \le 19$
Total data collected	8567
Unique data	1004
R(int)	0.048
Observed data, $I > 2\sigma$	989
Paramenter refined	87
F(000)	990
Goodness–of–fit (on F^2)	1.215
R1/wR2, $I > 2\sigma$ (I)	0.037 / 0.090
R1/wR2, all data	0.038 / 0.090
Residual electron density (max. / min.) ($eÅ^{-3}$)	0.352 / –0.480

Appendix 59: *$Ca_{0.5}Co(H_2O)_2[BP_2O_8]\cdot H_2O$: Crystallographic data and refinement parameters (sub cell solution)*

Crystallographic data

Formula weight (g / mol)	333.77
Dimensions of the crystal (mm^3)	0.20 × 0.20 × 0.04
Crystal color and habit	violet, hexagonal bipyramid
Temperature of measurement (K)	293
Crystal system	hexagonal
Space group	$P6_522$ (No.179)
Unit cell parameters	a = 9.4526(3) Å c = 15.9680(7) Å
Cell volume ($Å^3$)	1214.72
Formula units Z	6
Calculated density, ρ_{calc} (g / cm^3)	2.688

Data collection and refinement parameters

Diffractometer	RIGAKU AFC7 CCD, MoK_α–radiation (λ = 0.7107 Å), Graphite monochromator
Absorption coefficient, μ (MoK_α), mm^{-1}	2.884
Scan type	φ / ω
2θ range (°)	4.98 – 59.98
Limiting indices	$-13 \le h \le 13$, $-13 \le k \le 13$, $-20 \le l \le 21$
Total data collected	9768
Unique data	1180
R(int)	0.028
Observed data, $I > 2\sigma$	1164
Paramenter refined	79
F(000)	960
Goodness–of–fit (on F^2)	1.161
R1/wR2, $I > 2\sigma$ (I)	0.038 / 0.088
R1/wR2, all data	0.039 / 0.089
Residual electron density (max. / min.) ($eÅ^{-3}$)	0.430 / –0.454

Appendix 60: *$Ca_{0.5}Ni(H_2O)_2[BP_2O_8]\cdot H_2O$: Crystallographic data and refinement parameters*

Crystallographic data

Formula weight (g / mol)	333.35
Dimensions of the crystal (mm^3)	0.12 × 0.11 × 0.05
Crystal color and habit	yellow, hexagonal bipyramid
Temperature of measurement (K)	293
Crystal system	hexagonal
Space group	$P6_122$ (No.178)
Unit cell parameters	a = 9.3715(3) Å c = 15.7261(6) Å
Cell volume ($Å^3$)	1196.11
Formula units Z	6
Calculated density, ρ_{calc} (g / cm^3)	2.778

Data collection and refinement parameters

Diffractometer	RIGAKU AFC7 CCD, MoK_α–radiation (λ = 0.7107 Å), Graphite monochromator
Absorption coefficient, μ (MoK_α), mm^{-1}	3.212
Scan type	φ / ω
2θ range (°)	5.02 – 63.28
Limiting indices	$-11 \le h \le 13$, $-13 \le k \le 11$, $-20 \le l \le 19$
Total data collected	9797
Unique data	1248
R(int)	0.043
Observed data, $I > 2\sigma$	1173
Paramenter refined	87
F(000)	1002
Goodness–of–fit (on F^2)	1.221
R1/wR2, $I > 2\sigma$ (I)	0.052 / 0.120
R1/wR2, all data	0.056 / 0.130
Residual electron density (max. / min.) ($eÅ^{-3}$)	0.973 / –0.842

Appendix 61: *$Sr_{0.5}Co(H_2O)_2[BP_2O_8]\cdot H_2O$: Crystallographic data and refinement parameters (sub cell solution)*

Crystallographic data

Formula weight (g / mol)	357.52
Dimensions of the crystal (mm^3)	0.14 × 0.15 × 0.06
Crystal color and habit	violet, hexagonal bipyramid
Temperature of measurement (K)	293
Crystal system	hexagonal
Space group	$P6_122$ (No.178)
Unit cell parameters	a = 9.4434(3) Å c = 15.8287(8) Å
Cell volume ($Å^3$)	1222.45
Formula units Z	6
Calculated density, ρ_{calc} (g / cm^3)	2.865

Data collection and refinement parameters

Diffractometer	RIGAKU AFC7 CCD, MoK_α–radiation (λ = 0.7107 Å), Graphite monochromator
Absorption coefficient, μ (MoK_α), mm^{-1}	5.789
Scan type	φ / ω
2θ range (°)	4.98 – 60
Limiting indices	$-10 \le h \le 13$, $-13 \le k \le 13$, $-19 \le l \le 22$
Total data collected	9914
Unique data	1191
R(int)	0.042
Observed data, $I > 2\sigma$	1133
Paramenter refined	79
F(000)	1014
Goodness–of–fit (on F^2)	1.105
R1/wR2, $I > 2\sigma$ (I)	0.044 / 0.110
R1/wR2, all data	0.047 / 0.110
Residual electron density (max. / min.) ($eÅ^{-3}$)	0.608 / –0.701

Appendix 62: *$Ba_{0.5}Fe(H_2O)_2[BP_2O_8]\cdot H_2O$: Crystallographic data*

Crystallographic data

Formula weight (g / mol)	379.27
Dimensions of the crystal (mm^3)	0.15 × 0.15 × 0.05
Crystal color and habit	colorless, hexagonal bipyramid
Temperature of measurement (K)	293
Space group	—
Crystal system	hexagonal
Unit cell parameters	a = 9.4447(3) Å[a]
	c = 15.7337(9) Å[a]
Cell volume ($Å^3$)	1215.45

[a] only lattice parameters were determined by a single crystal diffractometer

Appendix 63: *$Ba_{0.5}Ni(H_2O)_2[BP_2O_8]\cdot H_2O$: Crystallographic data*

Crystallographic data

Formula weight (g / mol)	382.12
Dimensions of the crystal (mm^3)	0.12 × 0.11 × 0.06
Crystal color and habit	yellow, hexagonal bipyramid
Temperature of measurement (K)	293
Crystal system	hexagonal
Space group	—
Unit cell parameters	a = 16.11 Å[a]
	c = 15.81 Å[a]
Cell volume ($Å^3$)	3553.47

[a] only lattice parameters were determined by a single crystal diffractometer

Appendix 64: *$Ba_{0.5}Co(H_2O)_2[BP_2O_8]\cdot H_2O$: Crystallographic data and refinement parameters (sub cell solution)*

Crystallographic data

Formula weight (g / mol)	382.36
Dimensions of the crystal (mm^3)	0.25 × 0.25 × 0.06
Crystal color and habit	violet, hexagonal bipyramid
Temperature of measurement (K)	293
Crystal system	hexagonal
Space group	$P6_522$ (No.179)
Unit cell parameters	a = 9.4333(3) Å c = 15.7984(8) Å
Cell volume ($Å^3$)	1217.51
Formula units Z	6
Calculated density, ρ_{calc} (g / cm^3)	3.080

Data collection and refinement parameters

Diffractometer	RIGAKU AFC7 CCD, MoK_α–radiation (λ = 0.7107 Å), Graphite monochromator
Absorption coefficient, μ (MoK_α), mm^{-1}	4.938
Scan type	φ / ω
2θ range (°)	4.98 – 59.96
Limiting indices	$-13 \le h \le 13$, $-12 \le k \le 11$, $-19 \le l \le 22$
Total data collected	9282
Unique data	1179
R(int)	0.032
Observed data, $I > 2\sigma$	1166
Paramenter refined	79
F(000)	1068
Goodness–of–fit (on F^2)	1.120
R1/wR2, $I > 2\sigma$ (I)	0.060 / 0.14
R1/wR2, all data	0.061 / 0.14
Residual electron density (max. / min.) ($eÅ^{-3}$)	1.637 / –1.252

Appendix 65: *$Ca_{0.5}Fe(H_2O)_2[BP_2O_8]\cdot H_2O$: Atomic coordinates and equivalent / isotropic displacement parameters ($Å^2$)*

Atom	Site	*x*	*y*	*z*	U_{eq} / U_{iso}
Ca [a]	12*c*	0.3560(4)	0.2506(4)	0.9231(2)	0.021(1)*
Fe	6*b*	0.5507(1)	0.1015(1)	3/4	0.020(1)
P	12*c*	0.3866(1)	0.1674(1)	0.5861(1)	0.014(1)
B	6*b*	0.8481(3)	0.6963(7)	3/4	0.013(1)
O1	12*c*	0.4167(3)	0.1820(3)	0.4878(1)	0.017(1)
O2	12*c*	0.2145(3)	0.0198(3)	0.6005(2)	0.016(1)
O3	12*c*	0.5149(4)	0.1380(4)	0.6232(2)	0.023(1)
O4	12*c*	0.3822(4)	0.3131(3)	0.6206(2)	0.019(1)
O5	12*c*	0.4860(4)	0.2947(4)	0.7855(2)	0.027(1)
O6	12*c*	0.1503(17)	0.1459(17)	0.8490(6)	0.036(1)
H5A	12*c*	0.562(8)	0.385(6)	0.789(5)	0.10(3)*
H5B	12*c*	0.447(9)	0.327(8)	0.749(4)	0.08(3)*

[a] The occupation of the Ca site was refined freely and in the final refinement cycles it was fixed to 0.25.

* refined with isotropic displacement parameters.

Appendix 66: *$Ca_{0.5}Fe(H_2O)_2[BP_2O_8]\cdot H_2O$: Anisotropic displacement parameters U_{ij} ($Å^2$ × 10^3). The anisotropic displacement factor exponent takes the form: $-2\pi\,[h^2a^{*2}U_{11} + \cdots + 2hka^*b^*\,U_{12}]$.*

Atom	U_{11}	U_{22}	U_{33}	U_{23}	U_{13}	U_{12}
Fe	20(1)	17(1)	20(1)	0	–8(1)	9(1)
P	15(1)	13(1)	12(1)	0(1)	–1(1)	5(1)
B	16(2)	17(2)	6(2)	0	0(2)	9(1)
O1	16(1)	21(1)	13(1)	2(1)	–2(1)	8(1)
O2	18(1)	12(1)	15(1)	–1(1)	4(1)	7(1)
O3	22(1)	29(2)	20(1)	3(1)	–3(1)	14(1)
O4	26(1)	11(1)	19(1)	–1(1)	–1(1)	8(1)
O5	26(2)	21(2)	29(2)	2(1)	–7(1)	8(1)
O6	38(5)	36(4)	34(8)	9(5)	2(5)	19(3)

Appendix 67: *$Ca_{0.5}Co(H_2O)_2[BP_2O_8]\cdot H_2O$: Atomic coordinates and equivalent displacement parameters ($Å^2$)*

Atom	Site	*x*	*y*	*z*	U_{eq}
Ca [a]	12*c*	0.2488(4)	0.8936(4)	0.0890(2)	0.018(1)
Co	6*b*	0.4491(1)	0.8982(1)	1/4	0.014(1)
P	12*c*	0.6121(1)	0.8310(1)	0.0865(1)	0.010(1)
B	6*b*	0.8472(3)	0.1528(3)	0.0833(1)	0.010(1)
O1	12*c*	0.7854(3)	0.9799(3)	0.1010(2)	0.014(1)
O2	12*c*	0.1921(3)	0.7071(3)	0.2155(2)	0.021(1)
O3	12*c*	0.6174(3)	0.6845(3)	0.1204(2)	0.016(1)
O4	12*c*	0.5808(3)	0.8170(3)	–0.0120(1)	0.014(1)
O5	12*c*	0.4822(3)	0.8598(3)	0.1246(2)	0.018(1)
O6	6*a*	0.1461(6)	0	0	0.060(1)

[a] Ca occupancy is 0.25.

Appendix 68: *$Ca_{0.5}Co(H_2O)_2[BP_2O_8]\cdot H_2O$: Anisotropic displacement parameters U_{ij} ($Å^2 \times 10^3$). The anisotropic displacement factor exponent takes the form: $-2\pi [h^2a^{*2}U_{11} + \cdots + 2hka^*b^* U_{12}]$.*

Atom	U_{11}	U_{22}	U_{33}	U_{23}	U_{13}	U_{12}
Ca	19(1)	28(1)	11(1)	0(1)	–1(1)	14(1)
Co	15(1)	14(1)	14(1)	0	3(1)	7(1)
P	11(1)	10(1)	9(1)	–1(1)	1(1)	4(1)
B	11(2)	11(2)	8(2)	1(2)	1(2)	5(2)
O1	14(1)	9(1)	15(1)	0(1)	–3(1)	4(1)
O2	25(1)	17(1)	22(1)	0(1)	6(1)	11(1)
O3	24(2)	10(2)	13(2)	2(1)	1(1)	7(1)
O4	13(2)	17(1)	10(2)	–1(1)	2(1)	7(1)
O5	16(1)	24(1)	16(1)	–2(1)	4(1)	11(1)
O6	32(2)	30(3)	117(6)	–6(3)	–3(2)	15(1)

Appendix 69: *$Ca_{0.5}Ni(H_2O)_2[BP_2O_8]\cdot H_2O$: Atomic coordinates and equivalent / isotropic displacement parameters ($Å^2$)*

Atom	Site	*x*	*y*	*z*	U_{eq} / U_{iso}
Ca [a]	12*c*	0.6396(5)	0.7526(5)	0.0768(3)	0.029(1)
Ni	6*b*	0.4458(1)	0.8916(1)	1/4	0.022(1)
P	12*c*	0.6112(1)	0.8286(1)	0.4139(1)	0.018(1)
B	6*b*	0.6972(8)	0.8486(4)	0.5833(1)	0.017(1)
O1	12*c*	0.5819(4)	0.8164(4)	0.5120(2)	0.020(1)
O2	12*c*	0.7866(4)	0.9780(4)	0.3994(2)	0.022(1)
O3	12*c*	0.4821(4)	0.8607(4)	0.3763(2)	0.025(1)
O4	12*c*	0.6153(4)	0.6802(4)	0.3800(2)	0.024(1)
O5	12*c*	0.5109(5)	0.7085(4)	0.2176(2)	0.028(1)
O6	12*c*	0.8471(15)	0.8551(19)	0.1523(10)	0.039(1)
H5A	12*c*	0.549(6)	0.677(6)	0.259(3)	0.013(1) *
H5B	12*c*	0.436(5)	0.622(5)	0.205(3)	0.015*

[a] Ca site was refined freely and in the final refinement cycles it was fixed to 0.25. * refined with isotropic displacement parameters, hydrogen positions were refined as free variables, whereas the isotropic displacement parameters were restrained to 1.2 U_{iso}(O5).

Appendix 70: *$Ca_{0.5}Ni(H_2O)_2[BP_2O_8]\cdot H_2O$: Anisotropic displacement parameters U_{ij} ($Å^2$ × 10^3). The anisotropic displacement factor exponent takes the form: $-2\pi\,[h^2a^{*2}U_{11} + \cdots + 2hka^*b^*\,U_{12}]$.*

Atom	U_{11}	U_{22}	U_{33}	U_{23}	U_{13}	U_{12}
Ni	22(1)	20(1)	23(1)	0	–3(1)	10(1)
P	18(1)	17(1)	18(1)	–1(1)	–2(1)	8(1)
B	19(1)	14(1)	20(1)	–1(1)	0(1)	10(1)
O1	19(1)	25(1)	16(1)	0(1)	–2(1)	10(1)
O2	24(1)	15(1)	24(2)	–1(1)	2(1)	8(1)
O3	25(2)	28(2)	24(2)	–2(1)	–4(1)	14(1)
O4	31(2)	18(1)	23(2)	0(1)	–1(1)	11(1)
O5	29(1)	22(1)	28(1)	0(1)	–6(1)	10(1)
O6	32(1)	47(1)	43(1)	14(1)	1(1)	23(1)

Appendix 71: *$Sr_{0.5}Co(H_2O)_2[BP_2O_8]\cdot H_2O$: Atomic coordinates and equivalent displacement parameters ($Å^2$)*

Atom	Site	*x*	*y*	*z*	U_{eq}
Sr [a]	12*c*	0.2216(2)	0.8589(2)	0.0867(2)	0.033(1)
Co	6*b*	0.4475(1)	0.8949(1)	1/4	0.020(1)
P	12*c*	0.6112(1)	0.8299(1)	0.0854(1)	0.016(1)
B	6*b*	0.8464(3)	0.1536(3)	0.0833(1)	0.015(1)
O1	12*c*	0.7844(4)	0.9802(3)	0.0997(2)	0.020(1)
O2	12*c*	0.1943(4)	0.7067(4)	0.2197(2)	0.033(1)
O3	12*c*	0.6180(4)	0.6840(3)	0.1188(2)	0.022(1)
O4	12*c*	0.5805(3)	0.8161(3)	–0.0123(2)	0.017(1)
O5	12*c*	0.4815(4)	0.8579(4)	0.1236(2)	0.024(1)
O6	6*a*	0.1314(9)	0	0	0.073(2)

[a] Sr occupancy is 0.25.

Appendix 72: *$Sr_{0.5}Co(H_2O)_2[BP_2O_8]\cdot H_2O$: Anisotropic displacement parameters U_{ij} ($Å^2 \times 10^3$). The anisotropic displacement factor exponent takes the form: $-2\pi\,[h^2a^{*2}U_{11} + \cdots + 2hka^*b^*\,U_{12}]$.*

Atom	U_{11}	U_{22}	U_{33}	U_{23}	U_{13}	U_{12}
Sr	40(1)	48(1)	26(1)	1(1)	1(1)	32(1)
Co	19(1)	17(1)	22(1)	0	5(1)	8(1)
P	16(1)	15(1)	14(1)	–1(1)	1(1)	6(1)
B	14(2)	14(2)	15(3)	–2(2)	–2(2)	5(2)
O1	19(1)	14(1)	22(1)	1(1)	–1(1)	5(1)
O2	30(2)	21(2)	41(2)	–6(1)	10(1)	7(1)
O3	29(2)	13(1)	22(1)	1(1)	0(1)	8(1)
O4	19(2)	19(1)	12(2)	–3(1)	1(1)	9(1)
O5	22(1)	24(1)	22(1)	–4(1)	6(1)	10(1)
O6	65(4)	51(4)	98(6)	–5(3)	–3(2)	25(1)

Appendix 73: *$Ba_{0.5}Co(H_2O)_2[BP_2O_8]\cdot H_2O$: Atomic coordinates and equivalent displacement parameters ($Å^2$)*

Atom	Site	*x*	*y*	*z*	U_{eq}
Ba [a]	12*c*	0.1842(14)	0.8400(14)	0.0809(9)	0.033(1)
Co	6*b*	0.4468(1)	0.8937(1)	1/4	0.051(2)
P	12*c*	0.6112(2)	0.8296(2)	0.0855(1)	0.013(1)
B	6*b*	0.8472(5)	0.1528(5)	0.0833(1)	0.014(1)
O1	12*c*	0.7846(5)	0.9792(5)	0.1008(3)	0.016(1)
O2	12*c*	0.1920(9)	0.7088(8)	0.2189(5)	0.056 (1)
O3	12*c*	0.6179(7)	0.6831(5)	0.1180(3)	0.022(1)
O4	12*c*	0.5806(5)	0.8175(5)	–0.0126(3)	0.016(1)
O5	12*c*	0.4816(6)	0.8575(7)	0.1239(3)	0.023(1)
O6	6*a*	0.170(20)	0	0	0.078(12)

[a] Ba occupancy is 0.25.

Appendix 74: *$Ba_{0.5}Co(H_2O)_2[BP_2O_8]\cdot H_2O$: Anisotropic displacement parameters U_{ij} ($Å^2 \times 10^3$). The anisotropic displacement factor exponent takes the form: $-2\pi [h^2a^{*2}U_{11} + \cdots + 2hka^*b^* U_{12}]$.*

Atom	U_{11}	U_{22}	U_{33}	U_{23}	U_{13}	U_{12}
Ba	77(6)	37(2)	36(2)	–9(1)	–23(3)	26(3)
Co	19(1)	14(1)	20(1)	0	7(1)	7(1)
P	13(1)	13(1)	11(1)	–1(1)	1(1)	5(1)
B	12(3)	12(3)	13(4)	0(3)	0(3)	2(3)
O1	17(2)	11(2)	19(2)	1(2)	–1(2)	6(2)
O2	44(4)	35(3)	65(5)	–27(3)	30(3)	1(3)
O3	35(3)	12(2)	16(2)	2(2)	1(2)	11(2)
O4	16(2)	17(2)	13(2)	–3(1)	2(1)	7(2)
O5	14(2)	36(3)	18(2)	–8(2)	2(2)	11(2)
O6	17(2)	59(9)	17(3)	–98(15)	–49(8)	29(5)

Appendix 75: *$Ca_{0.5}Fe(H_2O)_2[BP_2O_8]\cdot H_2O$: Selected interatomic distances (Å) and angles (°)*

Atom contact	Distance	Atom contact	Distance
Ca—O6[e]	2.38(2)	Fe—O3	2.082(2)
Ca—O6[h]	2.397(11)	Fe—O3[a]	2.082(2)
Ca—O4[h]	2.447(4)	Fe—O4[b]	2.102(3)
Ca—O3[k]	2.457(4)	Fe—O4[c]	2.102(3)
Ca—O5[e]	2.529(4)	Fe—O5[a]	2.280(4)
Ca—O5[h]	2.663(5)	Fe—O5	2.280(4)
Ca—O6[b]	2.674(19)		
		B—O2[j]	1.456(4)
P—O1	1.567(2)	B—O2[g]	1.456(4)
P—O2	1.550(3)	B—O1[f]	1.477(4)
P—O3	1.508(3)	B—O1[k]	1.477(4)
P—O4	1.500(3)		
O5—H5A	0.80(5)	O5—H5B	0.82(4)
O5—H5A···O1	2.758(1)	O5—H5B···O4	2.813(1)

Atoms	Angle	Atoms	Angle
O3—Fe—O3[a]	163.39(17)	O4—P—O3	115.51(16)
O3—Fe—O4[b]	101.16(11)	O3—P—O2	111.31(16)
O3[a]—Fe—O4[b]	89.97(10)	O4—P—O2	106.12(15)
O3—Fe—O4[c]	89.97(10))	O3—P—O1	105.73(15)
O3[a]—Fe—O4[c]	101.16(11)	O4—P—O1	111.21(15)
O4[b]—Fe—O4[c]	96.10(16)	O2—P—O1	106.69(14)
O3—Fe—O5[a]	80.25(11)		
O3[a]—Fe—O5[a]	88.16(12)	O2[j]—B—O2[g]	103.9(4)
O4[b]—Fe—O5[a]	177.25(11)	O2[j]—B—O1[f]	113.51(14)
O4[c]—Fe—O5[a]	86.24(12)	O2[g]—B—O1[f]	112.21(14)
O3—Fe—O5	88.16(11)	O2[j]—B—O1[k]	112.21(14)
O3[a]—Fe—O5	80.25(11)	O2[g]—B—O1[k]	113.51(14)
O4[b]—Fe—O5	86.24(12)	O1[a]—B—O1[k]	101.9(4)
O4[c]—Fe—O5	177.25(11)		
O5[a]—Fe—O5	91.47(17)	O5—H5A···O1	166.09(1)
		O5—H5B···O4	145.14(1)

Symmetry transformation used to generate equivalent atoms: [a] –x+y+1, y, –z+3/2; [b] y, –x+y, z+1/6; [c] –x+1, –x+y, –z+4/3; [d] –y+1, x–y, z-1/3; [e] x, x–y, –z+1/6; [f] –y+1, –x+1, –z+7/6; [g] –x+1, –x+y+1, –z+4/3; [h] y, x, –z+5/3; [i] x–y, x, z–1/6; [j] y+1, –x+y+1, z+1/6; [k] –x+y+1, –x+1, z+1/3.

Appendix 76: *$Ca_{0.5}Co(H_2O)_2[BP_2O_8]\cdot H_2O$: Selected interatomic distances (Å) and angles (°)*

Atom contact	Distance	Atom contact	Distance
Ca—O6	2.210(5)	Co—O5[a]	2.054(2)
Ca—O2[d]	2.419(4)	Co—O5	2.054(2)
Ca—O5	2.447(4)	Co—O3[b]	2.070(2)
Ca—O3	2.449(4)	Co—O3[c]	2.070(2)
Ca—O6[b]	2.505(3)	Co—O2	2.252(3)
Ca—O2	2.528(4)	Co—O2[a]	2.252(3)
Ca—O5[e]	2.654(4)		
		B—O1[f]	1.461(4)
P—O5	1.508(2)	B—O1[g]	1.461(4)
P—O3	1.508(2	B—O2[h]	1.477(4)
P—O1	1.553(3)	B—O2[i]	1.477(4)
P—O4	1.567(2)		

Atoms	Angle	Atoms	Angle
O5[a]—Co—O5	162.40(15)	O5—P—O3	115.48(15)
O5[a]—Co—O3[b]	101.88(10)	O5—P—O1	111.30(15)
O5—Co—O3[b]	89.91(10)	O3—P—O1	106.01(14)
O5[a]—Co—O3[c]	89.91(10)	O5—P—O4	105.66(14)
O5—Co—O3[c]	101.88(10)	O3—P—O4	111.27(14)
O3[b]—Co—O3[c]	96.21(16)	O1—P—O4	106.89(13)
O5[a]—Co—O2	87.78(10))		
O5—Co—O2	80.00(10)	O1[f]—B—O1[g]	103.0(3)
O3[b]—Co—O2	85.92(11)	O1[f]—B—O4[h]	112.16(13)
O3[c]—Co—O2	177.14(10)	O1[l]—B—O4[h]	113.99(13)
O5[a]—Co—O2[a]	80.00(10)	O1[f]—B—O4[i]	113.99(13)
O5—Co—O2[a]	87.78(10)	O1[g]—B—O4[i]	112.16(13)
O3[b]— Co—O2[a]	177.14(10)	O4[h]—B—O4[i]	102.0(3)
O3[c]—Co—O2[a]	85.92(10)		
O2—Co—O2[a]	92.02(15)		

Symmetry transformation used to generate equivalent atoms: [a] -x+y, y, –z+1/2; [b] –x+1, –x+y+1, –z+1/3; [c] y, –x+y+1, z+1/6; [d] –y+1, –x+1, –z+1/6; [e] x–y+1, x+1, z–1/6; [f] –y+2, –x+1, –z+1/6; [g] x, y–1, z; [h] x–y+1, –y+1, –z; [i] y, –x+y, z+1/6.

Appendix 77: *$Ca_{0.5}Ni(H_2O)_2[BP_2O_8]\cdot H_2O$: Selected interatomic distances (Å) and angles (°)*

Atom contact	Distance	Atom contact	Distance
Ca—O6[e]	2.328(17)	Ni—O4[a]	2.056(3)
Ca—O3[k]	2.392(5)	Ni—O4[b]	2.056(3)
Ca—O6[h]	2.400(11)	Ni—O3	2.060(3)
Ca—O4[h]	2.463(5)	Ni—O3[c]	2.060(3)
Ca—O5[e]	2.505(5)	Ni—O5[c]	2.150(4)
Ca—O6[b]	2.652(16)	Ni—O5	2.150(4)
Ca—O5[h]	2.718(5)		
		B—O2[i]	1.452(5)
P—O1	1.561(3)	B—O2[f]	1.452(5)
P—O2	1.553(3)	B—O1[j]	1.481(5)
P—O3	1.507(3)	B—O1	1.481(5)
P—O4	1.507(3)		
O5—H5A	0.87(4)	O5—H5B	0.79(4)
O5—H5A···O4	2.795(1)	O5—H5B···O1	2.727(1)

Atoms	Angle	Atoms	Angle
O4[a]—Ni—O4[b]	93.7(2)	O4—P—O3	116.05(19)
O4[a]—Ni—O3	88.39(13)	O3—P—O2	110.87(19)
O4[b]—Ni—O3	101.25(13)	O4—P—O2	106.05(19)
O4[a]—Ni—O3[c]	101.25(13)	O3—P—O1	105.81(17)
O4[b]—Ni—O3[c]	88.39(13)	O4—P—O1	111.49(17)
O3—Ni—O3[c]	165.98(19)	O2—P—O1	106.21(17)
O4[a]—Ni—O5[c]	86.94(14)		
O4[b]—Ni—O5[c]	177.43(13)	O2[i]—B—O2[f]	103.0(5)
O3—Ni—O5[c]	81.25(13)	O2[i]—B—O1	111.99(17)
O3[c]—Ni—O5[c]	89.04(13)	O2[f]—B—O1[f]	114.39(17)
O4[a]—Ni—O5	177.43(13)	O2[i]—B—O1[j]	114.39(17)
O4[b]—Ni—O5	86.94(14)	O2[f]—B—O1[j]	111.99(17)
O3—Ni—O5	89.04(13)	O1—B—O1[j]	101.6(4)
O3[c]—Ni—O5	81.25(13)		
O5[c]—Ni—O5	92.5(2)	O5—H5A···O4	153.19(1)
		O5—H5B···O1	173.47(1)

Symmetry transformation used to generate equivalent atoms: [a] –x+1, –x+y+1, –z+2/3; [b] y, –x+y+1, z–1/6; [c] –x+y, y, –z+1/2; [d] –y+1, x–y+1, z+1/3; [e] x, x–y+1, –z+1/6; [f] x–y+1, –y+2, –z+1; [g] –x+1, –x+y, –z+2/3; [h] y, x, –z+1/3; [i] x–y+1, x, z+1/6; [j] x, x–y+1, –z+7/6; [k] –x+y, –x+1, z–1/3.

Appendix 78: *$Sr_{0.5}Co(H_2O)_2[BP_2O_8]\cdot H_2O$: Selected interatomic distances (Å) and angles (°)*

Atom contact	Distance	Atom contact	Distance
Sr—O6	2.349(6)	Co—O3[a]	2.075(3)
Sr—O2[d]	2.438(5)	Co—O3[b]	2.075(3)
Sr—O6[d]	2.486(5)	Co—O5	2.083(3)
Sr—O2	2.489(4)	Co—O5[c]	2.083(3)
Sr—O5	2.528(4)	Co—O2	2.203(4)
Sr—O3[b]	2.693(4)	Co—O2[c]	2.203(4)
Sr—O2[f]	2.945(4)		
Sr—O5[d]	2.993(4)	B—O1[j]	1.461(4)
Sr—O3[g]	3.303(4)	B—O1[k]	1.461(4)
		B—O4[p]	1.472(4)
P—O5	1.504(3)	B—O4[h]	1.477(4)
P—O3	1.507(3)		
P—O1	1.556(3)		
P—O4	1.566(3)		

Atoms	Angle	Atoms	Angle
O3[a]—Co—O3[b]	95.21(18)	O5—P—O3	115.47(17)
O3[a]—Co—O5	101.20(11)	O5—P—O1	110.96(17)
O3[b]—Co—O5	90.09(12)	O3—P—O1	106.06(17)
O3[a]—Co—O5[c]	90.09(12)	O5—P—O4	106.23(16)
O3[b]—Co—O5[c]	101.20(11)	O3—P—O4	111.20(15)
O5—Co—O5[c]	163.30(17)	O1—P—O4	106.63(16)
O2[a]—Co—O2	176.64(13)		
O3[b]—Co—O2	86.78(14)	O1[j]—B—O1[l]	103.0(3)
O5—Co—O2	81.47(12)	O1[j]—B—O4[l]	112.16(13)
O5[c]—Co—O2	86.87(12)	O1[k]—B—O4[l]	113.99(13)
O3[a]—Co—O2[c]	86.78(14)	O1[j]—B—O4[h]	113.99(13)
O3[b]—Co—O2[c]	176.64(13)	O1[j]—B—O4[h]	112.16(13)
O5—Co—O2[c]	86.87(12)	O4[l]—B—O4[h]	102.0(3)
O5[c]—Co—O2[c]	81.47(12)		
O2—Co—O2[c]	91.4(2)		

Symmetry transformation used to generate equivalent atoms: [a] y, –x+y+1, z+1/6; [b] –x+1, –x+y+1, –z+1/3; [c] –x+y, y, –z+1/2; [d] –y+1, –x+1, –z+1/6; [e] –x+y, –x+1, z+1/3; [f] x–y+1, x+1, z–1/6; [g] x–y, x, z–1/6; [h] y, –x+y, z+1/6; [i] x–y, –y+1, –z; [j] –y+2, –x+1, –z+1/6; [k] x, y–1, z; [l] x–y+1, –y+1, –z.

Appendix 79: *$Ba_{0.5}Co(H_2O)_2[BP_2O_8]\cdot H_2O$: Selected interatomic distances (Å) and angles (°)*

Atom contact	Distance	Atom contact	Distance
Ba—O6	2.295(14)	Co—O3[a]	2.069(4)
Ba—O6[d]	2.392(14)	Co—O3[b]	2.069(4)
Ba—O2[d]	2.416(16)	Co—O5	2.074(4)
Ba—O2	2.525(15)	Co—O5[c]	2.074(4)
Ba—O5	2.810(10)	Co—O2	2.207(7)
Ba—O5[d]	2.921(10)	Co—O2[c]	2.207(7)
Ba—O3[b]	2.922(15)		
Ba—O3[f]	3.031(15)	B—O1[i]	1.463(7)
Ba—O2[g]	3.133(15)	B—O1[j]	1.463(7)
		B—O4[k]	1.476(7)
P—O5	1.501(5)	B—O4[h]	1.476(7)
P—O3	1.505(5)		
P—O1	1.555(5)		
P—O4	1.571(4)		

Atoms	Angle	Atoms	Angle
O3[a]—Co—O3[b]	94.7(3)	O5—P—O3	115.8(3)
O3[a]—Co—O5	100.72(19)	O5—P—O1	111.0(3)
O3[b]—Co—O5	90.38(19)	O3—P—O1	105.8(3)
O3[a]—Co—O5[c]	90.38(19)	O5—P—O4	106.0(3)
O3[b]—Co—O5[c]	100.72(18)	O3—P—O4	111.2(2)
O5—Co—O5[c]	163.6(3)	O1—P—O4	106.9(2)
O3[a]—Co—O2	177.5(2)		
O3[b]—Co—O2	85.9(3)	O1[i]—B—O1[j]	103.4(7)
O5—Co—O2	81.7(2)	O1[i]—B—O4[k]	112.4(3
O5[c]—Co—O2	87.1(2)	O1[j]—B—O4[k]	113.6(2)
O3[a]—Co—O2[c]	85.9(3)	O1[i]—B—O4[h]	113.6(2)
O3[b]—Co—O2[c]	177.5(2)	O1[j]—B—O4[h]	112.4(3)
O5—Co—O2[c]	87.1(2)	O4[k]—B—O4[h]	101.9(6)
O5[c]—Co—O2[c]	81.7(2)		
O2—Co—O2[c]	93.7(5)		

Symmetry transformation used to generate equivalent atoms: [a] y, –x+y+1, z+1/6; [b] –x+1, –x+y+1, –z+1/3; [c] –x+y, y, –z+1/2; [d] –y+1, –x+1, –z+1/6; [e] –x+y, –x+1, z+1/3; [f] x–y, x, z–1/6; [g] x–y+1, x+1, z–1/6; [h] y, –x+y, z+1/6; [i] –y+2, –x+1, –z+1/6; [j] x, y–1, z; [k] x–y+1, –y+1, –z.

5.2.9 $M^{II}(H_2O)_2[B_2P_2O_8(OH)_2]\cdot H_2O$ (M^{II} = Fe, Co, Ni)

Appendix 80: *$Fe(H_2O)_2[B_2P_2O_8(OH)_2]\cdot H_2O$: Crystallographic data and refinement parameters*

Crystallographic data

Formula weight (g / mol)	355.47
Dimensions of the crystal (mm^3)	0.040 × 0.040 × 0.080
Crystal color and habit	transparent, block
Temperature of measurement (K)	293
Crystal system	monoclinic
Space group	$P2_1/c$ (No. 14)
Unit cell parameters	a = 7.7449(4) Å b = 14.7900(10) Å β = 90.304(4)° c = 8.2429(6) Å
Cell volume ($Å^3$)	944.19(11)
Formula units Z	2
Calculated density, ρ_{calc} (g / cm^3)	2.5

Data collection and refinement parameters

Diffractometer	RIGAKU AFC7 CCD, MoK_α–radiation (λ = 0.7107 Å), Graphite monochromator
Absorption coefficient, μ (MoK_α), mm^{-1}	1.006
Scan type	φ / ω
2θ range (°)	5.26 – 58.58
Limiting indices	$-10 \le h \le 10$, $-20 \le k \le 13$, $-10 \le l \le 11$
Total data collected	7822
Unique data	2493
R(int)	0.025
Observed data, $I > 2\sigma$	2266
Paramenter refined	188
F(000)	356
Goodness–of–fit (on F^2)	1.128
R1/wR2, $I > 2\sigma$ (I)	0.035 / 0.073
R1/wR2, all data	0.039 / 0.077
Residual electron density (max. / min.) ($eÅ^{-3}$)	0.508 / –0.556

Appendix 81: *$Co(H_2O)_2[B_2P_2O_8(OH)_2]\cdot H_2O$: Crystallographic data and refinement parameters*

Crystallographic data

Formula weight (g / mol)	358.55
Dimensions of the crystal (mm^3)	0.065 × 0.070 × 0.095
Crystal color and habit	violet, block
Temperature of measurement (K)	293
Crystal system	monoclinic
Space group	$P2_1/c$ (No. 14)
Unit cell parameters	a = 7.7408(4) Å b = 14.6975(5) Å β = 90.26(2)° c = 8.2219(4) Å
Cell volume ($Å^3$)	935.40(7)
Formula units Z	2
Calculated density, ρ_{calc} (g / cm^3)	2.546

Data collection and refinement parameters

Diffractometer	RIGAKU AFC7 CCD, MoK_α–radiation (λ = 0.7107 Å), Graphite monochromator
Absorption coefficient, μ (MoK_α), mm^{-1}	1.127
Scan type	φ / ω
2θ range (°)	5.26 – 58.58
Limiting indices	$-11 \le h \le 11$, $-21 \le k \le 22$, $-11 \le l \le 12$
Total data collected	9531
Unique data	3014
R(int)	0.022
Observed data, $I > 2\sigma$	2905
Paramenter refined	188
F(000)	358
Goodness–of–fit (on F^2)	1.137
R1/wR2, $I > 2\sigma$ (I)	0.034 / 0.086
R1/wR2, all data	0.035 / 0.088
Residual electron density (max. / min.) ($eÅ^{-3}$)	0.718 / –0.655

Appendix 82: *$Ni(H_2O)_2[B_2P_2O_8(OH)_2]\cdot H_2O$: Crystallographic data and refinement parameters*

Crystallographic data

Formula weight (g / mol)	358.33
Dimensions of the crystal (mm^3)	0.05 × 0.04 × 0.09
Crystal color and habit	green, block
Temperature of measurement (K)	293
Crystal system	monoclinic
Space group	$P2_1/c$ (No. 14)
Unit cell parameters	a = 7.7389(7) Å b = 14.5735(11) Å β = 90.30(4)° c = 8.2060(4) Å
Cell volume ($Å^3$)	925.48(12)
Formula units Z	2
Calculated density, ρ_{calc} (g / cm^3)	2.572

Data collection and refinement parameters

Diffractometer	RIGAKU AFC7 CCD, MoK_α–radiation (λ = 0.7107 Å), Graphite monochromator
Absorption coefficient, μ (MoK_α), mm^{-1}	1.260
Scan type	φ / ω
2θ range (°)	5.26 – 59
Limiting indices	$-9 \le h \le 10$, $-20 \le k \le 19$, $-11 \le l \le 11$
Total data collected	7406
Unique data	2365
R(int)	0.030
Observed data, $I > 2\sigma$	2114
Paramenter refined	187
F(000)	360
Goodness–of–fit (on F^2)	1.134
R1/wR2, $I > 2\sigma$ (I)	0.039 / 0.092
R1/wR2, all data	0.044 / 0.097
Residual electron density (max. / min.) ($eÅ^{-3}$)	0.704 / –0.790

Appendix 83: *$Fe(H_2O)_2[B_2P_2O_8(OH)_2]\cdot H_2O$: Atomic coordinates and equivalent / isotropic displacement parameters ($Å^2$)*

Atom	Site	*x*	*y*	*z*	U_{eq} / U_{iso}
Fe	4*e*	0.2486(1)	0.5354(1)	0.7990(1)	0.010(1)
P1	4*e*	0.5712(1)	0.2876(1)	0.0607(1)	0.008(1)
P2	4*e*	0.0693(1)	0.1615(1)	0.2697(1)	0.008(1)
B1	4*e*	0.9197(3)	0.2844(1)	0.0570(3)	0.004(1)
B2	4*e*	0.4208(3)	0.3359(1)	0.7772(3)	0.004(1)
O1	4*e*	0.5514(2)	0.3700(1)	0.1681(2)	0.014(1)
O2	4*e*	0.5502(2)	0.1967(1)	0.1513(2)	0.010(1)
O3	4*e*	0.4368(2)	0.2139(1)	0.4227(2)	0.012(1)
O4	4*e*	0.2496(2)	0.7846(1)	0.5212(2)	0.009(1)
O5	4*e*	0.0460(2)	0.0610(1)	0.2938(2)	0.012(1)
O6	4*e*	0.0525(2)	0.1261(1)	0.4288(2)	0.011(1)
O7	4*e*	0.9375(2)	0.1956(1)	0.1424(2)	0.010(1)
O8	4*e*	0.2487(2)	0.1856(1)	0.1999(2)	0.009(1)
O9	4*e*	0.0648(2)	0.8624(1)	0.3359 (2)	0.012(1)
H9	4*e*	–0.0140(5)	0.869(2)	0.292(5)	0.018*
O10	4*e*	0.4370(2)	0.4333(1)	0.7862(2)	0.013(1)
H10	4*e*	0.528(5)	0.449(2)	0.827(5)	0.019*
O11	4*e*	0.2417(3)	0.9518(1)	0.0513(2)	0.026(1)
H11A	4*e*	0.236(6)	0.995(3)	–0.0100(6)	0.039*
H11B	4*e*	0.233(6)	0.907(3)	0.001(6)	0.039*
O12	4*e*	0.2553(2)	–0.0093(1)	0.5606(2)	0.015(1)
H12A	4*e*	0.277(5)	0.037(3)	0.573(5)	0.023*
H12B	4*e*	0.172(5)	–0.026(3)	0.603(5)	0.023*
O13	4*e*	0.2462(3)	0.1091(1)	0.8573(3)	0.022(1)
H13A	4*e*	0.240(5)	0.155(3)	0.923(5)	0.032*
H13B	4*e*	0.320(6)	0.119(3)	0.819(6)	0.032*

* U_{iso} values of the hydrogen atoms were kept at 1.5 U_{eq} of the oxygen atoms to which they are attached.

Appendix 84: *$Co(H_2O)_2[B_2P_2O_8(OH)_2]\cdot H_2O$: Atomic coordinates and equivalent / isotropic displacement parameters ($Å^2$)*

Atom	Site	*x*	*y*	*z*	U_{eq} / U_{iso}
Co	4*e*	0.2486(1)	0.5354(1)	0.7990(1)	0.010(1)
P1	4*e*	0.5712(1)	0.2876(1)	0.0607(1)	0.008(1)
P2	4*e*	0.0693(1)	0.1615(1)	0.2697(1)	0.008(1)
B1	4*e*	0.9197(3)	0.2844(1)	0.0570(3)	0.004(1)
B2	4*e*	0.4208(3)	0.3359(1)	0.7772(3)	0.004(1)
O1	4*e*	0.5514(2)	0.3700(1)	0.1681(2)	0.014(1)
O2	4*e*	0.5502(2)	0.1967(1)	0.1513(2)	0.010(1)
O3	4*e*	0.4368(2)	0.2139(1)	0.4227(2)	0.012(1)
O4	4*e*	0.2496(2)	0.7846(1)	0.5212(2)	0.009(1)
O5	4*e*	0.0460(2)	0.0610(1)	0.2938(2)	0.012(1)
O6	4*e*	0.0525(2)	0.1261(1)	0.4288(2)	0.011(1)
O7	4*e*	0.9375(2)	0.1956(1)	0.1424(2)	0.010(1)
O8	4*e*	0.2487(2)	0.1856(1)	0.1999(2)	0.009(1)
O9	4*e*	0.0648(2)	0.8624(1)	0.3359 (2)	0.012(1)
H9	4*e*	–0.0140(5)	0.869(2)	0.292(5)	0.018*
O10	4*e*	0.4370(2)	0.4333(1)	0.7862(2)	0.013(1)
H10	4*e*	0.528(5)	0.449(2)	0.827(5)	0.019*
O11	4*e*	0.2417(3)	0.9518(1)	0.0513(2)	0.026(1)
H11A	4*e*	0.236(6)	0.995(3)	–0.0100(6)	0.039*
H11B	4*e*	0.233(6)	0.907(3)	0.001(6)	0.039*
O12	4*e*	0.2553(2)	–0.0093(1)	0.5606(2)	0.015(1)
H12A	4*e*	0.277(5)	0.037(3)	0.573(5)	0.023*
H12B	4*e*	0.172(5)	–0.026(3)	0.603(5)	0.023*
O13	4*e*	0.2462(3)	0.1091(1)	0.8573(3)	0.022(1)
H13A	4*e*	0.240(5)	0.155(3)	0.923(5)	0.032*
H13B	4*e*	0.320(6)	0.119(3)	0.819(6)	0.032*

* U_{iso} values of the hydrogen atoms were kept at 1.5 U_{eq} of the oxygen atoms to which they are attached.

Appendix 85: *$Ni(H_2O)_2[B_2P_2O_8(OH)_2]\cdot H_2O$: Atomic coordinates and equivalent / isotropic displacement parameters ($Å^2$)*

Atom	Site	*x*	*y*	*z*	U_{eq} / U_{iso}
Ni	4*e*	0.2480(1)	0.5345(1)	0.8030(1)	0.012(1)
P1	4*e*	0.5703(1)	0.2889(1)	0.0616(1)	0.010(1)
P2	4*e*	0.0682(1)	0.1606(1)	0.2696(1)	0.010(1)
B1	4*e*	0.9185(4)	0.2848(2)	0.0579(4)	0.011(1)
B2	4*e*	0.4193(4)	0.3365(2)	0.7667(4)	0.010(1)
O1	4*e*	0.5531(3)	0.3716(1)	0.1700(3)	0.016(1)
O2	4*e*	0.5488(3)	0.1972(1)	0.1518(2)	0.012(1)
O3	4*e*	0.4349(3)	0.2118(2)	0.4237(3)	0.016(1)
O4	4*e*	0.2511(2)	0.7849(1)	0.5217(2)	0.012(1)
O5	4*e*	0.0459(3)	0.0593(1)	0.2930(3)	0.014(1)
O6	4*e*	0.9360(3)	0.1956(1)	0.1432(2)	0.012(1)
O7	4*e*	0.2469(2)	0.1859(1)	0.2004(2)	0.011(1)
O8	4*e*	0.0515(3)	0.2152(1)	0.4300(2)	0.014(1)
O9	4*e*	0.0684(3)	0.8637(2)	0.3353(3)	0.015(1)
H9	4*e*	–0.0040(6)	0.867(3)	0.293(5)	0.023*
O10	4*e*	0.4355(3)	0.4349(2)	0.7826(3)	0.016(1)
H10	4*e*	0.512(6)	0.447(3)	0.816(6)	0.024*
O11	4*e*	0.2450(4)	0.9509(2)	0.0570(3)	0.026(1)
H11A	4*e*	0.244(7)	0.988(4)	0(70)	0.039*
H11B	4*e*	0.237(6)	0.911(4)	0.015(6)	0.039*
O12	4*e*	0.2564(3)	–0.0078(2)	0.5569(3)	0.017(1)
H12A	4*e*	0.267(5)	0.054(3)	0.558(5)	0.025*
H12B	4*e*	0.173(5)	–0.021(3)	0.607(6)	0.025*
O13	4*e*	0.2443(3)	0.1082(2)	0.8576(3)	0.025(1)
H13A	4*e*	0.236(6)	0.149(4)	0.922(6)	0.038*
H13B	4*e*	0.322(7)	0.114(4)	0.821(7)	0.038*

* U_{iso} values of the hydrogen atoms were kept at 1.5 U_{eq} of the oxygen atoms to which they are attached.

Appendix 86: *$Fe(H_2O)_2[B_2P_2O_8(OH)_2]\cdot H_2O$: Anisotropic displacement parameters U_{ij} ($Å^2 \times 10^3$). The anisotropic displacement factor exponent takes the form: $-2\pi\,[h^2a^{*2}U_{11} + \cdots + 2hka^*b^*\,U_{12}]$.*

Atom	U_{11}	U_{22}	U_{33}	U_{23}	U_{13}	U_{12}
Fe	12(1)	10(1)	15(1)	–1(1)	1(1)	0(1)
P1	9(1)	10(1)	9(1)	1(1)	0(1)	–1(1)
P2	8(1)	10(1)	9(1)	1(1)	0(1)	0(1)
B1	10(1)	9(1)	10(1)	0(1)	1(1)	1(1)
B2	6(1)	10(1)	12(1)	0(1)	1(1)	1(1)
O1	14(1)	12(1)	19(1)	–4(1)	4(1)	–2(1)
O2	10(1)	18(1)	13(1)	–4(1)	–2(1)	2(1)
O3	10(1)	12(1)	13(1)	3(1)	3(1)	0(1)
O4	10(1)	14(1)	10(1)	–2(1)	1(1)	1(1)
O5	14(1)	9(1)	19(1)	2(1)	2(1)	–1(1)
O6	12(1)	12(1)	10(1)	4(1)	–3(1)	0(1)
O7	11(1)	16(1)	12(1)	–4(1)	3(1)	–2(1)
O8	8(1)	13(1)	10(1)	1(1)	0(1)	–1(1)
O9	13(1)	13(1)	18(1)	4(1)	–2(1)	–2(1)
O10	12(1)	11(1)	21(1)	–2(1)	–3(1)	1(1)
O11	58(2)	19(1)	16(1)	–2(1)	0(1)	–1(1)
O12	17(1)	19(1)	16(1)	0(1)	2(1)	–1(1)
O13	27(1)	21(1)	23(1)	–4(1)	4(1)	–5(1)

Appendix 87: *$Co(H_2O)_2[B_2P_2O_8(OH)_2]\cdot H_2O$: Anisotropic displacement parameters U_{ij} ($Å^2 \times 10^3$). The anisotropic displacement factor exponent takes the form: $-2\pi\,[h^2a^{*2}U_{11} + \cdots + 2hka^*b^*\,U_{12}]$.*

Atom	U_{11}	U_{22}	U_{33}	U_{23}	U_{13}	U_{12}
Co	10(1)	9(1)	11(1)	–1(1)	2(1)	0(1)
P1	7(1)	10(1)	7(1)	1(1)	2(1)	0(1)
P2	7(1)	9(1)	7(1)	1(1)	2(1)	1(1)
B1	3(1)	7(1)	2(1)	0(1)	1(1)	0(1)
B2	3(1)	5(1)	5(1)	–1(1)	2(1)	0(1)
O1	13(1)	12(1)	16(1)	–5(1)	5(1)	–1(1)
O2	8(1)	11(1)	10(1)	4(1)	4(1)	1(1)
O3	8(1)	19(1)	9(1)	–4(1)	0(1)	1(1)
O4	7(1)	13(1)	6(1)	–1(1)	2(1)	0(1)
O5	11(1)	9(1)	17(1)	3(1)	3(1)	0(1)
O6	8(1)	17(1)	9(1)	–3(1)	4(1)	–1(1)
O7	8(1)	12(1)	10(1)	4(1)	0(1)	0 (1)
O8	6(1)	13(1)	7(1)	1(1)	2(1)	0(1)
O9	10(1)	12(1)	14(1)	4(1)	–2(1)	–1(1)
O10	10(1)	10(1)	19(1)	–4(1)	0(1)	2(1)
O11	47(1)	18(1)	13(1)	–1(1)	1(1)	–2(1)
O12	15(1)	17(1)	14(1)	–1(1)	4(1)	–1(1)
O13	25(1)	20(1)	20(1)	–3(1)	6(1)	–6(1)

Appendix 88: *$Ni(H_2O)_2[B_2P_2O_8(OH)_2]\cdot H_2O$: Anisotropic displacement parameters U_{ij} ($Å^2 \times 10^3$). The anisotropic displacement factor exponent takes the form: $-2\pi [h^2a^{*2}U_{11} + \cdots + 2hka^*b^* U_{12}]$.*

Atom	U_{11}	U_{22}	U_{33}	U_{23}	U_{13}	U_{12}
Ni	12(1)	12(1)	12(1)	–1(1)	0(1)	0(1)
P1	9(1)	13(1)	9(1)	1(1)	0(1)	0(1)
P2	8(1)	12(1)	9(1)	1(1)	0(1)	1(1)
B1	10(1)	13(1)	9(1)	0(1)	–1(1)	1(1)
B2	7(1)	13(1)	11(1)	1(1)	0(1)	0(1)
O1	14(1)	14(1)	20(1)	–4(1)	5(1)	–2(1)
O2	8(1)	15(1)	13(1)	4(1)	4(1)	–1(1)
O3	11(1)	24(1)	12(1)	–5(1)	–3(1)	2(1)
O4	8(1)	19(1)	9(1)	–2(1)	–1(1)	0(1)
O5	11(1)	12(1)	18(1)	4(1)	0(1)	0(1)
O6	11(1)	13(1)	10(1)	4(1)	–1(1)	0(1)
O7	8(1)	16(1)	9(1)	1(1)	–1(1)	0(1)
O8	12(1)	20(1)	10(1)	–3(1)	2(1)	–2(1)
O9	13(1)	16(1)	16(1)	3(1)	–4(1)	–2(1)
O10	10(1)	10(1)	19(1)	–4(1)	0(1)	2(1)
O11	47(2)	18(1)	14(1)	–1(1)	– 2(1)	0(1)
O12	14(1)	21(1)	15(1)	0(1)	1(1)	0(1)
O13	26(1)	27(1)	23(1)	–5(1)	4(1)	–5(1)

Appendix 89: *$M^{II}(H_2O)_2[B_2P_2O_8(OH)_2]\cdot H_2O$ (M^{II} = Fe, Co, Ni): Selected bond distances (Å)*

	M^{II} = Fe	M^{II} = Co	M^{II} = Ni
M—O1[b]	2.1258(18)	2.0976(17)	2.070(2)
M—O5[c]	2.1385(18)	2.1130(16)	2.078(2)
M—O9[a]	2.1211(19)	2.0931(16)	2.051(2)
M—O10	2.1284(18)	2.0954(16)	2.060(2)
M—O11[a]$_w$	2.0780(2)	2.0460(2)	2.030(3)
M—O12[c]$_w$	2.2220(2)	2.1853(18)	2.120(2)
P1—O1	1.5050(18)	1.5069(17)	1.505(2)
P1—O2[f]	1.5371(17)	1.5364(19)	1.538(2)
P1—O3	1.5373(18)	1.5385(16)	1.537(2)
P1—O4[d]	1.5445(18)	1.5454(16)	1.547(2)
P2—O5	1.5014(18)	1.5017(16)	1.499(2)
P2—O6[g]	1.5385(16)	1.5406(17)	1.539(2)
P2—O7	1.5402(18)	1.5421(18)	1.544(2)
P2—O8	1.5426(18)	1.5460(15)	1.542(2)
B1—O4[d]	1.468(3)	1.457(3)	1.463(4)
B1—O6	1.485(3)	1.488(2)	1.482(3)
B1—O7[e]	1.479(3)	1.476(2)	1.474(4)
B1—O9[d]	1.446(3)	1.450(3)	1.449(4)
B2—O2[c]	1.481(3)	1.477(3)	1.473(4)
B2—O3[c]	1.468(3)	1.466(2)	1.465(4)
B2—O8[c]	1.481(3)	1.475(3)	1.475(3)
B2—O10	1.438(3)	1.445(2)	1.445(4)
O9—H9	0.68(4)	0.72(4)	0.66(4)
O9—H9···O13	2.897(1)	2.908(1)	2.914(1)
O10—H10	0.80(4)	0.81(4)	0.68(4)
O10—H10···O12	2.803(1)	2.819(1)	2.843(1)
O11—H11A	0.79(5)	0.81(5)	0.71(5)
O11—H11A···O13	2.800(1)	2.808(1)	2.816(1)
O11—H11B	0.74(5)	0.78(5)	0.68(6)
O11—H11B···O6	3.026(1)	3.022(1)	3.032(1)
O12—H12A	0.74(4)	0.71(4)	0.90(5)
O12—H12A···O13	3.017(1)	2.997(1)	3.171(1)
O12—H12B	0.79(4)	0.77(4)	0.79(5)
O12—H12B···O5	2.720(1)	2.734(1)	2.754(1)
O13—H13A	0.79(4)	0.87(4)	0.80(5)
O13—H13A···O8	3.046(1)	3.033(1)	3.035(1)
O132—H13B	0.75(4)	0.67(5)	0.68(5)
O13—H13B···O1	2.837(1)	2.864(1)	2.864(1)

Symmetry transformations used to generate equivalent atoms: [a] x, $-y+3/2$, $z+1/2$; [b] $-x+1$, $-y+1$, $-z+1$; [c] x, $-y+1/2$, $z+1/2$; [d] $-x+1$, $y-1/2$, $-z+1/2$; [e] $x+1$, $-y+1/2$, $z-1/2$; [f] x, $-y+1/2$, $z-1/2$; w = water.

Appendix 90: *$M^{II}(H_2O)_2[B_2P_2O_8(OH)_2]\cdot H_2O$ (M^{II} = Fe, Co, Ni): Selected bond angles (°)*

	M^{II} = Fe	M^{II} = Co	M^{II} = Ni
O1^{b}—*M*—O10	88.24(7)	88.17 (7)	87.18(9)
O1^{b}—*M*—O5^{c}	172.62(7)	173.77(7)	176.11(8)
O1^{b}—*M*—O12^{c}	88.96(7)	83.57(7)	89.84(9)
O5^{c}—*M*—O12^{c}	83.67(7)	85.24(7)	86.42(9)
O9^{a}—*M*—O1^{b}	90.56(7)	90.39(7)	90.68(9)
O9^{a}—*M*—O5^{c}	89.06(7)	88.80(6)	88.32(9)
O9^{a}—*M*—O10	173.56(7)	174.49(7)	176.69(9)
O9^{a}—*M*—O12^{c}	90.36(8)	89.78(7)	91.31(9)
O10—*M*—O5^{c}	91.32(7)	92.05(6)	93.65(9)
O10—*M*—O12^{c}	83.30(8)	84.87(7)	86.16(10)
O11^{a}—*M*—O1^{b}	94.22(9)	94.75(9)	92.37(11)
O11^{a}—*M*—O5^{c}	93.16(9)	91.46(9)	91.43(11)
O11^{a}—*M*—O9^{a}	93.34(9)	93.64(8)	92.77(11)
O11^{a}—*M*—O10	93.06(9)	91.78(9)	89.85(11)
O11^{a}—*M*—O12^{c}	175.09(9)	175.20(8)	175.33(10)
O1—P1—O2^{f}	112.10(10)	111.95(10)	112.23(13)
O1—P1—O3	113.68(10)	113.77(10)	113.69(12)
O1—P1—O4^{d}	111.83(10)	111.83(9)	111.90(12)
O2^{f}—P1—O3	105. 84(10)	105. 84(9)	105. 90(12)
O2^{f}—P1—O4^{d}	106.39(10)	106.45(8)	106.22(11)
O3—P1—O4^{d}	106.48(10)	106.48(9)	106.35(11)
O5—P2—O6^{g}	109.36(10)	109.26(10)	109.64(12)
O5—P2—O7	112.80(10)	112.93(10)	112.72(12)
O5—P2—O8	112.46(10)	112.55(9)	112.88(12)
O6^{g}—P2—O7	110.84(10)	110.41(9)	110.21(9)
O6^{g}—P2—O8	105.44(9)	105.44(9)	105.46(11)
O7—P2—O8	105.85(9)	105.97(9)	105.62(12)
O4^{d}—B1—O6	106.92 (19)	106.93(15)	107.0 (2)
O4^{d}—B1—O7^{e}	107.93(18)	108.24(17)	108.1(2)
O7^{e}—B1—O6	106.02(19)	105.64(15)	105.9(2)
O9^{d}—B1—O4^{d}	109.27(19)	109.77(16)	109.2(2)
O9^{d}—B1—O6	113.74(19)	113.54(17)	113.8(2)
O9^{d}—B1—O7^{e}	112.6(2)	112.41(16)	112.6(2)
O2^{c}—B2—O8^{c}	106.52(18)	107.75(16)	108.0(2)
O3^{c}—B2—O2^{c}	109.93(19)	110.23(16)	110.4(2)
O3^{c}—B2—O8^{c}	107.92(18)	106.88(15)	106.7(2)
O10—B2—O2^{c}	113.1(2)	112. 93(17)	112.9(2)
O10—B2—O3^{c}	109.9(2)	109.56(15)	109.3(2)
O10—B2—O8^{c}	109.29(19)	109.31(16)	109.3(2)
B1^{h}—O4—P1^{h}	128.88(15)	127.96(13)	127.21(18)
B1—O6—P2^{i}	131.45 (15)	131.68(14)	131.87 (18)
B1^{j}—O7—P2	132.01(16)	131.76(14)	131.94(19)

B2[f]—O2—P1[c]	133.09(16)	133.33(14)	133.87(19)
B2[f]—O3—P1	132.39(16)	132.25(13)	132.39(16)
B2[f]—O8—P2	129.24(15)	128.54(13)	128.50(18)
H11A—O11—H11B	110(5)	107(5)	108(6)
H12A—O12—H12B	107(4)	109(4)	108(4)
H13A—O13—H13B	100(4)	100(5)	106(5)
O9—H9···O13	171.69(1)	176.33(1)	174.29(1)
O10—H10···O12	170.77(1)	176.75(1)	174.23(1)
O11—H11A···O13	175.61(1)	172.13(1)	172.76(1)
O11—H11B···O6	153.06(1)	149.73(1)	150.03(1)
O12—H12A···O13	124.12(1)	120.05(1)	119.72(1)
O12—H12B···O5	174.94(1)	176.90(1)	173.39(1)
O13—H13A···O8	145.33(1)	138.58(1)	132.40(1)
O13—H13B···O1	165.83(1)	169.44(1)	171.77(1)

Symmetry transformations used to generate equivalent atoms: [a] x, $-y+3/2$, $z+1/2$; [b] $-x+1$, $-y+1$, $-z+1$; [c] x, $-y+1/2$, $z+1/2$; [d] $-x+1$, $y-1/2$, $-z+1/2$; [e] $x+1$, $-y+1/2$, $z-1/2$; [f] x, $-y+1/2$, $z-1/2$; [g] $x-1$, y, z.

5.2.10 $M^{II}(H_2O)_2[B_2P_2O_8(OH)_2]\cdot H_2O$ (M^{II} = $Ni_{0.5}Co_{0.5}$, $Ni_{0.8}Zn_{0.2}$, $Ni_{0.5}Mg_{0.5}$)

Appendix 91: *$Ni_{0.5}Co_{0.5}(H_2O)_2[B_2P_2O_8(OH)_2]\cdot H_2O$: Crystallographic data and refinement parameters*

Crystallographic data

Formula weight (g / mol)	358.44
Dimensions of the crystal (mm^3)	0.040 × 0.050 × 0.075
Crystal color and habit	orange, block
Temperature of measurement (K)	293
Crystal system	monoclinic
Space group	$P2_1/c$ (No. 14)
Unit cell parameters	a = 7.7411(7) Å b = 14.6307(9) Å β = 90.248(3)° c = 8.2146(4) Å
Cell volume ($Å^3$)	930.36(11)
Formula units Z	2
Calculated density, ρ_{calc} (g / cm^3)	2.560

Data collection and refinement parameters

Diffractometer	RIGAKU AFC7 CCD, MoK_α–radiation (λ = 0.7107 Å), Graphite monochromator
Absorption coefficient, μ (MoK_α), mm^{-1}	1.193
Scan type	φ / ω
2θ range (°)	4.96 – 59.50
Limiting indices	$-10 \le h \le 6$, $-20 \le k \le 15$, $-11 \le l \le 11$
Total data collected	7885
Unique data	2491
R(int)	0.023
Observed data, $I > 2\sigma$	2377
Paramenter refined	189
F(000)	359
Goodness–of–fit (on F^2)	1.087
R1/wR2, $I > 2\sigma$ (I)	0.034 / 0.077
R1/wR2, all data	0.036 / 0.079
Residual electron density (max. / min.) ($eÅ^{-3}$)	0.556 / –0.578

Appendix 92: *$Ni_{0.8}Zn_{0.2}(H_2O)_2[B_2P_2O_8(OH)_2]\cdot H_2O$: Crystallographic data and refinement parameters*

Crystallographic data

Formula weight (g / mol)	359.67
Dimensions of the crystal (mm^3)	0.045 × 0.045 × 0.09
Crystal color and habit	yellow, block
Temperature of measurement (K)	293
Crystal system	monoclinic
Space group	$P2_1/c$ (No. 14)
Unit cell parameters	a = 7.7411(5) Å b = 14.5893(10) Å β = 90.257(4)° c = 8.2928(7) Å
Cell volume ($Å^3$)	926.39(12)
Formula units Z	2
Calculated density, ρ_{calc} (g / cm^3)	2.578

Data collection and refinement parameters

Diffractometer	RIGAKU AFC7 CCD, MoK_α–radiation (λ = 0.7107 Å), Graphite monochromator
Absorption coefficient, μ (MoK_α), mm^{-1}	1.314
Scan type	φ / ω
2θ range (°)	5.26 – 59
Limiting indices	$-9 \le h \le 10$, $-19 \le k \le 20$, $-9 \le l \le 11$
Total data collected	7580
Unique data	2519
R(int)	0.027
Observed data, $I > 2\sigma$	2265
Paramenter refined	188
F(000)	361
Goodness–of–fit (on F^2)	1.136
R1/wR2, $I > 2\sigma$ (I)	0.038 / 0.082
R1/wR2, all data	0.042 / 0.087
Residual electron density (max. / min.) ($eÅ^{-3}$)	0.603 / –0.581

Appendix 93: *$Ni_{0.5}Mg_{0.5}(H_2O)_2[B_2P_2O_8(OH)_2]\cdot H_2O$: Crystallographic data and refinement parameters*

Crystallographic data

Formula weight (g / mol)	341.13
Dimensions of the crystal (mm^3)	0.04 × 0.04 × 0.08
Crystal color and habit	light green, block
Temperature of measurement (K)	293
Crystal system	monoclinic
Space group	$P2_1/c$ (No. 14)
Unit cell parameters	a = 7.7389(5) Å b = 14.5735(9) Å β = 90.254(3)° c = 8.2060(4) Å
Cell volume ($Å^3$)	925.49(9)
Formula units Z	2
Calculated density, ρ_{calc} (g / cm^3)	2.448

Data collection and refinement parameters

Diffractometer	RIGAKU AFC7 CCD, MoK_α–radiation (λ = 0.7107 Å), Graphite monochromator
Absorption coefficient, μ (MoK_α), mm^{-1}	0.784
Scan type	φ / ω
2θ range (°)	4.96 – 58.96
Limiting indices	$-7 \le h \le 10$, $-19 \le k \le 13$, $-11 \le l \le 11$
Total data collected	7144
Unique data	2353
R(int)	0.027
Observed data, $I > 2\sigma$	2257
Paramenter refined	186
F(000)	344
Goodness–of–fit (on F^2)	1.080
R1/wR2, $I > 2\sigma$ (I)	0.041 / 0.097
R1/wR2, all data	0.043 / 0.099
Residual electron density (max. / min.) ($eÅ^{-3}$)	0.455 / –0.487

Appendix 94: *$Ni_{0.5}Co_{0.5}(H_2O)_2[B_2P_2O_8(OH)_2]\cdot H_2O$: Atomic coordinates and equivalent / isotropic displacement parameters ($Å^2$)*

Atom	Site	*x*	*y*	*z*	U_{eq} / U_{iso}
M^x	4*e*	0.2483(1)	0.5349(1)	0.8014(1)	0.011(1)
P1	4*e*	0.5708(1)	0.2882(1)	0.0612(1)	0.009(1)
P2	4*e*	0.0687(1)	0.1611(1)	0.2699(1)	0.009(1)
B1	4*e*	0.9191(4)	0.2846(2)	0.0578(3)	0.008(1)
B2	4*e*	0.4203(3)	0.3363(2)	0.7666(3)	0.007(1)
O1	4*e*	0.5524(2)	0.3708(1)	0.1689(2)	0.015(1)
O2	4*e*	0.4360(2)	0.2129(1)	0.4235(2)	0.014(1)
O3	4*e*	0.5495(2)	0.1971(1)	0.1518(2)	0.011(1)
O4	4*e*	0.2502(2)	0.7847(1)	0.5215(2)	0.010(1)
O5	4*e*	0.0464(2)	0.0601(1)	0.2941(2)	0.013(1)
O6	4*e*	0.9372(2)	0.1956(1)	0.1431(2)	0.011(1)
O7	4*e*	0.0523(2)	0.2157(1)	0.4296(2)	0.013(1)
O8	4*e*	0.2480(2)	0.1859(1)	0.2002(2)	0.010(1)
O9	4*e*	0.0667(3)	0.8630(1)	0.3359(2)	0.014(1)
H9	4*e*	–0.010(5)	0.865(3)	0.293(5)	0.021*
O10	4*e*	0.4361(3)	0.4339(1)	0.7849(2)	0.014(1)
H10	4*e*	0.520(5)	0.448(3)	0.816(5)	0.022*
O11	4*e*	0.2428(4)	0.9514(2)	0.547(3)	0.028(1)
H11A	4*e*	0.244(6)	0.992(3)	–0.005(6)	0.041*
H11B	4*e*	0.234(6)	0.910(4)	0.006(6)	0.041*
O12	4*e*	0.2561(3)	–0.0089(3)	0.05593(2)	0.016(1)
H12A	4*e*	0.268(5)	0.040(3)	0.568(5)	0.024*
H12B	4*e*	0.159(5)	–0.022(3)	0.607(5)	0.024*
O13	4*e*	0.2454(3)	0.1085(2)	0.8573(3)	0.024(1)
H13A	4*e*	0.233(6)	0.146(3)	0.919(6)	0.035*
H13B	4*e*	0.329(6)	0.115(3)	0.821(6)	0.035*

[x] $M = Ni_{0.5}Co_{0.5}$; * U_{iso} values of the hydrogen atoms were kept at 1.5 U_{eq} of the oxygen atoms to which they are attached.

Appendix 95: *$Ni_{0.8}Zn_{0.2}(H_2O)_2[B_2P_2O_8(OH)_2]\cdot H_2O$: Atomic coordinates and equivalent / isotropic displacement parameters ($Å^2$)*

Atom	Site	*x*	*y*	*z*	U_{eq} / U_{iso}
M[x]	4*e*	0.2482(1)	0.5348(1)	0.8013(1)	0.012(1)
P1	4*e*	0.5707(1)	0.2887(1)	0.0617(1)	0.009(1)
P2	4*e*	0.0685(1)	0.1607(1)	0.2698(1)	0.009(1)
B1	4*e*	0.9189(3)	0.2848(2)	0.0583(3)	0.008(1)
B2	4*e*	0.4196(3)	0.3365(2)	0.7669(3)	0.008(1)
O1	4*e*	0.5532(2)	0.3712(1)	0.1704(2)	0.015(1)
O2	4*e*	0.4355(2)	0.2120(1)	0.4241(2)	0.014(1)
O3	4*e*	0.5493(2)	0.1971(1)	0.1521(2)	0.012(1)
O4	4*e*	0.2507(2)	0.7848(1)	0.5216(2)	0.011(1)
O5	4*e*	0.0462(2)	0.0593(1)	0.2932(2)	0.013(1)
O6	4*e*	0.9364(2)	0.1956(1)	0.1435(2)	0.011(1)
O7	4*e*	0.0522(2)	0.2151(1)	0.4298(2)	0.012(1)
O8	4*e*	0.2476(2)	0.1858(1)	0.2003(2)	0.010(1)
O9	4*e*	0.0679(3)	0.8634(1)	0.3352(2)	0.014(1)
H9	4*e*	–0.010(5)	0.868(3)	0.295(5)	0.021*
O10	4*e*	0.4358(3)	0.4349(1)	0.7828(2)	0.015(1)
H10	4*e*	0.513(5)	0.448(3)	0.819(5)	0.022*
O11	4*e*	0.2442(4)	0.9507(2)	0.0549(3)	0.027(1)
H11A	4*e*	0.243(6)	0.988(4)	0(60)	0.040*
H11B	4*e*	0.235(6)	0.905(4)	0(60)	0.041*
O12	4*e*	0.2564(3)	–0.0082(2)	0.5578(3)	0.017(1)
H12A	4*e*	0.265(5)	0.041(3)	0.560(5)	0.025*
H12B	4*e*	0.172(6)	–0.022(3)	0.603(5)	0.025*
O13	4*e*	0.2444(3)	0.1085(2)	0.8573(3)	0.024(1)
H13A	4*e*	0.236(6)	0.147(3)	0.920(6)	0.036*
H13B	4*e*	0.319(6)	0.117(3)	0.823(6)	0.036*

[x] $M = Ni_{0.8}Zn_{0.2}$; * U_{iso} values of the hydrogen atoms were kept at 1.5 U_{eq} of the oxygen atoms to which they are attached.

Appendix 96: *$Ni_{0.5}Mg_{0.5}(H_2O)_2[B_2P_2O_8(OH)_2]\cdot H_2O$: Atomic coordinates and equivalent / isotropic displacement parameters ($Å^2$)*

Atom	Site	*x*	*y*	*z*	U_{eq} / U_{iso}
M^x	4*e*	0.2484(1)	0.5349(1)	0.8030(1)	0.014(1)
P1	4*e*	0.5717(1)	0.2876(1)	0.0613(1)	0.014(1)
P2	4*e*	0.0699(1)	0.1612(1)	0.2705(1)	0.014(1)
B1	4*e*	0.9208(5)	0.2842(3)	0.0576(5)	0.008(1)
B2	4*e*	0.4215(3)	0.3365(3)	0.7676(5)	0.009(1)
O1	4*e*	0.5550(4)	0.3708(2)	0.1676(3)	0.019(1)
O2	4*e*	0.4368(4)	0.2138(2)	0.4239(3)	0.016(1)
O3	4*e*	0.5504(3)	0.1964(2)	0.1523(3)	0.016(1)
O4	4*e*	0.2501(4)	0.7836(2)	0.5215(3)	0.014(1)
O5	4*e*	0.0495(3)	0.0600(2)	0.2948(4)	0.018(1)
O6	4*e*	0.9390(4)	0.1954(2)	0.1443(3)	0.015(1)
O7	4*e*	0.0517(3)	0.2160(2)	0.4298(3)	0.017(1)
O8	4*e*	0.2489(4)	0.1867(2)	0.2010(3)	0.014(1)
O9	4*e*	0.0675(4)	0.8633(2)	0.3362(3)	0.017(1)
H9	4*e*	–0.010(6)	0.859(3)	0.283(7)	0.021*
O10	4*e*	0.4359(4)	0.4338(2)	0.7873(3)	0.018(1)
O11	4*e*	0.2431(6)	0.9507(2)	0.0556(3)	0.031(1)
H11A	4*e*	0.268(9)	0.995(4)	–0.006(7)	0.046*
H11B	4*e*	0.304(7)	0.911(4)	–0.004(7)	0.046*
O12	4*e*	0.2544(4)	–0.0087(2)	0.5594(3)	0.019(1)
H12A	4*e*	0.290(6)	0.049(3)	0.573(6)	0.029*
H12B	4*e*	0.150(7)	–0.028(4)	0.617(7)	0.029*
O13	4*e*	0.2470(5)	0.1086(2)	0.8571(3)	0.028(1)
H13A	4*e*	0.230(8)	0.159(4)	0.920(7)	0.043*
H13B	4*e*	0.359(8)	0.116(4)	0.812(8)	0.043*

[x] $M = Ni_{0.5}Mg_{0.5}$; * U_{iso} values of the hydrogen atoms were kept at 1.5 U_{eq} of the oxygen atoms to which they are attached.

Appendix 97: *$Ni_{0.5}Co_{0.5}(H_2O)_2[B_2P_2O_8(OH)_2]\cdot H_2O$: Anisotropic displacement parameters U_{ij} ($Å^2 \times 10^3$). The anisotropic displacement factor exponent takes the form: $-2\pi [h^2a^{*2}U_{11} + \cdots + 2hka^*b^* U_{12}]$.*

Atom	U_{11}	U_{22}	U_{33}	U_{23}	U_{13}	U_{12}
M^x	11(1)	8(1)	15(1)	–2(1)	0(1)	0(1)
P1	8(1)	9(1)	10(1)	1(1)	0(1)	0(1)
P2	8(1)	8(1)	11(1)	1(1)	1(1)	1(1)
B1	7(1)	6(1)	11(1)	0(1)	1(1)	1(1)
B2	4(1)	7(1)	10(1)	–1(1)	–1(1)	1(1)
O1	13(1)	11(1)	12(1)	–5(1)	4(1)	–2(1)
O2	9(1)	18(1)	14(1)	–3(1)	–2(1)	2(1)
O3	9(1)	9(1)	16(1)	2(1)	2(1)	–(1)
O4	7(1)	12(1)	11(1)	–2(1)	0(1)	1(1)
O5	10(1)	8(1)	20(1)	2(1)	1(1)	0(1)
O6	9(1)	11(1)	13(1)	3(1)	–2(1)	1(1)
O7	10(1)	15(1)	13(1)	–4(1)	2(1)	–1(1)
O8	7(1)	10(1)	12(1)	1(1)	1(1)	0(1)
O9	11(1)	12(1)	19(1)	5(1)	–4(1)	–3(1)
O10	10(1)	9(1)	24(1)	–3(1)	–3(1)	1(1)
O11	49(2)	16(1)	18(1)	0(1)	0(1)	–1(1)
O12	17(1)	14(1)	18(1)	0(1)	1(1)	–1(1)
O13	27(1)	20(1)	24(1)	–4(1)	5(1)	–4(1)

[x] $M = Ni_{0.5}Co_{0.5}$

Appendix 98: *$Ni_{0.8}Zn_{0.2}(H_2O)_2[B_2P_2O_8(OH)_2]\cdot H_2O$: Anisotropic displacement parameters U_{ij} ($Å^2 \times 10^3$). The anisotropic displacement factor exponent takes the form: $-2\pi [h^2a^{*2}U_{11} + \cdots + 2hka^*b^* U_{12}]$.*

Atom	U_{11}	U_{22}	U_{33}	U_{23}	U_{13}	U_{12}
M^x	10(1)	11(1)	14(1)	–1(1)	0(1)	0(1)
P1	7(1)	12(1)	9(1)	1(1)	–1(1)	0(1)
P2	6(1)	11(1)	9(1)	1(1)	–1(1)	1(1)
B1	6(1)	10(1)	8(1)	1(1)	0(1)	2(1)
B2	5(1)	10(1)	11(1)	–1(1)	–2(1)	1(1)
O1	13(1)	13(1)	19(1)	–5(1)	4(1)	–3(1)
O2	8(1)	22(1)	12(1)	–4(1)	–3(1)	1(1)
O3	9(1)	14(1)	13(1)	3(1)	3(1)	–1(1)
O4	6(1)	17(1)	9(1)	–2(1)	0(1)	1(1)
O5	10(1)	10(1)	19(1)	3(1)	0(1)	0(1)
O6	8(1)	13(1)	11(1)	3(1)	–2(1)	0(1)
O7	8(1)	17(1)	11(1)	–3(1)	2(1)	–1(1)
O8	5(1)	14(1)	10(1)	1(1)	–1(1)	0(1)
O9	10(1)	14(1)	17(1)	4(1)	–4(1)	2(1)
O10	10(1)	11(1)	24(1)	–3(1)	–4(1)	1(1)
O11	45(2)	20(1)	16(1)	–1(1)	–2(1)	–2(1)
O12	14(1)	20(1)	16(1)	0(1)	2(1)	–1(1)
O13	25(1)	25(1)	23(1)	–5(1)	3(1)	–5(1)

[x] $M = Ni_{0.8}Zn_{0.2}$

Appendix 99: *$Ni_{0.5}Mg_{0.5}(H_2O)_2[B_2P_2O_8(OH)_2]\cdot H_2O$: Anisotropic displacement parameters U_{ij} ($Å^2 \times 10^3$). The anisotropic displacement factor exponent takes the form: $-2\pi [h^2a^{*2}U_{11} + \cdots + 2hka^*b^* U_{12}]$.*

Atom	U_{11}	U_{22}	U_{33}	U_{23}	U_{13}	U_{12}
M^x	13(1)	11(1)	16(1)	–1(1)	1(1)	0(1)
P1	13(1)	15(1)	14(1)	1(1)	0(1)	0(1)
P2	13(1)	14(1)	15(1)	1(1)	0(1)	1(1)
B1	4(2)	9(2)	11(2)	0(1)	3(2)	2(1)
B2	6(2)	9(2)	13(2)	–1(1)	3(2)	–1(1)
O1	19(1)	16(1)	22(1)	–4(1)	4(1)	–4(1)
O2	12(1)	22(1)	15(1)	–2(1)	0(1)	2(1)
O3	14(1)	16(1)	20(1)	2(1)	2(1)	–2(1)
O4	13(1)	17(1)	14(1)	–1(1)	1(1)	1(1)
O5	16(1)	12(1)	26(1)	3(1)	2(1)	1(1)
O6	14(1)	15(1)	15(1)	5(1)	–3(1)	–1(1)
O7	14(1)	19(1)	17(1)	–3(1)	2(1)	0(1)
O8	12(1)	17(1)	14(1)	2(1)	–1(1)	1(1)
O9	14(1)	16(1)	22(1)	3(1)	–3(1)	–5(1)
O10	16(1)	12(1)	25(1)	–3(1)	2(1)	2(1)
O11	49(2)	23(1)	20(1)	0(1)	4(2)	0(2)
O12	19(1)	21(1)	18(1)	0(1)	–1(2)	0(1)
O13	32(2)	25(1)	29(1)	–2(1)	6(1)	–1(1)

[x] $M = Ni_{0.5}Mg_{0.5.}$

Appendix 100: *$M^{II}(H_2O)_2[BP_2O_8(OH)_2]\cdot H_2O$ (M^{II} = $Ni_{0.5}Co_{0.5}$, $Ni_{0.8}Zn_{0.2}$, $Ni_{0.5}Mg_{0.5}$): Selected bond distances (Å)*

	M^{II} = $Ni_{0.5}Co_{0.5}$	M^{II} = $Ni_{0.8}Zn_{0.2}$	M^{II} = $Ni_{0.5}Mg_{0.5}$
M—O1[b]	2.0835(19)	2.0723(19)	2.064(3)
M—O5[c]	2.0922(19)	2.0820(19)	2.070(3)
M—O9[a]	2.0716(19)	2.057(2)	2.059(3)
M—O10	2.0767(19)	2.064(2)	2.072(3)
M—O11[a]$_w$	2.037(2)	2.033(2)	2.041(3)
M—O12[c]$_w$	2.153(2)	2.140(2)	2.138(2)
P1—O1	1.5046(19)	1.504(2)	1.500(3)
P1—O2[f]	1.536(2)	1.536(2)	1.533(3)
P1—O3	1.5361(18)	1.5383(19)	1.535(3)
P1—O4[d]	1.5467(19)	1.5459(18)	1.542(3)
P2—O5	1.5009(19)	1.501(2)	1.496(3)
P2—O6[g]	1.5381(19)	1.5394(19)	1.529(3)
P2—O7	1.5415(19)	1.539(2)	1.539(3)
P2—O8	1.5472(18)	1.5462(18)	1.546(3)
B1—O4[d]	1.461(3)	1.465(3)	1.471(4)
B1—O6	1.485(3)	1.484(3)	1.483(4)
B1—O7[e]	1.477(3)	1.479(3)	1.462(4)
B1—O9[d]	1.446(3)	1.445(3)	1.448(5)
B2—O2[c]	1.481(3)	1.476(3)	1.481(4)
B2—O3[c]	1.462(3)	1.464(3)	1.458(4)
B2—O8[c]	1.475(3)	1.473(3)	1.480(5)
B2—O10	1.441(3)	1.447(3)	1.432(4)
O9—H9	0.69(4)	0.69(4)	0.74(5)
O9—H9···O13	2.915(1)	2.911(1)	2.928(1)
O10—H10	0.72(4)	0.69(4)	–[a]
O10—H10···O12	2.827(1)	2.837(1)	–[a]
O11—H11A	0.77(5)	0.71(5)	0.84(6)
O11—H11A···O13	2.813(1)	2.815(1)	2.819(1)
O11—H11B	0.73(5)	0.81(5)	0.89(6)
O11—H11B···O6	3.031(1)	3.022(1)	3.176(1)
O12—H12A	0.72(4)	0.73(4)	0.89(5)
O12—H12A···O13	2.991(1)	2.991(1)	2.983(1)
O12—H12B	0.87(4)	0.78(4)	0.98(5)
O12—H12B···O5	2.742(1)	2.750(1)	2.747(1)
O13—H13A	0.76(5)	0.76(5)	0.91(6)
O13—H13A···O8	3.036(1)	3.031(1)	3.043(1)
O13—H13B	0.72(5)	0.66(5)	0.95(6)
O13—H13B···O1	2.857(1)	2.861(1)	2.867(1)

[a] The hydrogen atoms could not be localized from the Fourrier difference maps. Symmetry transformations used to generate equivalent atoms: [a] *x*, –*y*+3/2, *z*+1/2; [b] –*x*+1, –*y*+1, –*z*+1; [c] *x*, –*y*+1/2, *z*+1/2; [d] –*x*+1, *y*–1/2, –*z*+1/2; [e] *x*+1, –*y*+1/2, *z*–1/2; [f] *x*, –*y*+1/2, *z*–1/2; [g] *x*–1, *y*, *z*; w = water.

Appendix 101: *$M^{II}(H_2O)_2[B_2P_2O_8(OH)_2]\cdot H_2O$ (M^{II} = $Ni_{0.5}Co_{0.5}$, $Ni_{0.8}Zn_{0.2}$, $Ni_{0.5}Mg_{0.5}$): Selected bond angles (°)*

	M^{II} = $Ni_{0.5}Co_{0.5}$	M^{II} = $Ni_{0.8}Zn_{0.2}$	M^{II} = $Ni_{0.5}Mg_{0.5}$
O1^{b}—*M*—O10	87.74(8)	87.30(8)	87.94(11)
O1^{b}—*M*—O5^{c}	174.91(8)	175.39(8)	175.16(11)
O1^{b}—*M*—O12^{c}	89.11(8)	89.49(8)	89.47(12)
O5^{c}—*M*—O12^{c}	85.89(8)	86.03(8)	85.76(12)
O9^{a}—*M*—O1^{b}	90.52(8)	90.64(8)	90.35(11)
O9^{a}—*M*—O5^{c}	88.58(8)	88.33(8)	88.85(11)
O9^{a}—*M*—O10	175.69(8)	176.10(8)	175.78(11)
O9^{a}—*M*—O12^{c}	90.49(8)	90.89(9)	90.60(12)
O10—*M*—O5^{c}	85.53(8)	85.78(9)	85.53(12)
O10—*M*—O12^{c}	92.81(8)	93.45(8)	92.53(10)
O11^{a}—*M*—O1^{b}	93.08(9)	92.98(10)	92.68(14)
O11^{a}—*M*—O5^{c}	93.64(10)	92.89(10)	93.38(14)
O11^{a}—*M*—O9^{a}	90.97(10)	90.43(10)	91.27(14)
O11^{a}—*M*—O10	91.42(10)	91.65(10)	91.43(15)
O11^{a}—*M*—O12^{c}	175.47(9)	90.89(9)	175.64(11)
O1—P1—O2^{f}	111.10(11)	112.19(12)	112.23(16)
O1—P1—O3	113.69(11)	113.56(11)	114.07(16)
O1—P1—O4^{d}	111.88(10)	112.01(11)	111.53(15)
O2^{f}—P1—O3	105. 86(11)	105.90(11)	105. 81(15)
O2^{f}—P1—O4^{d}	106.44(10)	106.40(11)	106.43(16)
O3—P1—O4^{d}	106.35(10)	106.25(10)	106.22(14)
O5—P2—O6^{g}	109.68(11)	109.60(11)	109.95(15)
O5—P2—O7	112.83(11)	112.94 (11)	112.87(16)
O5—P2—O8	112.59(10)	112.58(11)	112.47(15)
O6^{g}—P2—O7	110.46(10)	110.29(11)	110.04(15)
O6^{g}—P2—O8	105.29(10)	105.52(10)	105.27(15)
O7—P2—O8	105.68(10)	105.61(10)	105.91(14)
O4^{d}—B1—O6	107.07(19)	106.9(2)	106.9(3)
O4^{d}—B1—O7^{e}	108.0(2)	107.9(2)	107.9(3)
O7^{e}—B1—O6	105.60(19)	105.9(2)	106.1(3)
O9^{d}—B1—O4^{d}	109.5(2)	109.4(2)	108.9(3)
O9^{d}—B1—O6	113.9(2)	113.9(2)	113.6(3)
O9^{d}—B1—O7^{e}	112.4(2)	112.5(2)	113.1(3)
O2^{c}—B2—O8^{c}	106.60(19)	106.8(2)	106.52(3)
O3^{c}—B2—O2^{c}	110.19(19)	110.3(2)	107.92(3)
O3^{c}—B2—O8^{c}	107.93(19)	108.0(2)	109.93(3)
O10—B2—O2^{c}	112.6(2)	113.0(2)	109.29(3)
O10—B2—O3^{c}	109.9(2)	109.3(2)	110.2(3)
O10—B2—O8^{c}	109.4(2)	109.3(2)	109.7(3)
B1^{h}—O4—P1^{h}	127.44(15)	127.10(16)	127.6(2)
B1—O6—P2^{i}	131.92(17)	131.77(17)	132.1(2)

B1[j]—O7—P2	131.70(17)	131.91(17)	132.4(2)
B2[f]—O2—P1[c]	133.54(27)	133.87(17)	133.0(2)
B2[f]—O3—P1	132.65(16)	132.57(17)	132.5(2)
B2[f]—O8—P2	128.49(15)	128.44(16)	128.11(19)
H11A—O11—H11B	107(5)	103(5)	92(5)
H12A—O12—H12B	107(4)	103(5)	118(4)
H13A—O13—H13B	107(5)	103(5)	105(5)
O9—H9···O13	170.93(1)	173.07(1)	168.83(1)
O10—H10···O12	171.67(1)	176.67(1)	
O11—H11A···O13	174.56(1)	173.89(1)	161.51(1)
O11—H11B···O6	150.89(1)	149.73(1)	176.51(1)
O12—H12A···O13	117.43(1)	112.94(1)	113.65(1)
O12—H12B···O5	175.19(1)	176.91(1)	175.01(1)
O13—H12A···O8	145.12(1)	145.81(1)	133.68(1)
O13—H12B···O1	169.08(1)	169.30(1)	165.17(1)

Symmetry transformations used to generate equivalent atoms: [a] *x*, –*y*+3/2, *z*+1/2; [b] –*x*+1, –*y*+1, –*z*+1; [c] *x*, –*y*+1/2, *z*+1/2; [d] –*x*+1, *y*–1/2, –*z*+1/2; [e] *x*+1, –*y*+1/2, *z*–1/2; [f] *x*, –*y*+1/2, *z*–1/2; [g] *x*–1, *y*, *z*; [h] –*x*+1, *y*+1/2, –*z*+1/2; [i] *x*+1, *y*, *z*; [j] *x*–1, –*y*+1/2, *z*+1/2.

5.2.11 $FeCo(H_2O)[BP_3O_9(OH)_4]$ and $Fe_{1.3}Co_{0.7}[P_2O_7]\cdot 2H_2O$

Appendix 102: *$FeCo(H_2O)[BP_3O_9(OH)_4]$: Crystallographic data and refinement parameters*

Crystallographic data

Formula weight (g / mol)	448.55
Dimensions of the crystal (mm^3)	0.065 × 0.080 × 0.140
Crystal color and habit	red, platelet
Temperature of measurement (K)	293
Crystal system	orthorhombic
Space group	$P\,2_1\,2_1\,2_1$ (No.19)
Unit cell parameters	a = 7.1353(4) Å b = 8.6742(4) Å c = 16.4052(7) Å
Cell volume ($Å^3$)	1015.37
Formula units Z	2
Calculated density, ρ_{calc} (g / cm^3)	1.467

Data collection and refinement parameters

Diffractometer	RIGAKU AFC7 CCD, MoK_α–radiation (λ = 0.7107 Å), Graphite monochromator
Absorption coefficient, μ (MoK_α), mm^{-1}	1.811
Scan type	φ / ω
2θ range (°)	5.12 – 59.98
Limiting indices	$-10 \le h \le 6$, $-12 \le k \le 19$, $-23 \le l \le 23$
Total data collected	8825
Unique data	2901
R(int)	0.023
Observed data, $I > 2\sigma$	2843
Paramenter refined	206
F(000)	442
Goodness–of–fit (on F^2)	1.145
R1/wR2, $I > 2\sigma$ (I)	0.027 / 0.062
R1/wR2, all data	0.028 / 0.063
Residual electron density (max. / min.) ($eÅ^{-3}$)	0.552 / –0.699

Appendix 103: *$Fe_{1.3}Co_{0.7}[P_2O_7]\cdot 2H_2O$: Crystallographic data and refinement parameters*

Crystallographic data

Formula weight (g / mol)	324.75
Dimensions of the crystal (mm^3)	0.125 × 0.075 × 0.060
Crystal color and habit	red, colorless block
Temperature of measurement (K)	293
Crystal system	monoclinic
Space group	$P2_1/n$ (No.14)
Unit cell parameters	a = 6.3868(5) Å b = 14.1318(11) Å β = 95.148(5)° c = 7.4051(8) Å
Cell volume ($Å^3$)	665.67
Formula units Z	4
Calculated density, ρ_{calc} (g / cm^3)	3.240

Data collection and refinement parameters

Diffractometer	RIGAKU AFC7 CCD, MoK_α–radiation Graphite monochromator
Absorption coefficient, μ (MoK_α), mm^{-1}	5.177
Scan type	φ / ω
2θ range (°)	5.76 – 59.56
Limiting indices	$-8 \le h \le 8$, $-19 \le k \le 15$, $-9 \le l \le 9$
Total data collected	5108
Unique data	1839
Observed data, $I > 2\sigma$	1551
R(int)	0.034
Paramenter refined	135
F(000)	636
Goodness–of–fit (on F^2)	1.108
R1/wR2, $I > 2\ \sigma(I)$	0.0454 / 0.0920
R1/wR2, all data	0.0560 / 0.0987
Residual electron density (max. / min.) ($eÅ^{-3}$)	0.801 / –0.866

Appendix 104: *$FeCo(H_2O)[BP_3O_9(OH)_4]$: Atomic coordinates and equivalent / isotropic displacement parameters ($Å^2$)*

Atom	Site	*x*	*y*	*z*	U_{eq} / U_{iso}
M1[x]	4*a*	0.3189(1)	0.6936(1)	0.7064(1)	0.010(1)
M2[x]	4*a*	0.3194(1)	0.3230(1)	0.6944(1)	0.011(1)
P1	4*a*	0.9473(1)	0.4978(1)	0.7635(1)	0.009(1)
P2	4*a*	0.4858(1)	0.5010(1)	0.8633(1)	0.009(1)
P3	4*a*	0.6340(1)	0.5249(1)	0.5810(1)	0.011(1)
B	4*a*	0.1531(5)	0.9158(4)	0.5835(2)	0.011(1)
O1	4*a*	0.8363(3)	0.3613(2)	0.7322(1)	0.013(1)
O2	4*a*	0.8430(3)	0.6500(2)	0.7493(1)	0.013(1)
O3	4*a*	0.1420(3)	0.5057(2)	0.7242(1)	0.011(1)
O4	4*a*	0.9828(3)	0.4775(3)	0.8570(1)	0.015(1)
O5	4*a*	0.4697(3)	0.3605(2)	0.8087(1)	0.012(1)
O6	4*a*	0.4688(3)	0.6524(2)	0.8170(1)	0.012(1)
O7	4*a*	0.6694(3)	0.5022(3)	0.9135(1)	0.014(1)
O8	4*a*	0.3335(3)	0.4951(3)	0.9325(1)	0.016(1)
O9	4*a*	0.4783(3)	0.5196(3)	0.6432(1)	0.013(1)
O10	4*a*	0.5581(3)	0.5545(3)	0.4949(1)	0.014(1)
O11	4*a*	0.7795(3)	0.6512(3)	0.5991(1)	0.015(1)
O12	4*a*	0.7350(4)	0.3659(3)	0.5750(2)	0.020(1)
O13	4*a*	0.1904(4)	0.7543(2)	0.5958(1)	0.016(1)
O14	4*a*	0.1982(4)	0.3077(3)	0.5785(2)	0.028(1)
H8	4*a*	0.246(6)	0.476(6)	0.913(3)	0.027(12)*
H11	4*a*	0.810(9)	0.659(7)	0.667(4)	0.080(20)*
H12	4*a*	0.781(7)	0.344(5)	0.619(3)	0.029(12)*
H13	4*a*	0.111(8)	0.704(6)	0.576(3)	0.047(16)*
H14A	4*a*	0.190(11)	0.380(9)	0.543(4)	0.090(30)*
H14B	4*a*	0.232(10)	0.243(9)	0.544(4)	0.080(30)*

[x] *M1 = M2* =$Fe_{0.5}Co_{0.5}$; * refined with isotropic displacement parameters.

Appendix 105: *$FeCo(H_2O)[BP_3O_9(OH)_4]$: Anisotropic displacement parameters U_{ij} ($Å^2 \times 10^3$). The anisotropic displacement factor exponent takes the form: $-2\pi [h^2a^{*2}U_{11} + \cdots + 2hka^*b^* U_{12}]$.*

Atom	U_{11}	U_{22}	U_{33}	U_{23}	U_{13}	U_{12}
M1[x]	9(1)	8(1)	13(1)	1(1)	0(1)	0(1)
M2[x]	11(1)	9(1)	14(1)	0(1)	1(1)	0(1)
P1	7(1)	10(1)	10(1)	0(1)	0(1)	0(1)
P2	7(1)	8(1)	11(1)	0(1)	0(1)	0(1)
P3	11(1)	12(1)	10(1)	0(1)	1(1)	0(1)
B	12(1)	11(1)	10(1)	–2(1)	0(1)	0(1)
O1	12(1)	12(1)	15(1)	0(1)	1(1)	–3(1)
O2	12(1)	11(1)	16(1)	–1(1)	1(1)	2(1)
O3	10(1)	9(1)	15(1)	1(1)	4(1)	0(1)
O4	11(1)	21(1)	12(1)	1(1)	1(1)	–3(1)
O5	10(1)	10(1)	15(1)	–1(1)	–3(1)	0(1)
O6	12(1)	8(1)	16(1)	1(1)	0(1)	–1(1)
O7	11(1)	14(1)	17(1)	–4(1)	–4(1)	2(1)
O8	10(1)	20(1)	17(1)	–3(1)	4(1)	–2(1)
O9	12(1)	13(1)	14(1)	1(1)	3(1)	0(1)
O10	11(1)	20(1)	13(1)	2(1)	1(1)	0(1)
O11	19(1)	20(1)	17(1)	–2(1)	1(1)	–6(1)
O12	25(2)	18(1)	16(1)	3(1)	6(1)	6(1)
O13	19(1)	10(1)	20(1)	–1(1)	–3(1)	–1(1)
O14	42(1)	20(1)	21(1)	–3(1)	–12(1)	2(1)

[x] *M1 = M2* = $Fe_{0.5}Co_{0.5}$

Appendix 106: *$Fe_{1.3}Co_{0.7}[P_2O_7]\cdot 2H_2O$: Atomic coordinates and equivalent / isotropic displacement parameters ($Å^2$)*

Atom	Site	*x*	*y*	*z*	U_{eq} / U_{iso}
M[x]	4*e*	0.7366(1)	0.6104(1)	–0.0807(1)	0.013(1)
Fe	4*e*	0.0488(1)	0.2480(1)	0.3482(1)	0.016(1)
P1	4*e*	0.7579(2)	0.4151(1)	0.1502(2)	0.009(1)
P2	4*e*	0.5655(2)	0.3123(1)	0.4261(2)	0.009(1)
O1	4*e*	0.7951(5)	0.5190(2)	0.1277(4)	0.014(1)
O2	4*e*	0.9602(5)	0.3579(2)	0.1583(4)	0.013(1)
O3	4*e*	0.5867(5)	0.3725(2)	0.182(4)	0.013(1)
O4	4*e*	0.6686(5)	0.4058(2)	0.3466(4)	0.011(1)
O5	4*e*	0.7236(5)	0.2322(2)	0.4066(4)	0.012(1)
O6	4*e*	0.3620(5)	0.2939(2)	0.3059(4)	0.013(1)
O7	4*e*	0.5321(5)	0.3382(2)	0.6201(4)	0.013(1)
O8	4*e*	0.7478(6)	0.5025(3)	–0.2802(5)	0.021(1)
O9	4*e*	0.0685(6)	0.3501(3)	0.5615(5)	0.020(1)
H5A	4*e*	0.664(11)	0.461(5)	–0.311(9)	0.04(2)*
H5B	4*e*	0.866(14)	0.480(6)	–0.270(11)	0.07(3)*
H9A	4*e*	0.140(20)	0.388(10)	0.560(19)	0.16(7)*
H9B	4*e*	0.075(15)	0.328(7)	0.650(13)	0.07(3)*

[x] M = $Fe_{0.3}Co_{0.7}$; * refined with isotropic displacement parameters.

Appendix 107: *$Fe_{1.3}Co_{0.7}[P_2O_7]\cdot 2H_2O$: Anisotropic displacement parameters U_{ij} ($Å^2 \times 10^3$). The anisotropic displacement factor exponent takes the form: $-2\pi [h^2a^{*2}U_{11} + \cdots + 2hka^*b^* U_{12}]$.*

Atom	U_{11}	U_{22}	U_{33}	U_{23}	U_{13}	U_{12}
M^x	13(1)	12(1)	13(1)	1(1)	1(1)	0(1)
Fe	10(1)	10(1)	10(1)	1(1)	1(1)	0(1)
P1	9(1)	9(1)	9(1)	1(1)	0(1)	–1(1)
P2	9(1)	11(1)	9(1)	0(1)	0(1)	0(1)
O1	21(1)	8(1)	13(1)	4(1)	–2(1)	1(1)
O2	12(1)	14(1)	13(1)	4(1)	4(1)	1(1)
O3	12(1)	14(1)	12(1)	–2(1)	1(1)	–1(1)
O4	13(1)	11(1)	9(1)	1(1)	–1(1)	–2(1)
O5	11(1)	12(1)	14(1)	2(1)	2(1)	2(1)
O6	9(1)	15(1)	13(1)	2(1)	–1(1)	–2(1)
O7	18(1)	12(1)	10(1)	–1(1)	2(1)	–2(1)
O8	22(1)	18(1)	21(1)	–9(1)	–1(1)	–4(1)
O9	20(1)	23(1)	15(1)	–5(1)	–1(1)	1(1)

[x] $M = Fe_{0.3}Co_{0.7}$

Appendix 108: *$FeCo(H_2O)[BP_3O_9(OH)_4]$: Selected interatomic distances (Å) and angles (°)*

Atom contact	Distance	Atom contact	Distance
M1^{x}—O3	2.082(2)	P1—O1	1.515(2)
M1^{x}—O1^{a}	2.087(2)	P1—O3^{c}	1.5328(19)
M1^{x}—O13	2.099(2)	P1—O2	1.533(2)
M1^{x}—O5^{a}	2.105(2)	P1—O4	1.564(2)
M1^{x}—O6	2.137(2)		
M1^{x}—O9	2.155(2)	P2—O5	1.517(2)
		P2—O6	1.522(2)
M2^{x}—O3	2.087(2)	P2—O7	1.5479(19)
M2^{x}—O14	2.093(2)	P2—O8	1.573(2)
M2^{x}—O2^{b}	2.109(2)		
M2^{x}—O6^{b}	2.123(2)	P3—O9	1.509(2)
M2^{x}—O5	2.184(2)	P3—O10	1.535(2)
M2^{x}—O9	2.213(2)	P3—O11	1.537(2)
		P3—O12	1.559(2)
B—O13	1.440(4)		
B—O7^{a}	1.473(4)	O12—H12	0.82(5)
B—O10^{d}	1.476(4)	O12—H12···O1	2.679(1)
B—O4	1.477(4)	O13—H13	0.79(6)
		O13—H13···O11	3.066(1)
O8—H8	0.72(4)		
O8—H8···O4	2.797(1)	O14—H14A	0.86(8)
O11—H11	1.15(6)	O14—H14A···O8	2.952(1)
O11—H11···O2	2.507(1)	O14—H14B	0.84(7)
		O14—H14B···O12	2.945(1)

Atoms	Angle	Atoms	Angle
O3—*M1*^{x}—O1^{a}	98.96(8)	O3—*M2**—O14	90.62(10)
O3—*M1*^{x}—O13	93.03(8)	O3—*M2**—O2^{b}	95.98(8)
O1^{a}—*M1*^{x}—O13	90.62(9)	O14—*M2**—O2^{b}	97.20(10)
O3—*M1*^{x}—O5^{a}	171.54(8)	O3—*M2**—O6^{b}	169.04(8)
O1^{a}—*M1*^{x}—O5^{a}	87.58(9)	O14—*M2**—O6^{b}	99.78(10)
O13—*M1*^{x}—O5^{a}	92.25(9)	O2^{b}—*M2**—O6^{b}	86.20(8)
O3—*M1*^{x}—O6	93.05(8)	O3—*M2**—O5	89.06(8)
O1^{a}—*M1*^{x}—O6	88.40(8)	O14—*M2**—O5	172.79(10)
O13—*M1*^{x}—O6	173.92(9)	O2^{b}—*M2**—O5	89.99(8)
O5^{a}—*M1*^{x}—O6	81.71(8)	O6^{b}—*M2**—O5	80.19(8)
O3—*M1*^{x}—O9	80.77(8)	O3—*M2**—O9	79.32(8)
O1^{a}—*M1*^{x}—O9	179.72(9)	O14—*M2**—O9	85.20(10)
O13—*M1*^{x}—O9	89.47(8)	O2^{b}—*M2**—O9	174.78(8)
O5^{a}—*M1*^{x}—O9	92.68(8)	O6^{b}—*M2**—O9	97.99(8)
O6—*M1*^{x}—O9	91.53(8)	O5—*M2**—O9	87.66(8)
O1—P1—O3^{c}	111.48(12)	O9—P3—O10	111.57(12)
O1—P1—O2	111.62(11)	O9—P3—O11	112.86(12)
O3^{c}—P1—O2	109.71(12)	O10—P3—O11	107.23(12)
O1—P1—O4	109.22(12)	O9—P3—O12	110.90(13)

O3[c]—P1—O4	105.67(11)	O10—P3—O12	104.59(13)
O2—P1—O4	108.93(12)	O11—P3—O12	109.29(14)
O5—P2—O6	113.12(11)	O13—B—O7[a]	109.4(2)
O5—P2—O7	112.57(12)	O13—B—O10[d]	112.2(2)
O6—P2—O7	109.09(13)	O7[a]—B—O10[d]	109.6(2)
O5—P2—O8	110.39(13)	O13—B—O4[a]	112.4(2)
O6—P2—O7	109.49(13)	O7[a]—B—O4[a]	111.0(2)
O7—P2—O8	101.55(11)	O10d—B—O4[a]	102.2(2)
O8—H8···O4	166.70(1)	H14A—O14—O14B	93(6)
O11—H11···O2	173.37(1)		
O12—H12···O1	158.13(1)	O14—H14A···O8	163.98(1)
O13—H13···O11	137.28(1)	O14—H14B···O12	155.50(1)

[x] *M1* = *M2* = $Fe_{0.5}Co_{0.5.}$ Symmetry transformation used to generate equivalent atoms: [a] –x+1, y+1/2, –z+3/2; [b] –x+1, y–1/2, –z+3/2; [c] x+1, y, z; [d] x–1/2, –y+3/2, –z+1;

Appendix 109: *$Fe_{1.3}Co_{0.7}[P_2O_7]\cdot 2H_2O$: Selected interatomic distances (Å) and angles (°)*

Atom–contact	Distance	Atom–contact	Distance
M^x—O1	2.022(3)	Fe—O7^d	2.078(3)
M^x—O2^a	2.116(3)	Fe—O3^e	2.119(3)
M^x—O8	2.129(4)	Fe—O9	2.134(4)
M^x—O5^b	2.151(3)	Fe—O2^f	2.137(3)
M^x—O3^c	2.170(3)	Fe—O6	2.152(3)
M^x—O6^c	2.195(3)	Fe—O5^f	2.171(3)
P1—O1	1.498(3)	P2—O7	1.516(3)
P1—O2	1.521(3)	P2—O6	1.530(3)
P1—O3	1.523(3)	P2—O5	1.532(3)
P1—O4	1.615(3)	P2—O4	1.611(3)
O8—H8A	0.82(7)	O9—H9A	0.70(15)
O8—H8A···O7	2.766(1)	O9—H9A···O7	2.958(1)
O8—H8B	0.81(9)	O9—H9B	0.73(10)
O8—H8B···O1	3.050(1)	O9—H9B···O5	2.900(1)

Atoms	Angle	Atoms	Angle
O1—M^x—O2^a	103.40(13)	O7^d—Fe—O3^e	90.35(12)
O1—M^x—O8	93.23(14)	O7^d—Fe—O9	173.36(15)
O2^a—M^x—O8	82.80(14)	O3^e—Fe—O9	96.19(15)
O1—M^x—O5^b	92.87(12)	O7^d—Fe—O2^f	84.26(12)
O2^a—M^x—O5^b	86.09(12)	O3^e—Fe—O2^f	169.90(12)
O8—M^x—O5^b	168.31(14)	O9—Fe—O2^f	89.46(15)
O1—M^x—O3^c	91.26(12)	O7^d—Fe—O6	92.24(12)
O2^a—M^x—O3^c	161.06(12)	O3^e—Fe—O6	105.69(12)
O8—M^x—O3^c	108.63(14)	O9—Fe—O6	84.85(14)
O5^b—M^x—O3^c	81.19(11)	O2^f—Fe—O6	83.11(11)
O1—M^x—O6^c	173.95(12)	O7^d—Fe—O5^f	96.96(12)
O2^a—M^x—O6^c	82.57(11)	O3^e—Fe—O5^f	81.90(11)
O8—M^x—O6^c	86.51(13)	O9—Fe—O5^f	85.19(13)
O5^b—M^x—O6^c	88.46(12)	O2^f—Fe—O5^f	90.26(11)
O3^c—M^x—O6^c	83.11(12)	O6—Fe—O5^f	168.08(12)
O1—P1—O2	112.51(18)	O7—P2—O6	114.06(17)
O1—P1—O3	115.29(18)	O7—P2—O5	114.71(18)
O2—P1—O3	111.94(18)	O6—P2—O5	110.62(18)
O1—P1—O4	104.59(18)	O7—P2—O4	104.15(17)
O3—P1—O4	106.78(17)	O6—P2—O4	106.28(17)
O3—P1—O4	104.75(17)	O5—P2—O4	106.11(17)
O8—H8A···O7	164.35(1)	O9—H9A···O7	112.89(1)
O8—H8B···O1	149.32(1)	O9—H9B···O5	158.23(1)

[x] M = $Fe_{0.3}Co_{0.7}$. Symmetry transformation used to generate equivalent atoms: [a] –x+2, –y+1, –z; [b] –x+3/2, y+1/2, –z+1/2; [c] –x+1, –y+1, –z; [d] x –1/2, –y+1/2, z –1/2; [e] x –1/2, –y+1/2, z+1/2; [f] x –1, y, z;

5.3 Shape Developement of Single Crystals of Helical Borophosphates

α–quartz comprises a chiral arrangement of tetrahedral building units [163] and crystallizes in the space groups $P3_122$ or $P3_222$. The SiO_4 tetrahedra are arranged around a 3_1 (left–handed quartz) or a 3_2 (right–handed quartz) screw axis (*Figure 5.1a*) [163].

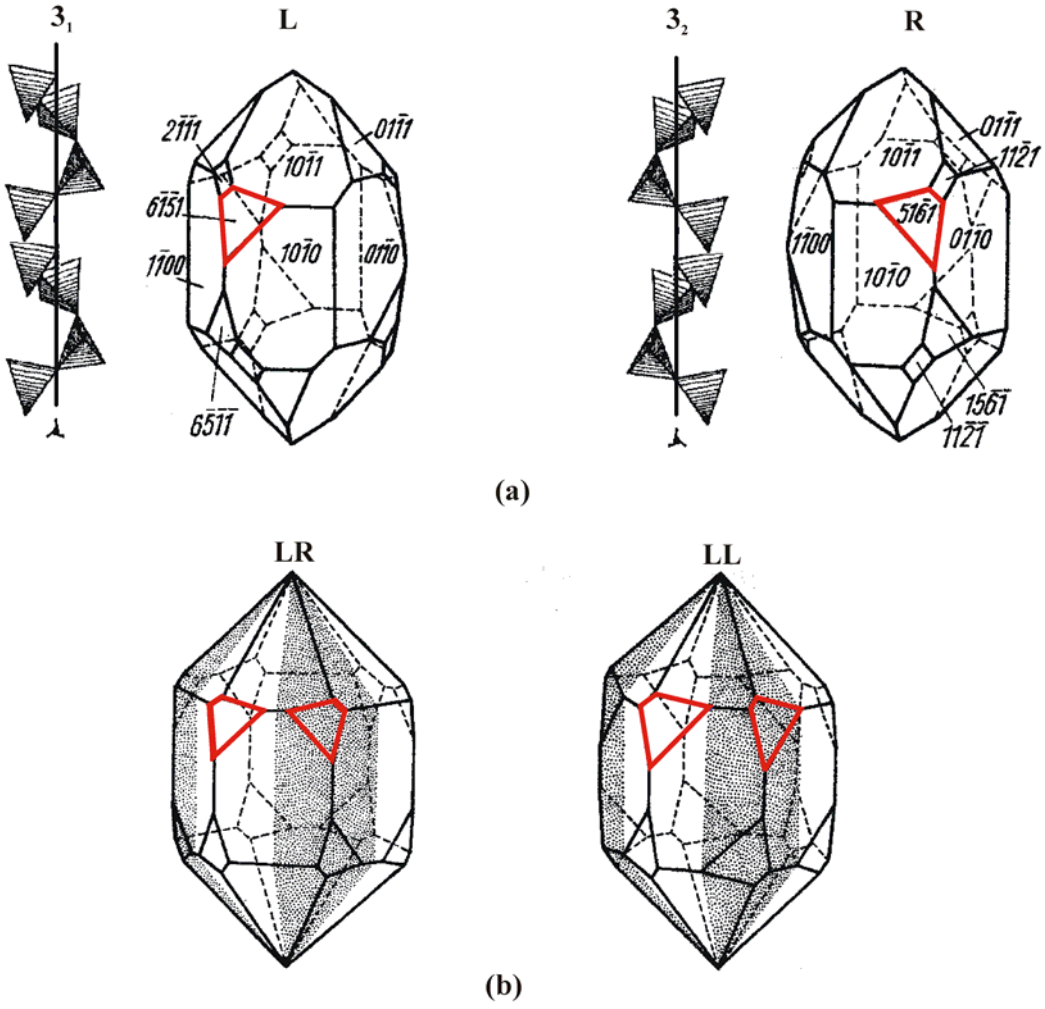

Figure 5.1: *(a) Structural arrangement of SiO_4 tetrahedra (3_1 or 3_2) and the idealized left–handed "L" and right–handed "R" crystals which can easily be identified by the positions of the trapezohedral faces (red). (b) Macroscopic "Brazilian" twin (LR) and "Dauphine" twin (LL) which are identified by the special combination of trapezohedral faces. (source of the pictures: W. Kleber, An Introduction to Crystallography, 1970)*

The macroscopic identification of single crystals of α–quartz, whether it is left handed "L" or right handed "R", can be distinguished from the morphology by the orientation of trapezohedral faces (*Figure 5.1a*) with respect to the trigonal pyramidal faces of the investigated individual. Similarly, whether a crystal is twinned "LL, RR…LLRR" (*Figure 5.1b*) can be seen by the combination of trapezohedral faces as observed for "Brazilian" twin (LR) and "Dauphine" twin (LL).

Borophosphates of compositions $M^{III}(H_2O)_2[BP_2O_8]\cdot H_2O$ (M^{III} = Fe, Sc, In) and $M^{I}M^{III}(H_2O)_2[BP_2O_8]\cdot H_2O$ (M^{I} = Na–Cs; M^{II} = Mn–Zn) crystallize in the chiral space groups $P6_522$ and $P6_122$, respectively [67, 69, 111] (*Figure 5.2*). The main structural features are the loop–branched helical $_\infty^1[BP_2O_8]^{3-}$ chains built of alternating borate and phosphate tetrahedra connected *via* common corners. The arrangement around a six–fold screw axis forms helices which are "left–handed" (6_5) or "right–handed" (6_1). The SEM image of single crystals of $Sc(H_2O)_2[BP_2O_8]\cdot H_2O$ (*Figure 5.2*) led to the question whether a macroscopic identification (L or R and twins LL, RR…LLRR, respectively) is possible by the examination of the face combinations of the individual crystals.

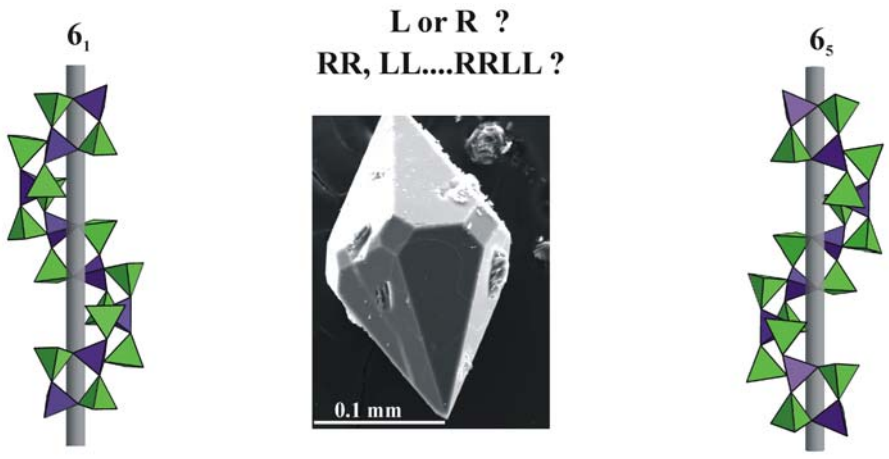

Figure 5.2: *Anionic partial structure of helical borophosphates (6_1 or 6_5) forms loop–branched helical $_\infty^1[BP_2O_8]^{3-}$ chains built of borate (blue) and phosphate (green) tetrahedra connected via common corners. A selected SEM image of a single crystal of $Sc(H_2O)_2[BP_2O_8]\cdot H_2O$ is shown in the middle.*

The aim of this project was to investigate the shape development of the well known and well defined helical borophosphates $M^{III}(H_2O)_2[BP_2O_8]\cdot H_2O$ (M^{III} = Sc, In) by

careful variation of the growth conditions (pressure, temperature, starting composition and time) [67, 111]. Further, to examine the crystal morphologies.

5.3.1 Synthesis

Single crystals of $M^{III}(H_2O)_2[BP_2O_8]\cdot H_2O$ (M^{III} = Sc, In) were synthesized under mild hydrothermal conditions by varying the temperature (120 – 240 ºC), the filling degree (30 – 80 %), the composition (Sc / In : B : P = 1: 2 : 6 – 3 : 4 : 8) and the reaction time (1 – 20 days). The reaction conditions were optimized and the growth of the single crystals was studied in detail. The optimized method of synthesis can be described as follows.

$Sc(H_2O)_2[BP_2O_8]\cdot H_2O$ was grown from a mixture of 0.750 g, Sc_2O_3, 0.897 g H_3BO_3 and 2.508 g H_3PO_4 (molar ratio of Sc : B : P = 3 : 4 : 6) homogenized in 10 ml water and acidified with 1.5 ml of HCl (37 %). By evaporating the water, the mixture was concentrated to form a colorless non–transparent gel that was then treated hydrothermally at 170 ºC for 1 – 20 days (filling degree of the autoclave: 30 %). Similarly, $In(H_2O)_2[BP_2O_8]\cdot H_2O$ was obtained hydrothermally from a mixture of 2.993 g of In_2O_3, 2.000 g H_3BO_3 and 6.2151 g H_3PO_4 which was homogenized (molar ratio 1 : 2 : 6) in 5 ml of water and then treated hydrothermally at 170 ºC from 1 – 20 days (pH = 1, degree of filling 70 %).

After reaction times of 1 to 20 days, the autoclave was allowed to cool down to ambient temperature, and the raw product was separated from the mother liquor by vacuum filtration. The transparent and colorless crystalline samples were washed with hot water, filtered, and washed again with acetone before they were dried in air at 60 ºC. The X–ray powder patterns of these samples showed that there is no evidence of any crystalline impurity even after 20 days of hydrothermal treatement (*Figure 5.3* and *Figure 5.4*).

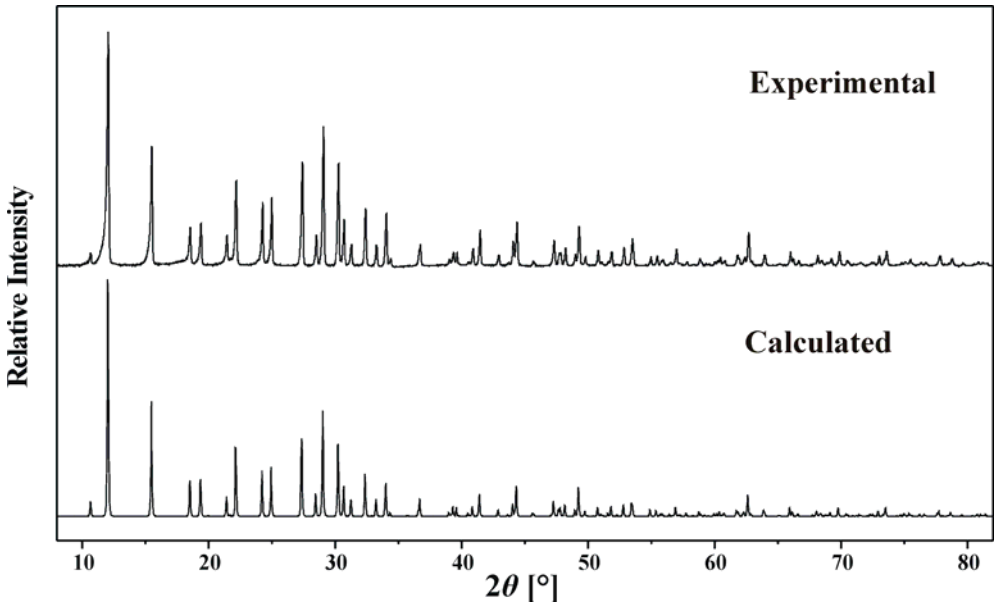

Figure 5.3: *Observed (background subtracted) and calculated powder X–ray diffraction patterns of* $Sc(H_2O)_2[BP_2O_8]\cdot H_2O$ *(Cu* $K_{\alpha 1}$*–radiation)*

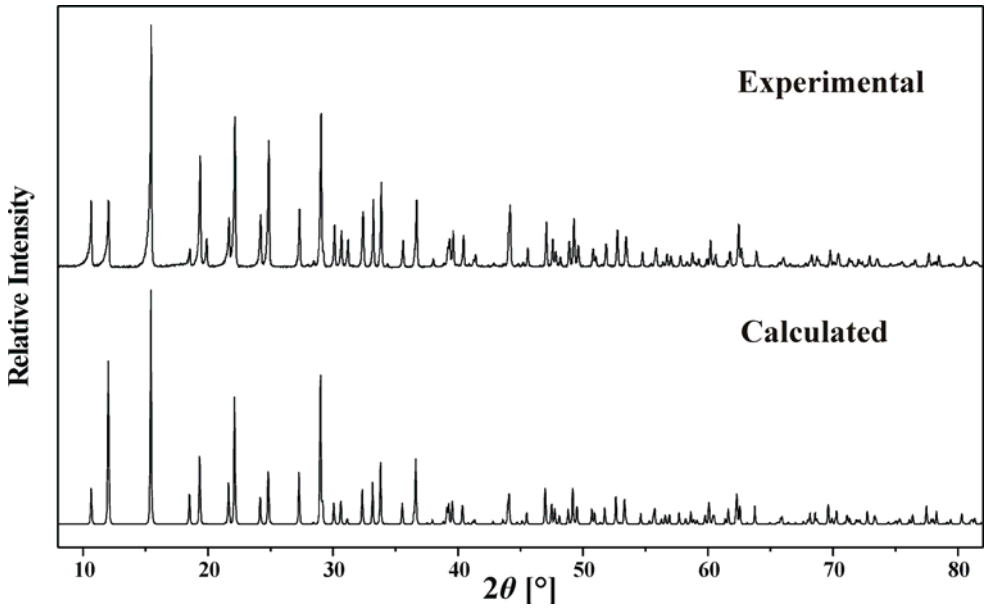

Figure 5.4: *Observed (background subtracted) and calculated powder X–ray diffraction patterns of* $In(H_2O)_2[BP_2O_8]\cdot H_2O$ *(Cu* $K_{\alpha 1}$*–radiation)*

5.3.2 Growth and Morphology

The change in the crystal morphology for both compounds was investigated by scanning electron microscopy (SEM). After each experiment (1 – 20 days) five well developed crystals were picked up from each batch and subjected to SEM analyses and respective images of the single crystals are shown in *Figure 5.5* ($Sc(H_2O)_2[BP_2O_8]\cdot H_2O$ **)** and in *Figure 5.6* ($In(H_2O)_2[BP_2O_8]\cdot H_2O$).

The shape development of single crystals of $Sc(H_2O)_2[BP_2O_8]\cdot H_2O$ and $In(H_2O)_2[BP_2O_8]\cdot H_2O$ can be described by four stages (*Table 5.2*). In the first stage the crystals are close to ideal hexagonal bipyramids (1 – 4 d, 0.05 – 0.01 mm). In the second stage a new face appears (*Figure 5.5* and in *Figure 5.6*) between two bipyramidal faces (4 – 8 d, 0.01 – 0.02 mm). The third stage shows that the new face grows with increasing size of the crystals (8 – 12d, 0.02 – 0.05 mm). After that the new face does no longer grow also the size of the crystal increases (12 – 16 d, 0.02 – 0.05 mm). Finally the new face starts to disappear and hexagonal bipyramids are formed without having a mirror plane perpendicular to the hexagonal axis (16 – 20 d, 0.05 – 0.1 mm). The reactions were also carried out for longer reaction periods (till 30 days) with neither change in morphology nor in size.

Table 5.2: *Stages involved in growth of single crystals of helical borophosphates*

Stages	Time (d)	Size (mm)	Morphology
Stage 1	1 – 4	0.05 – 0.01	Ideal hexagonal bipyramids (6/m)
Stage 2	4 – 8	0.01 – 0.02 mm	Hexagonal bipyramids with appearance of a new face
Stage 3	8 – 16	0.02 – 0.05 mm	Hexagonal bipyramids with growing of the new face
Stage 4	16 – 20	0.05 – 0.1 mm	Hexagonal bipyramids without the new face ($\neq$ 6/m)

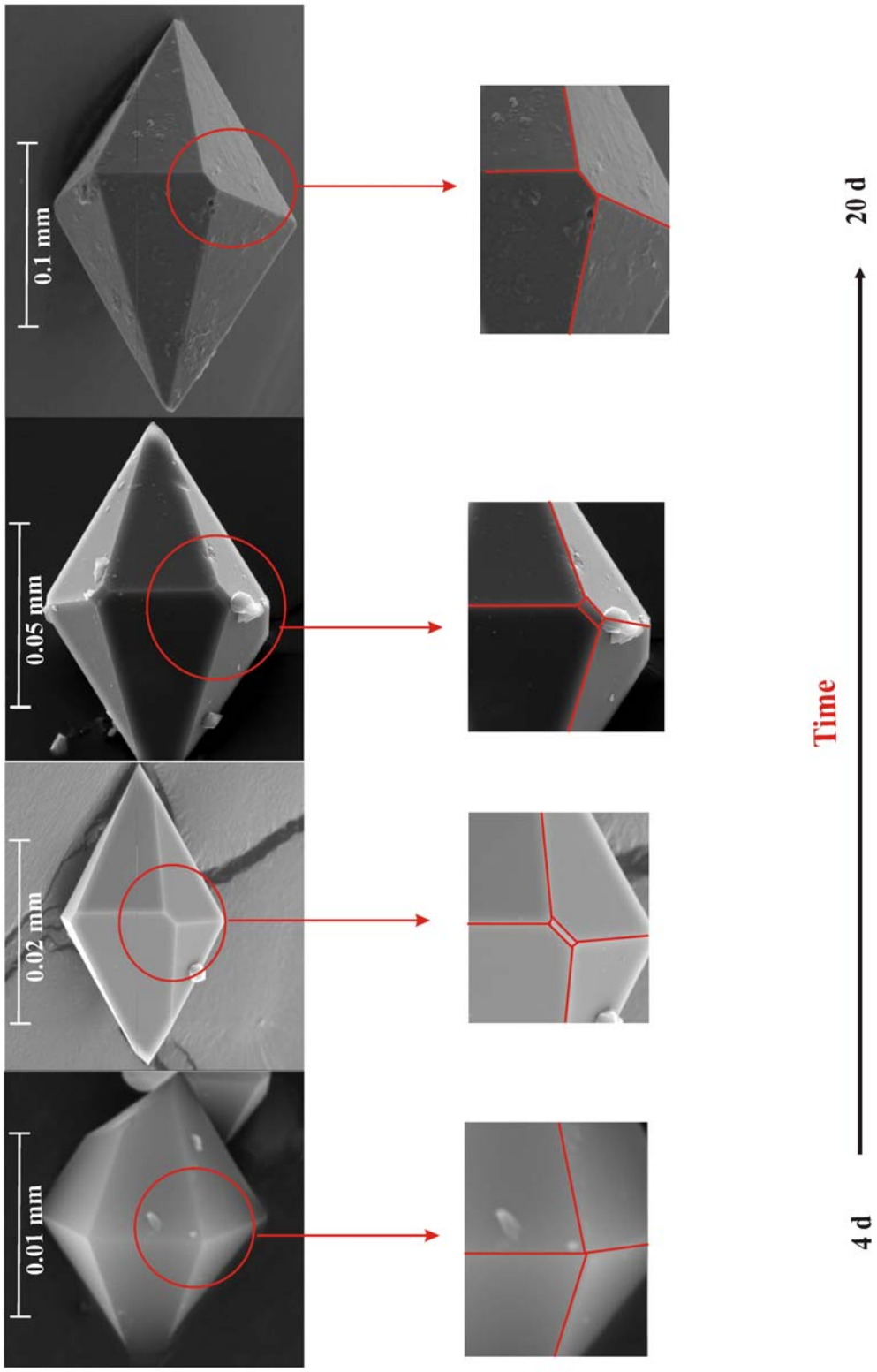

Figure 5.5: *Change in the morphology (SEM images) of single crystals of* $Sc(H_2O)_2[BP_2O_8]\cdot H_2O$ *with time (The edges of the growing face are outlined with red color).*

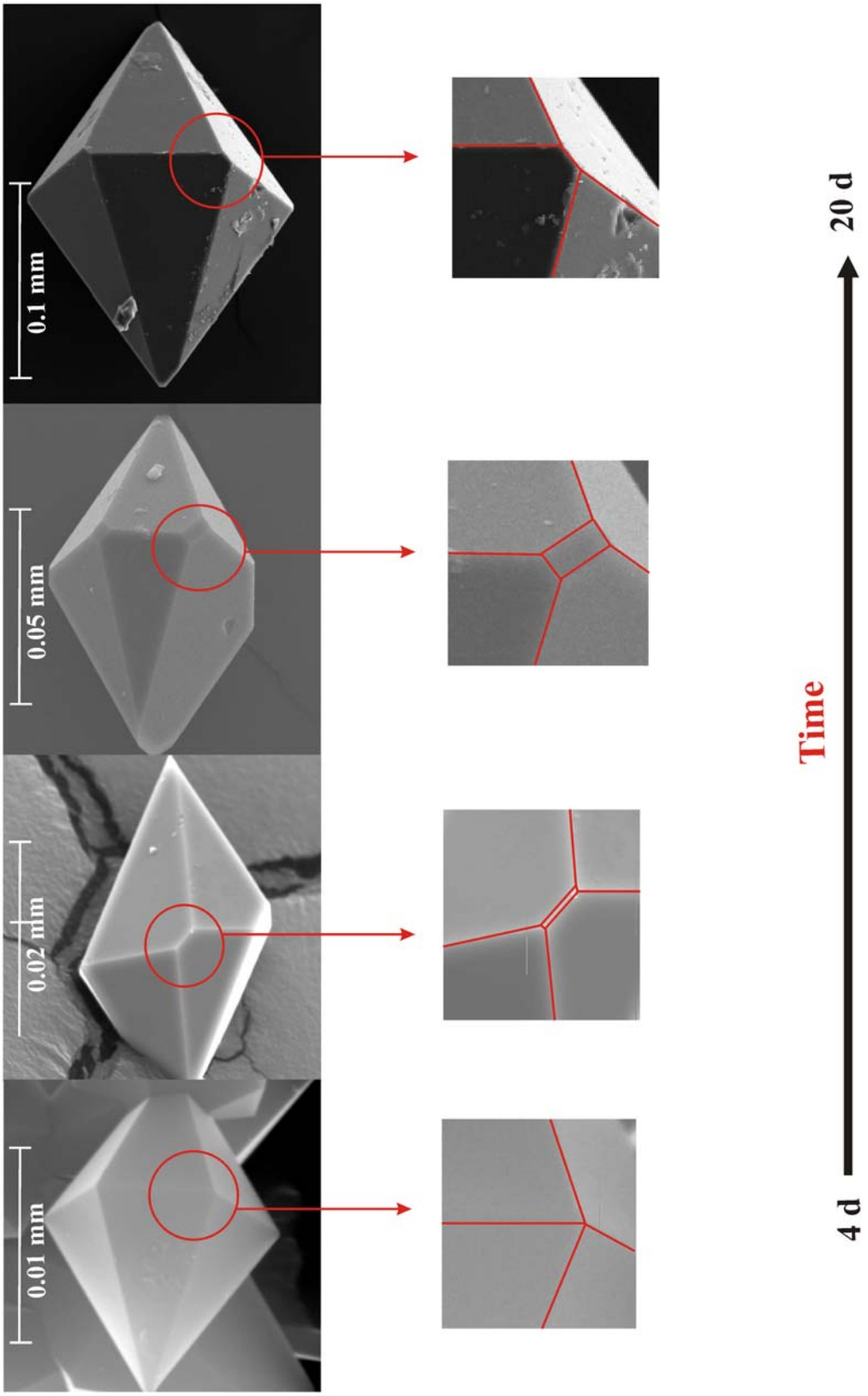

Figure 5.6: *Change in the morphology (SEM images) of single crystals of* $In(H_2O)_2[BP_2O_8]\cdot H_2O$ *with time (The edges of the growing face are outlined with red color).*

5.3.3 Conclusion

Single crystals of $Sc(H_2O)_2[BP_2O_8]\cdot H_2O$ and $In(H_2O)_2[BP_2O_8]\cdot H_2O$ were prepared under mild hydrothermal conditions by variation of temperature, filling degree, starting composition and reaction time. Morphology studies of crystals showed that a new face appears close to the equatorial area. The noticeable point is that (from the morphology) the symmetry of the starting crystal appears to be 6/m. Further, the crystal continues to grow with the additional new face. The main drawback of this study was that no bigger crystals could be obtained and that no clear indication for a chance to distinguish between L and R was found. So, we did not try to really index the faces or even did not investigate the 6/m hexagonal bipyramids (6/m morphology "against" chirality).

5.4 Infrared Spectroscopy

5.4.1 $M^{I}Sc[BP_2O_8(OH)]$ (M^{I} = K, Rb).

Infrared spectra of $M^{I}Sc[BP_2O_8(OH)]$ (M^{I} = K, Rb) were recorded (*Figure 5.7*) and the band at 3594 cm^{-1} confirmed the presence of O—H groups (O—H stretching vibration) in the crystal structures of $M^{I}Sc[BP_2O_8(OH)]$ (M^{I} = K, Rb).

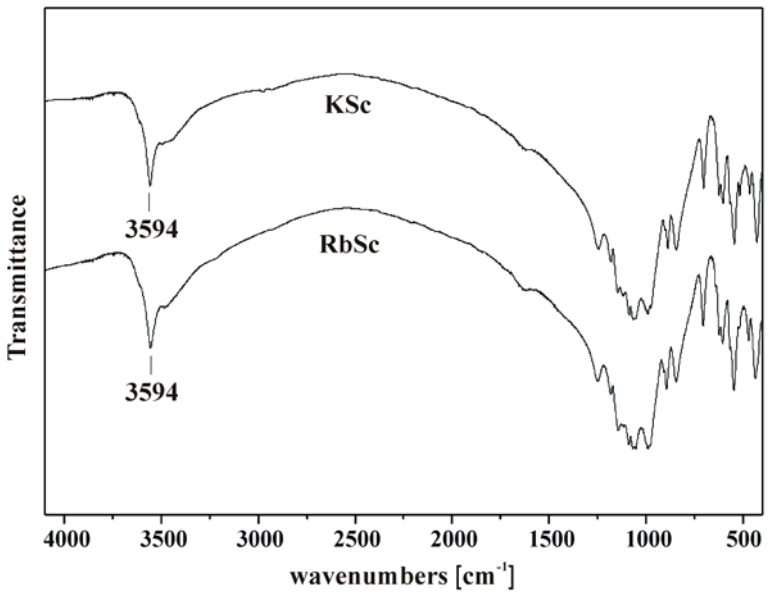

Figure 5.7: *Infrared spectra of $M^{I}Sc[BP_2O_8(OH)]$ (M^{I} = K, Rb) in the range of 4000 – 400 cm^{-1} confirming the presence of O—H groups (3594 cm^{-1}, O—H stretching vibration) in the crystal structures.*

5.4.2 $CsSc[B_2P_3O_{11}(OH)_3]$

The infrared spectra of $CsSc[B_2P_3O_{11}(OH)_3]$ is shown in *Figure 5.8*. The observed broad IR absorption band at 3250 cm^{-1} clearly indicates the presence of O—H groups (O—H stretching vibration).

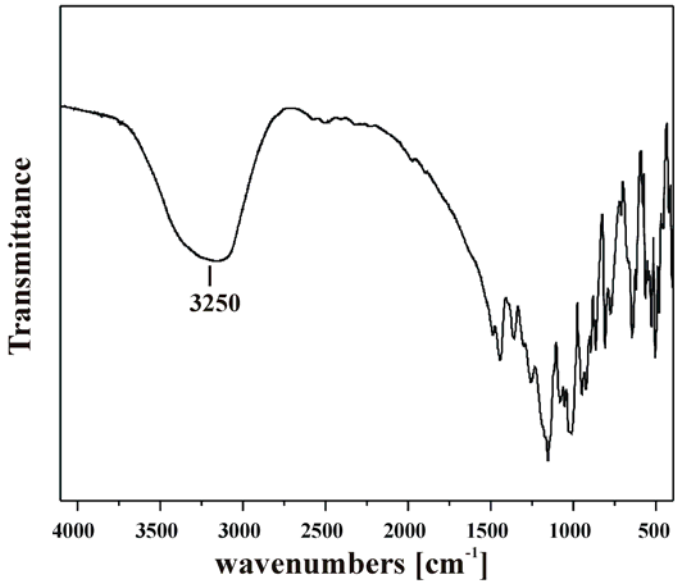

Figure 5.8: *IR spectra shows a characteristic absorption band at 3250 cm^{-1}, which indicated the presence of O—H groups (O—H stretching vibration) in the crystal structure of $CsSc[B_2P_3O_{11}(OH)_3]$*

5.4.3 $Li_2Sc[(PO_4)(HPO_4)]$ and $M^ISc(HPO_4)_2$ (M^I = K, Rb, Cs, NH_4)

The infrared spectra of $Li_2Sc[(PO_4)(HPO_4)]$ and $M^ISc(HPO_4)_2$ (M^I = K, Rb, Cs, NH_4) are shown in *Figure 5.9*. The observed broad infra red absorption band at 3430 – 3564 cm^{-1} clearly indicates the presence of O—H groups (O—H stretching vibration).

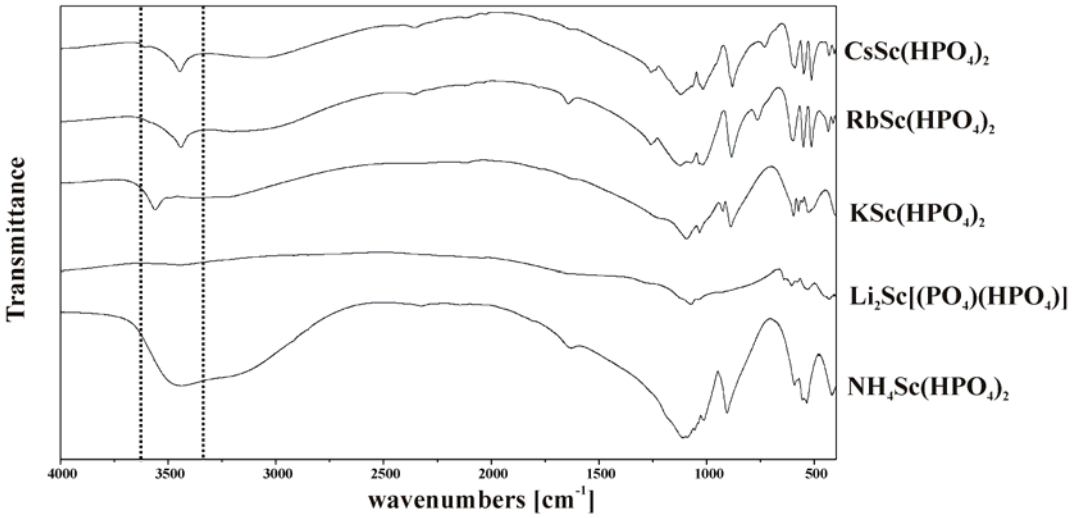

Figure 5.9: *IR spectra shows characteristic absorption bands in the range of 3430 – 3564 cm^{-1}, which indicated the presence of O—H groups in the crystal structures of $Li_2Sc[(PO_4)(HPO_4)$ and $M^ISc(HPO_4)_2$ (M^I = K, Rb, Cs, NH_4)*

5.4.4 $M^{II}(H_2O)_2[B_2P_2O_8(OH)_2]\cdot H_2O$ (M^{II} = Fe, Co, Ni)

The infrared spectra of $M^{II}(H_2O)_2[B_2P_2O_8(OH)_2]\cdot H_2O$ (M^{II} = Fe, Co, Ni) are shown in *Figure 5.10*. The observed broad IR absorption band at 1628 cm^{-1} (H_2O deformation) and 3594 cm^{-1} (O—H stretching) clearly indicates the presence of water in the crystal structures.

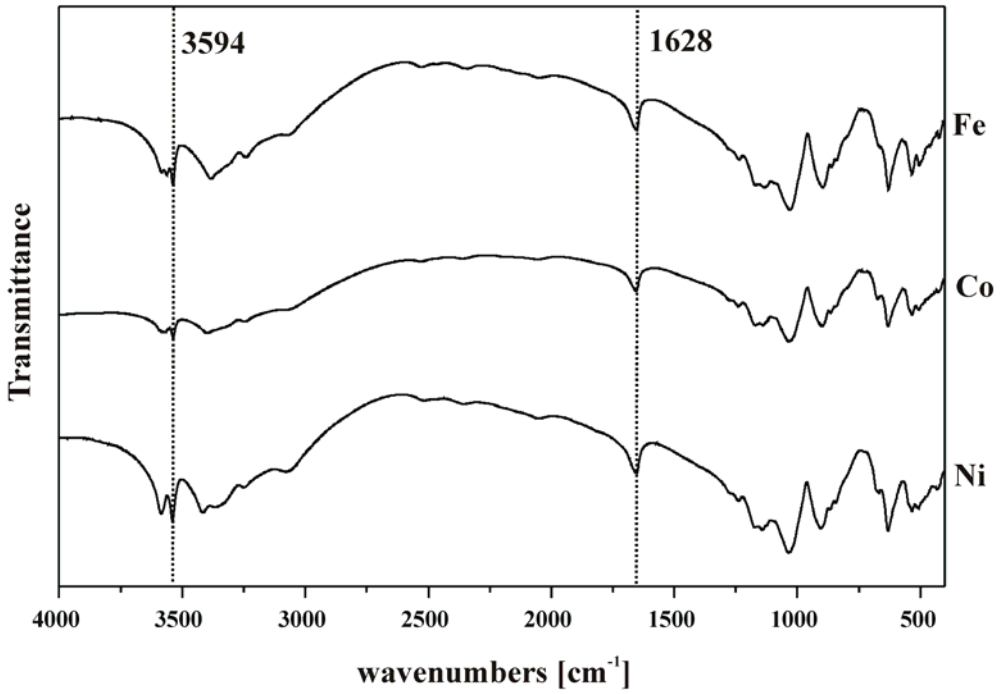

Figure 5.10: *IR spectra of $M^{II}(H_2O)_2[B_2P_2O_8(OH)_2]\cdot H_2O$ (M^{II} = Fe, Co, Ni) shows the presence of water by characteristic absorption bands at about 1628 cm^{-1} (H_2O deformation) and between 3000 and 3600 cm^{-1} (O—H stretching).*

5.4.5 $FeCo(H_2O)[BP_3O_9(OH)_4]$ and $Fe_{1.3}Co_{0.7}[P_2O_7]\cdot 2H_2O$

The IR spectra of $FeCo(H_2O)[BP_3O_9(OH)_4]$ and $Fe_{1.3}Co_{0.7}[P_2O_7]\cdot 2H_2O$ are shown in *Figure 5.11*. The characteristic absorption bands at 3250 – 3630 cm^{-1}, indicates the presence of O—H groups (O—H stretching vibration) in the crystal structures. In addition to this an absorption band at 1635 cm^{-1} confirms the deformation of H_2O.

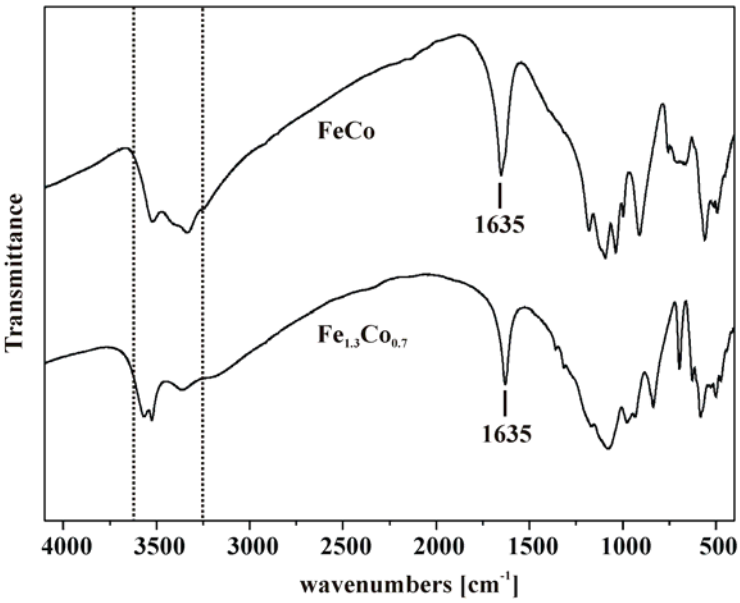

Figure 5.11: *IR spectra of $FeCo(H_2O)[BP_3O_9(OH)_4]$ and $Fe_{1.3}Co_{0.7}[P_2O_7]\cdot 2H_2O$: The characteristic absorption bands at 3250 – 3630 cm^{-1}, indicates the presence of O—H groups (O—H stretching vibration). The H_2O deformation vibration can be seen at 1635 cm^{-1}.*

Programs

[P1] ICSD, Inorganic Crystal Structure Database, Fachinformationszentrum (FIZ) Karlsruhe, **2008**.

[P2] PDF, Powder Diffraction File, The International Center for Diffraction Data, U.S.A. **2007**.

[P3] STOE Win XPOW, Visual XPOW software Package for STOE Powder Diffraction System, Version 1.2, Stoe & Cie GmbH, Darmstadt, **2001**.

[P4] WINCSD, Crystal Structure Determination Program Package, L. G. Akselrud, P. Y. Zavalii,Y. Grin, V. K. Pecharski, B. Baumgartner, E. Wölfel, *Mater. Sci. Forum**,** 335*, 133-136, **1993**.

[P5] SHELXS–97/2, A Computer Program for Crystal Structure Solution, G. M. Sheldrick, Universität Göttingen, **1997**.

[P6] SHELXL–97/2. Program for Crystal Structure Refinement, Universität Göttingen, **1997**.

[P7] WinGX 1.70.01 System Program, L. J. Farrugia, Universität Glasgow, **1997**.

[P8] PLATON – A Multipurpose Cyrstallographic Tool, Utrech University, **2000**. A. L. Spek, *Acta. Crystallogr. A 46*, C34, **1990**.

[P9] DIAMOND–Visual Crystal Sturcture Information System (Version 3.1f), Brandenburg, M. Berndt, Crystal Impact GbR, Bonn, **2007**.

References

[1] P. C. Burns
Borate Clusters and Fundamental Building Blocks Containing Four Polyhedra: Why Few Clusters are Utilized as Fundamental Building Blocks of Structures
Can. Mineral. **1995**, *33*, 1167-1176.

[2] P. C. Burns, J. D. Grice, F. C. Hawthorne
Borate Minerals.1. Polyhedral Clusters and Fundamental Building Blocks
Can. Mineral. **1995**, *33*, 1131-1151.

[3] C. T. Chen, Y. B. Wang, B. C. Wu, K. C. Wu, W. L. Zeng, L. H. Yu
Design and Synthesis of An Ultraviolet-Transparent Nonlinear-Optical Crystal $Sr_2Be_2B_2O_7$
Nature **1995**, *373*, 322-324.

[4] C. L. Christ, J. R. Clark
Crystal-Chemical Classification of Borate Structures with Emphasis on Hydrated Borates
Phys. Chem. Miner. **1977**, *2*, 59-87.

[5] J. D. Grice, P. C. Burns, F. C. Hawthorne
Borate Minerals. II. A Hierarchy of Structures Based Upon the Borate Fundamental Building Block
Can. Mineral. **1999**, *37*, 731-762.

[6] A. K. Cheetham, G. Férey, T. Loiseau
Open-framework Inorganic Materials
Angew. Chem. Int. Ed. Engl. **1999**, *38*, 3268-3292.

[7] R. Kniep, A. Wilms, M. Steffen
Structural Chemistry of Acid Aluminum Phosphates
Z. Kristallogr. **1979**, *149*, 142-143.

[8] R. Kniep
Ortho-Phosphates in the Ternary-System Al_2O_3-P_2O_5-H_2O
Angew. Chem. Int. Ed. Engl. **1986**, *25*, 525-534.

[9] J. M. Thomas, R. Raja, G. Sankar, R. G. Bell
Molecular Sieve Catalysts for the Regioselective and Shape-Selective Oxyfunctionalization of Alkanes in Air
Acc. Chem. Res. **2001**, *34*, 191-200.

[10] J. H. Yu, R. R. Xu
Rich Structure Chemistry in the Aluminophosphate Family
Acc. Chem. Res. **2003**, *36*, 481-490.

[11] R. Kniep, G. Gözel, B. Eisenmann, C. Röhr, M. Asbrand, M. Kizilyalli
Borophosphates - A Neglected Class of Compounds: Crystal Structures of $M^{II}[BPO_5]$ (M^{II}=Ca, Sr) and $Ba_3[BP_3O_{12}]$
Angew. Chem. Int. Ed. Engl. **1994**, *33*, 749-751.

[12] R. Kniep, H. Engelhardt, C. Hauf
A First Approach to Borophosphate Structural Chemistry
Chem. Mater. **1998**, *10*, 2930-2934.

[13] C. Hauf, T. Friedrich, R. Kniep
Crystal-Structure of Pentasodium Catena-(Diborato-Triphosphate), $Na_5[B_2P_3O_{13}]$
Z. Kristallogr. **1995**, *210*, 446-446.

[14] C. Hauf
Borophosphate der Alkalimetalle: Intermediäre Phasen in den Systemen M_2O-B_2O_3-P_2O_5-H_2O
Dissertaion, Technische Hochschule Darmstadt, **1997**.

[15] J.-X. Mi, J.-T. Zhao, S. Y. Mao, Y.-X. Huang, H. Engelhardt, R. Kniep
Crystal Structure of Dichromium Monoborotriphosphate, $Cr_2[BP_3O_{12}]$
Z. Kristallogr. - New Cryst. Struct. **2000**, *215*, 201-202.

[16] S. L. Pan, Y. C. Wu, P. Z. Fu, G. C. Zhang, Z. H. Li, C. X. Du, C. T. Chen
Growth, Structure, and Properties of Single Crystals of $SrBPO_5$
Chem. Mater. **2003**, *15*, 2218-2221.

[17] G. F. Wang, Y. C. Wu, P. Z. Fu, X. Y. Liang, Z. Y. Xu, C. T. Chen
Crystal Growth and Properties of β-Zn_3BPO_7
Chem. Mater. **2002**, *14*, 2044-2047.

[18] G. F. Wang, Y. C. Wu, H. J. Liu, P. Z. Fu, S. L. Pan, G. C. Zhang, C. T. Chen
Crystal Growth of Magnesium Zinc Borophosphate
Chem. Lett. **2002**, *31*, 620-621.

[19] Y. C. Wu, G. F. Wang, P. Z. Fu, X. Y. Liang, Z. Y. Xu, C. T. Chen
A New Nonlinear Optical Crystal β-Zn_3BPO_7
J. Cryst. Growth **2001**, *229*, 205-207.

[20] S. Gao, J. B. Moffat
The Isomerization of 1-Butene on Stoichiometric and Nonstoichiometric Boron Phosphate: The Dependence of the Acidity on Stoichiometry
J. Catal. **1998**, *180*, 142-148.

[21] G. J. Hutchings, I. D. Hudson, D. Bethell, D. G. Timms
Dehydration of 2-Methylbutanal and Methyl Isopropyl Ketone to Isoprene

Using Boron and Aluminium Phosphate Catalysts
J. Catal. **1999**, *188*, 291-299.

[22] Q. H. Zeng, N. Kilah, M. Riley
The Luminescence of Sm^{2+}-in Alkaline Earth Borophosphates
J. Lumin. **2003**, *101*, 167-174.

[23] J.-T.Zhao, C.-Z.Duan
Inorganic Chemistry in Focus III
Wiley InterScience, **2006**.

[24] H. B. Liang, Q. Su, Y. Tao, T. D. Hu, T. Liu, S. L. E. Shulin
XAFS at Eu-L-3 Edge and UV-VUV Excited Luminescence of Europium Doped Strontium Borophosphate Prepared in Air
J. Phys. Chem. Solids **2002**, *63*, 719-724.

[25] R. Ternane, M. T. Cohen-Adad, G. Panczer, C. Goutaudier, C. Dujardin, G. Boulon, N. Kbir-Ariguib, M. Trabelsi-Ayedi
Structural and Luminescent Properties of New Ce^{3+} Doped Calcium Borophosphate with Apatite Structure
Solid State Sci. **2002**, *4*, 53-59.

[26] M. Zhou, K. Li, D. Shu, B. D. Sun, J. Wang
Corrosion Resistance Properties of Enamels with High B_2O_3-P_2O_5 Content to Molten Aluminum
Mat. Sci. Eng. A-Strcut **2003**, *346*, 116-121.

[27] D. Koch
Untersuchungen zur Darstellung und Strukturchemie von Borophosphaten sowie zur Beschichtung von metallischen Substraten in Metallborat-Metallphosphat-Lösungen
Dissertaion, Technische Universität Darmstadt, **2002**.

[28] K.Götzman, D.Karlheinz, N.Hans-Dieter, G.Talf
Patent CA, C09K015, **1996**.

[29] B. Ewald, Y.-X. Huang, R. Kniep
Structural Chemistry of Borophosphates, Metalloborophosphates, and Related Compounds
Z. Anorg. Allg. Chem. **2007**, *633*, 1517-1540.

[30] B. Ewald, Yu. Prots, P. W. Menezes, S. Natarajan, H. Zhang, R. Kniep
Chain Structures in Alkali Metal Borophosphates: Synthesis and Characterization of $K_3[BP_3O_9(OH)_3]$ and $Rb_3[B_2P_3O_{11}(OH)_2]$
Inorg. Chem. **2005**, *44*, 6431-6438.

[31] A. Baykal, M. Kizilyalli, M. Toprak, R. Kniep
Hydrothermal and Microwave Synthesis of Boron Phosphate, BPO_4
Tur. J. Chem. **2001**, *25*, 425-432.

[32] C. Hauf, A. Yilmaz, M. Kizilyalli, R. Kniep
Borophosphates: Hydrothermal and Microwave-assisted Synthesis of $Na_5[B_2P_3O_{13}]$
J. Solid State Chem. **1998**, *140*, 154-156.

[33] A. F. Ali, P. Mustarelli, E. Quartarone, C. Tomasi, P. Baldini, A. Magistris
Sol-gel Lithium Borophosphates
J. Mater. Res. **1999**, *14*, 1510-1515.

[34] R. P. Bontchev, S. C. Sevov
$Co_5BP_3O_{14}$: The First Borophosphate with Planar BO_3 Groups Connected to PO_4 Tetrahedra
Inorg. Chem. **1996**, *35*, 6910-6913.

[35] M. Schmidt, B. Ewald, Yu. Prots, R. Cardoso-Gil, M. Armbrüster, I. Loa, L. Zhang, Y.-X. Huang, U. Schwarz, R. Kniep
Growth and Characterization of BPO_4 Single Crystals
Z. Anorg. Allg. Chem. **2004**, *630*, 655-662.

[36] A. Rabenau
The Role of Hydrothermal Synthesis in Preparative Chemistry
Angew. Chem. Int. Ed. Engl. **1985**, *24*, 1026-1040.

[37] S. H. Feng, R. R. Xu
New Materials in Hydrothermal Synthesis
Acc. Chem. Res. **2001**, *34*, 239-247.

[38] T. K. Pavlushkina, O. A. Gladushko
Synthesis and Properties of Sodium Borophosphate and Sodium Alumophosphate Glasses
Glass and Ceramics **2000**, *57*, 201-204.

[39] G. Sedmale, J. Vaivads, U. Sedmalis, V. O. Kabanov, O. V. Yanush
Formation of Borophosphate Glass Structure Within the System Bao-B_2O_3-P_2O_5
J. Non-Crys. Solids **1991**, *129*, 284-291.

[40] S. Natarajan, S. Mandal
Open-framework Structures of Transition Metal Compounds
Angew. Chem. Int. Ed. Engl. **2008**, *47*, 4798-4828.

[41] I. Boy
Zur Kristallchemie intermediärer Phasen der Systeme M_2O / MO / M_2O_3-

B_3O_3-P_2O_5-H_2O
Dissertaion, Technische Universität Darmstadt, **1999**.

[42] H. Engelhardt
Darstellung und Strukturchemie von quarternären Borophosphaten der schweren Alkalimetalle (Rb, Cs)
Dissertaion, Technische Universität Darmstadt, **2000**.

[43] G. Schäfer
Templatgesteuerte Synthesen von Borophosphaten
Dissertaion, Technische Universität Darmstadt, **2001**.

[44] Y.-X. Huang
Preparation and Characterization of Templated Borophosphate and Metalloborophosphates
Dissertaion, Technische Universität Dresden, **2004**.

[45] B. Ewald
Borophosphate der Haupt- und Nebengruppenmetalle: Synthese Charakterisierung und Strukurchemische Klassifizierung
Dissertaion, Technische Universität Dresden, **2006**.

[46] P. K. S. Gupta, G. H. Swihart, R. Dimitrijevic, M. B. Hossain
The Crystal Structure of Lüneburgite, $Mg_3(H_2O)_6(B_2(OH)_6(PO_4)_2$
Am. Mineral. **1991**, *76*, 1400-1407.

[47] P. B. Moore, S. Ghose
Novel Face-Sharing Octahedral Trimer in the Crystal Structure of Seamanite
Am. Mineral. **1971**, *56*, 1527-1538.

[48] I. Boy, G. Cordier, B. Eisenmann, R. Kniep
Oligomeric Tetrahedral Anions in Borophosphates: Synthesis and Crystal Structures of $NaFe[BP_2O_7(OH)_3]$ and $K_2Fe_2[B_2P_4O_{16}(OH)_2]$
Z. Naturforsch. , B: Chem. Sci. **1998**, *53*, 165-170.

[49] L. R. Zhang, H. Zhang, H. Borrmann, R. Kniep
Crystal Structure of Sodium Vanadium(III) (Monohydrogenmonophosphate-Dihydrogenmonoborate-Monophosphate), $NaV[BP_2O_7(OH)_3]$
Z. Kristallogr. - New Cryst. Struct. **2002**, *217*, 477-478.

[50] R. P. Bontchev, J. Do, A. J. Jacobson
Synthesis and Characterization of a Borophosphate Anion Containing a Single Vanadium Atom: $[N_2C_6H_{14}]_2VO(PO_3OH)_4(B_3O_3OH)\cdot 4H_2O$
Inorg. Chem. **1999**, *38*, 2231-2233.

[51] H. Engelhardt, H. Borrmann, W. Schnelle, R. Kniep
The First Vanadium(III) Borophosphate: Synthesis and Crystal Structure of

$CsV_3(H_2O)_2[B_2P_4O_{16}(OH)_4]$
Z. Anorg. Allg. Chem. **2000**, *626*, 1647-1652.

[52] W. Liu, Y.-X. Huang, Yu. Prots, W. Schnelle, H. Rosner, R. Kniep
$LiCu_2[BP_2O_8(OH)_2]$: A Lithium Copper Borophosphate with Chains of Distorted CuO_5 Square Pyramids
Z. Anorg. Allg. Chem. **2006**, *632*, 2143.

[53] R. P. Bontchev, J. Do, A. J. Jacobson
The Vanadium(V) Borophosphate $(NH_4)_5[V_3BP_3O_{19}]\cdot H_2O$
Inorg. Chem. **2000**, *39*, 4179-4181.

[54] M. Yang, J. H. Yu, L. Shi, P. Chen, G. H. Li, Y. Chen, R. R. Xu
Synthesis, Structure, and Magnetic Property of a New Open-framework Manganese Borophosphate, $(NH_4)_4[Mn_9B_2(OH)_2(HPO_4)_4(PO_4)_6]$
Chem. Mater. **2006**, *18*, 476-481.

[55] I. Boy, G. Schäfer, R. Kniep
$(Ni_{3-x}Mg_x)[B_3P_3O_{12}(OH)_6]\cdot 6\ H_2O$ (x = 1.5): A Novel Borophosphate-hydrate Containing Isolated Six-membered Rings of Tetrahedra
Z. Anorg. Allg. Chem. **2001**, *627*, 139-143.

[56] Z. S. Lin, Y.-X. Huang, Yu. Prots, J.-T. Zhao, R. Kniep
Crystal Structure of Potassium Vanadium (Monophosphate-Hydrogenmonoborate-Monophosphate), $KV[BP_2O_8(OH)]$
Z. Kristallogr. - New Cryst. Struct. **2008**, *223*, 323-324.

[57] A. Guesmi, A. Driss
Synthesis, Characterization and Crystal Structure of a New Cobalt Borophosphate, $NaCoH_2BP_2O_9$
Adv. Eng. Mat. **2004**, *6*, 840-842.

[58] I. Boy, G. Cordier, R. Kniep
Crystal Structure of Tetrasodium Tricopper(II) (Diboro-Diphosphate-Bis(Monohydrogenphosphate)) Bis(Monohydrogenphosphate), $Na_4Cu_3[B_2P_4O_{15}(OH)_2]\cdot 2HPO_4$
Z. Kristallogr. - New Cryst. Struct. **1998**, *213*, 29-30.

[59] I. Boy, G. Cordier, R. Kniep
Oligomeric Tetrahedral Anions in Borophosphates: Six-membered Rings with Open and Cyclic Phosphate Branchings in the Crystal Structure of $K_6Cu_2[B_4P_8O_{28}(OH)_6]$
Z. Naturforsch. , B: Chem. Sci. **1998**, *53*, 1440-1444.

[60] I. Boy, C. Hauf, R. Kniep
$Fe[B_2P_2O_7(OH)_5]$: A New Borophosphate Containing Non-branched

Tetrahedral Vierer-Einfach Chains
Z. Naturforsch. , B: Chem. Sci. **1998**, *53*, 631-633.

[61] Y.-X. Huang, B. Ewald, W. Schnelle, Yu. Prots, R. Kniep
Chirality and Magnetism in A Novel Series of Isotypic Borophosphates: $M^{II}[BPO_4(OH)_2]$ (M^{II} = Mn, Fe, Co)
Inorg. Chem. **2006**, *45*, 7578-7580.

[62] T. Yang, J. Ju, F. H. Liao, J. Sasaki, N. Toyota, J. H. Lin
Chirality and Ferromagnetism in $NiBPO_4(OH)_2$ Containing Helix Edge-sharing NiO_6 Chains
J. Solid State Chem. **2008**, *181*, 1110-1115.

[63] R. Kniep, I. Boy, H. Engelhardt
$RbFe[BP_2O_8(OH)]$: A New Borophosphate Containing Open-branched Tetrahedral Vierer-Einfach Chains
Z. Anorg. Allg. Chem. **1999**, *625*, 1512-1516.

[64] H. Engelhardt, H. Borrmann, R. Kniep
Crystal Structure of Rubidium Vanadium(III) Catena- [Monohydrogen-Monoborate-Bis(Monophosphate)], $RbV[BP_2O_8(OH)]$
Z. Kristallogr. - New Cryst. Struct. **2000**, *215*, 203-204.

[65] H. Engelhardt, R. Kniep
Crystal Structure of Caesium Iron(III) Catena-[Monohydrogenmonoborate-Bis(Monophosphate)], $CsFe[BP_2O_8(OH)]$
Z. Kristallogr. - New Cryst. Struct. **1999**, *214*, 443-444.

[66] M. Kritikos, E. Wikstad, K. Wallden
Hydrothermal Synthesis, Characterization and Magnetic Properties of Three Isostructural Chain Borophosphates; $NH_4M^{III}[BP_2O_8(OH)]$ with M^{III} = V or Fe and $NH_4(Fe_{0.53}V_{0.47})[BP_2O_8(OH)]$
Solid State Sci. **2001**, *3*, 649-658.

[67] B. Ewald, Yu. Prots, C. Kudla, D. Grüner, R. Cardoso-Gil, R. Kniep
Crystal Structure and Thermochemical Properties of a First Scandium Borophosphate, $Sc(H_2O)_2[BP_2O_8]\cdot H_2O$
Chem. Mater. **2006**, *18*, 673-679.

[68] A. Yilmaz, X. H. Bu, M. Kizilyalli, G. D. Stucky
$Fe(H_2O)_2[BP_2O_8]\cdot H_2O$, A First Zeotype Ferriborophosphate with Chiral Tetrahedral Framework Topology
Chem. Mater. **2000**, *12*, 3243-3245.

[69] R. Kniep, H. G. Will, I. Boy, C. Röhr
6_1 helices From Tetrahedral Ribbons $[BP_2O_8^{3-}]$: Isostructural Borophosphates $M^IM^{II}(H_2O)_2[BP_2O_8]\cdot H_2O$ (M^I =Na, K; M^{II} =Mg, Mn, Fe, Co, Ni, Zn) and

Their Dehydration to Microporous Phases $M^{I}M^{II}(H_2O)[BP_2O_8]$
Angew. Chem. Int. Ed. Engl. **1997**, *36*, 1013-1014.

[70] O. V. Yakubovich, I. Steel, O. V. Dimitrova
$NaMn(H_2O)_2[BP_2O_8]\cdot H_2O$: Crystal Structure Refinement
Kristallografiya **2009**, *54*, 20-25.

[71] H. Z. Shi, Y. K. Shan, M. Y. He, Y. Y. Liu, L. H. Weng
Synthesis and Structure of the First Protonated Zincoborophosphate:
$(H_3O)Zn(H_2O)_2BP_2O_8\cdot H_2O$
Chin. J. Chem. **2003**, *21*, 1170-1173.

[72] I. Boy, G. Schäfer, R. Kniep
Crystal Structure of Sodium Iron (II) Diaqua Catena-Monoboro-Diphosphate] Monohydrate, $NaFe(H_2O)_2[BP_2O_8]\cdot H_2O$, and of Potassium Iron (II) Diaqua Catena-[Monoboro-Diphosphate] Hemihydrate, $KFe(H_2O)_2[BP_2O_8]\cdot 0.5H_2O$
Z. Kristallogr. - New Cryst. Struct. **2001**, *216*, 13-14.

[73] A. Yilmaz, L. T. Yildirim, X. Bu, M. Kizilyalli, G. D. Stucky
New Zeotype Borophosphates with Chiral Tetrahedral Topology:
$(H)_{0.5}M_{1.25}(H_2O)_{1.5}[BP_2O_8]\cdot H_2O$ (M = Co(II) and Mn(II))
Cryst. Res. Technol. **2005**, *40*, 579-585.

[74] Y.-X. Huang, G. Schäfer, W. Carrillo-Cabrera, R. Cardoso, W. Schnelle, J.-T. Zhao, R. Kniep
Open-framework Borophosphates:
$(NH_4)_{0.4}(Fe_{0.5}Fe^{III}_{0.5})Fe^{II}(H_2O)_2[BP_2O_8]\cdot 0.6H_2O$ and $NH_4Fe^{III}[BP_2O_8(OH)]$
Chem. Mater. **2001**, *13*, 4348-4354.

[75] H. Z. Shi, Y. K. Shan, L. Y. Dai, Y. Y. Liu
Open-framework Borophosphate: $(NH_4)_{0.5}(Fe_{0.5}Fe^{III}_{0.5})Fe^{II}(H_2O)_2[BP_2O_8]\cdot 0.5$ H_2O
Chin. Chem. Lett. **2003**, *14*, 744-747.

[76] G. Schäfer, W. Carrillo-Cabrera, W. Schnelle, H. Borrmann, R. Kniep
Synthesis and Crystal Structure of $\{(NH_4)_xCo_{(3-x)/2}\}(H_2O)_2[BP_2O_8]\cdot(1-x)\ H_2O$ ($x = 0.5$)
Z. Anorg. Allg. Chem. **2002**, *628*, 289-294.

[77] H. Z. Shi, M. Li, H. Tangbo, A. G. Kong, B. Chen, Y. K. Shan
A Novel Open-framework Copper Borophosphate: $Cu(H_2O)_2[B_2P_2O_8(OH)_2]$
Inorg. Chem. **2005**, *44*, 8179-8181.

[78] B. Ewald, Y. Öztan, Yu. Prots, R. Kniep
Crystal Structure of Diaqua (Magnesium, Cobalt) Bis (Hydroxyboro) Bisphosphate Monohydrate, $Mg_{1-x}Co_x(H_2O)_2[B_2P_2O_8(OH)_2]\cdot H_2O$ ($x = 0.25$)
Z. Kristallogr. - New Cryst. Struct. **2005**, *220*, 535-536.

[79] H. Engelhardt, W. Schnelle, R. Kniep
$Rb_2Co_3(H_2O)_2[B_4P_6O_{24}(OH)_2]$: A Borophosphate with Tetrahedral Anionic Partial Structure and Trimers of Octahedra $Co^{II}{}_3O_{12}(H_2O)_2$
Z. Anorg. Allg. Chem. **2000**, *626*, 1380-1386.

[80] H. H. Chen, M. H. Ge, X. X. Yang, J.-X. Mi, J.-T. Zhao
Synthesis and Crystal Structure of $Fe_2BP_3O_{12}$
J. Inorg. Mater. **2004**, *19*, 429-432.

[81] M. Meisel, M. Päch, L. W. B. Lutz, D. Wulff-Molder
Synthesis and Crystal Structure of Vanadium (III) Borophosphate, $V_2[B(PO_4)_3]$
Z. Anorg. Allg. Chem. **2004**, *630*, 983-985.

[82] W. Liu, Y.-X. Huang, R. Cardoso-Gil, W. Schnelle, R. Kniep
$Na_6Cu_3\{B_6P_6O_{27}(O_2BOH)_3\}\cdot 2H_2O$: A Novel Copper Borophosphate with a Tubelike Borophosphate Anion
Z. Anorg. Allg. Chem. **2006**, *632*, 2143.

[83] Y. Tao, G. H. Li, J. Ju, F. H. Liao, Xiong M., J. H. Lin
A Series of Borate-rich Metalloborophosphates $Na_2[M^{II}B_3P_2O_{11}(OH)]\cdot 0.67H_2O$ (M^{II} = Mg, Mn, Fe, Co, Ni, Cu, Zn): Synthesis, Structure and Magnetic Susceptibility
J. Solid State Chem. **2006**, *179*, 2534-2540.

[84] M. Yang, J. H. Yu, J. C. Di, J. Y. Li, P. Chen, Q. R. Fang, Y. Chen, R. R. Xu
Syntheses, Structures, Ionic Conductivities, and Magnetic Properties of Three New Transition-metal Borophosphates $Na_5(H_3O)\{M_3{}^{II}[B_3O_3(OH)]_3(PO_4)_6\}\cdot 2H_2O$ (M^{II} = Mn, Co, Ni)
Inorg. Chem. **2006**, *45*, 3588-3593.

[85] R. Kniep, G. Schäfer, H. Engelhardt, I. Boy
$K[ZnBP_2O_8]$ and $A[ZnBP_2O_8]$ (A = NH_{4+}, Rb^+, Cs^+): Zincoborophosphates as a New Class of Compounds with Tetrahedral Framework Structures
Angew. Chem. Int. Ed. Engl. **1999**, *38*, 3642-3644.

[86] R. Kniep, G. Schäfer, H. Borrmann
Crystal Structure of Ammonium [Monozinco-Monoboro-Diphosphate], $NH_4[ZnBP_2O_8]$
Z. Kristallogr. - New Cryst. Struct. **2000**, *215*, 335-336.

[87] G. Schäfer, H. Borrmann, R. Kniep
Synthesis and Crystal structure of $NH_4[(Zn_{1-x}Co_x)BP_2O_8]$ ($0 < x < 0.14$), A Metallo-Borophosphate Analogue of the Zeolite Gismondine
Micropor. Mesopor. Mat. **2000**, *41*, 161-167.

[88] I. Boy, F. Stowasser, G. Schäfer, R. Kniep
$NaZn(H_2O)_2[BP_2O_8]\cdot H_2O$: A Novel Open-framework Borophosphate and its Reversible Dehydration to Microporous Sodium Zincoborophosphate $Na[ZnBP_2O_8]\cdot H_2O$ with CZP Topology
Chem-Euro. J. **2001**, *7*, 834-839.

[89] Y.-X. Huang, Yu. Prots, R. Kniep
$Zn[BPO_4(OH)_2]$: A Zinc Borophosphate with the Rare Moganite-Type Topology
Chem-Euro. J. **2008**, *14*, 1757-1761.

[90] J. Liebertz, S. Stahr
Existence and Mono-Crystal Growth of Zn_3BPO_7 and Mg_3BPO_7
Z. Kristallogr. **1982**, *160*, 135-137.

[91] K. Bluhm, C. H. Park
Synthesis and Crystal Structure of the Borate-Phosphate: α-$Zn_3(BO_3)(PO_4)$
Z. Naturforsch. , B: Chem. Sci. **1997**, *52*, 102-106.

[92] A. Yilmaz, X. H. Bu, M. Kizilyalli, R. Kniep, G. D. Stucky
Cobalt Borate Phosphate, $Co_3[BPO_7]$, Synthesis and Characterization
J. Solid State Chem. **2001**, *156*, 281-285.

[93] I. Bull, V. Young, S. J. Teat, L. M. Peng, C. P. Grey, J. B. Parise
Hydrothermal Synthesis and Structural Characterization of Four Scandium Phosphate Frameworks
Chem. Mater. **2003**, *15*, 3818-3825.

[94] S. R. Miller, E. Lear, J. Gonzalez, A. M. Z. Slawin, P. A. Wright, N. Guillou, G. Ferey
Synthesis and Structure of the Framework Scandium Methylphosphonates $ScF(H_2O)CH_3PO_3$ and $NaSc(CH_3PO_3)_2$ center dot $0.5H_2O$
Dalton Transactions **2005**, 3319-3325.

[95] S. R. Miller, A. M. Z. Slawin, P. Wormald, P. A. Wright
Hydrothermal Synthesis and Structure of Organically Templated Chain, Layered and Framework Scandium Phosphates
J. Solid State Chem. **2005**, *178*, 1738-1752.

[96] D. Riou, F. Fayon, D. Massiot
Hydrothermal Synthesis, Structure Determination, and Solid-State NMR Study of the First Organically Templated Scandium Phosphate
Chem. Mater. **2002**, *14*, 2416-2420.

[97] R. M. Barrer
Hydrothermal Chemistry of Zeolites
Academic Press London, **1982.**

[98] K.Byrappa
Handbook of Crystal Growth: Bulk Crystal Growth
Elsevier Science, **1994**.

[99] L. R. Taylor, R. B. Papp, and B. D. Pollard
Instrumental Methods for Determining Elements
VCH Publishers, **1994.**

[100] Ch. Bärlocher and L. B. McCusker
Atlas Zeolite Structures Types
http://www.iza-sc.ethz.ch/IZA-SC/Atlas/data/CZP.html., **2008.**

[101] W. H. Baur
Geometry of Polyhedral Distortions - Predictive Relationships for Phosphate Group
Acta Crystallogr. **1974**, *B 30*, 1195-1215.

[102] O. A. Gurbanova, E. L. Belokoneva, O. V. Dimitrova
Synthesis and Crystal Structure of New Borophosphate NaIn[BP_2O_8(OH)]
Russ. J. Inorg. Chem. **2002**, *47*, 6-9.

[103] R. Kniep, D. Koch, T. Hartmann
Crystal Structure of Potassium Aluminum Catena-(Monohydrogenmonoborate)-Bis(Monophosphate), KAl[BP_2O_8(OH)]
Z. Kristallogr. - New Cryst. Struct. **2002**, *217*, 186-186.

[104] J.-X. Mi, J.-T. Zhao, Y.-X. Huang, J. F. Deng, H. Borrmann, R. Kniep
Crystal Structure of Rubidium Aluminum Catena-[Monohydrogen-Monoborate-Bis(Monophosphate)], RbAl[BP_2O_8(OH)]
Z. Kristallogr. - New Cryst. Struct. **2002**, *217*, 171-172.

[105] J.-X. Mi, H. Borrmann, Y.-X. Huang, S.-Y. Mao, J.-T. Zhao, R. Kniep
Crystal Structure of Caesium Gallium(III) Catena-[Monohydrogenmonoborate-Bis(Monophosphate)], CsGa[BP_2O_8(OH)]
Z. Kristallogr. - New Cryst. Struct. **2003**, *218*, 171-172.

[106] J.-X. Mi, H. Borrmann, S.-Y. Mao, Y.-X. Huang, H. Zhang, J.-T. Zhao, R. Kniep
Crystal Structure of Rubidium Gallium Catena-[Monohydrogen-Monoborate-Bis(Monophosphate)] RbGa[BP_2O_8(OH)], from a Twinned Crystal
Z. Kristallogr. - New Cryst. Struct. **2003**, *218*, 17-18.

[107] D. Koch, R. Kniep
Crystal Structure of Sodium Aluminum (Monohydrogenmonophosphate-Dihydrogenmonoborate-Monophosphate), NaAl[$BP_2O_7(OH)_3$]
Z. Kristallogr. - New Cryst. Struct. **1999**, *214*, 441-442.

[108] J.-X. Mi, Y.-X. Huang, S. Y. Mao, H. Borrmann, J.-T. Zhao, R. Kniep
Crystal Structure of Potassium Gallium (Monophosphate-Hydrogenmonoborate-Monophosphate), $KGa[BP_2O_7(OH)_3]$
Z. Kristallogr. - New Cryst. Struct. **2002**, *217*, 167-168.

[109] Y.-X. Huang, J.-T. Zhao, J.-X. Mi, H. Borrmann, R. Kniep
Crystal Structure of Rubidium Indium (Monophosphate-Hydrogenmonoborate-Monophosphate), $RbIn[BP_2O_8(OH)]$
Z. Kristallogr. - New Cryst. Struct. **2002**, *217*, 163-164.

[110] S.-Y. Mao, M. R. Li, Y.-X. Huang, J.-X. Mi, Z. B. Wei, J.-T. Zhao, R. Kniep
Crystal Structure of Potassium Indium (Monophosphate-Hydrogenmonoborate-Monophosphate), $KIn[BP_2O_8(OH)]$
Z. Kristallogr. - New Cryst. Struct. **2002**, *217*, 3-4.

[111] B. Ewald, Yu. Prots, P. W. Menezes, R. Kniep
Crystal Structure of Diaqua-Indium Catena-Monoboro-Bisphosphate Monohydrate, $In(H_2O)_2[BP_2O_8]\cdot H_2O$
Z. Kristallogr. - New Cryst. Struct. **2004**, *219*, 351-352.

[112] C. Hauf, R. Kniep
Crystal Structure of Diammonium Catena-(Monoboro-Mono-Dihydrogendiboratemonophosphate), $(NH_4)_2[B_3PO_7(OH)_2]$
Z. Kristallogr. **1996**, *211*, 705-706.

[113] C. Hauf, R. Kniep
Crystal Structure of Tripotassium Catena-[Triboro-Monohydrogenphosphate Bis(Monohydrogenborate)], $K_3[B_5PO_{10}(OH)_3]$
Z. Kristallogr. **1996**, *211*, 707-708.

[114] C. Hauf, R. Kniep
Crystal Structure of Lithium Catena-[Monoboro-Mono-Dihydrogendiborate-Monohydrogenphosphate], $Li[B_3PO_6(OH)_3]$
Z. Kristallogr. - New Cryst. Struct. **1997**, *212*, 313-314.

[115] J.-X. Mi, J. F. Deng, S.-Y. Mao, Y.-X. Huang, H. Borrmann, J.-T. Zhao, R. Kniep
Crystal Structure of Dilithium Indium (Monophosphate-Monohydrogen-Monophosphate), $Li_2In[(PO_4)(HPO_4)]$
Z. Kristallogr. - New Cryst. Struct. **2002**, *217*, 307-308.

[116] J.-X. Mi, H. Borrmann, H. Zhang, Y.-X. Huang, W. Schnelle, J.-T. Zhao, R. Kniep
Synthesis, Magnetism, and Crystal Structure of $Li_2Fe[(PO_4)(HPO_4)]$ and its Hydrogen Position Refinement
Z. Anorg. Allg. Chem. **2004**, *630*, 1632-1636.

[117] R. C. Haushalter, Z. W. Wang, M. E. Thompson, J. Zubieta
Hydrothermal Synthesis and Structural Characterization of Reduced Vanadium Phosphates, α-Rb[$V^{III}(HPO_4)_2$], β-Rb[$V^{III}(HPO_4)_2$] and $NH_4[V^{III}(HPO_4)_2]$, Octahedral-Tetrahedral Framework Solids
Inorg. Chim. Acta **1995**, *232*, 83-89.

[118] I. P. Kondratyuk, M. I. Sirota, B. A. Maksimov, L. A. Muradyan, V. I. Simonov
An X-Ray Structural Investigation of Microtwinning of $Li_3Sc_2(PO_4)_3$ and $Li_3Fe_2(PO_4)_3$ Crystals
Kristallografiya **1986**, *31*, 488-494.

[119] G. Vitins, Z. Kanepe, A. Vitins, J. Ronis, A. Dindune, A. Lusis
Structural and Conductivity Studies in $LiFeP_2O_7$, $LiScP_2O_7$, and $NaScP_2O_7$
J. Solid State Electr. **2000**, *4*, 146-152.

[120] Z. Kanepe, V. Krasinkov, Z. Konstants
Potassium Scandium Phosphate, $KScP_2O_7$
Kim. Ser. **1987**, *1*, 29-30.

[121] F. C. Hawthorne
Structural Aspects of Oxide and Oxysalt Crystals
Acta Crystallogr. **1994**, *50*, 481-510.

[122] R. D. Shannon
Revised Effective Ionic-Radii and Systematic Studies of Interatomic Distances in Halides and Chalcogenides
Acta Crystallogr. , Sect. A: Found. Crystallogr. **1976**, *32*, 751-767.

[123] L. N. Komissarova, M. G. Zhizhin, A. A. Filaretov
Complex Phosphates Containing Mono- and Trivalent Cations
Russ. Chem. Rev. **2002**, *71*, 619-650.

[124] O. V. Yakubovich
Crystal Structure of $NH_4Fe(HPO_4)_2$
Kristallografiya **1993**, *38*, 43-48.

[125] K. H. Lii, L. S. Wu
$RbFe(HPO_4)_2$ - An Iron(IIII) Phosphate with An Intersecting Tunnel Structure
J. Chem. Soc. , Dalton Trans. **1994**, 1577-1580.

[126] J. Lesage, L. Adam, A. Guesdon, B. Raveau
Four New Hydroxymonophosphates with Closely Related Intersecting Tunnels Structures: The Series $AM(PO_3(OH))_2$ with *A* = Rb, Cs,; *M* = Fe, Al, Ga, In
J. Solid State Chem. **2007**, *180*, 1799-1808.

[127] Z. Bircsak, W. T. A. Harrison
α-Ammonium Vanadium Hydrogen Phosphate, α-$(NH_4)V(HPO_4)_2$
Acta Crystallogr. , Sect. C: Cryst. Struct. Commun. **1998**, *54*, 1195-1197.

[128] B. Ewald, Yu. Prots, H. Zhang, R. Kniep
Crystal Structure of Sodium Scandium Bis(Monohydrogenphosphate), $NaSc(HPO_4)_2$
Z. Kristallogr. - New Cryst. Struct. **2004**, *219*, 343-344.

[129] J. E. Huheey, E. A. Keiter, and R. L. Keiter
Inorganic Chemistry
HarperCollins College Publisher, **1993.**

[130] Y.-X. Huang, M. R. Li, J.-X. Mi, S.-Y. Mao, H. H. Chen, J.-T. Zhao
New Indium (III) Phosphate $CsIn[PO_3(OH)]_2$ with A New Type of Structure
Chin. J. Inorg. Chem **2004**, *20*, 1191-1196.

[131] A. A. Filaretov, M. G. Zhizhin, A. V. Olenev, A. A. Gurkin, A. P. Bobylev, B. I. Lazoryak, V. P. Danilov, L. N. Komissarova
Hydrothermal Synthesis, Structures, and Properties: Indium Hydrogen Phosphates ($M^{I}In(HPO_4)_2$ (M^{I} = K, Rb, and NH_4)
Russ. J. Inorg. Chem. **2002**, *47*, 1773-1789.

[132] O. A. Gurbanova, E. L. Belokoneva, O. V. Dimitrova, A. G. Al-Ama
The New Phosphate $LiIn[PO_3(OH)]_2$: Synthesis and Crystal Structure
Russ. J. Inorg. Chem. **2001**, *46*, 1302-1307.

[133] Y.-X. Huang, S.-Y. Mao, J.-X. Mi, Z. B. Wei, J.-T. Zhao, R. Kniep
Crystal Structure of Sodium Gallium [Monohydrogenmonophosphate-Dihydrogenmonoborate-Monophosphate],$NaGa[BP_2O_7(OH)_3]$
Z. Kristallogr. - New Cryst. Struct. **2001**, *216*, 15-16.

[134] Y.-X. Huang, J.-X. Mi, S.-Y. Mao, Z. B. Wei, J.-T. Zhao, R. Kniep
Crystal Structure of Sodium Indium (Monohydrogenmonophosphate-Dihydrogenmonoborate-Monophosphate), $NaIn[BP_2O_7(OH)_3]$
Z. Kristallogr. - New Cryst. Struct. **2002**, *217*, 7-8.

[135] J.-X. Mi, M. R. Li, S.-Y. Mao, Y.-X. Huang, Z. B. Wei, J.-T. Zhao, R. Kniep
Crystal Structure of Ammonium Indium (Monophosphate-Hydrogenmonoborate-Monophosphate), $(NH_4)In[BP_2O_8(OH)]$
Z. Kristallogr. - New Cryst. Struct. **2002**, *217*, 5-6.

[136] R. L. Carlin
Magnetochemistry
Springer, Berlin, **1986.**

[137] W. T. A. Harrison, T. E. Gier, G. D. Stucky, R. W. Broach, R. A. Bedard
$NaZnPO_4 \cdot H_2O$, An Open-framework Sodium Zincophosphate with a New Chiral Tetrahedral Framework Topology
Chem. Mater. **1996**, *8*, 145-151.

[138] N. Rajic, N. Z. Logar, V. Kaucic
A Novel Open Framework Zincophosphate - Synthesis and Characterization
Zeolites **1995**, *15*, 672-678.

[139] M. Helliwell, J. R. Helliwell, V. Kaucic, N. Z. Logar, L. Barba, E. Busetto, A. Lausi
Determination of the Site of Incorporation of Cobalt in CoZnPO-CZP by Multiple Wavelength Anomalous Dispersion Crystallography
Acta Crystallogr. **1999**, *55*, 327-332.

[140] G. E. R. Schulze
The Crystal Structure of BPO_4 and $BAsO_4$
Z. Phys . Chem. Abt. B **1934**, *24*, 215-240.

[141] C. Hauf, I. Boy, R. Kniep
Crystal Structure of Dimagnesium (Monohydrogenmonophosphate-Dihydrogenmonoborate-Monophosphate), $Mg_2[BP_2O_7(OH)_3]$
Z. Kristallogr. - New Cryst. Struct. **1999**, *214*, 3-4.

[142] Y.-X. Huang, O. Hochrein, D. Zahn, Yu. Prots, H. Borrmann, R. Kniep
Control of Channel Shapes in a Microporous Manganese(II)-Borophosphate Framework By Variation of Size and Shape of Organic Template Cations
Chem-Euro. J. **2007**, *13*, 1737-1745.

[143] N. Shin, J. Kim, D. Ahn, K. S. Sohn
A new strontium borophosphate, $Sr_6BP_5O_{20}$, from synchrotron powder data
Acta Crystallogr. , Sect. C: Cryst. Struct. Commun. **2005**, *61*, I54-I56-I56.

[144] H. Y. Zhang, Z. X. Chen, L. H. Weng, Y. M. Zhou, D. Y. Zhao
Hydrothermal Synthesis of New Berylloborophosphates $M^I[BeBP_2O_8]$ (M^I = K^+, Na^+ and NH_{4+}) with Zeolite ANA Framework Topology
Micropor. Mesopor. Mat. **2003**, *57*, 309-316.

[145] B. Ewald, Y. Öztan, Yu. Prots, R. Kniep
Structural Patterns and Dimensionality in Magnesium Borophosphates: The Crystal Structures of $Mg_2(H_2O)[BP_3O_9(OH)_4]$ and $Mg(H_2O)_2[B_2P_2O_8(OH)_2] \cdot H_2O$
Z. Anorg. Allg. Chem. **2005**, *631*, 1615-1621.

[146] Liebau F.
Structural Chemistry of Silicates
Springer-Verlag, Berlin Heidelberg, **1985.**

[147] G. Heller
A Survey of Structural Types of Borates and Polyborates
Top. Curr. Chem. **1986**, *131*, 39-98.

[148] G. A. Sharpataya, K. S. Gavrichev, V. E. Gorbunov, Z. P. Ozerova, I. D. Sokolova, A. D. Fedoseev, A. V. Filatov
Phase-Transitions of Cobalt Diphosphate
Zh. Neorg. Khim. **1994**, *39*, 398-406.

[149] N. Krishnam, C. Calvo
Crystal Structure of Cobalt Diphosphate
Acta Crystallogr. **1972**, *B 28*, 2883-2886.

[150] R. Masse, J. C. Guitel, A. Durif
Crystalline Structure of New Form of Nickel Pyrophosphate - $Ni_2P_2O_7$
Mat. Res. Bull. **1979**, *14*, 337-341.

[151] C. Parada, J. Perles, R. Saez-Puche, C. Ruiz-Valero, N. Snejko
Crystal Growth, Structure, and Magnetic Properties of a New Polymorph of $Fe_2P_2O_7$
Chem. Mater. **2003**, *15*, 3347-3351.

[152] V. Kahlenberg, G. Dorsam, M. Wendschuh-Josties, R. X. Fischer
The Crystal Structure of δ-$Na_2Si_2O_5$
J. Solid State Chem. **1999**, *146*, 380-386.

[153] S. Natarajan, B. Ewald, Yu. Prots, R. Kniep
$[C_{10}N_2H_{10}][ZnCl(HPO_4)]_2$: A New Templated Zincophosphate Containing Tetrahedral Nets With 6^3 Topology
Z. Anorg. Allg. Chem. **2005**, *631*, 1622-1626.

[154] N. Stock, G. D. Stucky, A. K. Cheetham
Synthesis and Characterization of the Manganese Pyroarsenate $Mn_2As_2O_7{\cdot}2H_2O$
Z. Naturforsch. , B: Chem. Sci. **2001**, *56*, 359-363.

[155] H. G. Giesber, M. B. Korzenski, W. T. Pennington, J. W. Kolis
$Fe_2P_2O_7(H_2O)_2$
Acta Crystallogr. , Sect. C: Cryst. Struct. Commun. **2000**, *56*, 399-400.

[156] H. Effenberger, F. Pertlik
Comparison of the Crystal Structures of $Co_2(X_2O_7){\cdot}2H_2O$, X = P and As
Monat. Chem. **1993**, *124*, 381-389.

[157] A. Elbelghitti, A. Boukhari, E. M. Holt
β-Dicobalt Pyrophosphate
Acta Crystallogr. , Sect. C: Cryst. Struct. Commun. **1994**, *50*, 482-484.

[158] T. Yang, J. Ju, G. B. Li, S. H. Yang, J. L. Sun, F. H. Liao, J. H. Lin, J. Sasaki, N. Toyota
$M H_2P_2O_7$ (M = Co, Ni): Metamagnetic Interaction between the Zigzag Octahedral Chains
Inorg. Chem. **2007**, *46*, 2342-2344.

[159] M. Asnani, A. Ramanan, J. J. Vittal
Hydrothermal Synthesis and Structural Characterisation of a Vanadium (V) Borophosphate Cluster Containing Solid: $[Coen_3][enH_2]\{V_3BP_3O_{19}\}\cdot 4.5H_2O$
Inorg. Chem. Comm. **2003**, *6*, 589-592.

[160] Y. Wang, J. H. Yu, O. H. Pan, Y. Du, Y. C. Zou, R. R. Xu
Synthesis and Structural Characterization of 0D Vanadium Borophosphate $[Co(en)_3]_2[V_3P_3BO_{19}][H_2PO_4]\cdot 4H_2O$ and 1D vanadium oxides $[Co(en)_3][V_3O_9]\cdot H_2O$ and $[Co(dien)_2][V_3O_9]\cdot H_2O$ Templated by Cobalt Complexes: Cooperative Organization of the Complexes and the Inorganic Networks
Inorg. Chem. **2004**, *43*, 559-565.

[161] C. H. Park, K. Bluhm
Synthesis and Crystal-Structure of Trilead-Diphosphato-Borate-Phosphate, A Compound with a Infinite $[(PO_4)_2BPO_4]^{6-}$ Anion
Z. Naturforsch. , B: Chem. Sci. **1995**, *50*, 1617-1622.

[162] A. Durif
Crystal Chemistry of Condensed Phosphates
Plenum, **1995.**

[163] W. Kleber
An Introduction to Crystallography
VEB Verlag Technik Berlin, **1970.**

Curriculum Vitae

PERSONAL DATA:

Name:	Prashanth Wilfred Menezes
Date of Birth:	2nd May 1979
Place of Birth:	Puttur
Marital Status:	Single
Nationality:	Indian

EDUCATION

June 1996 – June 1999	**Bachelor of Science** St. Philomena College Mangalore University, Karnataka, INDIA.
June 1999 – June 2001	**Master of Science** Department of Chemistry Mangalore University, Karnataka, INDIA. Supervisor: Prof. B. Narayana
October 2004 – Present	**Dissertation** Max Planck Institute for Chemical Physics of Solids, Dresden, GERMANY. Supervisor: Prof. Dr. R. Kniep

RESEARCH EXPERIENCE

June 2002 – December 2003	**CSIR Research Fellow** Indian Institute of Science Bangalore, INDIA. Supervisor: Prof. D. D. Sarma
January 2004 – October 2004	**Visiting Scientist** Max Planck Institute for Chemical Physics of Solids, Dresden, GERMANY. Supervisor: Prof. Dr. R. Kniep
October 2004 – Present	**Ph.D. Student** Max Planck Institute for Chemical Physics of Solids, Dresden, GERMANY. Supervisor: Prof. Dr. R. Kniep

Publications

1. Debangshu Chaudhuri, Prashanth W. Menezes and D. D. Sarma,
   Remarkable thermal stability of BF3-doped polyaniline
   Appl. Phys. Lett., **2003***, 83,* 2348-2350.

2. Bastian Ewald, Prashanth W. Menezes, Yurii Prots and Rüdiger Kniep
   Solvothermal Synthesis of Alkali–Metal Borophosphates: Crystal Structure of $Rb_3[B_2P_3O_{10}(OH)_3]$
   Z. Anorg. Allg. Chem. **2004**, *630*, 1721-1722.

3. Bastian Ewald, Yurii Prots, Prashanth W. Menezes and Rüdiger Kniep
   Crystal Structure of Diaqua Indium Catena Monoboro–Bisphosphate Monohydrate, $In(H_2O)_2[BP_2O_8]\cdot H_2O$
   Z. Kristallogr. - New Cryst. Struct. **2004**, *219*, 351-352.

4. Bastian Ewald, Yurii Prots, Prashanth W. Menezes, Srinivasan Natarajan, Hui Zhang and Rüdiger Kniep
   Chain Structures in Alkali–Metal Borophosphates: Synthesis and Characterization of $K_3[BP_3O_9(OH)_3]$ and $Rb_3[B_2P_3O_{11}(OH)_2]$
   Inorg. Chem. **2005**, *44*, 6431-6438.

5. Prashanth W. Menezes, Stefan Hoffmann, Yurii Prots and Rüdiger Kniep
   $CsSc[B_2P_3O_{11}(OH)_3]$: A New Borophosphate Oligomer Containing Boron in CN = 3 and 4
   Z. Anorg. Allg. Chem. **2006**, 632, 2131-2132.

6. Prashanth W. Menezes, Stefan Hoffmann, Yurii Prots and Rüdiger Kniep
   Crystal Structure of Potassium Scandium (Monophosphate–Hydrogenmonoborate–Monophosphate), $KSc[BP_2O_8(OH)]$
   Z. Kristallogr. - New Cryst. Struct. **2006**, *221*, 251-252.

7. Prashanth W. Menezes, Stefan Hoffmann, Yurii Prots and Rüdiger Kniep
   Crystal Structure of Rubidium Scandium (Monophosphate–Hydrogenmonoborate–Monophosphate), $RbSc[BP_2O_8(OH)]$
   Z. Kristallogr. - New Cryst. Struct. **2006**, *221*, 253-254.

8. Prashanth W. Menezes, Stefan Hoffmann, Yurii Prots and Rüdiger Kniep
   Crystal Structure of Calcium Nickel (II) Monohydrogen–Monophosphate–Dihydrogenmonoborate–Monophosphate, $CaNi[BP_2O_7(OH)_3]$
   Z. Kristallogr. - New Cryst. Struct. **2006**, *221*, 429-430.

9. Harold Brice Tanh Jeazet, Prashanth W. Menezes, Stefan Hoffmann, Yurii Prots and Rüdiger Kniep
   Crystal Structures of Lead Cobalt (Monophosphate–Hydrogenmonoborate–Monophosphate), $PbCo[BP_2O_8(OH)]$, and Lead Zinc (Monophosphate–Hydrogenmonoborate–Monophosphate), $PbZn[BP_2O_8(OH)]$
   Z. Kristallogr. - New Cryst. Struct. **2006**, *221*, 431-433.

10. Prashanth W. Menezes, Stefan Hoffmann, Yurii Prots and Rüdiger Kniep

Crystal Structure of Hemicalcium Diaquanickel (II) Catena–(Monoborodiphosphate) Monohydrate, $Ca_{0.5}Ni(H_2O)_2[BP_2O_8]\cdot H_2O$
Z. Kristallogr. - New Cryst. Struct. **2007**, *222*, 1-2.

11. Prashanth W. Menezes, Stefan Hoffmann, Yurii Prots and Rüdiger Kniep
$CsSc[B_2P_3O_{11}(OH)_3]$: A New Borophosphate Oligomer Containing Boron in Three– and Four Fold Coordination
Inorg. Chem. **2007**, *46*, 7503-7508.

12. Prashanth W. Menezes, Stefan Hoffmann, Yurii Prots and Rüdiger Kniep
Crystal Structure of Hemicalcium Diaquanickel (II) Catena–(Monoborodiphosphate) Monohydrate, $Ca_{0.5}Fe(H_2O)_2[BP_2O_8]\cdot H_2O$
Z. Kristallogr. - New Cryst. Struct. **2008**. 223, 9-10.

13. Prashanth W. Menezes, Stefan Hoffmann, Yurii Prots and Rüdiger Kniep
Crystal Structure of Dilithium Monoscandium (Monophosphate–Monohydrogen–Monophosphate), $Li_2Sc[(PO_4)(HPO_4)]$
Z. Kristallogr. - New Cryst. Struct. **2008**, *223*, 319-320.

14. Prashanth W. Menezes, Stefan Hoffmann, Yurii Prots and Rüdiger Kniep
Crystal Structure of Monocesium Monoscandium Bis Monohydrogenphosphate, $CsSc(HPO_4)_2$
Z. Kristallogr. - New Cryst. Struct. **2008**, *223*, 321-322.

15. Prashanth W. Menezes, Stefan Hoffmann, Yurii Prots and Rüdiger Kniep
Crystal Structure of Lithium Diaquacobalt (II) Catena–(Monoboro–Diphosphate) Monohydrate, $LiCo(H_2O)_2[BP_2O_8]\cdot H_2O$
Z. Kristallogr. - New Cryst. Struct. **2008,** *223*, 333-334.

16. Prashanth W. Menezes, Stefan Hoffmann, Yurii Prots and Rüdiger Kniep
Crystal Structure of Calcium (II) Iron (II) Monohydrogen–Monophosphate–Dihydrogenmonoborate–Monophosphate), $CaFe[BP_2O_7(OH)_3]$
Z. Kristallogr. - New Cryst. Struct. **2008,** *223*, 335-336.

17. Prashanth W. Menezes, Stefan Hoffmann, Yurii Prots and Rüdiger Kniep
Crystal Structure of Barium (II) Iron (II) (Monophosphate–Hydrogenmonoborate–Monophosphate), $BaFe[BP_2O_8(OH)]$
Z. Kristallogr. - New Cryst. Struct. **2008,** *223*, 337-338.

18. Prashanth W. Menezes, Stefan Hoffmann, Yurii Prots and Rüdiger Kniep
Crystal Structure of Barium (II) Cobalt (II) (Monophosphate–Hydrogenmonoborate–Monophosphate), $BaCo[BP_2O_8(OH)]$
Z. Kristallogr. - New Cryst. Struct. **2008,** *223*, 339-340.

19. Stefan Hoffmann, Harold Brice Tanh Jeazet, Prashanth W. Menezes,Yurii Prots and Rüdiger Kniep
$Na_3Pb(II)[B(O_3POH)_4]$: An Alkali Metal Lead Borophosphate with Hetero Cubane–like Units Na_3PbO_4
Inorg. Chem. **2008**, *47*, 10193-10197

20. Prashanth W. Menezes, Stefan Hoffmann, Yurii Prots and Rüdiger Kniep
Crystal Structure of Diceasium Diaquatricobalt (II) (Monophosphate–Monoborate–Hydrogenmonophosphate), $Cs_2Co_3(H_2O)_2[B_4P_6O_{24}(OH)_2]$
Z. Kristallogr. - New Cryst. Struct. **2009,** *224*, 1-2.

21. Prashanth W. Menezes, Stefan Hoffmann, Yurii Prots and Rüdiger Kniep
Crystal Structure of Monorubidium Monoscandium Bis Monohydrogenphosphate) $RbSc(HPO_4)_2$ and Monoammonium Monoscandium Bis Monohydrogen Phosphate) $NH_4Sc(HPO_4)_2$
Z. Kristallogr. - New Cryst. Struct. **2009,** *224*, 21-23.

22. Prashanth W. Menezes, Stefan Hoffmann, Yurii Prots and Rüdiger Kniep
Synthesis and Crystal Structure of $KSc(HPO_4)_2$
Z. Anorg. Allg. Chem. **2009**, *65*, 33-35.

23. Prashanth W. Menezes, Stefan Hoffmann, Yurii Prots and Rüdiger Kniep
Synthesis and Crystal Structure of a Novel Layered $CaCo(H_2O)[BP_2O_8(OH)]\cdot H_2O$
Z. Anorg. Allg. Chem. **2009**, *635*, 614-617.

24. Prashanth W. Menezes, Stefan Hoffmann, Yurii Prots, Walter Schnelle and Rüdiger Kniep
Synthesis and Crystal Structure of $SrFe[BP_2O_7(OH)_2]$
Z. Anorg. Allg. Chem. **2009**, *635* (in press)

25. Prashanth W. Menezes, Stefan Hoffmann, Yurii Prots, Gudrun Auffermann and Rüdiger Kniep
Crystal Structures of $M^{II}(H_2O)_2[B_2P_2O_8(OH)_2]\cdot H_2O$ (M^{II} = $Ni_{0.5}Co_{0.5}$, $Ni_{0.8}Zn_{0.2}$, $Ni_{0.5}Mg_{0.5}$)
Z. Kristallogr. - New. Cryst. Struct. **2009** (to be submitted).

26. Prashanth W. Menezes, Stefan Hoffmann, Yurii Prots, Walter Schnelle and Rüdiger Kniep
Layered Borophosphates: Syntheses, Crystal Structures and Properties of $M^{II}(H_2O)_2[BP_2O_8(OH)_2]\cdot H_2O$ (M^{II} = Fe, Co, Ni)
Chem. A. Eur. J. **2009** (to be submitted).

27. Zhi-Sheng Lin, Ya-Xi Huang, Stefan Hoffmann, Prashanth W. Menezes, Yurii Prots, Jing-Tai Zhao and Rüdiger Kniep
$K_6M^{II}_3[B_9P_6O_{33}(OH)_3]\cdot 2H_2O$ (M^{II} = Mn, Fe, Co): Structure and Ion Exchange of Isotypic Chiral Borophosphates with One–dimensional Tubes
Chem. Mater. **2009** (to be submitted).

28. Prashanth W. Menezes, Stefan Hoffmann, and Rüdiger Kniep
Thermochemical Properties of Alkali–Metal Scandium Hydrogenphosphates
Thermochem. Acta **2009** (to be submitted).

29. Prashanth W. Menezes, Stefan Hoffmann, Yurii Prots and Rüdiger Kniep
$NaSc[BP_2O_6(OH)_3][(HO)PO_3]$: Synthesis and Crystal Structure of the First Alkali–Metal Scandium Borophosphate Hydrogenphosphate

Z. Anorg. Allg. Chem. **2009** (to be submitted).

30. Prashanth W. Menezes, Stefan Hoffmann, Yurii Prots and Rüdiger Kniep
Synthesis and Crystal Structure of $LiFe(H_2O)_2[BP_2O_8]\cdot H_2O$
Z. Anorg. Allg. Chem. **2009** (in preparation).

31. Prashanth W. Menezes, Stefan Hoffmann, Yurii Prots and Rüdiger Kniep
Synthesis and Crystal Structure of $FeCo(H_2O)[BP_3O_9(OH)_4]$ and $Fe_{1.3}Co_{0.7}[P_2O_7]\cdot 2H_2O$
J. Solid. State. Chem. **2009** (in preparation).

Poster Contributions

1. Bastian Ewald, Prashanth W. Menezes, Yurii Prots and Rüdiger Kniep
Solvothermal Synthesis of Alkali–Metal Borophosphates: Crystal Structure of $Rb_3[B_2P_3O_{10}(OH)_3]$
12. Fachgruppentagung Festkörperchemie und Materialforschung
13.–15. September **2004**, Marburg, GERMANY.

2. Bastian Ewald, Prashanth W. Menezes, Yurii Prots and Rüdiger Kniep
Chiral borophosphates $M^{III}(H_2O)_2[BP_2O_8]\cdot H_2O$ *(*M^{III} *= Sc, In,): Properties and Morphological Studies*
The 10th European Conference on Solid State Chemistry
29. August – 1. September **2005**, Sheffield, ENGLAND (Poster Prize).

3. Prashanth W. Menezes, Stefan Hoffmann, Yurii Prots and Rüdiger Kniep
CsSc$[B_2P_3O_{11}(OH)_3]$ *: A New Borophosphate Oligomer Containing Boron in CN = 3 and 4*
13. Fachgruppentagung Festkörperchemie und Materialforschung
13. – 15. September **2006**, Aachen, GERMANY.

4. Prashanth W. Menezes, Stefan Hoffmann, Yurii Prots and Rüdiger Kniep
Layered borophosphates $M^{II}(H_2O)_2[B_2P_2O_8(OH)_2]\cdot H_2O$ *(*M^{II} *= Co,.Fe, Ni)*
The 11th European Conference on Solid State Chemistry
11. – 13. September **2007**, Caen, FRANCE.

5. Stefan Hoffmann, Harold Brice Tanh Jeazet, Prashanth W. Menezes, Yurii Prots and Rüdiger Kniep
New Borophosphate Containing Lone Pair Ion Pb^{2+}
ZING – Solid State Chemistry Conference
10. – 13. March **2008**, Cancun, MEXICO.

6. Prashanth W. Menezes, Stefan Hoffmann, Yurii Prots and Rüdiger Kniep
Syntheses, Crystal structures and Properties of Borophosphates Containing Transition Metals (Sc, Fe, Co, Ni)
ZING – Solid State Chemistry Conference
10. – 13. March **2008**, Cancun, MEXICO.

7. Prashanth W. Menezes, Stefan Hoffmann, Yurii Prots and Rüdiger Kniep

Synthesis and Crystal Structure of $FeCo(H_2O)[BP_3O_9(OH)_4]$ and $Fe_{1.3}Co_{0.7}[P_2O_7]\cdot 2H_2O$
Solid State and Tansition Metal Elements Conference
24. – 30. July **2008**, Dresden, GERMANY.

8. Prashanth W. Menezes, Stefan Hoffmann and Rüdiger Kniep
Thermochemical Properties of $Li_2Sc[(PO_4)(HPO_4)]$ and $M^ISc(HPO_4)_2$ (M^I = K, Rb, Cs, NH_4)
18. Ulm – Freiberger Kalorimetrietage
18. – 21. March **2009**, Freiberg, GERMANY.

Oral Contributions

1. Prashanth W. Menezes, and Rüdiger Kniep
Back to the Roots of Crystallography
Fifth Baltic Boat Solid State Chemistry Conference
14. – 16. May **2004**, Stockholm, SWEDEN.

2. Prashanth W. Menezes, Stefan Hoffmann and Rüdiger Kniep
The family of Alkali–Metal Scandium Borophosphates: Synthesis, Crystal Structure and Properties
Sixth Baltic Boat Solid State Chemistry Conference
11. – 14. May **2006**, Stockholm, SWEDEN.

3. Stefan Hoffmann, Prashanth W. Menezes and Rüdiger Kniep
Alkali–Metal Scandium Borophosphates
MPI-CPfS – SICCAS Meeting
18. – 19. November **2008**, Shanghai, CHINA.

Workshops / Schools Attended

1. *MPI CPfS – NIMS Workshop on Development of Novel Functions in Network Materials*
11. April **2005**, Max-Planck Institute for Chemical Physics of Solids, Dresden, GERMANY.

2. *Experimental Physics of Emergent Materials*
16. January **2006**, Max-Planck Institute for Chemical Physics of Solids, Dresden, GERMANY.

3. *Phase Transformation in Metals and Alloys*
First European School in Material Science
22. – 27. May **2006**, Mons Hotel and Congress Center, Ljubljana, SLOVENIA.

4. *Properties and Applications of Complex Metallic Alloys*
Second European School in Material Science
21. – 26. May **2007**, Mons Hotel and Congress Center, Ljubljana, SLOVENIA.

5. *Solid State and Materials Chemistry*
   Second Bilateral Workshop
   17. – 19. July **2007**, Max-Planck Institute for Chemical Physics of Solids, Dresden, GERMANY.

Versicherung

Hiermit versichere ich, dass ich die vorliegende Arbeit ohne unzulässige Hilfe Dritter und ohne Benutzung anderer als der angegebenen Hilfsmittel angefertigt habe; die aus fremden Quellen direkt oder indirekt übernommenen Gedanken sind als solche kenntlich gemacht. Die Arbeit wurde bisher weder im Inland noch im Ausland in gleicher oder ähnlicher Form einer anderen Prüfungsbehörde vorgelegt.

Die vorliegende Dissertation wurde unter Betreuung von Herrn Prof. Dr. R. Kniep in der Zeit von Oktober 2004 bis Juni 2009 am Max-Planck-Institut für Chemische Physik fester Stoffe in Dresden angefertigt.

Es haben keine früheren erfolglosen Promotionsverfahren stattgefunden.

Ich erkenne die Promotionsordnung der Fakultät Mathematik und Naturwissenschaften der Technischen Universität Dresden vom 20. März 2000 gemäß der letzten Änderung vom 17. Juli 2008 in vollem Umfang an.

Dresden, den

(Prashanth W. Menezes)